Abstract

MCDOWELL, CHRISTOPHER CARROLL. Sorption and Transport of Acetone in Random Copolymers of Poly(ethylene terephthalate) and Poly(ethylene 2,6-naphthalate)

Poly(ethylene terephthalate) (PET) is widely used as a barrier packaging material for several food and beverage products. However, PET does not have sufficient barrier properties for many food and beverage packaging applications. The shelf life of these products can be compromised by the migration of small molecules such as oxygen, water, or organic flavor molecules through packaging materials. Copolymerization of PET with poly(ethylene 2,6-naphthalate) (PEN) leads to polymers with a better barrier properties. The focus of this dissertation is to elucidate the fundamental sorption and transport properties of small molecules in random copolymers of PET and PEN in order to develop systematic structure/property relations for this family of polymers.

The sorption and kinetics of acetone uptake in solvent cast films of poly(ethylene terephthalate) are reported at 35˚C for acetone pressures ranging from 0 to 7.3 cm Hg. The equilibrium sorption isotherm is well described by the dual-mode sorption model with the following parameters: k_D = 61 cm^3(STP)/(cm^3·atm), C'_H = 7.2 cm^3(STP)/cm^3, and b = 50 atm^{-1}. Sorption kinetics are described using a two-stage model which incorporates both Fickian diffusion and protracted polymer structural relaxation. The characteristic time associated with the relaxation process is essentially independent of acetone concentration and has an average value of approximately 15 hours. The fraction of sorption associated with polymer relaxation increases linearly with acetone concentration in the equilibrium densified matrix of the polymer. Acetone diffusion coefficients increase with increasing acetone concentration. The concentration dependence of the acetone diffusion coefficient is well described by the dual-mobility model if the assumption of constant diffusion coefficients in the two modes is relaxed.

Random copolymers of poly(ethylene terephthalate) [PET] and poly(ethylene 2,6-naphthalate) [PEN] were synthesized by melt condensation. The glass/rubber transition temperatures of these materials rise monotonically with increasing PEN content. In a series of thin, solvent cast

films of varying PEN content, acetone diffusivity and solubility were determined at 35˚C and an acetone pressure of 5.4 cm Hg. The kinetics of acetone sorption in the copolymer films are well described by a Fickian model. Both solubility and diffusivity decrease with increasing PEN content. The acetone diffusion coefficient decreases 93% from PET to PET/85PEN. The acronym PET/85PEN refers to a polymer in which 85 weight percent of the dimethyl terephthalate in PET has been replace by dimethyl naphthalate 2,6-dicarboxylate. The acetone solubility coefficient in the amorphous regions of the polymer decreases by approximately a factor of two over the same composition range. Copolymers containing between 20 and 80 wt. % PEN are amorphous. Samples with less than 20% or more than 80% PEN contain measurable levels of crystallinity. Estimated fractional free volume in the amorphous regions of these samples is lower in the copolymers than in either of the homopolymers. Relative free volume as probed by positron annihilation lifetime spectroscopy [PALS] decreases systematically with increasing PEN content. Acetone diffusion coefficients correlate well with PALS results. Infrared spectroscopy suggests an increase in the fraction of ethylene glycol units in the trans conformation in the amorphous phase as the concentration of PEN in the copolymer increases.

The interval sorption kinetics of acetone in solvent cast films of random poly(ethylene terephthalate)-co-(ethylene 2,6-naphthalate) are reported at 35˚C and at acetone pressures ranging from 0 to 7.3 cm Hg. Equilibrium sorption is well described by the dual-mode sorption model. Interval sorption kinetics are described using a two-stage model, which incorporates both Fickian diffusion and protracted polymer structural relaxation. The incorporation of low levels of PEN into PET appears to reduce the excess free volume associated with the glassy state and, for these interval acetone sorption experiments in ~5µm thick films, decreases the fraction of acetone uptake controlled by penetrant-induced polymer structural relaxation.

A systematic series of copolyesters was prepared by replacing up to 10 weight percent of the dimethyl terephthalate [DMT] in poly(ethylene terephthalate) [PET] with dimethyl 2,6-naphthalene dicarboxylate [NDC], isophthalic acid [IPA], or 2,5-bis-(4-carboxyphenyl)-1,3,4-oxadiazole [ODCA]. Solution cast films of the resulting copolymers were prepared and characterized. Modification of PET with NDC and ODCA led to copolymers with glass transition temperatures higher than that of PET, while modification with IPA decreased the glass transition temperature. Copolymerization decreased crystallinity in all cases. The acetone solubility and acetone diffusion coefficient were determined by integral kinetic gravimetric sorption experiments at 35˚C and 5.4 cm Hg acetone pressure. PET containing low levels of NDC had lower acetone diffusivity and lower acetone solubility than PET, while PET modified with IPA had higher acetone diffusivity and lower acetone solubility than PET. PET modified with 5% ODCA had higher acetone diffusivity, while PET modified with 10% ODCA had an acetone diffusivity value similar to that of PET. PET copolymers containing ODCA had higher acetone solubilities that PET.

Sorption and Transport of Acetone in Random Copolymers of Poly(ethylene terephthalate) and Poly(ethylene 2,6-naphthalate)

Christopher Carroll McDowell

A dissertation submitted to the Graduate Faculty of
North Carolina State University in partial fulfillment of
the requirements for the Degree of Doctor of Philosophy

DEPARTMENT OF CHEMICAL ENGINEERING

Raleigh

1998

APPROVED BY:

[illegible] C. M. Balik

Carol K. Hall Benny D. Freeman
Chair of Advisory Committee

Dedication

This dissertation is dedicated to the author's parents, Charles and Louise McDowell, and to the rest of his family and friends.

Biography

The author was born on February 19, 1970 in Radford, Virginia. Following secondary education in Henrico County, Virginia, he matriculated at Virginia Polytechnic Institute and State University. He graduated from Virginia Tech in 1992 cum laude with a Bachelor's of Science degree in Chemical Engineering. He entered North Carolina State University in the fall of 1992 to pursue his doctoral degree. His hobbies include playing guitar, trombone, basketball, and softball.

Acknowledgments

The author would like to thank his advisor, Dr. Benny Freeman, and committee members: Prof. Vivian Stannett, Prof. Harold Hopfenberg, Prof. Carol Hall, Prof. C. Maury Balik, and Prof. Dennis Maher for assistance during his time as a graduate student. Each one has been very willing to help when approached.

In addition he would like to thank several employees of the Hoechst Celanese Corporation for their support, interest, and assistance: Dr. Mike Jaffe, Dr. Gerry McNeely, Dr. Ishaq Haider, Dr. Randy Jester, Dr. Doug Roth, Dr. Larry Charboneau, Dr. Jim Schweitert, and Ms. Inessa Levin. The author would also like to thank his collaborators at the University of North Carolina - Chapel Hill: Theo Dingemanns, Dr. Klaus Semmler, and Dr. Ed Samulski. The positron annihilation lifetime spectroscopy experiments reported in this thesis were kindly performed by Anita Hill at CSIRO in Australia.

The author's professors at Virginia Tech, especially Dr. Bill Conger, Dr. Richey Davis, Dr. Peter Rony, and the late Dr. Gerhard Beyer, are thanked for their support during his time in Blacksburg.

Each and every labmate in the polymer research group is thanked for their support and patience: Dr. Nate Miranda, Dr. Vincent Shen, Dr. Atsushi Morisato, Dr. G.R. "Rusty" Cantrell, Dr. Steve Smith, Suresh Sunderajan, Michelle Arnold, Lora Toy, Sabrina Dixon, George Serad, Tim Merkel, and especially Dr. Anuraag Singh. Very special thanks are due to the undergraduate researchers that assisted the author: David Coker, Ranjit Mathur, Henry Hui, and Jason Partin.

Table of Contents

List of Tables

List of Figures

Chapter 1. Introduction

I. Overview

The focus of this experimental research program has been to determine the effect of systematic variation of chemical structure in the backbone of high barrier polyesters on small molecule sorption and transport properties in these polymers. These sorption and transport data are rationalized based on primary chemical structure, higher order molecular structure, and macromolecular chain dynamics. In the context of this dissertation, higher order molecular structure includes crystallinity and packing properties in the amorphous phase, including distribution of free volume between the equilibrium and non-equilibrium excess volume associated with the glassy state.

In this dissertation, the sorption and transport properties of an organic vapor, acetone, in a systematic series of random copolyesters based on poly(ethylene terephthalate) (PET) are reported. One of the principal systems considered was a series of random copolymers of PET and poly(ethylene 2,6-naphthalate) (PEN). PET is a commercial polymer used in barrier packaging for carbonated beverage products. PEN is a related polymer which has a more rigid molecular backbone and higher barrier properties than PET.

An organic marker penetrant, acetone, was used to probe solubility and diffusivity in the polyesters under study. An important consideration in barrier packaging for food products is the loss of organic flavor molecules, such as d-limonene in fruit juices, through sorption of the flavor molecules into package walls.[1] Flavor molecule carry-over is emerging as a concern with refillable plastic beverage bottles. In carry-over, flavor molecules sorbed into package walls from an initially-packaged product desorb after refill to influence the taste of the product in the refilled package. To understand the sorption of flavor molecules into barrier packaging materials, organic penetrants are used as model flavor molecules.[2]

This dissertation is organized in the following manner. The first chapter provides a short overview of the research, presents a synopsis of the relevant fundamentals from literature, and presents a short section outlining the kinetic gravimetric sorption technique, the primary experimental method used in this research program. The second chapter describes the automation of a spring balance system used for kinetic gravimetric sorption experiments. The third chapter presents and discusses results from a study of acetone sorption and diffusion in PET. The fourth chapter describes results from a systematic study of sorption and diffusion of acetone in PET/PEN random copolymers. Chapter 4 also presents and discusses characterization of these copolymers by differential scanning calorimetry [DSC], wide-angle X-ray diffraction [WAXD], infrared [IR] spectroscopy, and positron annihilation lifetime spectroscopy [PALS]. The fifth chapter presents equilibrium acetone sorption and kinetics of acetone sorption in random copolymers of PET/PEN from interval sorption experiments. The sixth chapter presents acetone sorption, differential scanning calorimetry, wide angle X-ray diffraction, and infrared spectroscopy results for copolymers of PET with low (≤10 weight percent) concentrations of polyester comonomers. The seventh chapter summarizes conclusions from the dissertation research and provides suggestions for future work in this research area. Appendix A presents results from additional sorption experiments on high barrier polyesters which are outside the scope of this dissertation. Appendix A also presents results from experiments that are considered supplementary to the dissertation. Appendix B provides a tabulation of data for the figures in the body of the dissertation.

II. Fundamentals of Sorption and Transport of Small Molecules in Polymers

Permeability

In a dense polymer film, the permeability, P, is defined as the molar flux of penetrant through the polymer relative to a fixed coordinate system, N_A, normalized by the film thickness, ℓ, and the difference between upstream (p_2) and downstream (p_1) partial pressure.[3]

$$P = \frac{N_A \ell}{p_2 - p_1} \tag{1.1}$$

According to the solution-diffusion model, permeation of a penetrant through a film occurs in three steps: the penetrant dissolves into the upstream face of the polymer film, diffuses through the material, and desorbs from the downstream face of the film. When upstream pressure and dissolved penetrant concentration are much greater than the downstream dissolved penetrant pressure and concentration, Equation 1.1 can be rewritten as:

$$P = \overline{D} x S \tag{1.2}$$

where $\overline{D}$ is the concentration average diffusion coefficient, a measure of penetrant mobility in the polymer matrix, and S is the solubility, a measure of the partitioning coefficient of the penetrant between the polymer and contiguous penetrant phases. Penetrant permeability, therefore, depends on a combination of a kinetic parameter, $\overline{D}$, and a thermodynamic parameter, S.[4]

Diffusivity

One-dimensional diffusion in an isotropic medium was described by Fick in 1855 through an analogy of Fourier's equations for conductive heat transfer:

$$J_A = -D\frac{\partial C}{\partial x} \tag{1.3}$$

where D is the effective diffusion coefficient, $\partial C/\partial x$ is concentration gradient and J_A is the diffusion flux of A.[5]

In a plane sheet whose thickness is much less than its length or width, conservation of mass, Equation 1.3, and an assumption of constant diffusion coefficient may be combined to yield Fick's second law:[6]

$$\frac{\partial C}{\partial t} = D\frac{\partial^2 C}{\partial x^2} \tag{1.4}$$

In integral gravimetric sorption experiments, the penetrant concentration is zero at all values of x for times less than zero, and the surface concentration of penetrant in the polymer is constant for times greater than zero. From these experimental conditions, appropriate boundary conditions can be formulated, and Equation 1.4 can be solved to provide two equivalent solutions:[5]

$$\frac{M_t}{M_\infty} = \left[4\left(\frac{Dt}{\ell^2}\right)^{1/2}\left(\pi^{1/2} + 2\sum_{n=1}^{\infty}(-1)^n \operatorname{ierfc}\left(\frac{n\ell}{\sqrt{4Dt}}\right)\right)\right] \tag{1.5}$$

$$\frac{M_t}{M_\infty} = \left[1 - \sum_{n=1}^{\infty} \left(\frac{8}{(2n+1)^2\pi^2} \exp\frac{-D(2n+1)^2\pi^2 t}{\ell^2}\right)\right] \qquad (1.6).$$

where M_t and M_∞ are the penetrant mass uptake (normalized by the initial penetrant-free polymer sample weight) at time t and at equilibrium, respectively, D is the diffusion coefficient, and ℓ is the sheet thickness.[5] From these solutions, diffusivities can be estimated using the experimental fractional mass uptake (*i.e.* M_t / M_∞) from sorption data. A Pascal program employing a least-squares, non-linear regression is available to calculate a diffusivity from the best fit of the experimental data to Equation 1.6.

In practical systems, D is a function of penetrant concentration, however Equations 1.5 and 1.6 are still valid provided that D is replaced by $\bar{D}$, which is defined as:[5]

$$\bar{D} = \frac{1}{C_f - C_i} \int_{C_i}^{C_f} D dC \qquad (1.7)$$

where C_i and C_f are the penetrant concentrations at the beginning and end of the experiment, respectively.

Solubility

The solubility of small molecules in polymers is the equilibrium concentration, C, of the penetrant dissolved in the polymer matrix divided by the pressure, p, of the penetrant in the gas phase:[7]

$$S = \frac{C}{p}. \qquad (1.8)$$

The equilibrium concentration of penetrant can be calculated from M_∞ using the following expression:

$$C = M_{\infty} \frac{\rho_{polymer}}{MW_{penetrant}} 22{,}414 \tag{1.9}$$

where C has units of $cm^3(STP)/cm^3$ polymer. The polymer density is given in g/cm^3 and 22,414 is the conversion factor from moles to cm^3 at standard conditions.

The dependence of penetrant concentration on the penetrant pressure contiguous to the polymer is described by a sorption isotherm. There are four general isotherms that describe sorption of small molecules in a polymer matrix, as shown in Figure 1.1. These isotherms are known as the (a) Henry's Law, (b) Dual Mode, (c) Flory-Huggins, and (d) Generalized isotherms.

Henry's Law Isotherm:

Figure 1.1a shows a Henry's Law sorption isotherm, where k_D is the solubility coefficient.

$$C = k_D p \tag{1.10}$$

This behavior is typical of permanent gas sorption in a rubbery polymer. [8]

Dual-Mode Sorption Isotherm:

Sorption of gases and low activity vapors into polymers below their glass transition temperature [T_g] follows an isotherm described by the dual mode model (Figure 1.1b)

$$C = C_D + C_H = k_D p + \frac{C'_H bp}{1 + bp} \tag{1.11}$$

where C_H' is the Langmuir capacity constant and b is the Langmuir affinity constant related to polymer-penetrant interactions. The model is based on the notion that penetrant sorption occurs in two modes: a Henry's law mode in the dense, equilibrium packed polymer matrix (C_D), and a Langmuir-type mode in so-called "microvoids" (C_H) associated with the non-equilibrium excess volume present in the glassy state.[7]

Figure 1.2 presents a cartoon describing the basis for this model. The polymer specific volume, V, as a function of temperature, T, has a discontinuity in the slope at the T_g. The glass transition temperature is the temperature above which the polymer behaves as a low modulus, rubbery material. Below the glass transition temperature, the material behaves as a glass, where long relaxation times for molecular motion prevent the polymer from relaxing into a fully densified equilibrium state. The theoretical line for the hypothetical equilibrium specific volume below T_g is given by the dashed line in Figure 1.2. A portion of the actual specific volume exists as non-equilibrium excess volume. This excess volume is the difference between the actual glassy specific volume, V_g, and the theoretical liquidous specific volume, V_l.

According to the dual mode theory, sorption follows Henry's law in the equilibrium, densified regions of the polymer. The non-equilibrium excess volume associated with the glassy state, V_g-V_l, of the polymer exists as molecular scale holes or microvoids. The long relaxation times for molecular motion in glassy materials allow these microvoids to be trapped over experimentally accessible time scales in the polymer matrix. Sorption occurs in these microvoids following a Langmuir-type isotherm. The Langmuir capacity constant can be estimated using the following expression:[9]

$$C'_H = \left[\frac{V_g - V_l}{V_g}\right]\rho^* \tag{1.12}$$

where V_g is the actual glassy specific volume, V_l is the equilibrium volume of the densified glass, and ρ^* is the condensed density of the penetrant.

Flory-Huggins Sorption Isotherm:

Organic vapors and highly sorbing gases at high pressure in rubbery polymers often follow a Flory-Huggins isotherm (Figure 1.1c):[4]

$$\ln(a) = \ln\varphi + (1-\varphi) + \chi(1-\varphi)^2 \tag{1.13}$$

where a is the penetrant activity, which, for an ideal gas, is the partial pressure, p , divided by the penetrant vapor pressure, p_o. φ is the volume fraction of penetrant in the polymer matrix. χ is the Flory interaction parameter and is related to energetic and entropic interactions between the specific polymer and penetrant.[4]

Generalized Sorption Isotherm:

The generalized isotherm, shown in Figure 1.1d, is a combination of the Langmuir and Flory-Huggins isotherms.[10] This isotherm can be used to describe the sorption of condensable vapors in glassy polymers. The isotherm is concave relative to the pressure axis at low pressures. This curvature is associated with sorption into non-equilibrium excess free volume of the polymer matrix. At higher penetrant pressures, the sorption curve is convex upward relative to the pressure axis due to swelling of the polymer matrix. As the penetrant dissolves into the polymer matrix, the polymer is plasticized and swells, creating additional free volume for penetrant uptake.

III. Factors Influencing the Sorption and Transport of Small Molecules in Polymers

Free Volume

The dependence of penetrant transport properties on chain packing in polymers is often described in terms of correlations involving the fractional free volume of polymers.[11] Fractional free volume (FFV) is the fraction of polymer that is not occupied by polymer molecules and can be estimated using the expression:[4]

$$FFV = \frac{V - V_o}{V} \tag{1.14}$$

where V is the polymer specific molar volume and V_o is an estimation of the volume occupied by polymer chains. V_o is estimated using the equation $V_o=1.3V_w$, where V_w is the van der Waals volume estimated using the group contribution method suggested by Bondi.[12] FFV has been related to diffusion coefficients through the Doolittle equation:[4]

$$D = A\exp\left(\frac{-B}{FFV}\right) \tag{1.15}$$

where B and A are empirical constants. Figure 1.3 presents an example of a series of polymers which follow this relationship. In this figure, carbon dioxide and methane diffusivity in tetramethylhexaflouro bisphenol A polycarbonate (TMHFPC), poly(phenylene oxide) (PPO), tetramethyl bisphenol A polysulfone (TMPSF), bisphenol A polycarbonate (PC), and bisphenol A polysulfone (PSF) are presented as a function of FFV.[4]

Figure 1.4 presents the dependence of carbon dioxide and methane solubility on fractional free volume in the same polymer series shown in

Figure 1.3. While penetrant solubility is also a function of free volume, the dependence of solubility on free volume is usually weaker than the dependence of diffusivity on free volume.[4] Therefore, penetrant permeability often follows a similar dependence on free volume as penetrant diffusivity, as illustrated in Figure 1.5.[13]

Crystallinity

Crystallinity influences both solubility and diffusion coefficients [14] and is an important factor to consider since many polyesters are semicrystalline. In most polymer systems, crystalline regions preclude penetrant sorption, thereby hindering diffusion.[15-20]

Michaels and Barker used the following model to describe the effect of crystallinity on penetrant diffusion coefficients:

$$D = \frac{D_a}{\tau\beta} \tag{1.16}$$

where D_a is the diffusivity of wholly amorphous polymer, τ is a geometric impedance factor, and β is a chain immobilization factor.[16] In this model, a penetrant can only diffuse through amorphous material. Therefore, the crystallites create a tortuous pathway for the penetrant by acting as impermeable barriers to diffusion. This effect is taken into account by the factor τ, which is the ratio of the distance traveled by a penetrant molecule in crossing a sample to the sample thickness. Crystallites may also restrict chain mobility in the amorphous phase by acting as virtual crosslinks and reducing the volume that can be used for the penetrant to make a diffusional jump.[17] This effect is accounted for by the chain immobilization factor, β. β is equal to one in glassy polymers and is greater than one in rubbery polymers.[16,19]

A two-phase model (Equation 1.17) is typically used to describe the sorption of penetrants in semicrystalline polymers:

$$S = S_a \Phi_a \tag{1.17}$$

where S_a is the solubility of penetrant in the amorphous phase and Φ_a is the amorphous volume fraction of the polymer.[14] This model was introduced by Myers, *et al.*,[15] and later tested by Michaels[18] with gases in rubbery polyethylene; some of these data are presented in Figure 1.6. The solubility data extrapolate to zero at zero percent amorphous phase, suggesting that the crystalline regions do not allow penetrant sorption.[18] Polymer chains in crystallites usually pack very efficiently in a rigid three-dimensional lattice. For example, the amorphous density of polyethylene is 0.855 g/cm^3 and the density of crystalline polyethylene is 1.002 g/cm^3,[21] leading to calculated fractional free volumes of 0.188 for amorphous and 0.048 for crystalline polyethylene. The reduction in free volume accompanying crystallization is apparently sufficient to preclude penetrant sorption. For the penetrant to dissolve into the crystal, it would need to disrupt (*i.e.* melt) the crystallites and there is not usually enough energy available from sorption to accommodate this process.

The CO_2 sorption isotherms for amorphous and semicrystalline PET were both well-described by the dual-mode sorption isotherm. Michaels, however, observed a decrease in CO_2 solubility in poly(ethylene terephthalate) less than that predicted by Equation 1.17.[20] Michaels hypothesized that crystallization would occur preferentially in the dense regions of the polymer leaving sorption in the microvoids associated with the non-equilibrium excess volume less affected by crystallization than sorption in the densified polymer matrix.[20]

Puleo and Paul describe a polymer that is the only reported exception to Equation 1.17. When carbon dioxide and methane are sorbed into poly (4-methyl-1-pentene) (PMP) of varying degrees of crystallinity, the data do not predict zero solubility at 0% amorphous material (Figure 1.7).[22] These data suggest that gases dissolve into the crystals of PMP. X-ray diffraction and density data show a very open structure for PMP crystals which presumably permits limited penetrant sorption.[22] The density of crystalline PMP, 0.828 g/cm^3, is lower than the density of amorphous PMP, 0.838 g/cm^3. This trend is exactly opposite of most polymers, where the crystalline density is substantially higher than the amorphous density.

IV. Models for Sorption and Transport in Copolymers

This research program focuses on the sorption and transport properties of polyesters, and many of the systems under study are copolymers. There are several models to describe sorption and transport in phase separated and homogeneous copolymers and blends. The copolymers in this study are believed to be random and homogeneous (due to a single glass transition temperature). However, blends of these polymers or block copolymers could exhibit phase segregation. Therefore models for both phase separated and homogeneous copolymers are presented.

Homogeneous Systems:

Based on results from activated state theory, the effect of polymer composition on the diffusion coefficient of small molecules in amorphous random copolymers is given by the relationship:[23]

$$\ln D = \Phi_1 \ln D_1 + \Phi_2 \ln D_2 + (aRT - 1)\frac{\Delta E_{12}}{RT} \tag{1.18}$$

where D_1 and D_2 are penetrant diffusivities in the homopolymers, Φ_1 and Φ_2 are volume fractions of the homopolymers, a is a constant, and ΔE_{12} is a term that corrects for deviations from additive activation energies of diffusion. The constant a, the linear free energy coefficient, has been reported to be 0.001/R for glassy polymers.[8] Ternary thermodynamic polymer solution theory may be used to derive the following relationship for penetrant solubility in an amorphous random copolymer or compatible blend,[23]

$$\ln S = \Phi_1 \ln S_1 + \Phi_2 \ln S_2 + \frac{\gamma \tilde{V}_3}{RT}\Phi_1 \Phi_2 \tag{1.19}$$

where S_1 and S_2 are the penetrant solubilities of the homopolymers, γ is the binary interaction parameter for mixing of the homopolymers, and $\tilde{V}_3$ is the molar volume of the penetrant. Combining Equations 1.18 and 1.19 yields the following equation for permeability.[23]

$$\ln P = \Phi_1 \ln P_1 + \Phi_2 \ln P_2 + (aRT - 1)\frac{\Delta E_{12}}{RT} + \frac{\gamma \tilde{V}_3}{RT}\Phi_1 \Phi_2 \tag{1.20}$$

These equations have been tested for several amorphous polymer systems.[23]

The following empirical mixing rule for gas permeability coefficients of blends and copolymers, similar in form to Equation 1.20 but neglecting the last two terms, has often been used to describe gas permeation in homogeneous copolymers and blends.[24]

$$\ln P = \Phi_1 \ln P_1 + \Phi_2 \ln P_2 \tag{1.21}$$

This model describes experimental data when the energetic terms are both zero,[23] or, since both ΔE_{12} and β can be either positive or negative,[23] when these terms cancel each other. For data that follow this model, the logarithm of permeability is a linear function of the volume fraction of one component. As a result, this model is referred to as the log linear model.

Another model assuming additive free volume has been used to characterize random copolymers and homogeneous blends.[23] Following the equation of Lee,[13] the following model has been suggested:[23]

$$\ln(P/A) = \left[\frac{\Phi_1}{\ln(P_1/A)} + \frac{\Phi_2}{\ln(P_2/A)}\right]^{-1} \tag{1.22}$$

where A is a constant associated with the particular penetrant.[13] The constant A comes from correlations of free volume with permeability. This model has the benefit of requiring none of the energetic parameters used in Equation 1.21. The constant A is tabulated for many penetrants.[13]

These gas transport models (Equations 1.18-1.22) have been used to describe glassy polymer systems such as polycarbonate / polyester blends and polystyrene / poly(methacrylonitrile) copolymers[23] and rubbery systems such as low-density polyethylene / high-density polyethylene blends.[24] The models do not take into account the effects of crystallinity on the solubility, diffusivity, and permeability coefficients. The models may be extended to semicrystalline systems if the solubility, diffusivity, and permeability coefficients are corrected for the effect of crystallinity.

Heterogeneous Systems:

Transport in phase separated systems (both copolymer and blends) depends both on the permeabilities of the component polymers and the morphology of the system.[25] Many models have been suggested to describe the permeation properties of such systems. The Maxwell model for permeability in composite structures provides an example of this class of models. The permeability of the blend or copolymer is given by the following equation:[25]

$$\frac{P}{P_1} = 1 + \frac{(1+G)\Phi_2}{\frac{(R+G)}{(R-1)} - \Phi_2} \tag{1.23}$$

where P is the observed permeability, P_1 is the permeability of the continuous phase, Φ_2 is the volume fraction of the dispersed phase, R is the ratio of permeabilities of phase 1 to phase 2 (P_1/P_2), and G is a geometric factor determined by the morphology of the non-homogeneous material. G can range from zero to infinity depending on the shape of the structures formed by the dispersed phase and their orientation relative to flow. G is zero if the dispersed phase forms platelets parallel to the direction of penetrant transport; G is infinity for flat platelets of the dispersed phase aligned perpendicular to penetrant transport.

V. Experimental

Kinetic Gravimetric Sorption

In gravimetric sorption, a polymer film is exposed to vapor at a constant pressure, and the weight increase of the film is measured as a function of time. Two different experimental devices are available for this purpose: a McBain type quartz spring system and a Cahn RG electronic microbalance. Schematics of these instruments are presented in Figure 1.8.

The spring system consists of a water-jacketed glass chamber serviced by a vacuum pump for penetrant removal and degassing. Pressure inside the system is monitored with a MKS Baratron pressure transducer. The cap of the glass chamber is sealed with an O-ring; a quartz spring similar to that described by McBain is suspended from the cap.[26] The springs are manufactured by Ruska, Incorporated. The sensitivity of these Hookean springs is typically 5 mm of extension per mg of load(Ruska model no. 4501.3, non-rotating, with reference pointer). The polymer film is suspended from this quartz spring. A wire reference rod hangs from the cap of the chamber. The weight of the polymer is monitored with a cathetometer by recording the position of a reference pointer on the spring relative to the tip of the reference rod. These position readings are used to determine changes in sample weight with time.

The Cahn balance system consists of a glass chamber connected to a pump and penetrant source. The entire system is encased in a heated wooden cabinet for temperature control. The polymer film hangs from the left side of the electrobalance; the right side of the balance is the reference side and is weighted with ballast. The electrobalance produces a voltage signal which is fed to a chart recorder. The McBain spring system and Cahn electrobalance system are used interchangeably.[27]

A typical polymer film, 5 microns thick and 6 square inches in area, is degassed for at least 24 hours to remove any dissolved gasses. The sample is then exposed to a controlled pressure of penetrant, and the film weight is recorded as a function of time. Once the system reaches equilibrium (*i.e.* no further uptake for ~10 hours), the system is exposed to vacuum to desorb the penetrant. From the data collected during the experiment, diffusivity and solubility can be calculated independently; permeability can be estimated from these two parameters.[6]

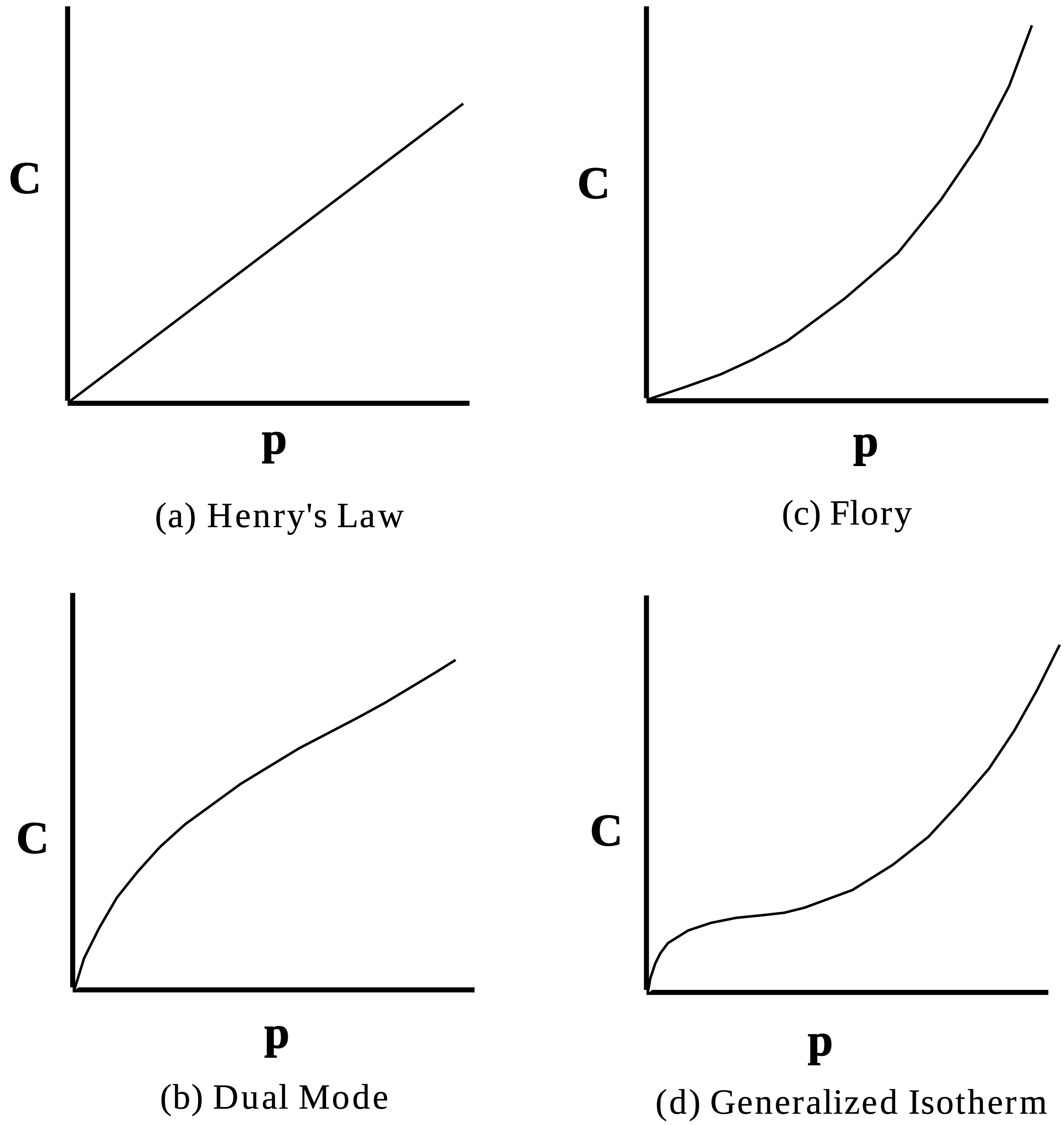

Figure 1.1. Sorption Isotherms for Gases and Vapors in Polymers

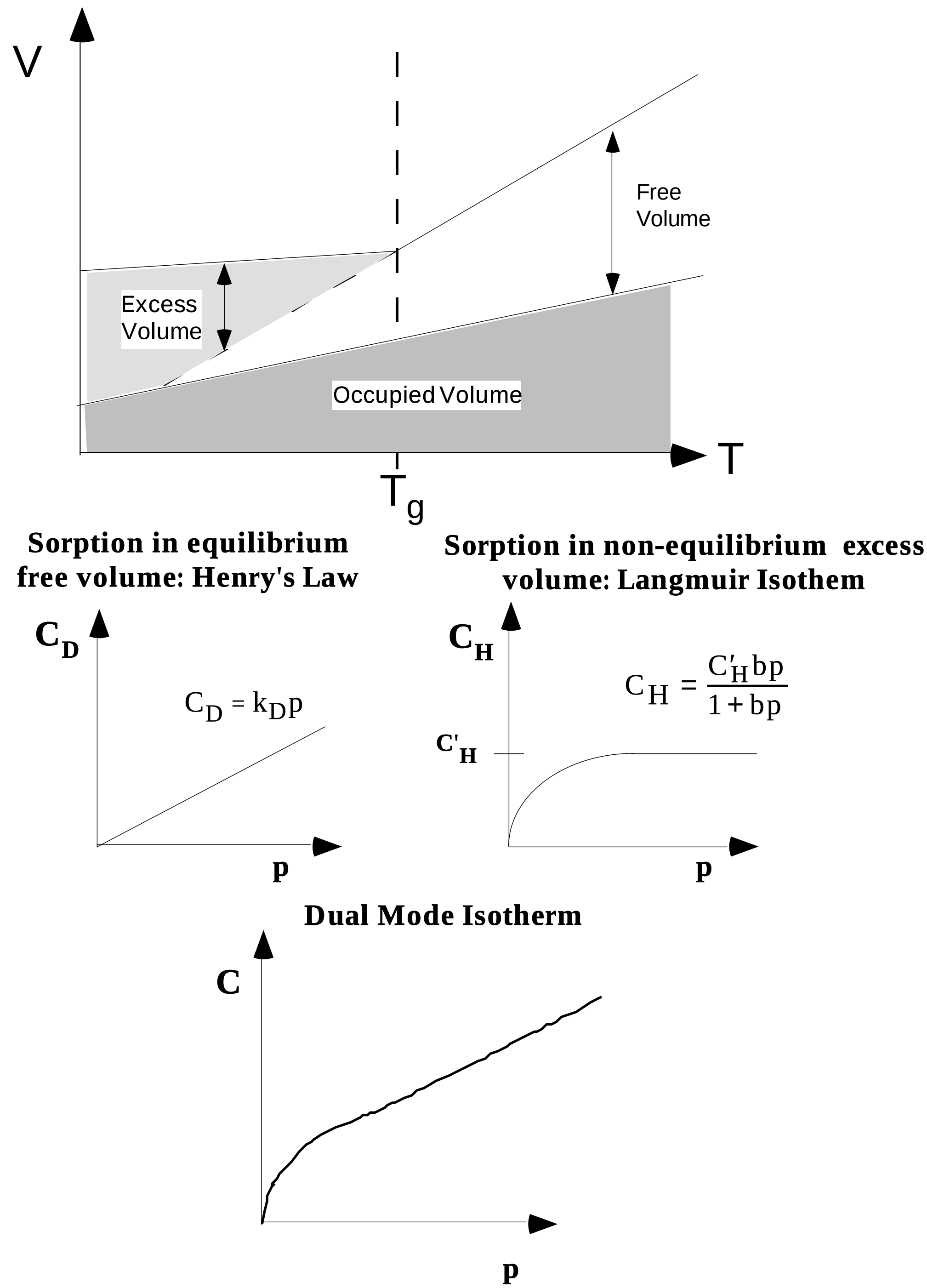

$$C = C_D + C_H = k_D p + \frac{C'_H bp}{1+bp}$$

Figure 1.2. Physical Basis for the Dual-Mode Isotherm

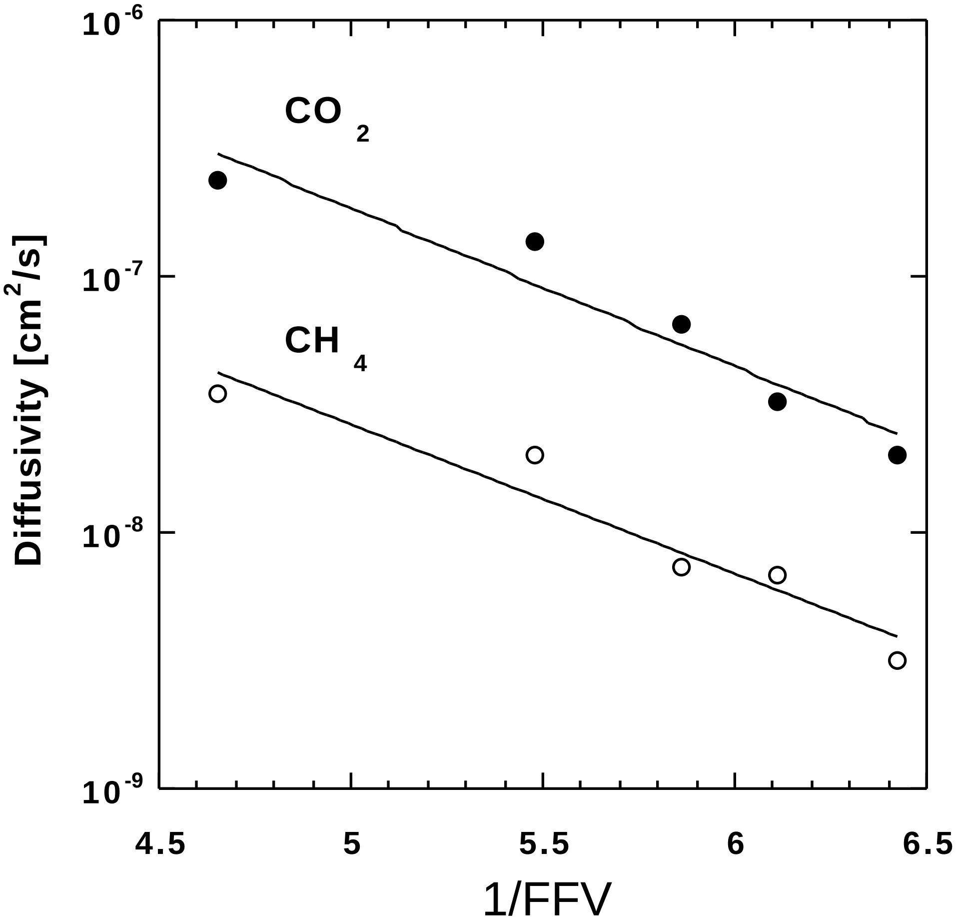

Figure 1.3. The Relationship Between Polymer Fractional Free Volume and Penetrant Diffusivity[4]

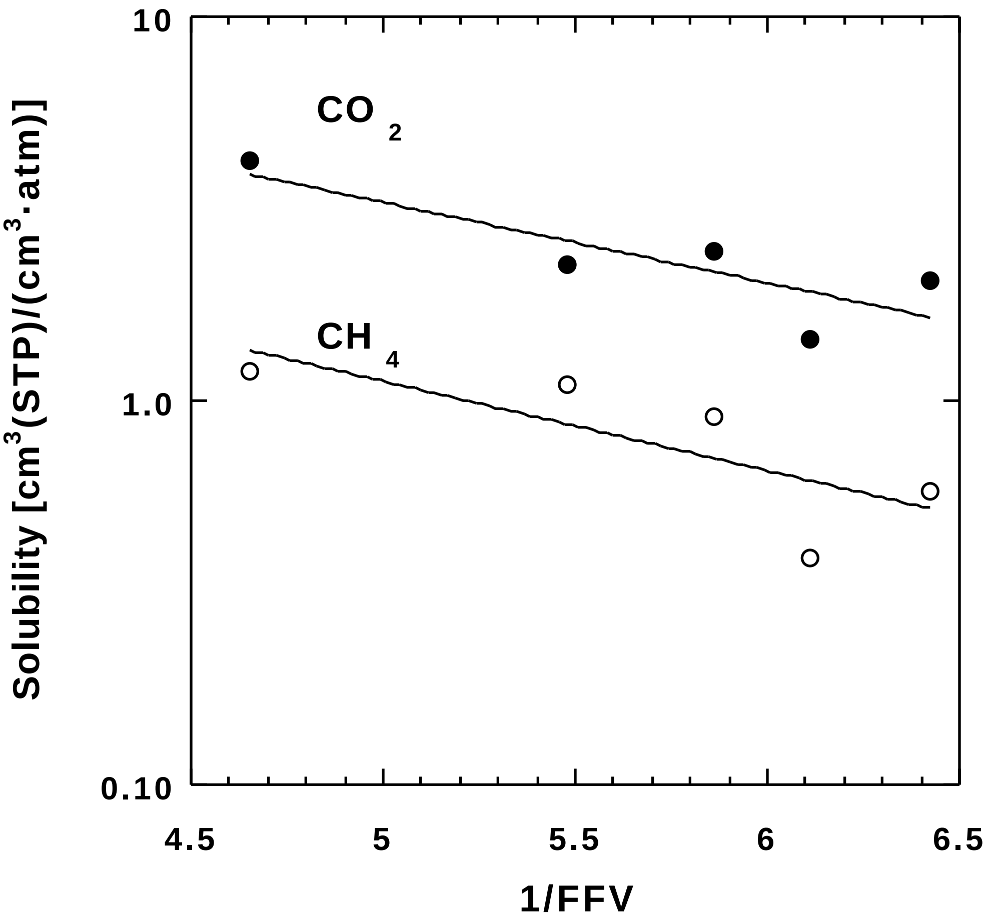

Figure 1.4. The Relationship Between Polymer Fractional Free Volume and Penetrant Solubility[4]

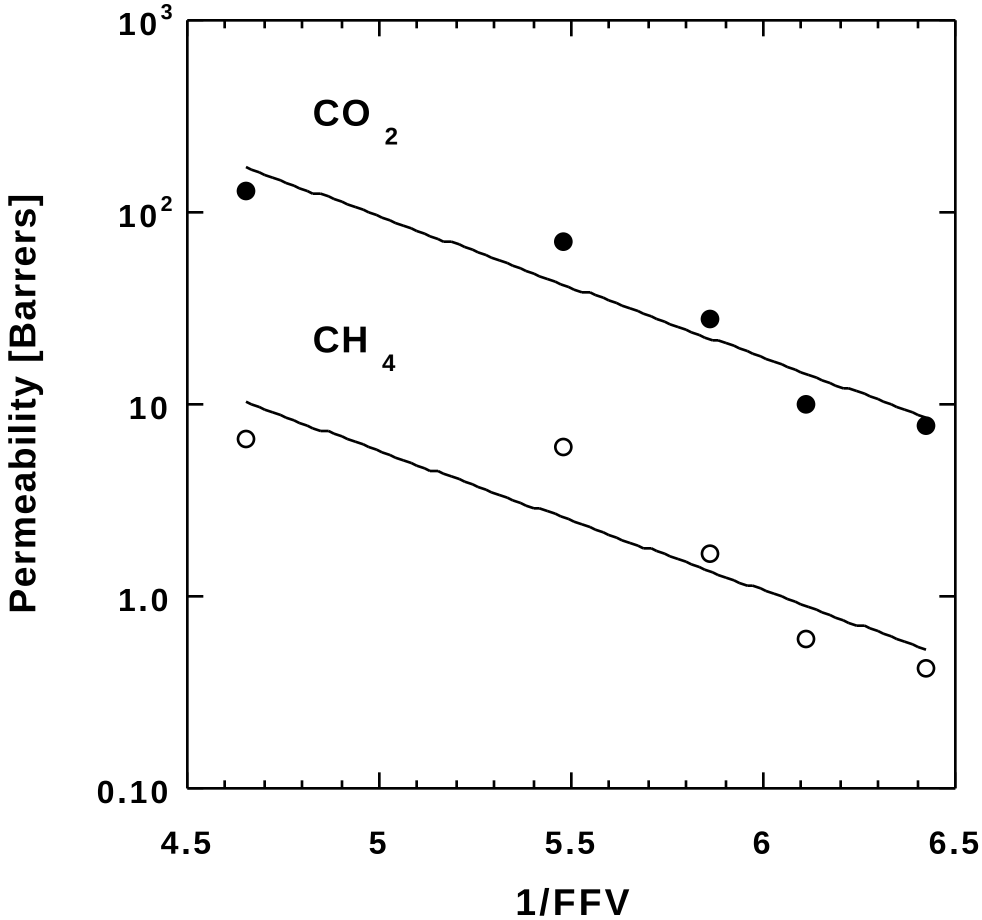

Figure 1.5. The Dependence of Penetrant Permeability on Polymer Fractional Free Volume[4]

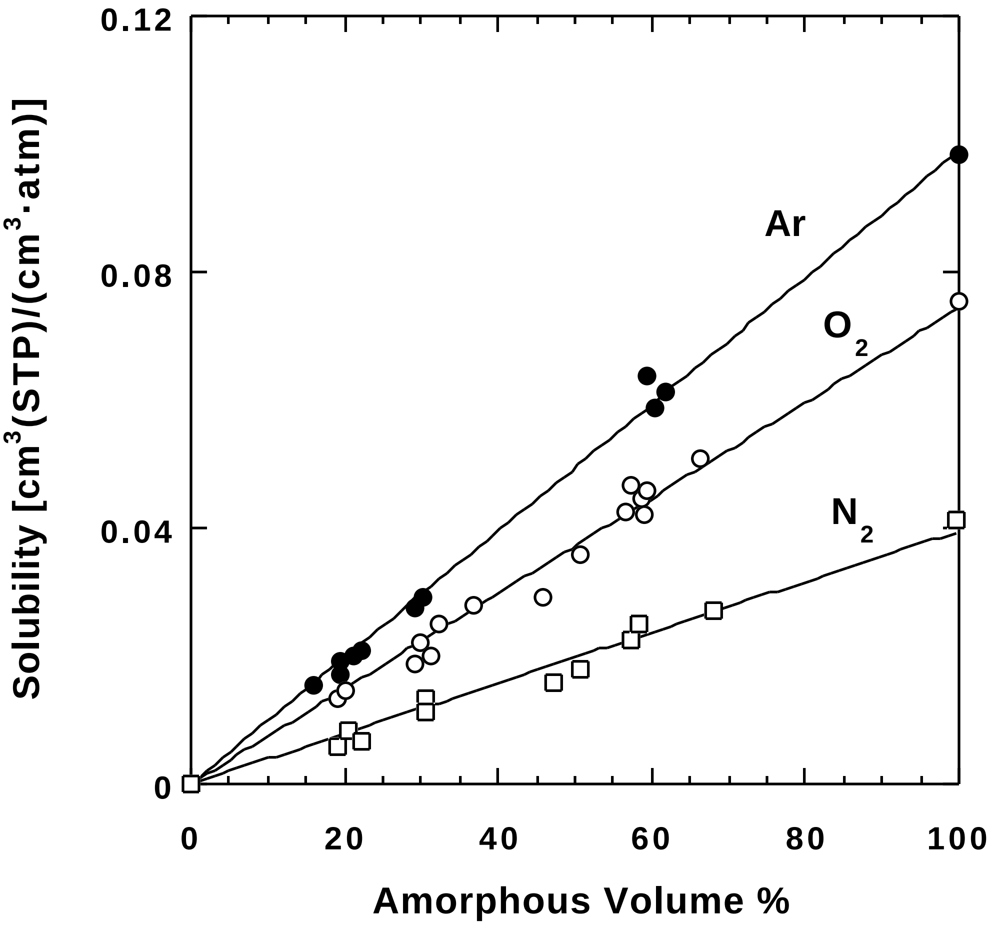

Figure 1.6. Solubility of Various Gases in Polyethylene as a Function of Amorphous Volume Fraction[18]

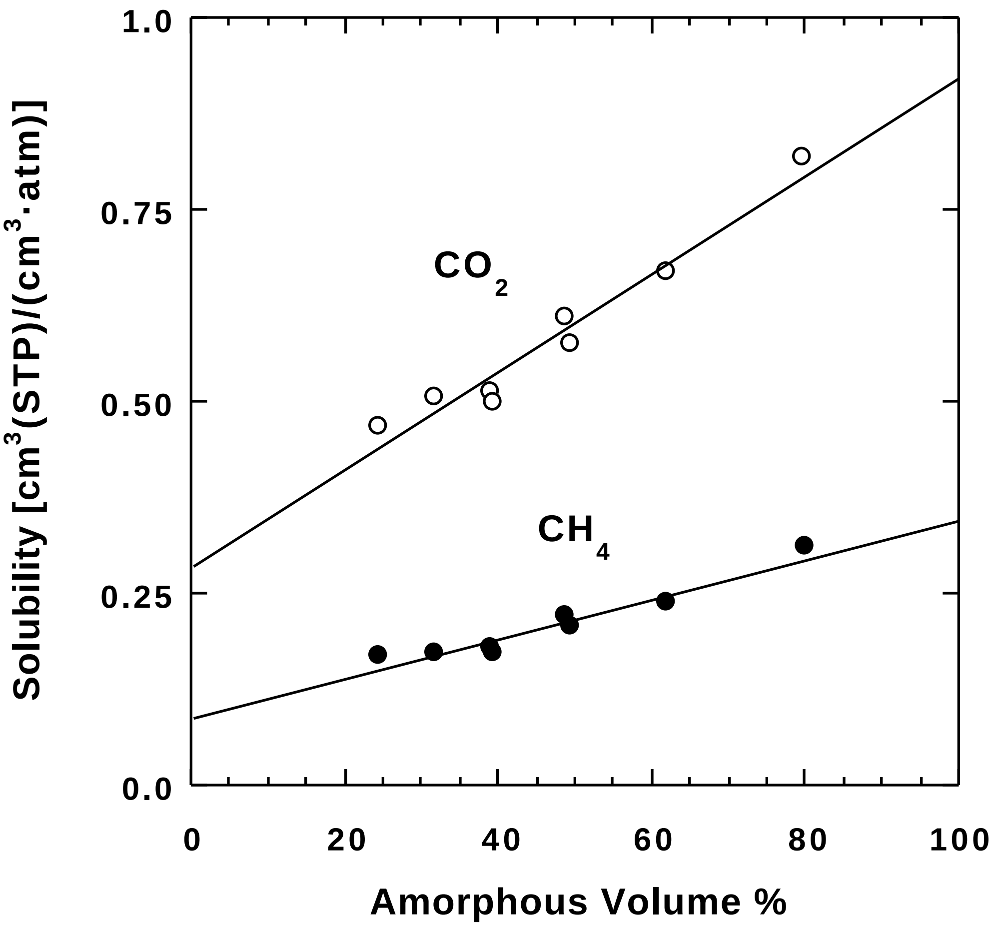

Figure 1.7. Solubility of Gases in Poly(4-methyl-1-pentene) as a Function of Amorphous Volume Fraction[22]

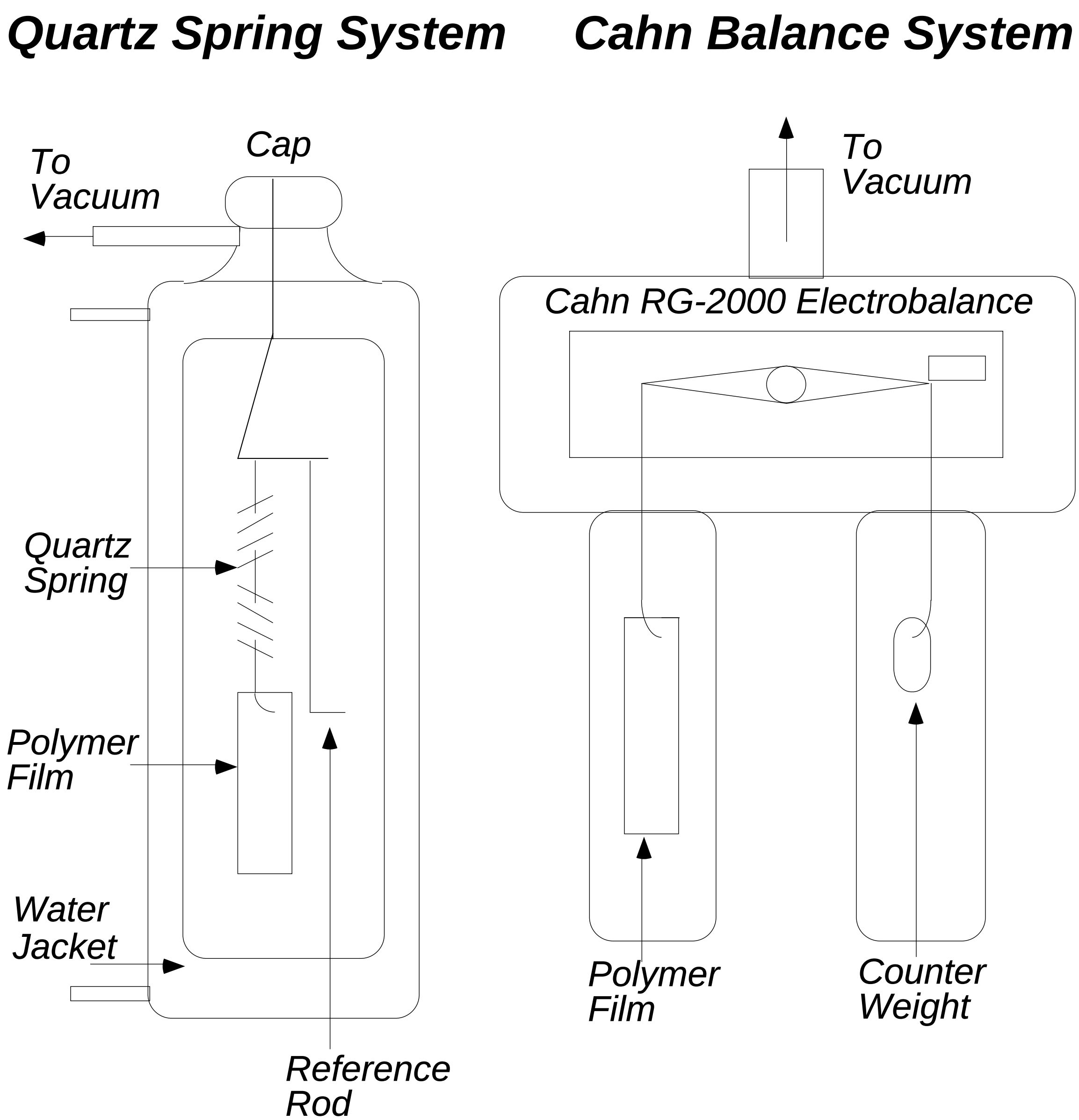

Figure 1.8. Schematic of Gravimetric Sorption Instruments

Chapter 2. An Automated Spring Balance for Kinetic Gravimetric Sorption of Gases and Vapors in Polymers

I. Introduction

The sorption and transport of small penetrant molecules in polymeric materials is important in applications such as food packaging and membrane-based separations.[4] A common experiment used to explore sorption and transport properties of materials is the kinetic gravimetric sorption of penetrant by a thin sheet of polymer.[6] This method provides an independent determination of penetrant solubility and diffusivity in a single experiment. A widely used device for gravimetric sorption is the McBain spring balance.[26] A thin, uniform polymer film is placed on the end of a calibrated spring and contacted with penetrant at fixed pressure. As penetrant sorbs into the polymer matrix, the load on the spring increases, and the spring extends. The time dependent mass uptake of penetrant by the polymer is measured by recording the spring extension. Typically, such measurements are made using a manual cathetometer to observe the position of the spring relative to a reference rod of fixed length.

For many studies of high barrier packaging polymers, diffusion coefficients can be quite low ($<10^{-12}$ cm^2/s).[27] Even using thin polymer samples (*ca.* 5µm), experiment duration can be on the order of many hours to several days, and as a result, automation of data collection is desirable.

This paper describes the automation of a McBain spring system using a CCD camera, a personal computer equipped with a frame-grabber card, and the public domain NIH Image program (developed at the U.S. National Institutes of Health and available at http://rsb.info.nih.gov/nih-image/). This approach for automating engineering experiments has previously been used to investigate flow instabilities in polymeric fluids.[28] In addition, digital imaging has also been used to monitor sub-micron motions in a torsion balance.[29]

II. Principle of Operation

Figure 2.1 presents a schematic of the sorption system. A glass bulb (12 liters), A, is part of a glass manifold used as a penetrant vapor reservoir. Liquid penetrant is stored in a glass ampule, B, before being vaporized into the glass manifold. Alternately, gaseous penetrant can be introduced into the system by connecting a gas cylinder to the manifold in place of the ampule. A ventilation valve, C, is used to expose the system to air at ambient conditions. The system is connected, via valve D, to a vacuum pump used for sample degassing and system evacuation. The water-jacketed vessel, E, provides temperature control for the sample environment. The glass manifold is wrapped with heating tape, which is connected to variable autotransformers for temperature control. Alternatively, the system can be placed in a temperature-controlled box. A sensitive quartz spring, F, and reference rod, G, are suspended from the cap of the vessel, H, which is sealed to the main vessel with an O-ring seal, I, and a metal clamp. The spring is a model 4501.3 spring from Ruska Instruments (Houston, TX). The spring is non-rotating and has a reference pointer. The reference rod is fabricated from metal wire and is adjusted so that the tip of the reference rod is in the same plane as the reference pointer on the spring to permit both the spring and reference rod to be in focus during the experiment. The polymer sample is hung directly on a hook at the end of the spring or placed in a quartz pan (also available from Ruska) at position J.

The camera, K, is a COHU (San Diego, CA) model 4915-2000 CCD camera. It is outfitted with a C-mount adapter to accommodate photographic camera lenses. A Nikor M 55 mm macro lens was used along with a Nikon PK-3 extender for additional magnification. The camera interfaces with a Power MacIntosh 7600/132 personal computer through a Scion (Frederick, MD) LG-3 Frame grabber card. The cathetometer, L, previously used for tracking the spring displacement, is used to calibrate distance measurements by the camera. A lamp is placed behind the jacketed vessel opposite the camera, and a translucent sheet of plastic is placed between the vessel and the lamp to provide diffuse back lighting for maximum image contrast.

An Image macro is used to automate data collection for the experiment (See Table 2.1 for the Macro). Since penetrant uptake proceeds linearly with the square root of time for Fickian diffusion in a plane sheet,[6] the macro instructs the Scion LG-3 card to capture a frame from the camera at equal intervals in $t^{1/2}$. The macro prompts the user for two inputs: 'Number of Frames,' which corresponds to the number of data points to be collected during the experiment, and 'Delay Factor,' which sets the time between successive data point collection events. The delay factor is defined as follows:

$$\text{Delay Factor} = \text{Interval}^2 * 60 \tag{2.1}$$

where Interval is the spacing, in square root minutes, between two data points. For example, to obtain a data point each 0.5 $min^{1/2}$, the Delay Factor is 15.

Figure 2.2 presents a typical image captured by the frame grabber card using NIH Image version 1.59. Upon launching Image, this picture is obtained by using the 'Start Capturing' command in the 'Special' menu on the toolbar or by using the keystroke z-G. The reference pointer on the spring and the reference rod are shown in this figure.

To calibrate the distance measurement scale in Image, the distance between the reference rod and the reference pointer is measured in millimeters using the cathetometer and in pixels using Image. The 'Set Scale' function under the 'Analyze' menu in Image is used to define the number of pixels per millimeter, thereby calibrating the distance measurement in Image. The camera (which has a resolution of 640 by 480 pixels) is positioned so that the maximum number of pixels (640) is used to monitor spring displacement.

Before running the macro to begin data collection, a region of interest (ROI) is defined within Image. The specification of a ROI is illustrated in Figure 2.2 as the box with a dashed border. The ROI should be as thin as possible in the direction perpendicular to the direction of spring displacement to minimize the possibility of extraneous objects appearing in the ROI. Additionally, it should be as long as the Image window in the direction of spring displacement to maximize the range of spring displacement that can be monitored. Finally, the ROI must include portions of both the spring reference pointer and the reference rod because they are the two objects whose locations are needed to monitor spring displacement. Care must be taken when preparing the length and shape of the reference rod to meet this last requirement.

After beginning the experiment by introducing penetrant into the sample chamber and starting the macro, each captured image is analyzed in real time using the one-dimensional array 'PlotProfile' in Image. After each frame is captured, 'PlotProfile' contains the average pixel number versus horizontal pixel location. Pixel number is a measure of light intensity, 0 being brightest and 255 being darkest. Sample results from the 'PlotProfile' function are presented in Figure 2.3. The location of the spring reference pointer and the reference rod are indicated in the figure. The macro searches each array for the pointer and reference rod using the following algorithm: 1) search from low to high horizontal pixel location, which corresponds to left to right in Figure 2.2 and 2.3, to find the first occurrence of a pixel number greater than 140 (which signals the location of the leading edge of the spring reference pointer. marked "1" in Figure 2.3), 2) search for the next location with a pixel number less than 140 and at least 10 pixels away from the location identified in step 1 (which corresponds to the bright region in the center of the transparent quartz reference pointer, marked "2" in Figure 2.3), 3) search for the next location with a pixel number greater than 200 (which is the location of the leading edge of the opaque reference rod, marked "3" in Figure 2.3), and 4) search for the next point with a pixel number less than 200 and at least 10 pixels away from the location identified in step 3 (which is the trailing edge of the reference rod, marked "4" in Figure 2.3). The values of pixel number (140 and 200) and pixel dimension (10) are selected empirically so that smaller objects (*i.e.* dust or other extraneous material on the water jacket or in the water in the water jacket) are not recorded by the macro. These parameters can be tuned for experiments with varying backlighting conditions, size of spring, and size of reference rod. Using the results of this algorithm, the macro calculates the distance between the spring reference pointer and the reference rod as the number of pixels between points 1 and 4 in Figure 2.3 and converts this value to distance (in mm) using the scale previously defined.

The macro creates a text file containing the time and distance between the spring reference pointer and the reference rod for each frame. This file can be opened with a spreadsheet or graphing program, and the distance data may be converted into penetrant mass uptake data using the calibration constant, k, for the spring. The spring constant is determined by suspending known calibration weights on the spring and measuring the displacement by the camera or cathetometer. According to Hooke's law,[30]

$$d = kx \tag{2.2}$$

where d is the calibration weight and x is the spring extension.

III. Experimental Results

The sorption kinetics of acetone vapor in a random copolymer of 50 weight % poly(ethylene terephthalate) and 50 weight % poly(ethylene 2,6-naphthalate) were determined at 35˚C. The film, approximately 5 µm thick, was cast from a solution of 5% (w/v) solution of triflouroacetic acid as described previously.[27] Prior to beginning a sorption experiment, the polymer film was placed on the end of the spring and exposed to vacuum to remove atmospheric gases dissolved in the film.

Figure 2.4 presents experimental data from two separate sorption experiments. The main chamber containing the spring and sample (E in Figure 1) was pressurized to 5.4 cm Hg with acetone vapor and the displacement of the spring was monitored by either the cathetometer (points labeled "Manual" in Figure 4) or the CCD camera/NIH Image system (points labeled "Automatic" in Figure 4). The square root of the time since sorption began, $t^{1/2}$, normalized by sample thickness, ℓ, is the abscissa; mass uptake at time t, M_t, normalized by mass uptake at equilibrium, M_∞, is the ordinate. M_t is calculated using the equation:

$$M_t = kx_t \tag{2.3}$$

where k is calibration constant determined in Equation 2.2, and x_t is the displacement of the spring at time t from the text file created by the Image macro. The concentration-average diffusion coefficient, $\bar{D}$, and the equilibrium weight uptake, M_∞, are obtained from a best fit of the data to the following equation, which describes Fickian penetrant uptake in a plane sheet:[5]

$$\frac{M_t}{M_\infty} = 1 - \frac{8}{\pi^2}\sum_{n=0}^{\infty}\frac{1}{(2n+1)^2}\exp\left(\frac{-\bar{D}(2n+1)^2\pi^2 t}{\ell^2}\right), \tag{2.4}$$

where n is the integer counter in the infinite summation. The equilibrium concentration of acetone in the polymer is M_∞ divided by the weight of the penetrant-free polymer sample.

The values of $\bar{D}$ and M_∞ determined from these separate experiments are in excellent agreement. The diffusion coefficients determined from the cathetometer and camera experiments are $1.1 \pm 0.2 \times 10^{-12}$ cm^2/s and $1.0 \pm 0.2 \times 10^{-12}$ cm^2/s, respectively. The equilibrium acetone uptake was 1.47 ± 0.15 g acetone/ 100g polymer in the cathetometer experiment and 1.52 ± 0.15 g acetone / 100g polymer when the camera was used to record the data.

Since the value of k is typically 0.2 mg/mm, and the long (640 pixel) dimension of the image is typically 3 mm, the spring balance is sensitive to changes in weight as small as ±1 µg. There are four sources in the uncertainty of estimating the diffusion coefficients: uncertainty in determining M_t (± 1 µg), uncertainty in determining M_∞ (± 1 µg), uncertainty in measuring ℓ (± 1 µm) the uncertainty in measuring t (± .02 s). As the film in this study is very thin (~ 5 µm), most (over 95%) of the systematic uncertainty in the diffusion coefficient comes from this measurement. There are two sources of error in determining the equilibrium acetone uptake: the uncertainty in determining M_∞ (± 1 µg) and the uncertainty in measuring the weight of the penetrant-free polymer sample, M_o (± 1 mg). For a typical 15 mg value of M_o, the relative uncertainty in determining M_o, $\Delta M_o/M_o$, is much larger (~0.07) than the relative uncertainty in determining M_∞, $\Delta M_\infty/M_\infty$, (~0.004) because the measurement of M_o relies on the initial weight of the sample as determined by an analytical balance. Therefore, the uncertainty of measuring M_o dominates the uncertainty in determining the equilibrium acetone concentration.

IV. Discussion

The spring balance equipped with a CCD camera, frame-grabber card, MacIntosh computer, and NIH Image software provides a straightforward, inexpensive mechanism for automation of spring balance systems to collect equilibrium uptake and kinetic sorption data. Automation of the spring balance is particularly useful when studying systems where diffusion is slow, and data collection may last several days. For example, acetone uptake in the PET/PEN copolymer occurred over 2.5 days. This device may also be useful for monitoring kinetics of penetrant uptake in membrane polymers with high diffusion coefficients. In these materials, even for relatively thick film samples, the kinetics of sorption may be inconveniently fast for manual data collection.

Moreover, the automated spring balance has the inherent advantage, relative to commercially available recording electrobalances, of being useful for studying the uptake of reactive or highly condensable vapors in polymers. Such penetrants may sorb into the epoxy or electronic components in electrobalances, thereby introducing spurious responses in such instruments. The relevant components exposed to penetrant in the automated spring system are the reference rod (which may be fabricated from metal or glass), the glass sample chamber, and the quartz spring, all of which are resistant to even chemically aggressive penetrants.

V. Conclusions

A method for automation of a McBain-type spring balance using a charge coupled device [CCD] camera, a computer equipped with a frame-grabber card, and National Institute of Health [NIH] Image software is presented. This balance is used to study the sorption and transport of small molecules in polymeric materials. Kinetic gravimetric sorption data of acetone uptake in a random copolymer of 50 wt% poly(ethylene terephthalate) and 50 wt% poly(ethylene 2,6-naphthalate) at 35˚C are provided to illustrate the utility of the method. The diffusion coefficients determined from the cathetometer and camera experiments are $1.1 \pm 0.2 \times 10^{-}$

^{12} cm^2/s and $1.0 \pm 0.2 \times 10^{-12}$ cm^2/s, respectively. At an acetone partial pressure of 5.4 cm Hg, the equilibrium acetone uptake was 1.47 ± 0.15 g acetone/ 100g polymer using the cathetometer to determine spring extension and 1.52 ± 0.15 g acetone/ 100g polymer when the camera was used to determine mass uptake of acetone by the polymer. The camera-based balance was determined to be sensitive to weight changes as small as ±1 μg.

Table 2.1. Code for Image 1.59 Macro

```
macro 'Sorption Run...';
{
Captures images as a function of square root time.
Select an area of interest within the Camera window before starting.
by David Coker (2/27/97)...
}
var
  nFrames,n,Left,Top,Width,Height:integer;
  interval,EndTicks,secs:integer;
  offset:integer;
  year,month,day,hour,minute,second,dayofweek:integer;
  ymin,ymax:real;
  scale:real;
  unit:string;
  AspectRatio:real;
  x11,x12,x21,x22:integer;
  count,ppv,i:integer;
  FirstTime:boolean;
begin
  GetRoi(Left,Top,Width,Height);
  if width=0 then begin
    PutMessage('First select the area of interest in the Camera window.');
    exit;
  end;
  nFrames:=GetNumber('Number of Frames?',10);
  secs:=GetNumber ('Delay Factor (seconds)?',60.0);
  interval:=round(secs*60);
  FirstTime:=true;
  offset:=10;
  NewTextWindow('Sorption Run Text',350,400);
  Save;
  SelectWindow('Camera');
  for n:=1 to nFrames do begin
    StopCapturing;  beep;

    GetTime(year,month,day,hour,minute,second,dayofweek);

    MoveTo(Left+offset, Top+offset);
    Write(month:2);
    if (day<10) then begin
      Write('/0',day:1);
    end;
    if (day>9) then begin
      Write('/',day:2);
    end;
```

```
Write('/',year:4);
Write(' - ');
Write(hour:2);
if (minute<10) then begin
   Write(':0',minute:1);
end;
if (minute>9) then begin
   Write(':',minute:2);
end;
if (second<10) then begin
   Write(':0',second:1);
end;
if (second>9) then begin
   Write(':',second:2);
end;

MakeRoi(Left,Top,Width,Height);
GetPlotData(count,ppv,ymin,ymax);
GetScale(scale,unit,AspectRatio);
x11:=0;
x12:=0;
x21:=0;
x22:=0;
for i:=0 to count-1 do begin
  if (PlotData[i] > 140) and (x11 = 0) then begin
    x11:=i;
  end;
  if (PlotData[i] < 140) and (x11 > 0) and (x12 = 0) then begin
    if ((i-x11) >= 10) then begin
      x12:=i;
    end;
    if ((i-x11) < 10) then begin
      x11:=i;
    end;
  end;
  if (PlotData[i] > 200) and (x12 > 0) and (x21 = 0) then begin
    x21:=i;
  end;
  if (PlotData[i] < 200) and (x21 > 0) and (x22 = 0) then begin
    if ((i-x21) >= 10) then begin
      x22:=i;
    end;
    if ((i-x21) < 10) then begin
      x21:=i;
    end;
  end;
```

```
    end;
    SelectWindow('Sorption Run Text');
    Write(hour:2);
    if (minute<10) then begin
      Write(':0',minute:1);
    end;
    if (minute>9) then begin
      Write(':',minute:2);
    end;
    if (second<10) then begin
      Write(':0',second:1);
    end;
    if (second>9) then begin
      Write(':',second:2);
    end;
    Write(chr(9),(x22-x11) / scale,chr(9),unit,chr(13));

   SelectWindow('Camera');
    MakeRoi(Left,Top,Width,Height);
    SaveAs('Plastics-O-Rama:Applications:Scion Image 1.59:Sorption
Folder:Frame ',n);

    if FirstTime then begin
      EndTicks:=TickCount+sqr(n)*interval;
      FirstTime:=false;
    end;

    if button then begin
      StopCapturing;
      exit;
    end;

    StartCapturing;

    while TickCount<EndTicks do begin
       secs:=(EndTicks-TickCount) div 60;
       ShowMessage(n:1,' / ',nFrames,' ',secs:4);
    end;
    EndTicks:=EndTicks+(sqr(n+1)-sqr(n))*interval;
  end;
  StopCapturing;
  SelectWindow('Sorption Run Text');
  Save;
end;
```

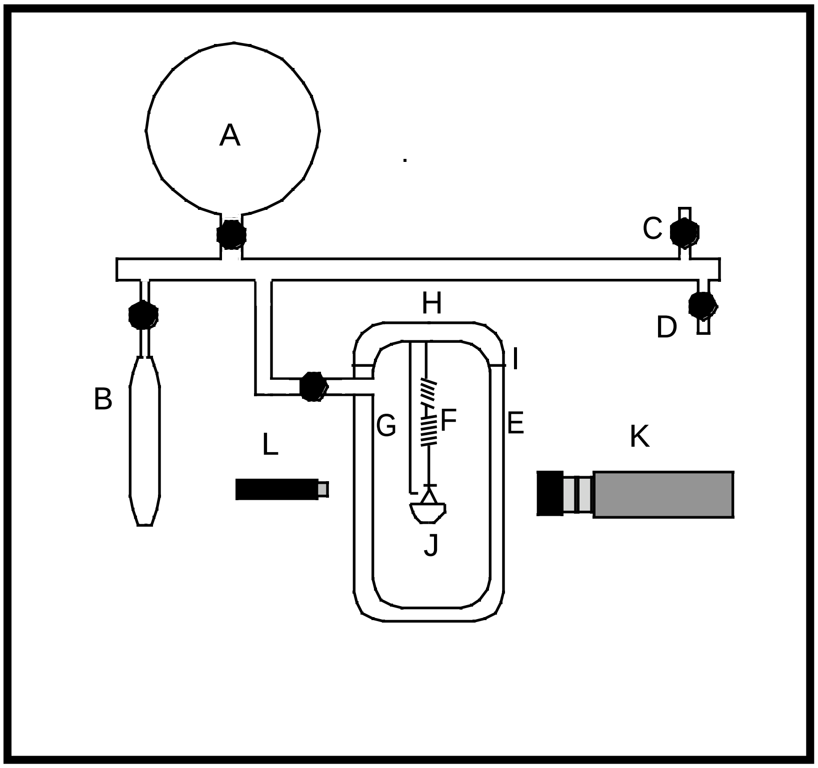

Figure 2.1. Schematic Diagram of Automated Spring Balance

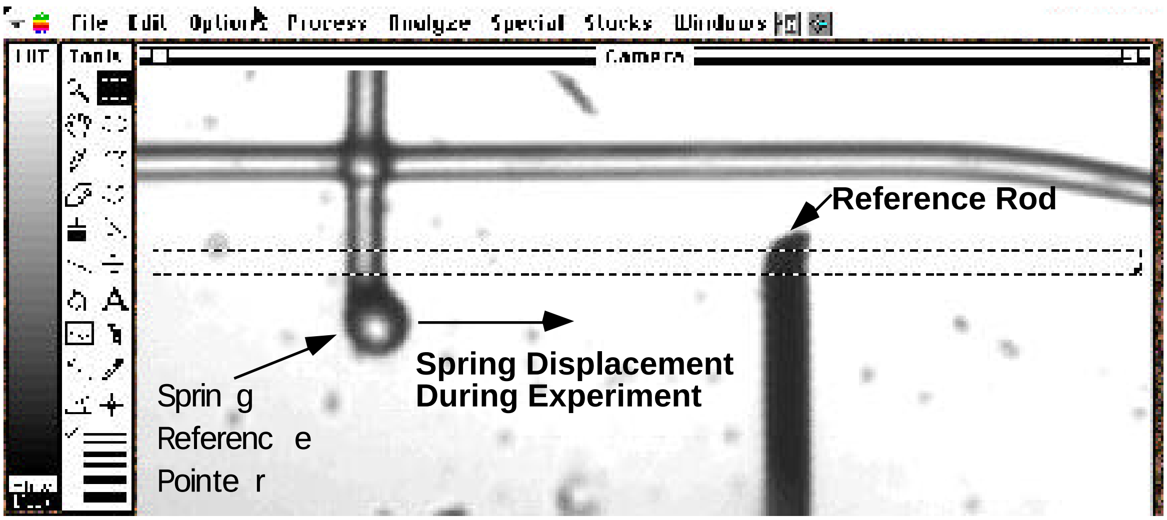

Figure 2.2. View of Scion Image version 1.59 main window showing a captured frame with spring, reference rod, and the selected region of interest (ROI)

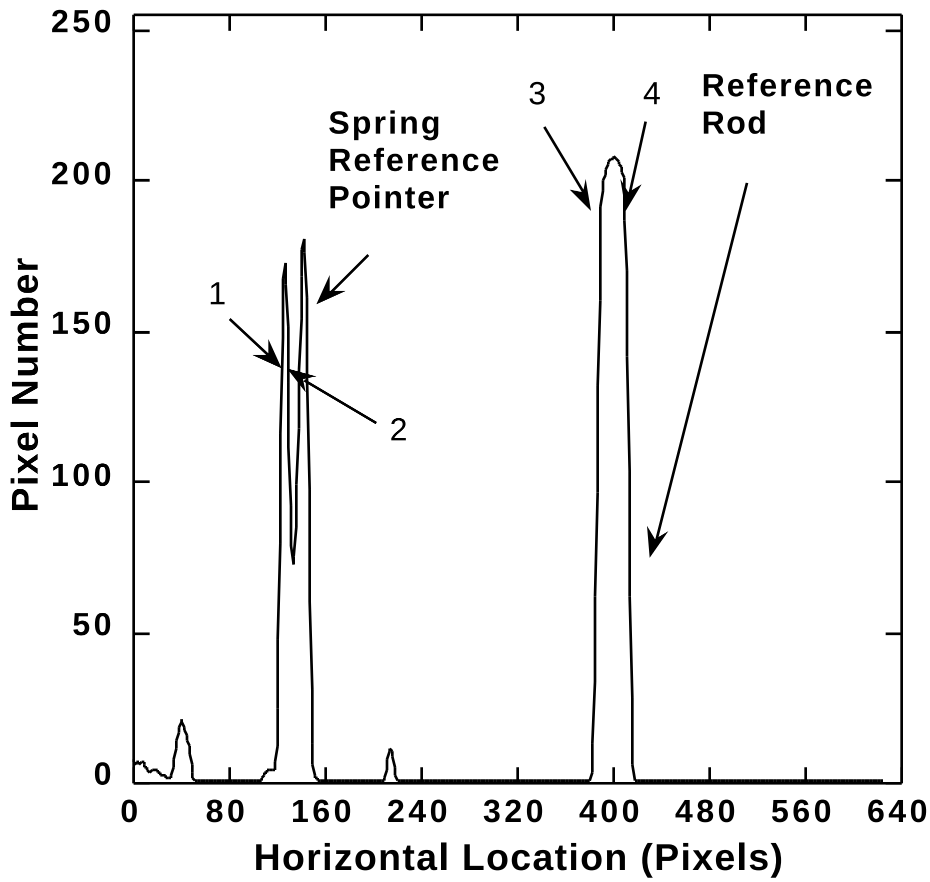

Figure 2.3. Plot Profile from Scion Image. The points (1-4) correspond to markers used by the Image manual to determine the separation of the spring and reference rod in each frame.

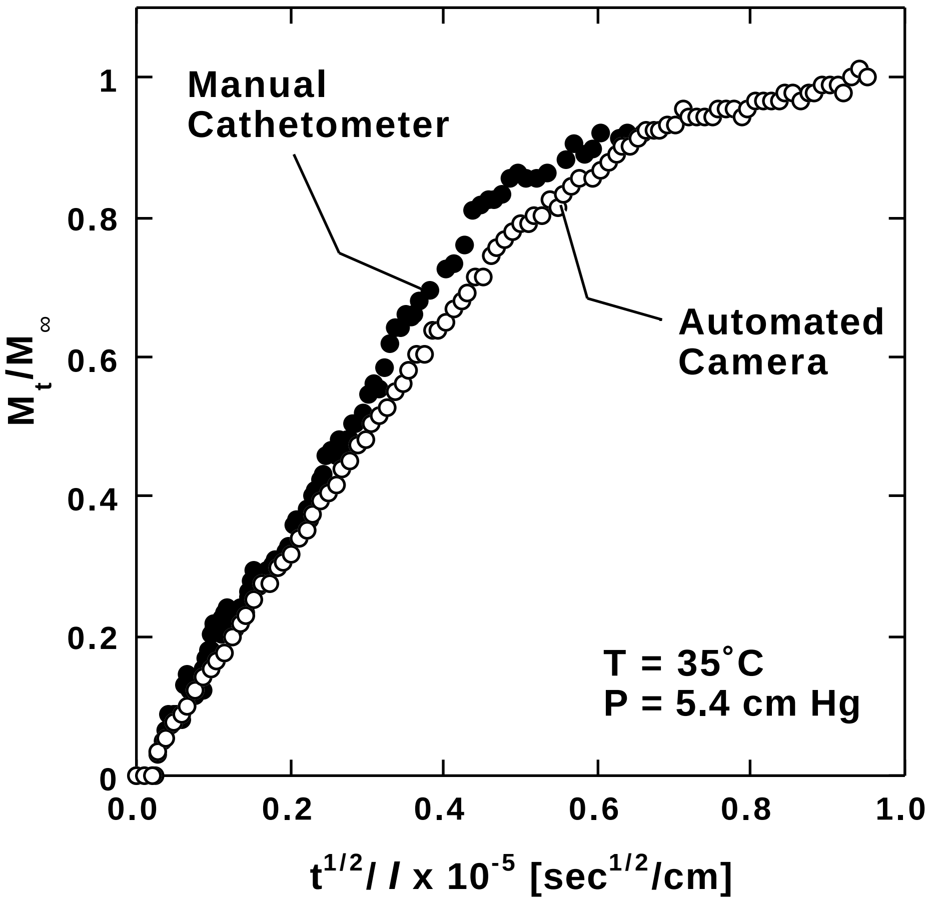

Figure 2.4. Comparison of Camera and Cathetometer Data for Sorption of Acetone in 50/50 PEN/PET Copolymer at 35˚C and 5.4 cm Hg (●=manual cathetometer system, $\overline{D}$ = 1.1 ± 0.2 x 10^{-12} cm^2/s, M_∞ = 1.47 ± 0.15 g acetone/ 100g polymer; ❍=automated CCD/Image system, $\overline{D}$ = 1.0 ± 0.2 x 10^{-12} cm^2/s, M_∞ = 1.52 ± 0.15 g acetone/ 100g polymer)

Chapter 3. Acetone Sorption and Uptake Kinetics in Poly(ethylene terephthalate)

I. Introduction

Poly(ethylene terephthalate) [PET] is an important barrier material that is widely used to package foods and beverages.[31] An important consideration in such barrier packaging applications is the loss of organic flavor molecules, such as d-limonene in fruit juices, as a result of scalping, (*i.e.* sorption of the flavor molecules into package walls).[1] Additionally, flavor molecule carry-over is emerging as a concern for refillable plastic beverage bottles. Flavor molecules sorbed into package walls from an initially-packaged product desorb after refill to influence the taste of the product in the refilled package. To understand better the sorption and transport of flavor components (such as esters, ketones, and aromatics) into barrier polymers such as PET, small organic penetrants are used as model marker molecules.[2]

The sorption of organics in PET has been the subject of several investigations. As PET is a glassy polymer, the equilibrium sorption isotherms of a variety of organic vapors (*e.g.* methanol,[32] ethyl acetate,[32] and benzene[33]) are reported to be well-described by the dual mode sorption model[7] or the so-called generalized dual mode sorption model.[10] Liu and Neogi measured methylene chloride vapor sorption kinetics in PET over a wide range of penetrant activity and observed Fickian mass uptake kinetics.[34] The sorption isotherm of methylene chloride in PET was well-described by the generalized dual-mode model.[34] In another study, the kinetics of benzene uptake in PET were rationalized using a model which combined Fickian diffusion, within the context of the dual mode transport theory (the so-called dual mobility model), and structural relaxation of the polymer upon penetrant sorption (i.e. swelling-controlled penetrant uptake).[33] Sorption of liquid dimethylformamide in PET obeyed Fickian kinetics in a set of films prepared with draw ratios ranging from 1.6 to 4.0.[35]

Durning and Russel proposed a model for diffusion with induced crystallization to describe sorption kinetics of organic liquids which can trigger PET crystallization.[36] In another study, Durning *et al.* measured sorption and transport of methylene chloride and dimethylformamide in PET films and observed that both polymer swelling and solvent-induced crystallization influence penetrant sorption kinetics.[37] Billovits and Durning found that organic penetrant transport properties in PET were sensitive to film processing conditions.[38] In particular, the sorption kinetics of strongly swelling penetrants such as acetone and dimethylformamide (DMF) are influenced by thermal annealing and prior exposure to penetrants such as liquid methylene chloride. Initially amorphous PET films were crystallized by exposure to methylene chloride (*i.e.* solvent-induced crystallization), low temperature annealing (120˚C), or high temperature annealing (230˚C). The sample annealed at high temperature had the highest level of crystallinity (47 wt%), and the film crystallized by exposure to methylene chloride had the lowest level of crystallinity (23 wt%). DMF diffusion coefficients determined from desorption experiments decreased with increasing crystallinity. For example, at 65˚C, the diffusion coefficient of DMF was 74 x 10^{-9} cm^2/s in the film crystallized with methylene chloride and 5 x 10^{-9} cm^2/s in the film annealed at high temperature. DMF sorption kinetics were non-Fickian. At short times, the fractional mass uptake was convex to the $t^{1/2}$ axis. The lengths of the convex portions of the uptake kinetics are reported as induction times, or the time necessary to establish diffusion control of mass uptake. The induction time increased with increasing crystallinity. At longer times, uptake kinetics are a linear function of $t^{1/2}$, where t is the time since the beginning of the experiment, and the slope of the linear region were used to estimate the diffusion coefficient. Like DMF diffusion coefficients, the diffusivity of methylene chloride decreased with increasing crystallinity.

Transport properties of organic molecules such as acetone can be more sensitive than those of smaller molecules, such as carbon dioxide and oxygen, to subtle effects of processing and polymer structure on sorption and transport properties in high barrier polymers.[39-41] Penetrant diffusion coefficients are commonly understood to depend sensitively on free volume in the polymer matrix. One of the most widely used models of the effect of free volume on penetrant diffusion coefficients, the Cohen-Turnbull model,[42] suggests that the diffusion coefficients of larger penetrants are more sensitive than those of smaller penetrants to changes in the amount of free volume in the polymer matrix. The Lennard-Jones diameters of acetone, CO_2, and O_2, are 4.6 Å, 3.94 Å, and 3.47 Å, respectively.[43] As acetone is substantially larger than the other two molecules, it's diffusion coefficient should be more sensitive than those of O_2 and CO_2 to subtle processing-induced changes in the free volume in the polymer matrix. As a result, several studies have used acetone as a marker organic molecule to probe the effect of polymer chemistry and processing on sorption and transport properties of high barrier polyesters.[27,40] In these studies, the transport properties of acetone were observed to be more strongly influenced by polymer thermal history than the transport properties of small molecules such as O_2 and CO_2.[41]

In this study, the equilibrium uptake and kinetics of acetone sorption in a solution-cast film of PET are reported. The dual-mode model is used to analyze the equilibrium sorption isotherms. An empirical two-stage model incorporating Fickian diffusion and relaxation-controlled kinetics describes the kinetics of acetone uptake. The effect of acetone concentration on acetone diffusion coefficient is analyzed in the context of the dual mobility model.[33]

II. Experimental

Polymer Synthesis

PET was synthesized in a two-stage process. Dimethyl terephthalate (5.15 moles), an excess of ethylene glycol, and the catalyst mixture (manganese diacetate, 90 ppm Mn; cobalt diacetate, 90 ppm Co; and antimony trioxide, 350 ppm Sb) were added to a reaction vessel. Heat was applied to begin the ester interchange reaction. The methanol byproduct was removed, and when the reaction temperature had increased to 250˚C, the ester interchange was complete.

In the polycondensation stage, a phosphorus-containing stabilizer in the form of polyphosphoric acid (82 ppm P) was added to the ester interchange product, and the pressure was gradually reduced to about 0.1 cm Hg as the temperature was increased to approximately 290˚C to obtain the product.

The solution viscosity, percent diethylene glycol [DEG], and percent carboxylic acid were determined for the as-synthesized polymer. The solution viscosity, SV, is given by:

$$SV = (\eta_{rel} - 1)x100, \tag{3.1}$$

where η_{rel} is the relative viscosity. The relative viscosity of a 1 weight percent solution of the polymer in dichloroacetic acid was measured using a capillary viscometer at 25˚C, and Equation 1.1 was used to compute solution viscosity. To determine the percentage of diethylene glycol in the final polymer, the polymer sample was first dissolved in 30% NH_4OH by heating in a high pressure vessel at 220 ˚C for 2 hours. This process completely hydrolyzed the sample to monomer. The percent diethylene glycol in the polymer was then determined by gas chromatography using diethylene glycol as a standard. For end group (percent carboxylic acid) analysis, 0.14 grams of the sample was dissolved in 6 ml of benzyl alcohol at 206 ˚C. The solution was then titrated with an aqueous KOH solution using phenol red as the indicator.

Film Preparation

The kinetics of acetone sorption were recorded using a Cahn RG-2000 electrobalance at 35˚C over a pressure range of 0-5.4 cm Hg. The details of this experimental procedure are recorded elsewhere.[44] Each film was conditioned by exposure to 7.2 cm Hg of acetone and then degassed prior to the gravimetric sorption studies described in this report. This conditioning protocol alleviates penetrant-induced crystallization during the subsequent sorption experiments. Gravimetric sorption studies suggest that exposure of as-cast films to high relative pressures of acetone could increase crystallinity by as much as 4 percent (*cf*. Appendix A). However, DSC studies on samples before and after exposure never revealed a systematic, measurable increase in crystallinity.

Thermal and Physical Characterization

A Perkin-Elmer DSC-7 was used at a scan rate of 20˚C/minute to characterize the thermal transitions of the PET film. The second DSC scan is reported for thermal transition measurements. However, results from the first DSC scan are used for crystallinity measurements to characterize the polymer properties in the as-cast state. A wide angle X-ray diffraction [WAXD] spectrum was obtained using a Siemens Kristalloflex 4 X-ray Generator and a Siemens type FΘ/2Θ goniometer. The X-rays were produced by a CuKα (λ=1.54 Å) source. Density measurements were performed with a Techne density gradient column using aqueous calcium nitrate solutions with a density range of approximately 1.2 to 1.5 g/cm^3.

Kinetic Gravimetric Sorption

The kinetics of acetone sorption were recorded using a Cahn RG-2000 electrobalance at 35˚C and a pressure range of 0-7.2 cm Hg. A more detailed description of the experimental procedure is available elsewhere.[44] The film was conditioned by exposure to 7.2 cm Hg of acetone and then degassed prior to the gravimetric sorption studies described in this report. This conditioning protocol alleviates penetrant-induced crystallization during the subsequent sorption experiments. Based on DSC experiments, there was no measurable difference in crystallinity levels in the films before and after sorption.

III. Results and Discussion

Polymer Characterization

The solution viscosity of the as-synthesized polymer was 919. From this value, an intrinsic viscosity of 0.70 dL/g was estimated using a correlation available from Hoechst-Celanese. The concentration of carboxylic acid end groups in the polymer was 40 milliequivalents per kilogram, which corresponds to a number average molecular weight of 25,000 g/mole. The concentration of DEG was 0.86 weight percent (based on the total mass of the polymer sample).

A second scan DSC thermogram of an as-cast PET film is presented in Figure 3.1. The thermogram exhibits a glass/rubber transition, T_g, at 81˚C, a cold crystallization exotherm, T_c, centered at 141˚C, and a melting point, T_m, at 255˚C. These transition temperatures agree well with literature values for T_g (81˚C) and T_m (250-265˚C).[45] As kinetic constraints on macromolecular mobility are relieved, at temperatures above T_g, the polymer crystallizes on the time scale of the DSC experiment.[46] Therefore, the cold crystallization exotherm is observed, as expected, above T_g. The weight percent crystallinity was calculated by subtracting the enthalpy of cold crystallization from the enthalpy of melting (both determined by measuring the area under the respective peaks in the DSC thermogram) and dividing by the heat of fusion of PET, 140 J/g.[47] The weight percent crystallinity is 40%.

Figure 3.2 presents a wide-angle X-ray diffraction spectrum of the as-cast PET film. The three strong diffraction peaks centered at 2θ = 16.4, 22.0, and 25.1˚ are associated with PET crystallites. The vertical lines in Figure 3.2 represent values of WAXD peak locations expected for the $(0\bar{1}1)$, (010), $(\bar{1}10)$, and (100) reflections in PET.[48] These are the strongest reflections reported in a previous crystallography study of PET.[48] The unit cell of PET is triclinic, with one monomer unit per unit cell, and the following unit cell parameters: a = 4.56 Å, b = 5.94 Å, c = 10.75 Å, α =98.5˚, β = 118˚, γ = 112˚.[48] The broad amorphous halo in the WAXD spectrum is centered at approximately 2θ = 20.6˚. From this value of 2θ, using Bragg's law[49] [$\lambda = 2d\sin\theta$], the d-spacing of the amorphous material was estimated to be 4.3 Å. Murthy, *et al.*, separate the amorphous halo of PET into two peaks, one centered at 2θ = 17.5˚ (5.0 Å) and the other at 23.5˚ (3.9 Å).[48] The peak with a d-spacing of 3.9 Å is ascribed to interchain spacing normal to the plane of aligned aromatic rings in the PET matrix. The peak with a d-spacing of 5.0 Å is attributed to interchain spacing in the plane of the aligned aromatic rings. The relative areas of the two amorphous peaks were used to evaluate the amount of orientation and order in the amorphous PET matrix.[48] The data in Figure 3.2 are considered to be consistent with those of Murthy, *et al.* However, in our WAXD spectrum, there is not sufficient resolution to extract definitively two amorphous halos from the spectrum of this semicrystalline sample.

The weight percent crystallinity was estimated to be 38% from the WAXD spectrum in Figure 3.2. This value was obtained by computing the areas under the amorphous peak and crystalline peaks after establishing a baseline for the spectrum. The crystalline content was then estimated as $A_C/(A_A+A_C)$ where A_C is the area associated with the crystalline peaks and A_A is the area associated with the amorphous halo.

The density of the film was 1.373 g/cm^3. The densities of completely crystalline and wholly amorphous PET are 1.440 and 1.327 g/cm^3, respectively.

[25] Based on our measured density value, the weight percent crystallinity, X_c, is estimated to be 41% using the relation:

$$X_C = (\rho - \rho_A)/(\rho_C - \rho_A) \times 100 \tag{3.2}$$

where ρ is the polymer density, ρ_A is the density of amorphous PET, and ρ_C is the density of completely crystalline PET. The independent estimates of crystalline from WAXD (38%), DSC (40%), and densitometry (41%) are in excellent agreement.

Equilibrium Acetone Uptake

Interval gravimetric sorption experiments were used to determine the sorption isotherm presented in Figure 3.3. The shape of this isotherm is typical of that for isotherms of condensable low activity organic vapors in glassy polymers,[7] and the isotherm is well-described by the dual mode model:[7]

$$C = C_D + C_H, \tag{3.3}$$

where C is the equilibrium concentration of penetrant in the polymer, C_D is the equilibrium concentration of penetrant in the Henry's law mode, and C_H is the equilibrium concentration of penetrant in the Langmuir mode. The analytical expressions for C_D and C_H are:[7]

$$C_D = k_D p \tag{3.4}$$

and

$$C_H = \frac{C'_H bp}{1 + bp}, \tag{3.5}$$

so that,

$$C = k_D p + \frac{C'_H bp}{1 + bp}\,. \qquad (3.6)$$

In these expressions, k_D is the Henry's Law coefficient, which characterizes equilibrium sorption of the penetrant into the equilibrium densified polymer matrix. The Langmuir capacity parameter, C'_H, characterizes penetrant sorption in the non-equilibrium excess volume associated with the glassy polymer matrix. The Langmuir affinity parameter, b, characterizes the affinity of the penetrant for a Langmuir site in the matrix. C_D is, therefore, the equilibrium concentration of penetrant in the densified polymer matrix, and C_H is the equilibrium concentration of penetrant in the non-equilibrium excess volume. The curve in Figure 3.3 represents a least-squares fit of the sorption data to the dual mode model. This non-linear regression yielded the following model parameters: $k_D = 61 \pm 7.4$ $cm^3(STP)/(cm^3{\cdot}atm)$, $C'_H = 7.2 \pm 1.1$ $cm^3(STP)/cm^3$ and $b = 50 \pm 12$ atm^{-1}.

The logarithm of gas solubility or Henry's law coefficients of various penetrants in both rubbery[50,51] and glassy[52] polymers often increases linearly with penetrant critical temperature. Solubility coefficients for several permanent gases,[20] as well as the dual mode parameters for carbon dioxide[53] and benzene,[33] in PET are available. The solubility coefficients for the permanent gases and the Henry's law coefficients for CO_2, acetone, and benzene, divided by amorphous volume fraction, Φ_A, to correct for crystallinity,[15,18] are presented in Figure 3.4a as a function of penetrant critical temperature. The data were collected in different laboratories and at three different temperatures. The correlation is impressive and suggests that the Henry's law coefficient determined in this study is reasonable.

For the permanent gases (He, N_2, Ar, O_2, CH_4), the Henry's law parameter reported in Figure 3.4a is actually the infinite dilution solubility, k_D^*, where $k_D^* = k_D + bC'_H$, because sorption isotherms for the permanent gases (*i.e.* He, N_2, Ar, O_2, CH_4) are linear functions of pressure and, consequently, separate estimates for k_D, b, and C'_H are not available. However, for CO_2, acetone, and benzene, bC'_H is at least as large as k_D. Therefore, to provide what is perhaps a more appropriate comparison of the sorption data for different penetrants, Figure 3.4b presents the infinite dilution solubility coefficient, k_D^*, versus penetrant critical temperature. The correlation of the data with critical temperature is also excellent, again confirming that the acetone sorption parameters are reasonable.

Langmuir affinity parameters have also been correlated with penetrant critical temperature.[54] In this regard, Figure 3.4c presents the Langmuir affinity parameter, b, as a function of critical temperature for carbon dioxide, acetone, and benzene. As with k_D, there is excellent agreement of our acetone Langmuir affinity parameter with those of other penetrants.

Acetone Sorption Kinetics

Figure 3.5 presents results from four representative acetone kinetic sorption experiments in PET. The time since the penetrant pressure surrounding the polymer sample was increased from its initial value, p_i, to its final value, p_f, is t, M_t is the mass of acetone sorbed by the polymer from the beginning of the experiment until t, and M_∞ is the equilibrium mass uptake during the interval sorption experiment. At short times, the fractional mass uptake, M_t/M_∞, increases linearly with $t^{1/2}$, which is characteristic of sorption kinetics controlled by Fickian diffusion.[6] At longer times, the mass uptake exhibits a protracted, non-Fickian asymptotic approach towards equilibrium. Such so-called two stage kinetics[5] are often observed for organic vapor sorption in glassy polymers. Examples include vinyl chloride monomer in PVC[55] and benzene in PET,[33] methyl acetate in poly(methyl methacrylate) and cellulose acetate,[56] benzene in polystyrene,[56] acetone in cellulose nitrate,[56] and ethyl benzene in polystyrene.[57] Often, such sorption kinetics are described using the following empirical model:[55]

$$\frac{M_t}{M_\infty} = 1 - (1-\alpha_R)\frac{8}{\pi^2}\sum_{n=0}^{\infty}\frac{1}{(2n+1)^2}\exp\left(\frac{-\bar{D}(2n+1)^2\pi^2 t}{\ell^2}\right) - \alpha_R \exp\left(\frac{-t}{\tau_R}\right) \quad (3.7)$$

where $\bar{D}$ is the average diffusion coefficient (defined below), α_R is the fraction of weight uptake occurring during the protracted, non-Fickian approach to equilibrium, and τ_R is the time constant associated with the long time drift in mass uptake.[33] The long term drift in sorption kinetics is usually ascribed to mass uptake controlled by the viscoelastic relaxation of the polymer chains to accommodate penetrant.[33] $\bar{D}$ is approximately equal to the average effective diffusion coefficient over the concentration interval of the experiment:[5]

$$\bar{D} = \frac{1}{C_f - C_i}\int_{C_i}^{C_f} D(C)\,dC, \quad (3.8)$$

where C_i and C_f are penetrant concentrations in the polymer at the beginning and end of the sorption experiment, and D(C) is the effective diffusion coefficient..

Figure 3.6 presents a least squares fit of Equation 3.7 to the experimental data for an acetone pressure interval from 1.8 cm Hg to 2.7 cm Hg. While Equation 3.7 can describe the data, from this best fit, α_R is 0.60, suggesting that

60% of the mass uptake is controlled by relaxation. In contrast, M_t/M_∞ is linear with $t^{1/2}$ at short times and approaches a plateau at $M_t/M_\infty \approx 0.72$. Afterwards, there is a second stage of uptake which is not a linear function of $t^{1/2}$. Based on this qualitative examination of the experimental data, and in contrast to the result of the least squares fit of Equation 3.7 to the data, Fickian diffusion controls the initial 72% of mass uptake, and the remaining 28% is controlled by polymer relaxation. Additionally, the value of $\overline{D}$ from the best fit of Equation 3.6 to the data is 8.2×10^{-12} cm^2/s, which is approximately three times higher than would be expected from the initial slope of the data in Figure 3.6. That is, a fit of Equation 3.7 to the data in Figure 3.6 fails to provide reasonable parameter values.

For the simple empirical model represented in Equation 3.7, diffusion and relaxation occur in parallel, and therefore, the faster process controls initial mass uptake. Based on the linearity of initial uptake with $t^{1/2}$ in Figures 3.5 and 3.6, diffusion controls initial mass uptake for each pressure interval. The model, however, only describes two stage kinetics (with diffusion controlling the first stage) if the long time relaxation process is much slower than the diffusion process controlling initial uptake kinetics. As demonstrated below, the timescale for diffusion is actually longer than the timescale for relaxation for the data in Figure 3.6. Equation 3.7 cannot describe two stage mass uptake kinetics when the second stage (*i.e.* relaxation) occurs in series with a diffusion-controlled first stage and the relaxation timescale is faster than the diffusion timescale. The first three pressure intervals explored in this study (0-1.0, 1.0-1.8, and 1.8-2.7 cm Hg) are in this category. Therefore, the method described below was used to characterize the sorption kinetics for each interval.

At each pressure interval the diffusion-controlled process is essentially complete before polymer relaxation rate-controlled mass uptake begins. The presence of an intermediate plateau region in each graph in Figure 3.5 (indicated by arrows) between the diffusion-controlled and relaxation-controlled regimes of mass transfer is consistent with this simplified view of the kinetics of acetone sorption in PET and permits a separation of the two processes.

The fraction of weight uptake controlled by Fickian diffusion, $(1-\alpha_R)$, is estimated as the fraction of weight uptake at the intermediate plateau of the sorption data. The Fickian diffusion coefficient is estimated from a least squares fit of the data (from t=0 to the Fickian plateau) to the model for diffusion in a uniform plane sheet:[5]

$$\frac{\frac{M_t}{M_\infty}}{(1-\alpha_R)} = 1 - \frac{8}{\pi^2}\sum_{n=0}^{\infty}\frac{1}{(2n+1)^2}\exp\left(\frac{-\bar{D}(2n+1)^2\pi^2 t}{\ell^2}\right). \tag{3.9}$$

Figure 3.7 presents a characteristic example of a non-linear least squares fit of the data to Equation 3.9 for the acetone partial pressure interval from 1.8 to 2.7 cm Hg.

For this same kinetic sorption experiment, Figure 3.8 illustrates the procedure for estimating a first order time constant, τ_R, which characterizes the non-Fickian drift in mass uptake towards equilibrium after the initial diffusion-controlled regime. In the spirit of the model embodied in Equation 3.7, polymer relaxation-controlled mass uptake is described as a single exponential:

$$\ln\left(1-\frac{M_t}{M_\infty}\right) = \ln\alpha_R - \frac{t}{\tau_R}. \tag{3.10}$$

The curves in Figure 3.5 represent the separate diffusion and relaxation contributions to the acetone sorption kinetics as determined from Equations 3.9 and 3.10. The values of α_R determined from Equation 3.10 are higher than the values determined from the plateaus in Figure 3.5. For example, α_R determined from the data in Figure 3.8 is 1.4 ± 0.3, which is not consistent with the model, since α_R must lie between zero and one. Moreover, the plateau in the mass uptake data occurs at 0.72 (*i.e.* $1\text{-}\alpha_R=0.72$), which suggests an α_R value of 0.28. The graphically estimated plateau value is consistently lower than the value determined from Equation 3.10 for every pressure interval except the two highest intervals.

If the relaxation process did not begin at t=0 but, rather, started at some later time, then the data would be poorly described by Equation 3.7, which assumes that relaxation and diffusion occur simultaneously. Also, as described below, the values of α_R estimated from Equation 3.10 would be too high. The notion of a delay in the start of the relaxation process can be included simply in this empirical model by adding a delay time, t_D, to the second term of Equation 3.10, which would then be written as follows:

$$\ln\left(1-\frac{M_t}{M_\infty}\right)=\left[\ln\alpha_R+\frac{t_D}{\tau_R}\right]-\frac{t}{\tau_R}. \tag{3.11}$$

Initially, the mass uptake is controlled by Fickian diffusion, and the time for half of the total mass uptake controlled by Fickian diffusion to occur is given by:[55]

$$t_{1/2}=\frac{\ell^2}{20\overline{D}}=\frac{\tau_D}{20}, \tag{3.12}$$

where τ_D, the characteristic timescale for diffusion, is defined as $\ell^2/\overline{D}$. In all cases except for the highest two pressure intervals, the delay time estimated by

Equation 3.11 is at least 2 times the halftime for diffusion, $t_{1/2}$. Therefore, more than 80% of the mass uptake controlled by diffusion appears to be complete before the relaxation-controlled mass uptake begins. Within the context of this simple empirical model (Equation 3.11), this result is consistent with the notion that, for most of the pressure intervals considered, the diffusion-controlled process is essentially complete before relaxation-controlled mass uptake begins. For the highest two pressure intervals, the matrix may contain sufficient acetone and have, therefore, sufficiently high chain mobility, to permit the relaxation process to begin at or near t = 0.

The plateau value of mass uptake indicated by the arrows in Figure 3.5 is used to estimate α_R for each pressure interval. Equations 3.9 and 3.11 are used to estimate $\bar{D}$ and τ_R, respectively. These parameter values are recorded in Table 3.1 along with the Deborah number for diffusion, which is defined as τ_R/τ_D.[38] This dimensionless parameter characterizes the time scale for mass uptake due to structural relaxation relative to the timescale for Fickian diffusion.[38] The uncertainty in the diffusion coefficients in Table 3.1 is largely due to the uncertainty in determining sample thickness. Uncertainties in the parameters are estimated by the propagation of errors method described by Bevington.[58]

Figure 3.9 presents the structural relaxation time constant, τ_R, as a function of acetone concentration in the polymer at the end of each kinetic gravimetric sorption experiment, C_f. The relaxation time does not vary systematically over the range of acetone concentration investigated and has an average value of 53000 ± 4000 seconds. From Table 3.1, the diffusion Deborah number is less than one for the first three intervals (0-1.0, 1.0-1.8, and 1.8-2.7 cm Hg) and greater than one for the other pressure intervals. The increase in Deborah number results from the increase in acetone diffusion coefficient as acetone concentration increases.

Figure 3.10a presents the fraction of mass uptake controlled by relaxation as a function of acetone concentration in the polymer film at the end of each experiment. The value of α_R increases linearly with concentration and has a non-zero intercept. Interestingly, if α_R is presented as a function of acetone concentration in the Henry's Law mode (*cf.* Figure 3.10b), the best line describing the data passes through the origin, suggesting a strong correlation between the concentration of acetone in the Henry's law mode and the fraction of sorption controlled by structural relaxation. It is interesting that in conventional glassy polymers, such as polycarbonate, only penetrant molecules dissolved in the Henry's Law mode are understood to contribute to penetrant-induced swelling of the polymer matrix.[59]

Figure 3.11a presents the dependence of acetone diffusion coefficient on average acetone concentration during each interval sorption experiment. For lower values of average acetone concentration (*i.e.* 1.5-6.0 cm^3(STP) acetone/cm^3 polymer), acetone diffusion coefficients increase weakly with increasing acetone concentration. However, at higher acetone concentrations, the acetone diffusion coefficient increases more strongly with increasing concentration. C_i is the acetone concentration at the beginning of an interval sorption experiment, C_f is the acetone concentration at the end of an interval sorption experiment, and $\bar{C}$ is the average of C_i and C_f.

Figure 3.11b presents the diffusivity values on a semi-logarithmic scale. An exponential dependence of diffusivity on penetrant concentration is consistent with other reports of the concentration dependence of diffusion coefficients of organic vapors in glassy[60] and rubbery[61] polymers. The diffusivity is often expressed as the following empirical function of average concentration, $\bar{C}$:[4]

$$\bar{D} = D_o e^{\beta \bar{C}} \tag{3.13}$$

where D_o is the infinite dilution diffusion coefficient and β is an exponential factor describing the dependence of diffusion coefficient on concentration. The values of D_o and β are $9 \pm 5 \times 10^{-12}$ cm^2/s and 0.31 ± 0.05 $cm^3/cm^3(STP)$, respectively, based on a least squares fit of the data in Figure 3.11b to Equation 3.13.

Dual Mobility Analysis

A more fundamental model of the concentration dependence of diffusivity in glassy polymers is based on the notion that the two populations of penetrant molecules (Henry's law and Langmuir) in the dual mode theory have different mobilities.[62] In this so-called dual mobility model, one-dimensional penetrant transport is described by the following form of Fick's law:[62]

$$N = -D_H \frac{dC_H}{dx} - D_D \frac{dC_D}{dx} \tag{3.14}$$

where N is penetrant flux, C_D and D_D are the penetrant concentration and diffusion coefficient in the dense, equilibrium polymer matrix (Henry's law mode), and C_H and D_H are the penetrant concentration and diffusion coefficient in the non-equilibrium excess volume (Langmuir mode).

Within the context of the dual mobility model, the average effective diffusion coefficient determined in kinetic gravimetric sorption experiments is given by:[33]

$$\bar{D} = D_D \left[\frac{1 + FK/(1+bp_i)(1+bp_f)}{1 + K/(1+bp_i)(1+bp_f)} \right] \tag{3.15}$$

where $K = C_H'b/k_D$, and $F = D_H/D_D$. D_H and D_D are assumed to be independent of concentration. If this model adequately describes the experimental data, a plot of $\bar{D}[1+K/(1+bp_i)(1+bp_f)]$ versus $K/[(1+bp_i)(1+bp_f)]$ yields a straight line of slope D_H and intercept D_D. Such behavior has been reported for the diffusion of benzene in PET.[33]

Figure 3.12 presents our acetone diffusion coefficients plotted in the manner just described. A straight line describes the three data points at lowest acetone concentration, yielding $D_H = 6.4 \pm 5.3 \times 10^{-13}$ cm^2/s and $D_D = 96 \pm 2 \times 10^{-13}$ cm^2/s. However, at higher acetone concentration, this model does not adequately represent the experimental data, suggesting that acetone plasticizes the polymer matrix, thereby increasing D_D and/or D_H.

Stern and Saxena[63] presented a model to relax the assumption of constant (*i.e.* concentration independent) D_D and D_H. In the model proposed by Stern and Saxena, both D_D and D_H are presumed to be a function of the effective concentration C_m, where $C_m = C_D + FC_H$, and F is the ratio of D_H to D_D, which is taken to be a constant. A more general model where D_D and D_H have independent concentration dependences is presented below. The Stern and Saxena model is equivalent to the model described below when the ratio of D_H to D_D is held constant, and the diffusion coefficients are presumed to depend exponentially on the effective concentration, C_m.

The dual mobility model can be extended to account for concentration dependent Henry's law and Langmuir diffusion coefficients. Using Equation 3.14, the steady state permeability of a penetrant in a glassy polymer may be written as follows:[4]

$$P = \frac{\ell}{p_f - p_i}\left[-D_D\frac{dC_D}{dx} - D_H\frac{dC_H}{dx}\right] \tag{3.16}$$

where ℓ is the film thickness, p_f is the upstream pressure (at x=0) and p_i is the downstream pressure (at x=ℓ). This expression can be integrated from x=0 to ℓ to give:

$$P = \frac{\ell}{p_f - p_i}\left[\int_{C_{D_i}}^{C_{D_f}} D_D\,dC_D + \int_{C_{H_i}}^{C_{H_f}} D_H\,dC_H\right] \tag{3.17}$$

where C_{D_f} and C_{H_f} are the concentrations of penetrant dissolved in the Henry's law and Langmuir modes at pressure p_f, and C_{D_i} and C_{H_i} are the concentrations of penetrant dissolved in the Henry's law and Langmuir modes at pressure p_i. The permeability can also be defined in terms of the average diffusion coefficient:[4]

$$P = \frac{\ell}{p_f - p_i}\bar{D}(C_f - C_i). \tag{3.18}$$

Combining Equations 3.17 and 3.18 yields the following relationship:

$$\bar{D} = \frac{1}{C_f - C_i}\left[\int_{C_{D_i}}^{C_{D_f}} D_D\,dC_D + \int_{C_{H_i}}^{C_{H_f}} D_H\,dC_H\right]. \tag{3.19}$$

If $\bar{D}_D$ and $\bar{D}_H$ are defined by:

$$\bar{D}_D = \frac{1}{C_{D_f} - C_{D_i}}\int_{C_{D_i}}^{C_{D_f}} D_D\,dC_D \tag{3.20}$$

and:

$$\bar{D}_H = \frac{1}{C_{H_f} - C_{H_i}} \int_{C_{H_i}}^{C_{H_f}} D_H \, dC_H \tag{3.21}$$

then Equations 3.20 and 3.21 may be substituted into Equation 3.19 to give:

$$\bar{D} = \frac{1}{C_f - C_i}\left[(C_{D_f} - C_{D_i})\bar{D}_D + (C_{H_f} - C_{H_i})\bar{D}_H\right]. \tag{3.22}$$

Writing the penetrant concentrations in terms of pressure yields:

$$\bar{D} = \frac{1}{(k_D p_f - k_D p_i) - (\frac{C'_H b p_f}{1+bp_f} - \frac{C'_H b p_i}{1+bp_i})}\left[(k_D p_f - k_D p_i)\bar{D}_D + (\frac{C'_H b p_f}{1+bp_f} - \frac{C'_H b p_i}{1+bp_i})\bar{D}_H\right]. \tag{3.23}$$

Equation 3.23 reduces to Equation 3.15 when $\bar{D}_H$ and $\bar{D}_D$ are constants. $\bar{D}$ is measured experimentally and the other model diffusion coefficients ($\bar{D}_H$ and $\bar{D}_D$) in Equation 3.23 are fitted parameters. If $\bar{D}_H$ is arbitrarily assumed to be constant at the value determined from the dual mobility analysis, 6.4 x 10^{-13} cm^2/sec, the effect of acetone concentration on $\bar{D}_D$ can be determined using the equation:

$$\bar{D}_D = \frac{\bar{D}[(k_D p_f - k_D p_i) - (\frac{C'_H b p_f}{1+bp_f} - \frac{C'_H b p_i}{1+bp_i})] - (\frac{C'_H b p_f}{1+bp_f} - \frac{C'_H b p_i}{1+bp_i})\bar{D}_H}{(k_D p_f - k_D p_i)}. \tag{3.24}$$

The results of this analysis are presented in Figure 3.13a. The average Henry's law diffusion coefficients are reported as a function of average concentration in the Henry's law regions, $\bar{C}_D$, which is defined as $\bar{C}_D = \frac{1}{2}(k_D p_f + k_D p_i)$. The data are fit to an exponential relationship of the form:

$$\bar{D}_D = D_{D_o} e^{\beta_D \bar{C}_D} \tag{3.25}$$

where D_{D_o} is 7.9 ± 2.6 x 10^{-12} cm^2/s and β_D is 0.32 ± 0.08 cm^3/cm^3(STP). The value of D_{D_o} agrees well with the value of $\overline{D}_D$ determined by the classical dual mobility analysis at low concentration, 9.6 ± 0.2 x 10^{-12} cm^2/s. These values also agree well with the values determined from Figure 3.11b, where acetone diffusivity was related to overall average acetone concentration.

At the other extreme, one could assume that $\overline{D}_D$ is constant and confine all concentration dependence of the diffusivity to $\overline{D}_H$. In the following calculations, $\overline{D}_D$ is set to 9.6 x 10^{-12} cm^2/s, the value obtained from the dual mobility analysis of the low concentration data. The value of $\overline{D}_H$ can be calculated using the equation:

$$\overline{D}_H = \frac{\overline{D}(k_D(p_f - p_i) + C'_H(\frac{bp_f}{1+bp_f} - \frac{bp_i}{1+bp_i})) - k_D(p_f - p_i)\overline{D}_D}{C'_H(\frac{bp_f}{1+bp_f} - \frac{bp_i}{1+bp_i})} . \qquad (3.26)$$

These data are presented in Figure 3.13b as a function of $\overline{C}_H$, the average concentration of penetrant in the Henry's law mode. These data may be fit to:

$$\overline{D}_H = D_{H_o} e^{\beta_H \overline{C}_H} \qquad (3.27)$$

where D_{H_o} = 1.0 ± 0.9 x 10^{-15} cm^2/s and β_H = 2.0 ±0.2 cm^3/cm^3(STP). The value of D_{H_o} is very low and does not agree well with the value of D_H (6.4 x 10^{-13} cm^2/s) from the dual mobility analysis of the low concentration data. In addition, the value of β_H is almost an order of magnitude larger than the value of β determined from Figure 3.11b, where acetone diffusivity is related to overall average acetone concentration. Based on the magnitudes of the model parameters obtained using these two approaches, the relationship between concentration and diffusivity in Equation 3.25 yields more realistic values than the model embodied in Equation 3.27.

Using the experimentally determined parameters for D_{D_o} and β_D and substituting Equation 3.25 into Equation 3.23, the effect of concentration on acetone diffusion coefficient can be described within the context of the modified dual mobility model. A comparison of the model and the experimental data is presented in Figure 3.14. The error bars for the three data points at lowest average concentration are smaller than the size of the data points. In general, the data and the model agree well.

Two models have been compared to describe the concentration dependence of acetone diffusivity on acetone concentration in PET, an exponential dependence of diffusivity on concentration (Equation 3.13) and the modified dual mobility model (Equation 3.24). For the empirical model given by Equation 3.13, only two adjustable parameters are required to describe the data. The dual mobility model also provides a reasonable description of the experimental data if the assumption of constant Henry's law diffusion coefficient is relaxed. However, the dual mobility model does not provide guidance for the selection of the functional form of the concentration dependence of $\overline{D}_D$. In this study, we have elected to use the empirical expression given by Equation 3.24. However, it might prove useful and more satisfying from a theoretical point of view to combine the approach used in free volume theory to predict the concentration dependence of diffusivity[64] with the dual mobility model to obtain a more fundamental model for the concentration dependence of diffusion coefficients of organic vapors in glassy polymers.

IV. Conclusions

The dual mode model adequately describes the equilibrium sorption of acetone in PET. Interval kinetic gravimetric sorption results are described by an empirical two-stage model, with Fickian diffusion and polymer structural relaxation contributing to the control of mass uptake kinetics. The time constant of the relaxation process does not vary systematically with acetone concentration and has an average value of 53,000 ± 4,000 seconds (approximately 15 hours). The fraction of mass uptake associated with the relaxation process increases linearly with increasing concentration of acetone dissolved in the equilibrium densified region of the polymer matrix.

Acetone diffusivity increases with increasing concentration of acetone dissolved in the PET film. The standard dual mobility model cannot adequately account for this increase, implying that the acetone-induced polymer plasticization plays an important role in acetone diffusion. However, the experimental data were well described by an extended version of the dual mobility model where the diffusion coefficient of acetone in the Henry's law mode depends exponentially on concentration.

Table 3.1. Parameters from Analysis of the Kinetics of Acetone Sorption in PET

Pressure [cm Hg] p_i	p_f	$\bar{D}$ x 10^{12} [cm^2/s]	α_R	τ_R x 10^{-3} [s]	τ_D x 10^{-3} [s]	Deborah Number (τ_R/τ_D)
0	1.0	1.6 ± 0.1	0.04	33 ± 5	190	0.17
1.0	1.8	2.1 ± 0.2	0.18	60 ± 4	150	0.40
1.8	2.7	2.8 ± 0.3	0.28	58 ± 4	110	0.52
2.7	3.4	13 ± 1.2	0.40	51± 4	24	2.1
3.4	4.3	7.6 ± 0.7	0.45	46 ± 3	41	1.1
4.3	5.3	17 ± 1.6	0.55	79 ± 5	18	4.4
5.3	6.2	24 ± 2.1	0.76	47 ± 6	13	3.6
6.2	7.3	28 ± 2.4	0.74	54 ± 1	11	4.8

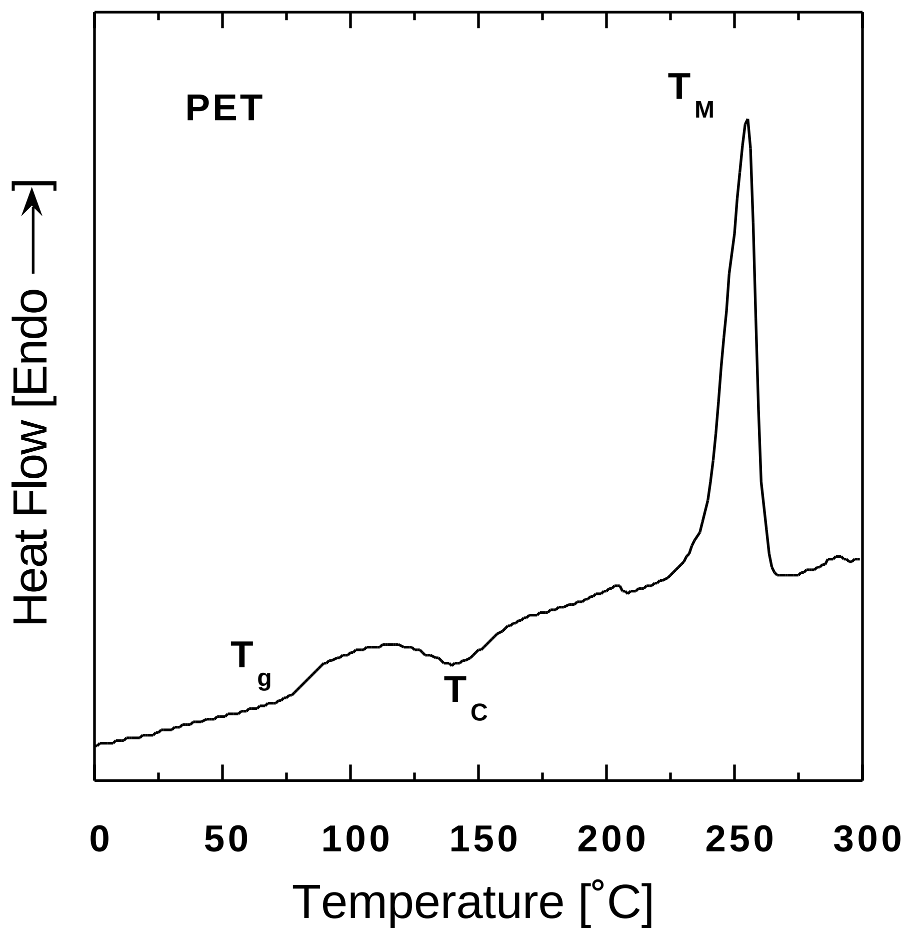

Figure 3.1. DSC Thermogram of As-Cast PET Film, Scan Rate = 20˚C / min.

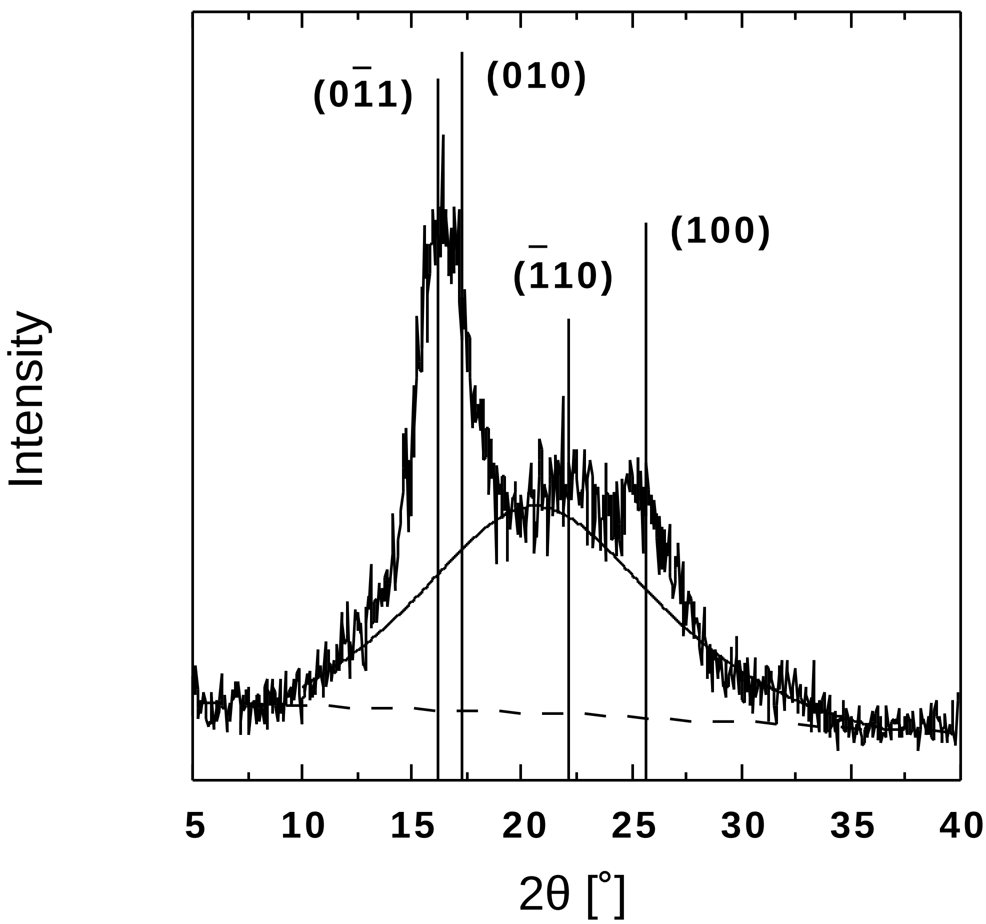

Figure 3.2. WAXD Spectrum of As-Cast PET Film. The smooth curve represents a Lorentzian curve representing the amorphous halo of the WAXD spectrum. The dashed line represents the baseline of the spectrum. The vertical lines represent expected diffraction peak locations based on literature reports of the crystal structure of PET.[48]

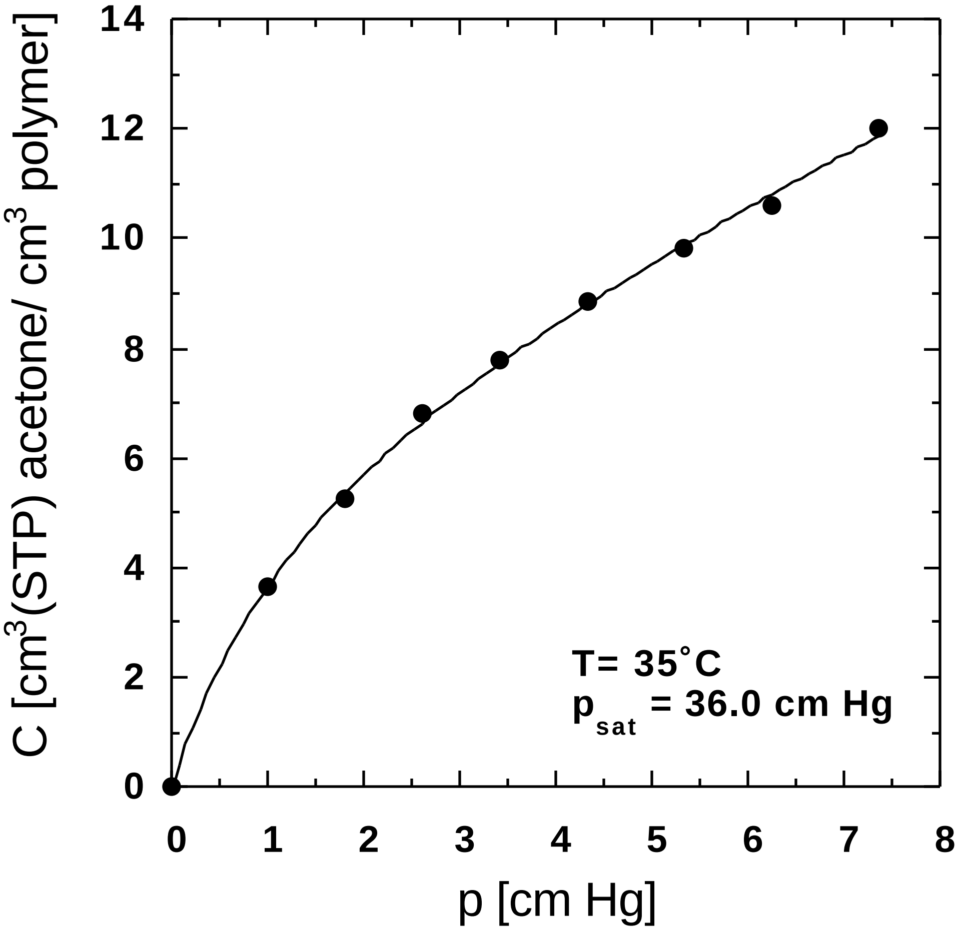

Figure 3.3. Acetone Sorption Isotherm in PET at 35˚C

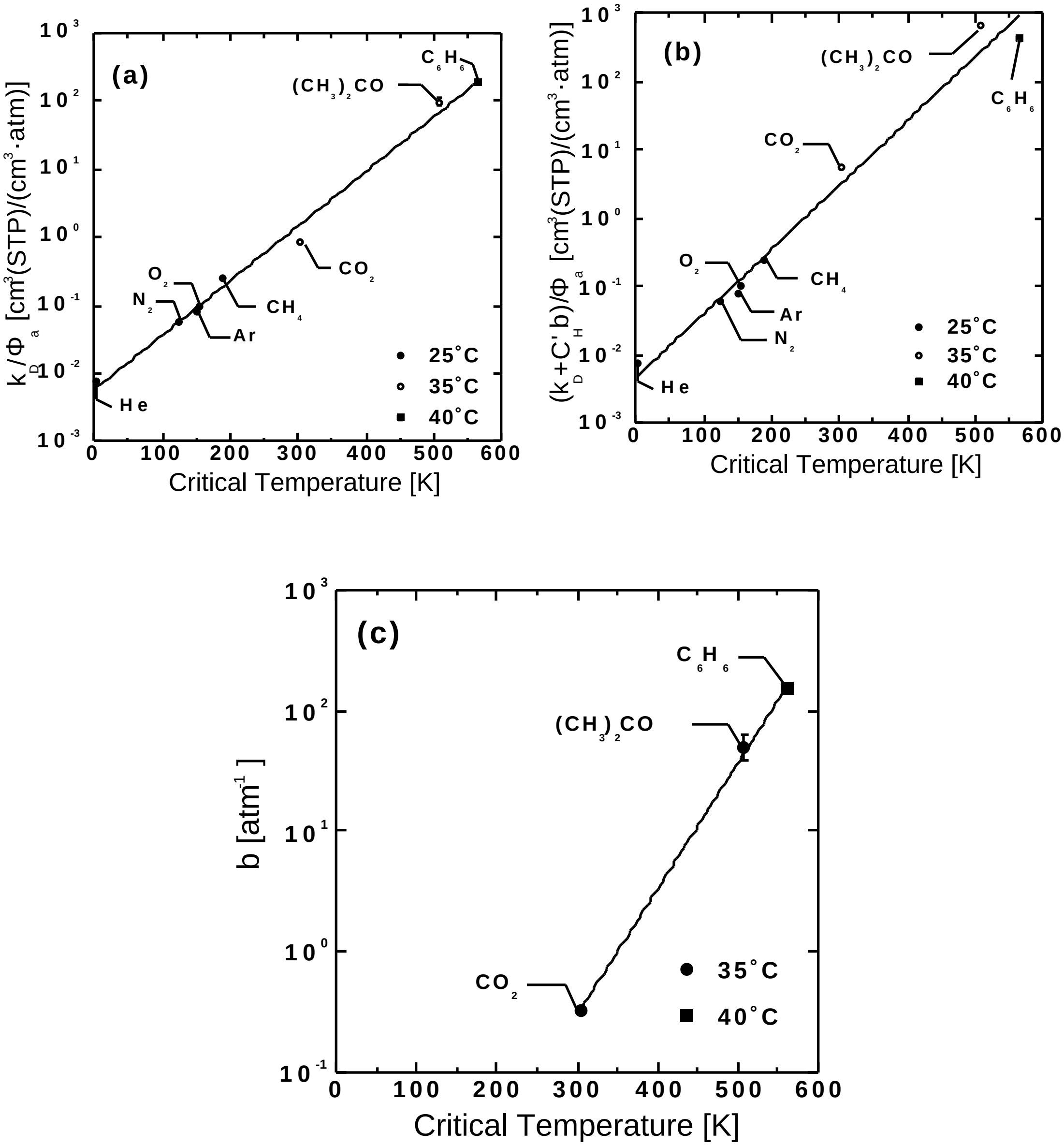

Figure 3.4. Dual Mode Sorption Parameters of PET as a Function of Penetrant Critical Temperature: (a) Henry's Law parameter, (b) Infinite dilution solubility, (c) Langmuir affinity parameter

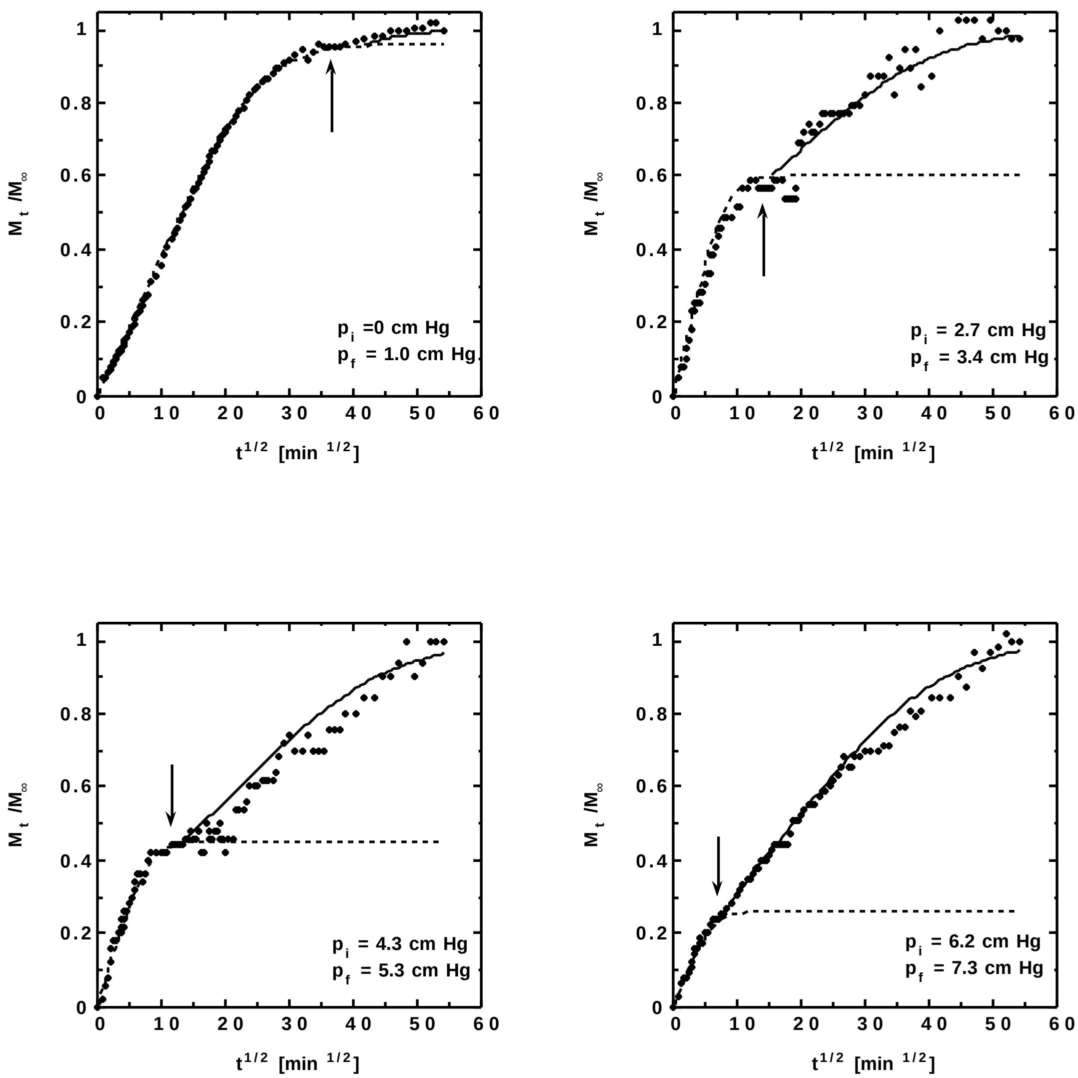

Figure 3.5. Examples of Interval Acetone Sorption Kinetics in PET at 35˚C. The dashed line is the contribution of Fickian-controlled mass uptake kinetics, and the solid line represents the contribution of relaxation-controlled uptake kinetics to the overall mass uptake.

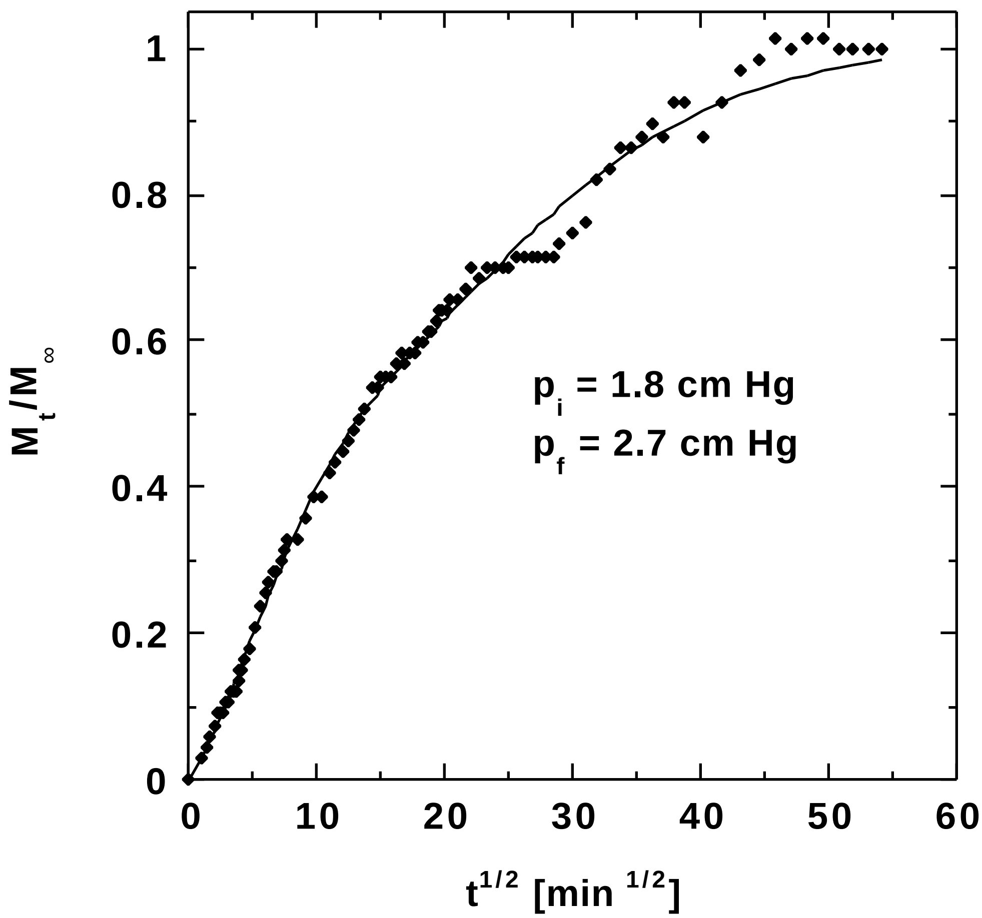

Figure 3.6. Fit of Equation 2 to Interval Kinetic Sorption Data for Acetone in PET

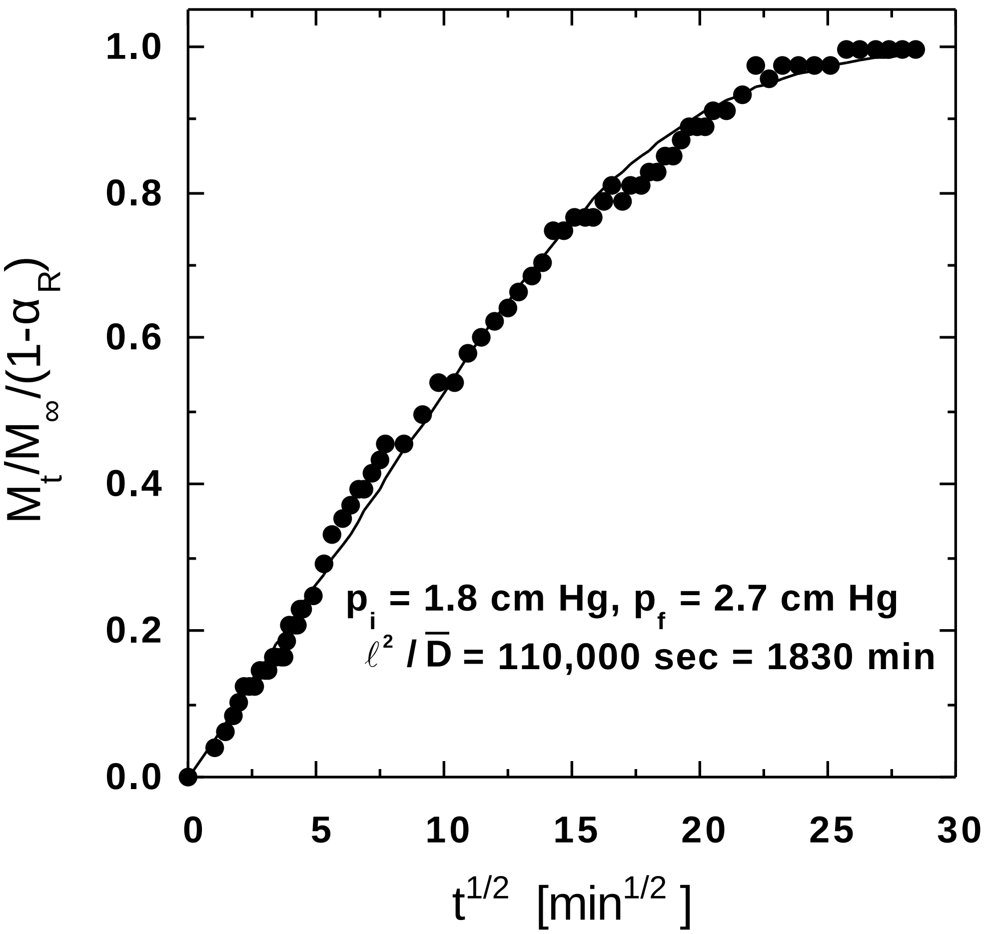

Figure 3.7. Analysis of Fickian Contribution to Acetone Sorption Kinetics in PET

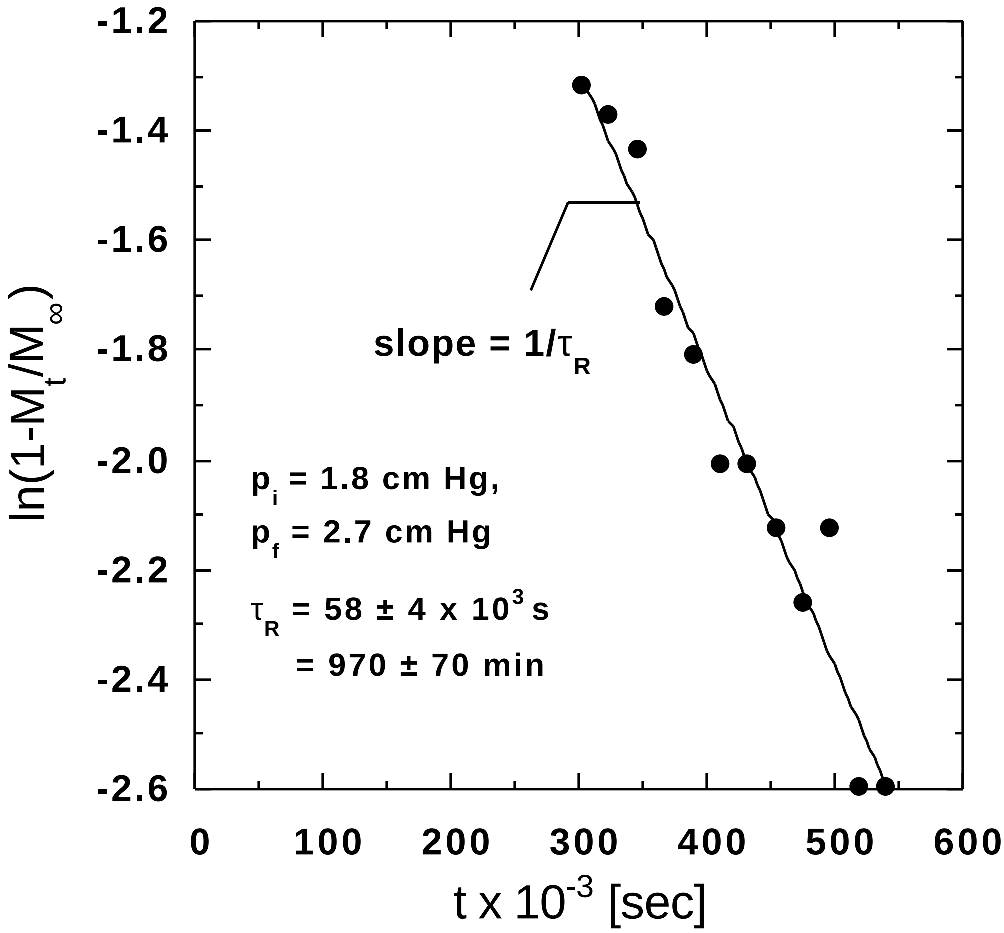

Figure 3.8. Analysis of Relaxation Contribution to Acetone Sorption Kinetics in PET

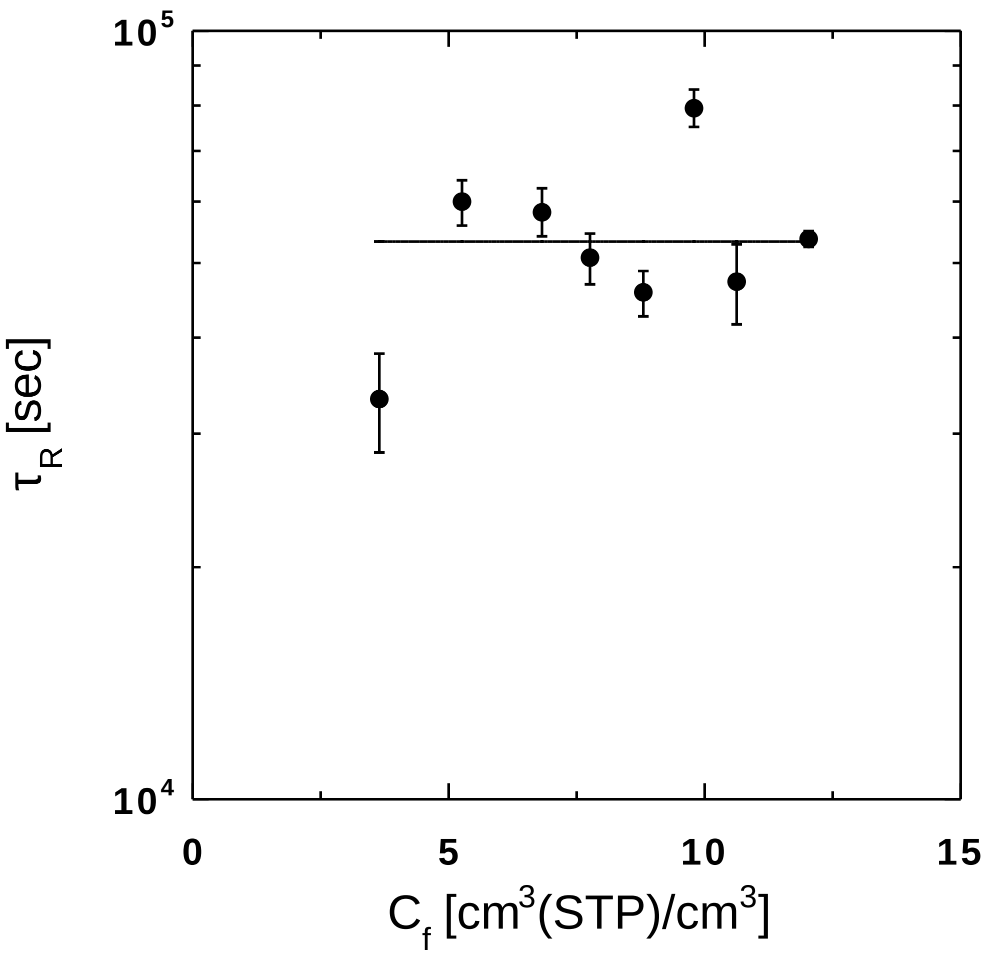

Figure 3.9. Characteristic Time of Relaxation During Incremental Acetone Sorption as a Function of Final Acetone Concentration

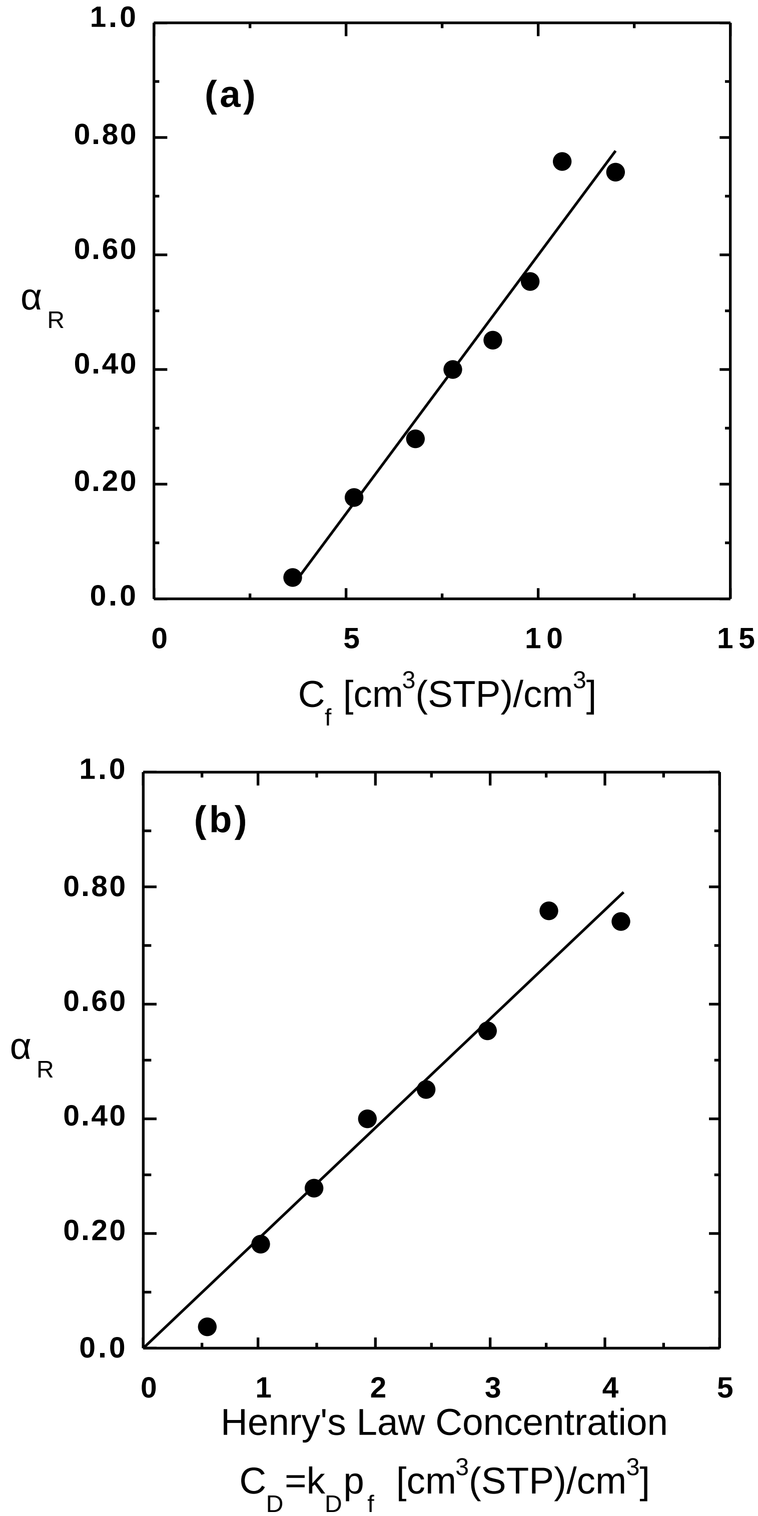

Figure 3.10. Effect of Acetone Concentration on Fraction of Acetone Sorption in PET Associated with Polymer Relaxation: (a) Effect of total acetone concentration, (b) Effect of Henry's law acetone concentration

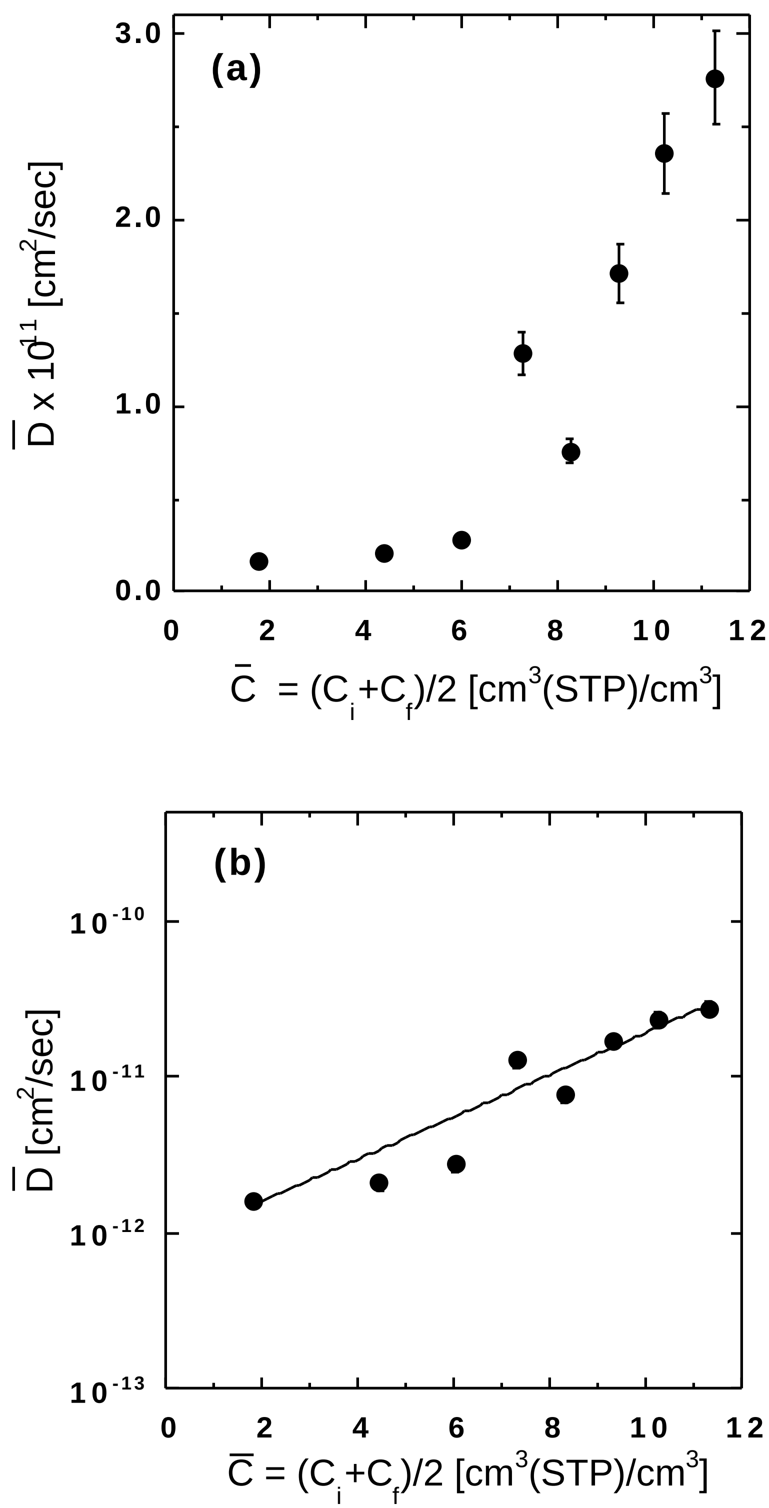

Figure 3.11. Acetone Diffusion Coefficient in PET as a Function of Average Acetone Concentration: (a) Linear scale, (b) Semi-logarithmic scale

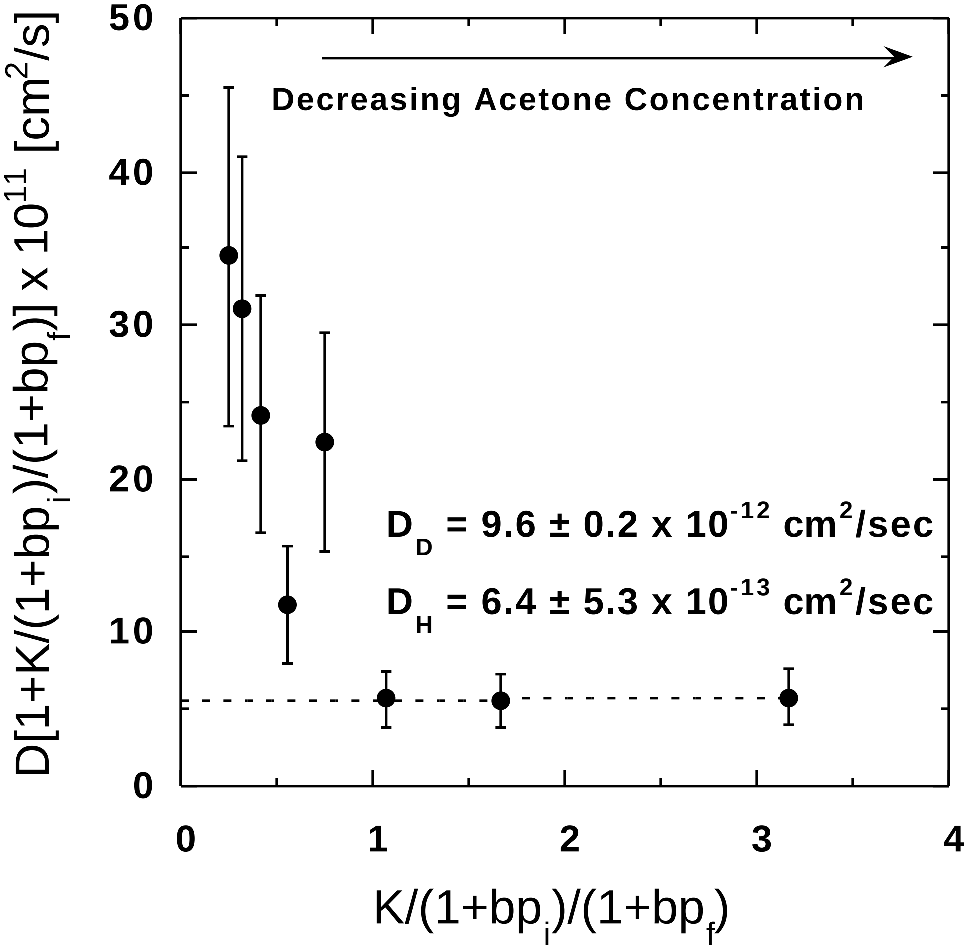

Figure 3.12. Dual Mobility Analysis of Acetone Diffusion in PET

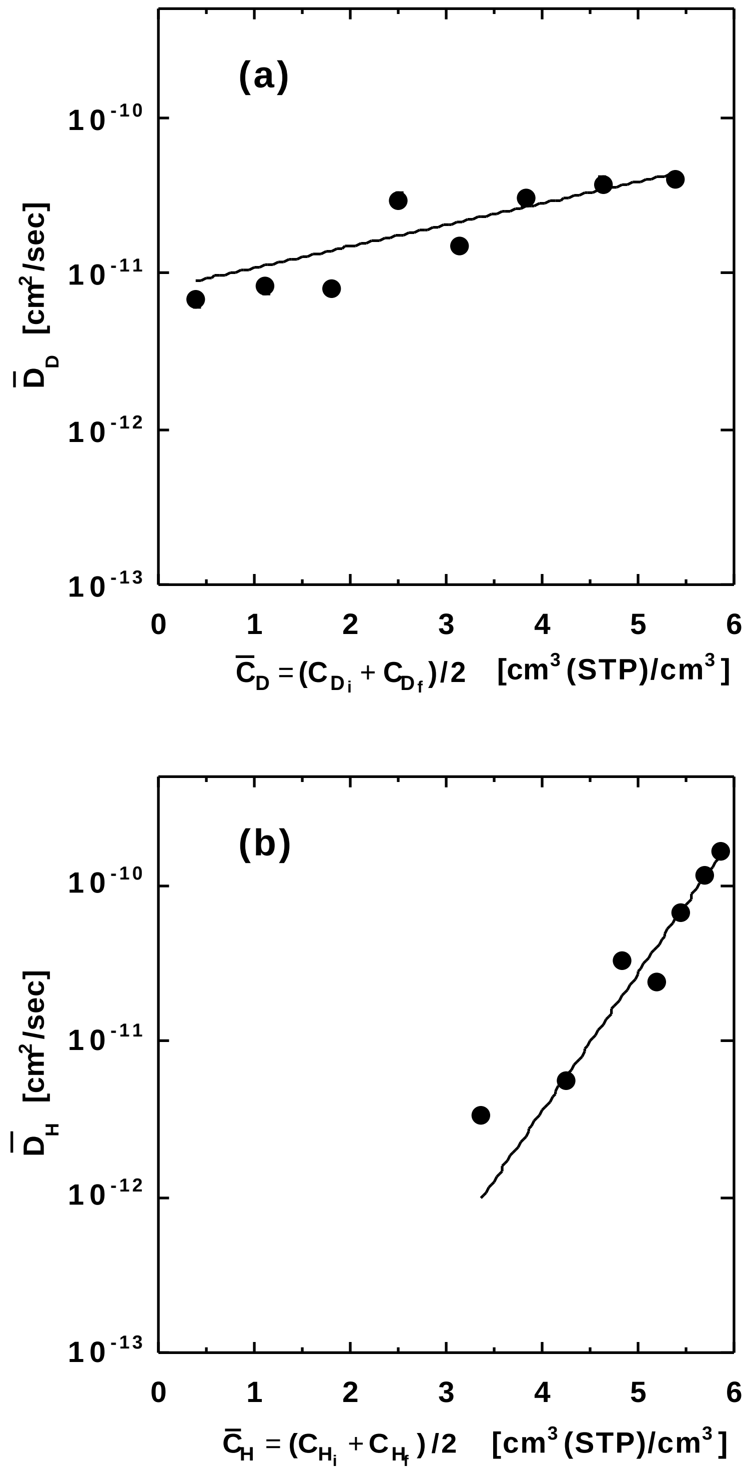

Figure 3.13. Dependence of Diffusivity on Acetone Concentration (a) Acetone Diffusivity in Henry's Law Regions as a Function of Average Acetone Concentration in Henry's Law Regions (b) Acetone Diffusivity in Langmuir Regions as a Function of Average Acetone Concentration in Langmuir Regions

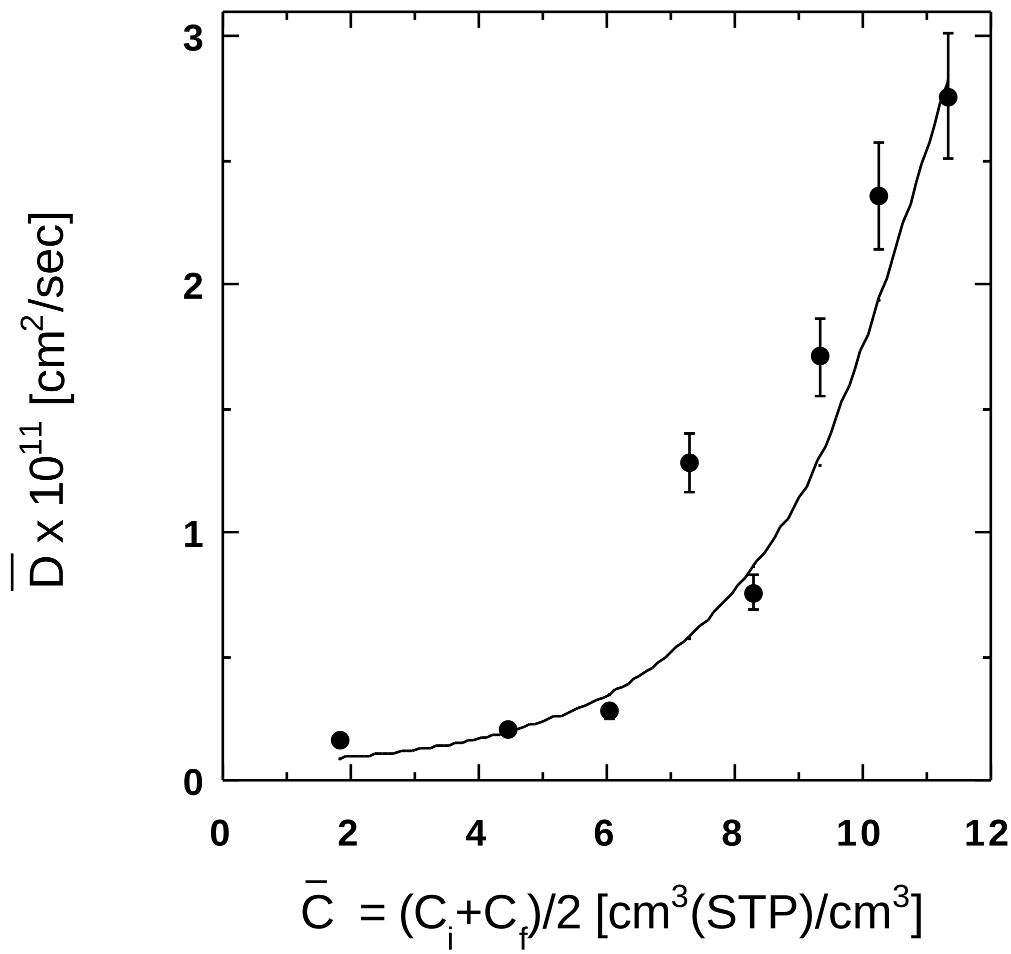

Figure 3.14. Composition Dependence of Acetone Diffusivity and Fit of the Modified Dual Mobility Model

Chapter 4. Synthesis, Physical Characterization, and Acetone Sorption Kinetics in Random Copolymers of Poly(ethylene terephthalate) and Poly(ethylene 2,6-naphthalate)

I. Introduction and Literature Review

Loss of CO_2 from carbonated beverage packages and O_2 ingress from the atmosphere into packages of oxygen-sensitive products can limit the shelf life of these products. Copolymers of poly(ethylene terephthalate) [PET] and poly(ethylene 2,6-naphthalate) [PEN] are of significant commercial interest since the addition of PEN to PET improves gas barrier properties and increases glass transition temperatures.[25] Improved gas barrier properties can increase the shelf life of package contents when the exchange of gas between the package contents and the contiguous atmosphere negatively impacts the packaged product. The increase in glass transition temperature with increasing PEN content makes higher temperature processing steps (*i.e.* hot-filling and retort) more accessible with polymer-based packaging.

The PEN content in PET/PEN copolymers is also known to influence mechanical properties. Santa Cruz, *et al.*[65] prepared quenched samples, which were assumed to be amorphous, and annealed samples, crystallized at about 20˚C below their melting points, of copolymers from 0 to 100% PEN and determined polymer microhardness. In glassy polyesters, microhardness is proportional to yield strength. Microhardness of quenched samples increased monotonically with increasing PEN composition. Crystallinity in annealed samples containing 0-30% PEN and 80-100% PEN was found to contribute to increased microhardness relative to the corresponding amorphous materials.

Blends of PET and PEN can be reactivity processed to form transparent samples at 10% transesterification, suggesting that even low levels of transesterification are sufficient to induce miscibility in blends of these polymers.[66] Dielectric relaxation experiments show that both the α relaxation (glass transition) and β relaxation (ascribed to local motions of ester groups) occur at higher temperatures in PEN than in PET.[67] The higher transition temperatures indicate more restricted long range (α) and local scale (β) molecular motion in the PEN-rich copolymers than in PET.[67]

Lu and Windle studied crystallinity of PEN/PET copolymers.[68] Copolymer melting points were lower than homopolymer melting points due to decreased crystallite size in the copolymers. No crystallinity was observed in annealed and slowly cooled samples containing 40, 50, and 60% PEN, suggesting no co-crystallization of PET and PEN. Samples containing 0-30% and 80-100% PEN contained significant levels of crystallinity. As-drawn fiber and annealed fiber samples exhibited measurable levels of crystallinity at all copolymer compositions. This observation suggested co-crystallization of PET and PEN in highly oriented fiber samples.[68]

The sorption and transport properties of some gases in PEN and PEN/PET copolymers have also been reported. Light and Seymour reported oxygen and carbon dioxide permeability in various polyesters including PET, PEN and a 50/50 copolymer of PET and PEN.[69] These results are presented in Table 1. At 30˚C, CO_2 and O_2 permeability was lower in PEN than in PET, and the permeability of the 50/50 PEN/PET copolymer was between that of homopolymers. The change in oxygen permeability with composition was linked to a change in oxygen diffusivity. Hoffman and Caldwell observed that the effect of polymer composition on oxygen permeability in PEN/PET blends and copolymers could be described using either a simple mixture rule or the Maxwell model.[25] Oxygen permeability was lower in drawn films than in undrawn films.[25] Water vapor sorption capacity is higher in PEN than in PET, however water vapor diffusion coefficients are lower in PEN than in PET.[70]

The transport properties of organic penetrant molecules such as acetone can be more sensitive than those of smaller molecules, such as carbon dioxide and oxygen, to subtle effects of processing and chemistry of polymers.[39-41] Several studies have used acetone to probe the effect of polymer chemistry and processing on the sorption and transport properties of high barrier polyesters.[27,40]

An important consideration in barrier packaging for food products is the loss of organic flavor molecules, such as d-limonene in fruit juices, through sorption of flavor molecules into package walls.[1] Flavor molecule carry-over is emerging as a concern with refillable plastic beverage bottles. In carry-over, flavor molecules sorbed into package walls from an initially-packaged product desorb after refill to influence the taste of the product in the refilled package. To characterize the sorption of flavor molecules into barrier packaging materials, organic penetrants are used as models for flavor molecules.[2]

In this study, the diffusivity and solubility of acetone in solution-cast films of PET/PEN random copolymers were determined as a function of polymer composition. These results are complemented by differential scanning calorimetry [DSC], wide-angle X-ray diffraction [WAXD], densitometry, positron annihilation lifetime spectroscopy [PALS], and infrared spectroscopy [IR] measurements.

II. Experimental

Polymer Synthesis

The PET/PEN copolymers were synthesized in a two-stage process as shown in Figure 4.1. In the first stage, mixtures of dimethyl terephthalate [DMT] and dimethyl 2,6-naphthalate [NDC] (a total of 5.15 moles), an excess of ethylene glycol, and a so-called Type IV catalyst mixture (manganese diacetate, 90 ppm Mn; cobalt diacetate, 90 ppm Co; and antimony trioxide, 350 ppm Sb) were added to a reaction vessel. Heat was applied to begin the ester interchange reaction. The methanol byproduct was removed, and when the reaction temperature had increased to 250˚C, the ester interchange was complete.

In the second stage, which is the polycondensation stage, a phosphorus-containing stabilizer in the form of polyphosphoric acid (82 ppm P) was added to the ester interchange product, and the pressure was gradually reduced to about 0.1 cm Hg as the temperature was increased to about 290˚C to obtain the product.

To prepare copolymers of various compositions, the fraction of the methyl ester monomer consisting of NDC was systematically varied. PET was synthesized using DMT as the only methyl ester monomer. PEN was synthesized using NDC as the only methyl ester monomer. Composition of the copolymers are reported as PET/xPEN, where x is the weight percent of NDC in the original mixture of NDC and DMT added to the reactor.

Film Preparation

Uniform polymer films (~5 μm thick) were prepared by casting a 5% (w/v) solution of the polymer in trifluoroacetic acid at ambient conditions onto a glass plate, and a doctor blade was used to control film uniformity. The samples were allowed to dry at ambient conditions for 24 hours. Afterwards, the films were soaked in a water bath for 24 hours and then in a methanol bath for 24 hours in remove residual solvent. Following the methanol bath, the films were placed in a vacuum oven for 24 hours at room temperature to completely remove the solvent. DSC and sensitive gravimetric desorption studies in a vacuum chamber showed no traces of residual solvent in the final films. Samples richer in PEN than PET/50PEN could not be dissolved in TFAA (or several other solvent systems, such as dichloroacetic acid, 30/70 (w/w) pentafluorophenol/ trichlorobenzene, and 60/40 (w/w) hexafluoroisopropanol/ pentafluorophenol). Therefore, thin films were not prepared for these compositions.

A PET/85PEN sample was extruded as thin tape using a micromelt extrusion apparatus (Hoechst Celanese, Summit, NJ). A slit die (0.005" thick x 0.250" wide) was used to make films approximately 0.25" in width and ranging in thickness from 8 to 12 μm. Before extrusion, the polymer sample was first dried overnight in a vacuum oven at 100˚C and then, with minimum exposure to air, cast into rods using a split tool die. The rod forming temperature was about 15˚C above the softening temperature. Initially, the polymer sample was extruded at melt temperatures ranging from 285˚C to 300˚C to determine the optimum extrusion conditions. The sample used in this study was prepared at the optimum temperature of 296˚C, a take up speed of 20 m/min, and a throughput of 0.45 cm^3/min. The micromelt sample was amorphous by DSC and WAXD.

Thermal and Physical Characterization

A Perkin-Elmer DSC-7, operating at a scan rate of 20˚C/minute, was used to characterize thermal transitions in the copolymers. Thermal transitions were determined from second DSC scans. First scan thermograms were used to evaluate the crystallinity levels of each sample. Wide angle X-ray diffraction spectra were obtained using a Siemens Kristalloflex 4 X-ray Generator and a Siemens type FΘ/2Θ goniometer. The X-rays were produced by a CuKα (λ=1.54 Å) source. Density measurements were performed with a Techne density gradient column using aqueous calcium nitrate solutions with a density range of approximately 1.2 to 1.5 g/cm^3.

Positron Annihilation Lifetime Spectroscopy

The PALS measurements were made in air at room temperature (22.5 ± 1^{o}C) using an automated EG&G Ortec fast-fast coincidence system. The timing resolution of the system was 275 ps determined using the prompt curve from a ^{60}Co source with the energy windows set to ^{22}Na events. Polymer films approximately 5 μm thick were stacked to a total thickness of 1.5 mm on either side of the 30 μCi ^{22}Na-Ti foil source. Five spectra for each sample were collected over a period of 8 hours and the results are the mean values for these spectra. The spectra were modeled as the sum of three decaying exponentials using the computer program PFPOSFIT.[71] The shortest lifetime was fixed at 125 ps characteristic of paraPositronium self annihilation. No source correction was used in the analysis based on a fit for pure Al standards of 169±2 ps, 99.3±0.3 %; 820 ps, 0.7%. Only the orthoPositronium (oPs) components (the longest lifetime, τ_3 and its intensity I_3) are reported as it is the oPs component that is related to annihilations in free volume cavities of the polymer matrix.[72]

Infrared Spectroscopy

Fourier transform infrared spectroscopy measurements were made using a Nicolet Magna-IR 750 FTIR spectrophotometer with a doped silicon carbide ceramic source. The detector was Deuterated Triglycine Sulfate [DTGS] KBr, the spectral resolution was 1 cm^{-1}, and 256 scans were collected per spectrum.

Kinetic Gravimetric Sorption

The kinetics of acetone sorption were recorded using a Cahn RG-2000 electrobalance at 35˚C over a pressure range of 0-5.4 cm Hg. The details of this experimental procedure are recorded elsewhere.[44] Each film was conditioned by exposure to 7.2 cm Hg of acetone and then degassed prior to the gravimetric sorption studies described in this report. This conditioning protocol alleviates penetrant-induced crystallization during the subsequent sorption experiments. Gravimetric sorption studies suggest that exposure of as-cast films to high relative pressures of acetone could increase crystallinity by as much as 4 percent (*cf*. Appendix A). However, DSC studies on samples before and after exposure did not reveal a systematic measurable increase in crystallinity in these samples.

III. Results and Discussion

Polymer Characterization

Figure 4.2a presents a second scan DSC thermogram for a PET/10PEN film. There are three thermal events evident in the thermogram: a glass/rubber transition [T_g], a cold crystallization exotherm [T_c], and a melting endotherm [T_m]. This thermogram is representative of those obtained for all of the other samples. Figure 4.2b presents thermal transition temperatures in the PET/PEN copolymers as a function of copolymer composition. These DSC results were obtained using as-cast films for compositions up to 50% PEN. Since higher PEN compositions could not be prepared as films, the as-synthesized samples were used for compositions of 80%, 90%, and 100% PEN. Glass/rubber transition temperatures [T_g] rise monotonically with increasing PEN content from 81˚C in PET to 123˚C in PEN. There is a single glass/rubber transition for each copolymer, and it's value is always between the glass transition temperatures of the homopolymers. This observation is consistent with a random ester monomer sequence distribution in the chain backbones. The solid curve in Figure 4.2b represents predicted glass transition temperatures based on the homopolymer glass transition temperatures and the Gordon-Taylor Equation for phase-continuous copolymers:[73]

$$\frac{1}{T_g} = \frac{w_{PET}}{T_{g_{PET}}} + \frac{w_{PEN}}{T_{g_{PEN}}} \tag{4.1}$$

where w_{PET} and w_{PEN} are the weight fractions of PET and PEN, respectively, in the copolymers. This equation describes the data well if w_{PET} and w_{PEN} are the weight fractions based on the entire copolymer compositions or the weight fractions based only on the amorphous regions of the polymer matrix.

The thermal transitions are recorded in Table 4.2 for each copolymer composition.

Copolymers rich in either homopolymer contain measurable levels of crystallinity, as indicated by cold crystallization exotherms centered at T_c and melting endotherms centered at T_m in the DSC thermograms. The weight percent crystallinity was calculated as follows:

$$X_c = \frac{\Delta H_m - \Delta H_c}{\Delta H_f} \times 100, \tag{4.2}$$

where ΔH_m is the enthalpy of melting determined by DSC, ΔH_c is the enthalpy of cold crystallization determined by DSC, and ΔH_f is the enthalpy of fusion of the crystallites. The enthalpy of fusion for PET and PEN are 140 J/g and 103 J/g, respectively.[47] For copolymers, the enthalpy of fusion of the crystallites is taken to be that of the homopolymer which is present in the highest amount. This calculation presumes no cocrystallization of PET and PEN, which is consistent with literature reports that cocrystallization occurs only in samples subject to high temperature annealing and high draw ratio.[68] There is no observed crystallinity in samples of intermediate composition, which also supports the notion of no cocrystallization in as-cast films of PET/PEN copolymers. The weight percent crystallinity in each copolymer film determined from DSC results and Equation 4.2 is recorded in Table 4.2.

Figure 4.3 presents wide-angle X-ray diffraction spectra of as-cast PET (Figure 4.3a) and PET/PEN (Figure 4.3b) films. The spectrum of the PET film is typical of other PET spectra[48] and has been described in detail previously (*cf.* Chapter 3). The vertical lines in Figure 4.3a represent the strongest expected diffraction peaks from the most common crystal form of PET.[48] The weight percent crystallinity, as determined from the WAXD spectrum in Figure 4.3a, is 38% for PET, in excellent agreement with the value of 40% determined by DSC (*cf*. Table 4.2). The spectra from the PET/10PEN and PET/20PEN as-cast films show hints of crystalline peaks, but the crystalline diffraction patterns are too weak for quantitative analysis. The WAXD spectrum of the PET/50PEN film exhibits no signs of crystalline diffraction peaks, which is consistent with the DSC result for this film.

As previously reported (*cf*. Chapter 3), the average amorphous peak maximum in the PET sample is at $2\theta = 20.6^{\circ}$, which corresponds to an average d-spacing (estimated from Bragg's Law, $n\lambda=2\sin\theta$)[74] of 4.3 Å. As PEN composition increases, the amorphous peak maximum appears to shift to lower values of 2θ. However, as the amorphous peaks are very broad and not easily discernible due to the presence of crystalline peaks in some of the spectra, the changes in the location of the amorphous peak maxima and associated d-spacings are near the uncertainty limits for this experiment. It should also be noted that other sources[48] represent two amorphous halos in PET, one centered at 3.9 Å and one centered at 5.0 Å. The peak with a d-spacing of 3.9 Å is ascribed to interchain spacing normal to the plane of aligned aromatic rings in the PET matrix. The peak with a d-spacing of 5.0 Å is attributed to interchain spacing in the plane of the aligned aromatic rings.[48] Since crystalline peaks overlap the amorphous region in our PET WAXD spectrum, we are unable to clearly resolve two amorphous halos from our data. Therefore, we report only the peak values of the broad amorphous region of the WAXD spectra. Table 4.3 presents the weight percent crystallinity, amorphous peak maximum, and estimated amorphous d-spacing for each as-cast film sample.

Table 4.4 presents densities of our as-synthesized pellets and as-cast films. For comparison, the data of SantaCruz *et al.*,[65] obtained using annealed and quenched melt-processed films, are also presented. The densities of our samples are lower than the densities reported by SantaCruz *et al.*[65] for annealed films, which should contain significant amounts of high density crystallites in compositions rich in either homopolymer. The density of our as-cast PET film is between the densities of annealed and quenched PET samples of SantaCruz *et al.*[65], which suggests a lower level of crystallinity in our as-cast PET film than in the annealed PET sample of Santa Cruz *et al.* and a higher crystalline content than their quenched sample. The quenched samples of SantaCruz *et al.*[65] were determined to be amorphous by WAXD. However, the densities of our as-synthesized pellets for PET/50PEN and PET/80PEN are lower than the densities of the quenched samples characterized by SantaCruz *et al.*[65] While the reason for this discrepancy is not clear, processing (*i.e.* thermal history) can influence crystalline content as well as the packing of the glassy amorphous phase.[75] Since our samples and those of SantaCruz *et al.* have different thermal histories, this may explain the difference in densities between our samples and those of SantaCruz *et al.*

Figure 4.4 presents amorphous density and amorphous fractional free volume as a function of copolymer composition for as-cast films and as-synthesized pellets. The amorphous density was estimated as follows:

$$\rho_a = \frac{\rho - \frac{X_c}{100}\rho_c}{(1 - \frac{X_c}{100})} \tag{4.3}$$

where ρ_a is the calculated density of the amorphous phase material in the sample, ρ is the measured density, X_c is the weight percent crystallinity determined by DSC, and ρ_c is the crystalline density. The crystalline density of

PET (1.440 g/cm^3)[25] was used as ρ_c for the PET-rich semicrystalline copolymers, and the crystalline density of PEN (1.407 g/cm^3)[76] was used as ρ_c for the PEN-rich semicrystalline copolymers. Fractional free volume in the amorphous phase of the sample [FFV$_a$] was estimated as follows:[4]

$$FFV_a = \frac{\frac{MW}{\rho_a} - V_o}{\frac{MW}{\rho_a}} \tag{4.4}$$

where MW is the average molecular weight of a monomer unit, and V_o is an estimation of the volume occupied by polymer chains. V_o is estimated using the equation:

$$V_o = 1.3 V_W, \tag{4.5}$$

where V_W is the van der Waals volume calculated using the group contribution method suggested by Bondi.[77]

Figure 4.4a shows the calculated amorphous density and amorphous fractional free volume in the PET/PEN as-cast films. There is a small increase in amorphous density, and, accordingly, a decrease in amorphous fractional free volume with increasing PEN content at PEN contents up to 5%. However, reliable density values could not be obtained for two of the as-cast films (PET/10PEN and PET/20PEN), probably due to voids in the sample which arose during the film processing. The apparent densities of those samples were unrealistically low and are not included in Figure 4.4a. Densities of the as-synthesized pellets were also measured for a wider range of copolymer composition.

As shown in Figure 4.4b, the calculated amorphous density values of PET/PEN as-synthesized pellets are higher than the amorphous density of either homopolymer. Accordingly, the fractional free volume of amorphous regions of the copolymers is lower than that of either homopolymer. Therefore, copolymerization of PEN with PET appears to promote more efficient chain packing in the amorphous regions of the polymer matrix than in either homopolymer. Deviations from simple linear additive mixing rules for density data are often exhibited in compatible multicomponent polymers.[23] For example, miscible amorphous blends of polystyrene and poly(2,6-dimethyl-1,4-phenylene oxide) have higher densities (and, therefore, lower fractional free volumes) than either polystyrene or poly(2,6-dimethyl-1,4-phenylene oxide) alone.[24]

Density provides a convenient characterization of so-called static (*i.e.* packing-related) free volume as a function of chemical structure in these copolymers. However, both static and dynamic (sub-T_g mobility related) free volume influence transport in glassy polymers.[4,72] Dynamic free volume can be probed by small angle X-ray scattering, xenon nuclear magnetic resonance, molecular dynamics, and positron annihilation lifetime spectroscopy [PALS]. PALS can be used to characterize both static and dynamic free volume cavity size and relative concentration of free volume cavities accessible to orthoPositronium (oPs).[72]

PALS probes the environment experienced by oPs localized in free volume cavities between and along the chains and at chain ends.[72] These cavities typically range in radius from 0.2 to 0.5 nm, which compares well with non-bonded interatomic distances in polymers and molecular radii of diffusing substances. The lifetime of the oPs component, τ_3, is generally believed to be related to the mean size of the free volume cavity in which oPs localizes in the polymer. The relative number of oPs annihilations, I_3, provides an indication of the concentration of free volume cavities. Thus the parameters τ_3 and I_3 can give information on the relative free volume cavity size and concentration accessible to oPs, which has a diameter of 3.88 Å. By assuming spherical cavities and relating the lifetime to the cavity radius, τ_3^3 characterizes the free volume cavity volume (since volume is proportional to the cube of the radius). A relative measure of total free volume accessible to oPs over the course of it's nanosecond-scale lifetime is provided by multiplying the cavity volume by the concentration (*i.e.* $\tau_3^3 I_3$).

For compositions from PET up to PET/50PEN, as-cast films were used for PALS measurements. Data for PEN was obtained using a melt-processed PEN film. The results of the PALS analysis are shown in Figure 4.5. Based on results from previous studies, oPs localizes in the disordered amorphous regions of polyesters rather than in the crystallites.[78,79] For this reason, the PALS free volume parameter $\tau_3^3 I_3$ has been normalized by the amorphous volume fraction, Φ_a, to provide an estimate of the total relative free volume in the amorphous regions of the polymer matrix as probed by PALS.[80] As shown in Figure 4.5, the PALS-based free volume decreases monotonically with increasing PEN composition, and most of the reduction occurs at low PEN content.

Integral Acetone Sorption Kinetics

Figure 4.6 presents the fractional mass uptake of acetone in a PET film as a function of $t^{1/2}$ for an integral sorption experiment at 5.4 cm Hg and 35˚C. The data for sorption in the PET film is representative of the sorption data for the other films. The integral sorption kinetics are well described by the following solution to Fick's Law for diffusion in a plane sheet of uniform thickness:[5]

$$\frac{M_t}{M_\infty} = 1 - \frac{8}{\pi^2}\sum_{n=0}^{\infty}\frac{1}{(2n+1)^2}\exp\left(\frac{-\bar{D}(2n+1)^2\pi^2 t}{\ell^2}\right) \tag{4.6}$$

where M_t and M_∞ are the penetrant mass uptake (normalized by the initial polymer sample weight) at time t and ℓ is the film thickness. $\bar{D}$ is approximately equal to the effective average diffusion coefficient over the concentration interval of the experiment:[5]

$$\bar{D} = \frac{1}{C_f - C_i}\int_{C_i}^{C_f} D\,dC, \tag{4.7}$$

where C_i and C_f are the penetrant concentrations at the beginning and end of the experiment, respectively, and D is the effective diffusion coefficient in the semicrystalline polymer.

A least squares fit of the data to Equation 4.6 is shown as the solid curve in Figure 4.6. From this least-squares fit, values of $\bar{D}$ and M_∞ are determined. The solubility coefficient, S, in $cm^3(STP)/(cm^3 \cdot atm)$, can be calculated from M_∞ as follows:

$$S = M_\infty \times \frac{\rho}{MW_{penetrant}} \times \frac{22{,}414}{p} \tag{4.8}$$

where p is the penetrant pressure in atm, $MW_{penetrant}$ is the penetrant molecular weight in g/mole, and 22,414 is a conversion factor.

Solubility of Acetone in PET/PEN Copolymers

Figure 4.7a presents acetone solubility in PEN/PET copolymers as a function of weight percent PEN for integral sorption experiments at 35˚C and an acetone relative pressure of 0.15 (5.4 cm Hg acetone pressure). The solubility coefficients decrease modestly with increasing PEN content. The acetone solubility in the PET/85PEN sample is approximately 30% lower than the acetone solubility in PET. From solubility parameter values, acetone is expected to be more soluble in PET than in PEN. The solubility parameter of acetone is 9.9 $(cal/cm^3)^{1/2}$,[81] while the estimated solubility parameters of PET and PEN are 10.8 $(cal/cm^3)^{1/2}$ and 11.2 $(cal/cm^3)^{1/2}$, respectively, based on the group contribution method of Hoy.[82] As the acetone solubility parameter is closer to that of PET than to that of PEN, it is not surprising that acetone is somewhat more soluble in PET than PEN.[82] Therefore, based solely on considerations of chemical structure, acetone solubility should decrease with increasing PEN content. However, crystallinity decreases with increasing PEN content for the films used in sorption experiments, and crystallinity generally precludes sorption of even the smallest penetrant molecules.[15,18,20]

In an attempt to separate the effects of composition and crystallinity on acetone solubility, Figure 4.7b presents amorphous phase acetone solubility as a function of the volume fraction of PEN in the amorphous regions of the copolymer. The solubility in the amorphous phase is estimated using a two phase model:[18]

$$S = \Phi_a S_a, \tag{4.9}$$

where Φ_a is the amorphous volume fraction in the semicrystalline polymer, and S_a is the solubility of penetrant in the amorphous regions of the polymer matrix. This model has been applied with excellent success to describe the effect of crystallinity on gas solubility in rubbery polymers[15,18] and provides a good description of the effect of crystallinity on gas solubility in PET.[20]

The volume fraction of PEN in the amorphous phase, $\Phi_{a,PEN}$, was estimated from the following equation:

$$\Phi_{a,PEN} = \frac{\dfrac{w_{PEN}}{\rho_{a,PEN}}}{\dfrac{w_{PEN}}{\rho_{a,PEN}} + \dfrac{X_C}{100\rho_{c,PET}} + \dfrac{\left[(1-w_{PEN}) - \dfrac{X_C}{100}\right]}{\rho_{a,PET}}} \tag{4.10}$$

where w_{PEN} is the weight fraction PEN in the copolymer, $\rho_{a,PEN}$ is the amorphous density of PEN (1.328 g/cm^3)[65], $\rho_{c,PET}$ is the crystalline density of PET (1.440 g/cm^3)[25], and $\rho_{a,PET}$ is the amorphous density of PET (1.327 g/cm^3).[25] This equation accounts for the fact that all of the crystallites in copolymers with high concentrations of PET are presumably composed of PET. Thus, PEN units are excluded from the crystalline regions and are, therefore, only present in the amorphous regions of the sample.

The estimated amorphous phase acetone solubility coefficients depend more strongly on polymer composition than the solubility coefficients in the semicrystalline samples (*cf*. Figure 4.7a). The trend with composition is, however, the same. Acetone solubility generally decreases with increasing PEN content. This trend is consistent with the order of the solubility parameters of acetone, PET, and PEN. Interestingly, most of the approximately two-fold variation of amorphous phase acetone solubility with composition occurs at low (i.e. <10 wt%) PEN content. To understand these trends in solubility with polymer composition better, the data were compared to two theoretical models.

A simple relation has been used to describe penetrant solubility in heterogeneous copolymers and blends (i.e. systems where there is no interaction between the two homopolymers):[83,84]

$$S_a = \Phi_{a,PEN} S_{a,PEN} + \Phi_{a,PET} S_{a,PET} \qquad (4.11)$$

where $\Phi_{a,PET}$ is the volume fraction of PET in the amorphous phase, $S_{PET,a}$ is the solubility in amorphous PET, and $S_{PEN,a}$ is the solubility in amorphous PEN. This model predicts a linear variation of solubility with PEN volume fraction in the amorphous phase and, as a result, clearly cannot describe the data in Figure 4.7b. As the components in these random copolymers are intimately mixed, and negative deviations from linear additivity of specific volume are not observed, it is not surprising that this simple two-phase, non-interacting model fails to describe the data.

The following relation, derived from ternary solution thermodynamics, has been used to describe penetrant solubility in homogeneous multicomponent polymers:[23]

$$\ln S_a = \Phi_{a,PEN} \ln S_{a,PEN} + \Phi_{a,PET} \ln S_{a,PET} + \frac{\gamma \tilde{V}_3}{RT} \Phi_{a,PEN} \Phi_{a,PET} \qquad (4.12)$$

where γ is a binary interaction parameter describing the mixing of the two polymer components, $\tilde{V}_3$ is the molar volume of the small molecule penetrant, and R is the ideal gas constant. Since we have not measured $S_{a,PEN}$ and do not wish to include it as an adjustable parameter in the model, we use the following method to eliminate $S_{a,PEN}$ from Equation 4.12. Based on the measured solubility data point at the highest PEN content, PET/85PEN, and the assumption that Equation 4.12 adequately describes solubility in the composition range from 85% PEN to 100% PEN, Equation 4.12 can be rearranged to eliminate $S_{a,PEN}$:

$$\ln S_a = \Phi_{a,PEN}\left(\frac{\ln S_{a,PET/85PEN} - 0.15\ln S_{a,PET} - \frac{\gamma\tilde{V}_3}{RT}(0.15)(0.85)}{0.85}\right) + \Phi_{a,PET}\ln S_{a,PET} + \frac{\gamma\tilde{V}_3}{RT}\Phi_{a,PEN}\Phi_{a,PET} \qquad (4.13)$$

where $S_{a,PET/85PEN}$ is the experimentally determined value of acetone solubility in amorphous PET/85PEN, 98 cm^3(STP)/(cm^3·atm). $S_{a,PET}$, the solubility of acetone in the amorphous phase of PET, is 208 cm^3(STP)/(cm^3·atm). This value is estimated from the measured solubility in the semicrystalline as-cast film, S, which was then corrected for crystallinity according to Equation 4.9. Equation 4.13 contains only one adjustable parameter, γ. The curve in Figure 4.7b represents the best fit of Equation 4.13 to the data. Using an acetone pure liquid molar volume calculated from the Hankinson-Brobst-Thomson correlation[43] (75 cm^3/mole), the parameter γ is estimated to be -21 ± 7 cal/cm^3 from the fit of Equation 4.13 to the data in Figure 4.7a. A negative value of γ generally results when the homopolymers exhibit specific interactions.[23] This result is qualitatively consistent with the increase in amorphous phase density (relative to the homopolymers) observed in the copolymers.

The model predicts a minimum in acetone solubility with PEN content. This minimum is not evident from the limited set of experimental data which are available. However, in general, Equation 4.13 provides reasonable agreement with the experimental data, particularly in light of the fact that it is typically used to describe gas solubility in amorphous multicomponent polymer systems. Moreover, since the model is based on an equilibrium description of multicomponent polymer mixing, it cannot predict changes in non-equilibrium excess volume in these glassy polymers. Finally, our experiments are performed at fixed acetone activity and, therefore, at finite acetone concentration in the polymer. We have attempted to extend Equation 4.13 to describe solubility data in systems such as ours, where solubility changes with penetrant pressure. In view of these approximations, the fit of the model provides tothe experimental data, with only one adjustable parameter, is good.

Diffusivity of Acetone in PET/PEN Copolymers

The values of $\bar{D}$ obtained from fitting acetone kinetic uptake data of as-cast films to Equation 4.6 are presented in Figure 4.8a. In contrast to the solubility data in Figure 4.7a, the acetone diffusion coefficient in PET/85PEN is 93% lower than the acetone diffusion coefficient in PET. Relative to acetone diffusivity in PET, a 53% reduction in acetone diffusivity is observed in the copolymer films containing only 10% PEN. Interestingly, the weight percent crystallinity in the copolymers decreases from 40% to 2% over the same composition range. Crystallites are commonly understood to act as impenetrable barriers to small molecules and act to increase the effective path length for diffusion, thereby depressing macroscopic effective diffusion coefficients.[14,17,19] Therefore, the observed dramatic decrease in diffusivity with increasing PEN content is in the opposite direction expected based simply on the crystalline content of the samples. The decrease in diffusivity with increasing PEN content may be expected based on improved packing in the amorphous phase of the copolymers (*i.e.* a reduction in FFV_a with increasing PEN content) and on restricted segmental motion in the copolymers (*i.e.* an increase in T_g with increasing PEN content). These two effects, which act to decrease diffusion coefficients, apparently override the crystallinity effect, which acts to increase diffusion coefficients with increasing PEN content.

The effect of crystallinity on diffusion coefficients in PET can be estimated from:[19]

$$\bar{D} = D_a / \tau \tag{4.14}$$

where D_a is the calculated diffusion coefficient in the amorphous region of the polymer matrix, and τ is a geometric impedance factor accounting for the increase in path length due to the impenetrable crystallites in the amorphous polymer matrix.[19] For gas diffusion in PET, Michaels *et al.* observed that τ can be expressed as a simple function of amorphous volume fraction of the polymer:[19]

$$\tau = 1/\Phi_a . \tag{4.15}$$

Figure 4.8b presents the calculated amorphous phase acetone diffusivity, estimated from Equations 4.14 and 4.15, as a function of PEN volume fraction in the amorphous region of the copolymers.

The following relationship has been used to describe the composition dependence of small molecule diffusion in homogeneous multicomponent polymer systems:[23]

$$\ln \bar{D}_a = \Phi_{a,PET} \ln \bar{D}_{a,PET} + \Phi_{a,PEN} \ln \bar{D}_{a,PEN} + (aRT - 1)\frac{\Delta E_{12}}{RT} \tag{4.16}$$

where $\bar{D}_{a,PET}$ is the diffusion coefficient in amorphous PET, $\bar{D}_{a,PEN}$ is the diffusion coefficient in amorphous PEN, and ΔE_{12} is a term accounting for deviations in the additivity of activation energies for diffusion. The constant a comes from the observed relationship between activation energy for diffusion and infinite dillution coefficient, D_o,[23]

$$\ln D_o = aE_D + c. \tag{4.17}$$

where a is 0.001/R for glassy polymers,[1,8] and c is an empirical parameter. Since the acetone diffusion coefficient was not measured for PEN, $D_{a,PEN}$ was eliminated from Equation 4.16 by using the measured value of the acetone diffusion coefficient in PET/85PEN and assuming Equation 4.16 could be used to describe the data from 85% PEN to 100% PEN. The composition dependence of ΔE_{12} is taken to be:[23]

$$\Delta E_{12} = \omega \Phi_{a,PET} \Phi_{a,PEN} \tag{4.18}$$

where ω is an adjustable parameter reflecting the magnitude of the activation energy deviation term, ΔE_{12}. The resulting modified form of Equation 4.16 is:

$$\ln \overline{D}_a = \Phi_{a,PEN} \left(\frac{\ln \overline{D}_{a,PET/85PEN} - 0.15 \ln \overline{D}_{a,PET} - (aRT - 1)\dfrac{\omega(0.15)(0.85)}{RT}}{0.85} \right) + \Phi_{a,PET} \ln \overline{D}_{a,PET} + (aRT - 1)\frac{\omega \Phi_{a,PET} \Phi_{a,PEN}}{RT} \tag{4.19}$$

where $\overline{D}_{a,PET/85PEN}$ is the measured acetone diffusivity in amorphous PET/85PEN. The results of fitting of the experimental data to Equation 4.19 are presented as the curve in Figure 4.8b. In this fit, $\overline{D}_{a,PET}$ is constrained to the average value of the estimated amorphous diffusion coefficient, which was calculated from two independent measurements of diffusion coefficients in the semicrystalline as-cast film and Equations 4.14 and 4.15.. From a least squares fit of the model to the data, the best value of ω is 11 ± 0.2 kcal/mol. There are no published results for activation energy of acetone diffusion in PET or PEN. However, the value of ΔE_{12}, which ranges from 0 to 2.75 kcal/mol based on Equation 4.18, is probably a non-negligible fraction of the activation energy of acetone diffusion in these stiff, glassy polyesters. This result, like the result of the fit of Equation 4.13 to the solubility data, suggests substantial specific interactions between PET and PEN in these copolymers. As with Equation 4.12, Equation 4.16 has previously only been used to describe gas diffusion coefficients in amorphous multicomponent polymer systems, and it does not account for the concentration dependence of the diffusion coefficients. Based on these simplifications, the agreement of the model with the experimental data should be regarded as excellent.

<u>Calculated Permeability of Acetone in PET/PEN Copolymers</u>

In polymers obeying the solution-diffusion mechanism, when downstream penetrant pressure is much less than upstream pressure, the steady-state permeability of the polymer film to acetone may be estimated as the product of solubility and diffusivity.[27] The results of this calculation are presented in Figure 4.9 as a function of weight percent PEN. Calculated acetone permeability decreases systematically as PEN concentration in the copolymer increases. For example, the calculated acetone permeability of PET/85PEN is 94% lower than the calculated acetone permeability of PET homopolymer. A 63% decrease in calculated acetone permeability (relative to PET permeability) is observed in PET/10PEN. This reduction is primarily due to a decrease in acetone diffusivity upon addition of low levels of PEN to PET. Error bars for Figures 4.7-4.9 were estimated using a propagation of error technique.[58] The largest source of error in diffusivity and calculated permeability values is the uncertainty associated with measurement of the thickness of the polymer films.

Figure 4.10 presents the estimated permeability of acetone from this study and the measured permeability of oxygen [25] in reactively processed, miscible PET/PEN blends as a function of weight percent PEN. For both oxygen and acetone, the permeability of the copolymers has been normalized by the permeability of PET. The two data sets were collected using different experimental protocols on samples prepared differently. The oxygen data are from direct permeation experiments using a MOCON Oxtran permeability tester operating at 23˚C and 75% relative humidity.[25] The films for these tests were melt processed from blends of pure PEN and PET that were subject to two extruder passes at 295˚C to make phase-miscible copolymers.[25] Despite the differences in processing and permeability measurement methodology, the reduction in permeability with increasing PEN content is greater for acetone (a large molecule with a Lennard-Jones diameter of 4.6 Å) [43] than for oxygen (a smaller molecule with a Lennard-Jones diameter of 3.47 Å).[43] This trend has been observed previously in a study of the effect of thermal annealing on gas and vapor permeation in a thermotropic copolyester.[41] One of the most widely used models of the effect of free volume on penetrant diffusion coefficients, the Cohen-Turnbull model,[42] suggests that the diffusion coefficients of larger penetrants are more sensitive than those of smaller penetrants to changes in the amount of free volume in the polymer matrix. As acetone is substantially larger than oxygen, it's diffusion coefficient, and, in turn, it's permeability coefficient should be a more sensitive probe of subtle processing-induced changes in the free volume or free volume distribution in the polymer matrix.

Effect of Free Volume on Acetone Diffusion Coefficients

Small molecule transport properties in polymers are very sensitive to chain packing in the solid state. A common characterization of chain packing is fractional free volume. The Doolittle equation presented below has been used with considerable success to describe qualitatively the influence of chain packing on gas diffusion coefficients in amorphous glassy polymers:[4]

$$\overline{D} = A\exp\left(\frac{-B}{FFV}\right) \tag{4.20}$$

where B and A are empirical constants. In our copolymer films, some of which are semicrystalline, the fractional free volume, FFV, in Equation 4.20 is replaced by FFV_a, the amorphous phase fractional free volume since FFV_a is presumably the free volume available to participate in molecular transport of penetrant molecules. $\overline{D}$ in Equation 4.20 is replaced by $\overline{D}/\Phi_a$ to provide an estimate of the diffusivity in amorphous regions of the polymer. Figure 4.11a presents estimated amorphous acetone diffusion coefficients in as-cast films as a function of reciprocal fractional free volume of the amorphous polymer in the as-cast films. While the correlation is somewhat scattered, there is a general decrease in amorphous diffusion coefficient with increasing reciprocal amorphous fractional free volume.

Figure 4.11b presents estimated amorphous acetone diffusion coefficients in the as-cast films as a function of the inverse PALS-based relative amorphous free volume in the as-cast films. The diffusion coefficients appear to be strongly correlated with this measure of relative free volume, suggesting that the free volume probed by PALS is important in the transport of acetone in the as-cast copolymer films. Support for this strong correlation comes from modeling of the diffusion coefficient for penetrants in glasses using molecular dynamics simulations and transition state theory.[85,86] Modeling has suggested that the rate determining factor for penetrant diffusion is the time spent by the penetrant in a free volume cavity while waiting for a neck opening to a neighboring cavity. This timescale is 1 ns or longer, similar to the nanosecond-scale lifetime of the PALS oPs probe.

Conformational Analysis by Infrared Spectroscopy

Infrared (IR) spectroscopy has been used to measure the conformation of ethylene glycol linkages in the polymer backbone of PET.[75] The ethylene glycol (EG) residue in PET can exist in either the trans or gauche conformation.[75] Gas transport properties of PET have been correlated with ethylene glycol linkage conformation determined by IR. Slee, *et al.* studied oxygen diffusion in films drawn under various conditions.[87] The oxygen diffusivity in PET was lowered by drawing the films. Drawing was accompanied by an increase of trans conformation of the ethylene glycol residues in the amorphous regions of the polymer matrix and an increase in crystallinity, which increases the total trans content of the sample. Vieth, *et al.*, considered IR measurements of glycol linkage conformation when studying carbon dioxide sorption in PET.[88] They observed a strong positive correlation between the fraction of ethylene glycol linkages in the gauche conformation and Langmuir sorption capacity, C'_H,[88] which is associated with the non-equilibrium excess volume in the amorphous regions of the glassy polymer matrix.[7]

The infrared spectra were collected for each solvent-cast copolymer film to characterize the fraction of EG units in the trans conformation in the amorphous regions of the polymer. As the EG unit can be in the gauche or trans conformation, the following equation represents an overall mass balance on EG units:

$$T + G = 1 \tag{4.21}$$

where T is the weight fraction of EG units in the trans conformation, and G is the weight fraction of EG units in the gauche conformation. The fractions T and G are calculated from IR peak areas using the following equations:

$$T = \frac{A_{1337\ cm^{-1}}}{A_{1337\ cm^{-1}} + A_{1365\text{-}70\ cm^{-1}}} \tag{4.22}$$

$$G = \frac{A_{1365\text{-}70\ cm^{-1}}}{A_{1337\ cm^{-1}} + A_{1365\text{-}70\ cm^{-1}}} \tag{4.23}$$

where $A_{1337\ cm^{-1}}$ is the area under the IR peak at 1337 cm^{-1} and $A_{1365\text{-}70\ cm^{-1}}$ is the area under the peak in the 1365-70 cm^{-1} wavenumber range. The 1337 cm^{-1} peak in both PET and PEN is attributed to wagging of CH_2 groups in the trans conformation.[89] The medium weak 1365 cm^{-1} peak in PET and the medium strong 1370 cm^{-1} peak in PEN are attributed to the wagging of CH_2 groups in the gauche conformation.[89] The peak of this band tends to shift to higher wavenumbers with increasing PEN content. A similar analysis was reported by Lin and Koenig[75] for PET. They observed a linear relationship between the amount of amorphous phase EG units in the trans conformation and amorphous phase density, suggesting a strong correlation between amorphous phase packing and EG conformation.

Since the 1337 and 1365-70 cm^{-1} bands are evident in both homopolymers and are attributed to the same vibration in different conformations, these bands were used in the following analysis. All of the ethylene glycol linkages in the crystalline phase are commonly understood to be in the trans conformation, but amorphous material contains a mixture of EG linkages in the trans and gauche conformations.[75] Therefore, Equation 21 can be rewritten as follows:

$$T_a + T_c + G = 1 \tag{4.24}$$

where T_a is the weight fraction of polymer that is amorphous and contains ethylene glycol linkages in the trans conformation. T_c is the weight fraction of polymer that is crystalline and contains ethylene glycol linkage in the trans conformation. Since all crystalline material is in the trans conformation:

$$T_c = X_c / 100. \tag{4.25}$$

Therefore, Equations 4.21-4.25 can be combined as follows to estimate the weight fraction of polymer in the amorphous phase and having ethylene glycol units in the trans conformation:

$$T_a = 1 - \frac{X_c}{100} - \frac{A_{1365-70\ cm^{-1}}}{A_{1337\ cm^{-1}} + A_{1365-70\ cm^{-1}}} \tag{4.26}$$

Figure 4.12a presents an IR spectrum of an as-cast PET/10PEN film. Figure 4.12b shows the same spectrum on a scale convenient for inspection of the two bands used in the analysis. These spectra are representative of the spectra of the other films. Based on the peak areas from the IR spectra, crystallinity values from Table 4.2 and Equation 4.26, the estimated fraction of amorphous phase EG units in the trans conformation was calculated for each of the solvent cast films. The results are presented in Figure 4.13. Within the approximate nature of the calculation and the uncertainty associated with each point, trans amorphous content increases systematically with increasing PEN content. In PET, the estimated density of amorphous material containing 100% trans EG units is approximately 8% higher than that of amorphous material containing 100% gauche EG units.[75] If this observation also applies to PET/PEN copolymers, then an increase in amorphous trans EG concentration with increasing PEN content suggests higher amorphous phase densities and lower amorphous phase free volume, consistent with the results in Figures 4.4 and 4.5.

Figure 4.14a presents acetone diffusion coefficients as a function of T_a. Acetone diffusion coefficients generally decrease with increasing values of T_a. An increase in the fraction of EG units in the trans conformation in the amorphous regions of the polymer may correlate with an increase in amorphous phase density, as shown previously, for PET[75] and therefore to a decrease in penetrant diffusivity. The correlation between acetone diffusion coefficient and T_a is slightly better if the calculated amorphous phase acetone diffusion coefficients are presented as a function of T_a as shown in Figure 4.14b.

IV. Conclusions

A series of random copolymers of PET and PEN were synthesized and characterized by DSC, WAXD, PALS, IR spectroscopy, and acetone sorption. The glass transition temperatures of the copolymers rise monotonically from 81°C in PET to 123°C in PEN. Copolymers with compositions rich in either homopolymer are semi-crystalline while copolymer of intermediate composition are amorphous. The estimated amorphous density is higher and amorphous fractional free volume is lower in the copolymers than in either homopolymer, suggesting that copolymerization leads to better chain packing in the amorphous regions of the polymer matrix even as copolymerization frustrates crystallinity. The amorphous phase free volume as probed by PALS decreases strongly with increasing PEN content, particularly at low concentration of PEN in PET. Acetone uptake kinetics in solvent cast PET/PEN copolymer films at 35˚C and 5.4 cm Hg are well-described by Fick's law. The acetone diffusion coefficient decreases 93% from PET to PET/85PEN. The amorphous phase acetone solubility coefficient decreases by approximately a factor of two over the same composition range. The diffusion coefficient decreases 53% from PET to PET/10PEN; over the same composition range the weight percent crystallinity decreases from 40% to 0. The acetone diffusion coefficients decrease as amorphous fractional free volume decreases. The acetone diffusion coefficients correlate well with the amorphous phase free volume as probed by PALS, suggesting that both static and dynamic free volume are important in the transport of acetone in these copolymers. Based on the results of an IR spectroscopy study, the fraction of amorphous phase EG units in the trans conformation increases with increasing PEN content. This increase in trans conformation may be associated with the observed increase in chain packing and decrease in amorphous phase free volume.

Table 4.1. Oxygen and Carbon Dioxide Permeability at 30˚C in PET, PEN, and a 50/50 PEN/PET Copolymer[69]

PEN Content [Weight %]	P_{CO_2} [Barrers]	P_{O_2} [Barrers]	$D_{O_2}x10^9$ [cm²/s]
0	0.32	0.054	6.5
50	0.24	0.04	4.8
100	0.11	0.02	2.2

Table 4.2. Summary of PET/PEN Copolymer DSC Results

Polymer	T_g [˚C]	T_c [˚C]	T_m [˚C]	X_c ‡
PET*	82	141	256	40
PET/1PEN*	82	-	252	28
PET/3PEN*	85	149	246	27
PET/5PEN*	79	136	244	15
PET/10PEN*	84	152	237	2
PET/20PEN*	91	-	221	0
PET/50PEN*	101	-	-	0
PET/80PEN**	113	-	-	0
PET/85PEN***	115	-	-	0
PET/90PEN**	117	209	247	11
PEN**	123	194	252	9

* As-cast films.
** As-synthesized pellets.
*** Melt extruded Film
‡ Crystallinity values estimated from first scan DSC thermograms using Equation 4.2.

Table 4.3. WAXD Measurements of Weight Percent Crystallites and Amorphous d-Spacing in As-Cast Films

Polymer	X_c	$2\theta_{max}$,	d (Å)
PET	38	20.6	4.3
PET/10PEN	*	18.9	4.7
PET/20PEN	*	18.3	4.8
PET/50PEN	0	18.1	4.9

* WAXD spectra show hints of crystalline peaks, but they are too weak for quantitative analysis.

Table 4.4. Density of PET/PEN Copolymers at 25˚C

Polymer	As-Synthesized Pellet Samples [g/cm^3]	As-Cast Film Samples [g/cm^3]	Annealed Film* [g/cm^3]	Quenched Film* [g/cm^3]
PET	1.366	1.366	1.408	1.337
PET/1PEN	1.391	1.362	-	-
PET/3PEN	1.392	1.360	-	-
PET/5PEN	1.366	1.351	-	-
PET/10PEN	1.341	-	1.375	1.335
PET/20PEN	1.340	-	1.361	1.334
PET/50PEN	1.319	1.326	1.331	1.332
PET/80PEN	1.317		1.353	1.331
PET/90PEN	1.336		1.354	1.331
PEN	1.353		1.357	1.328

* Data from SantaCruz, *et al.* [65]

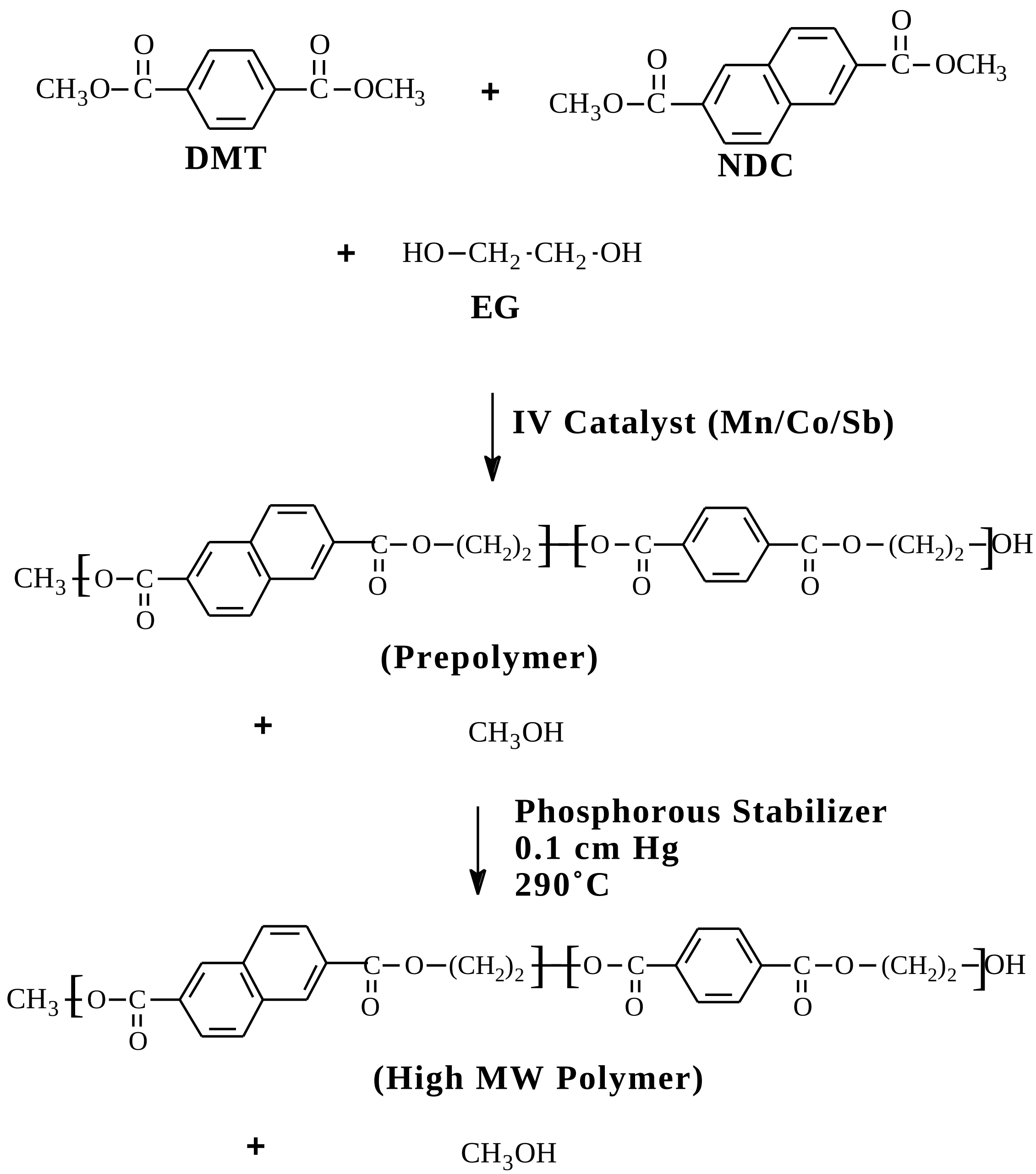

Figure 4.1. Reaction Scheme for PET/PEN Copolymers

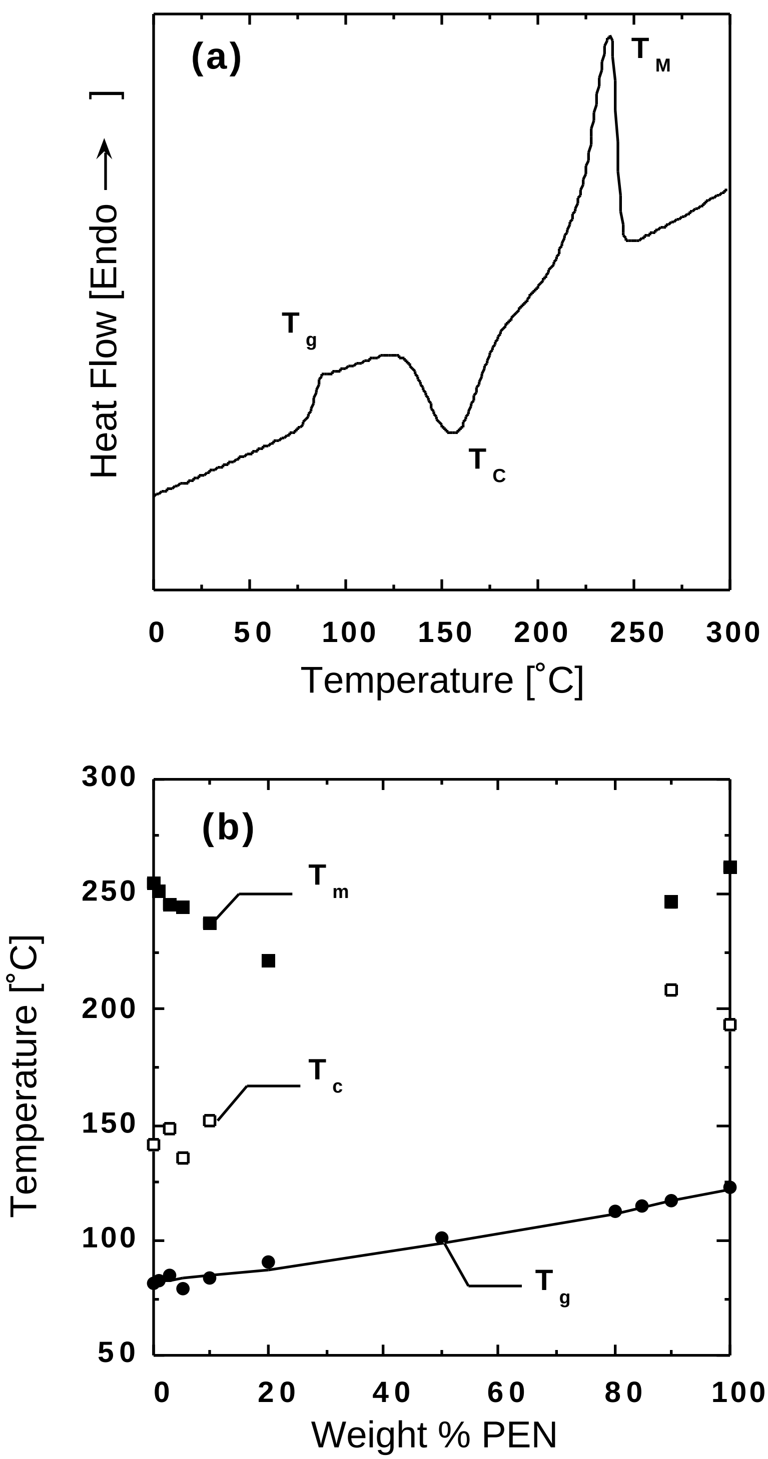

Figure 4.2 Thermal Analysis of PET/PEN Copolymers (a) DSC Thermogram of As-cast PET/10PEN Film (b) Thermal Transitions of PET/PEN Films as Determined by DSC. T_g (●), T_m(■), T_c(□)

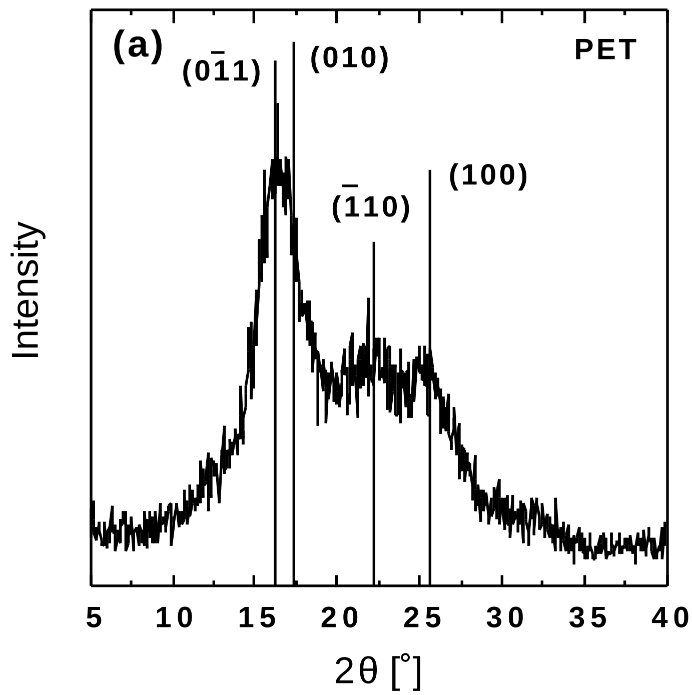

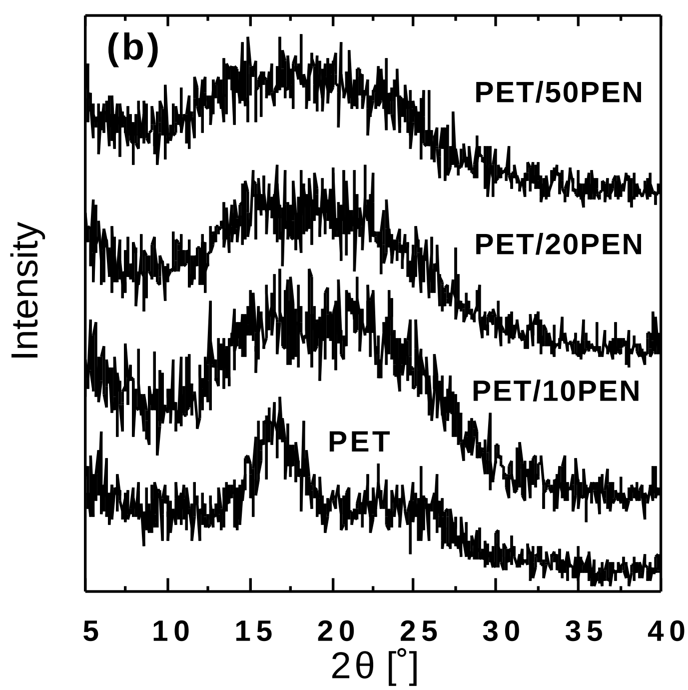

Figure 4.3. Wide-Angle X-ray Diffraction Spectra of (a) PET and (b) PET/PEN Films. The spectra in 4.3b have been displaced vertically for easier viewing.

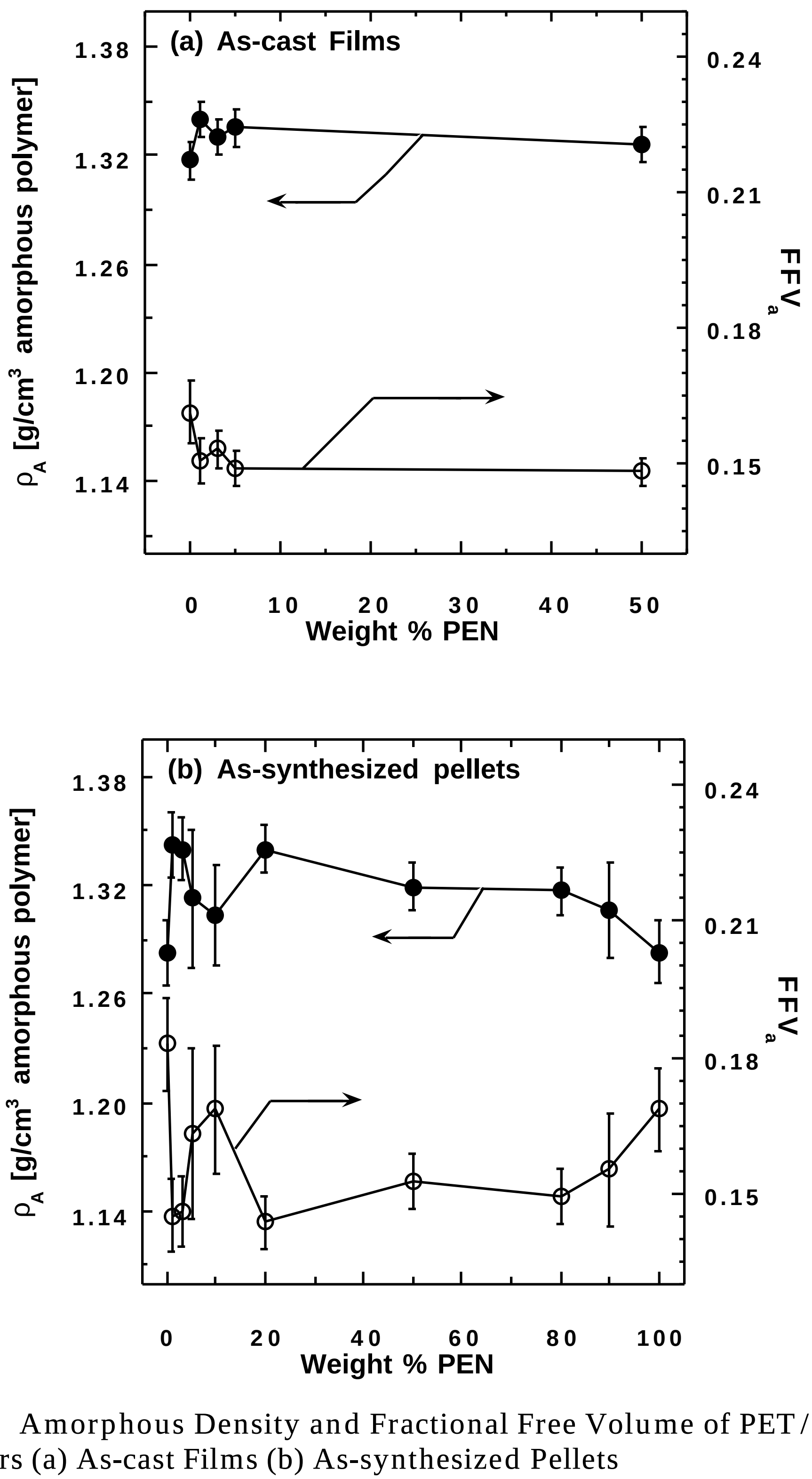

Figure 4.4. Amorphous Density and Fractional Free Volume of PET/PEN Copolymers (a) As-cast Films (b) As-synthesized Pellets

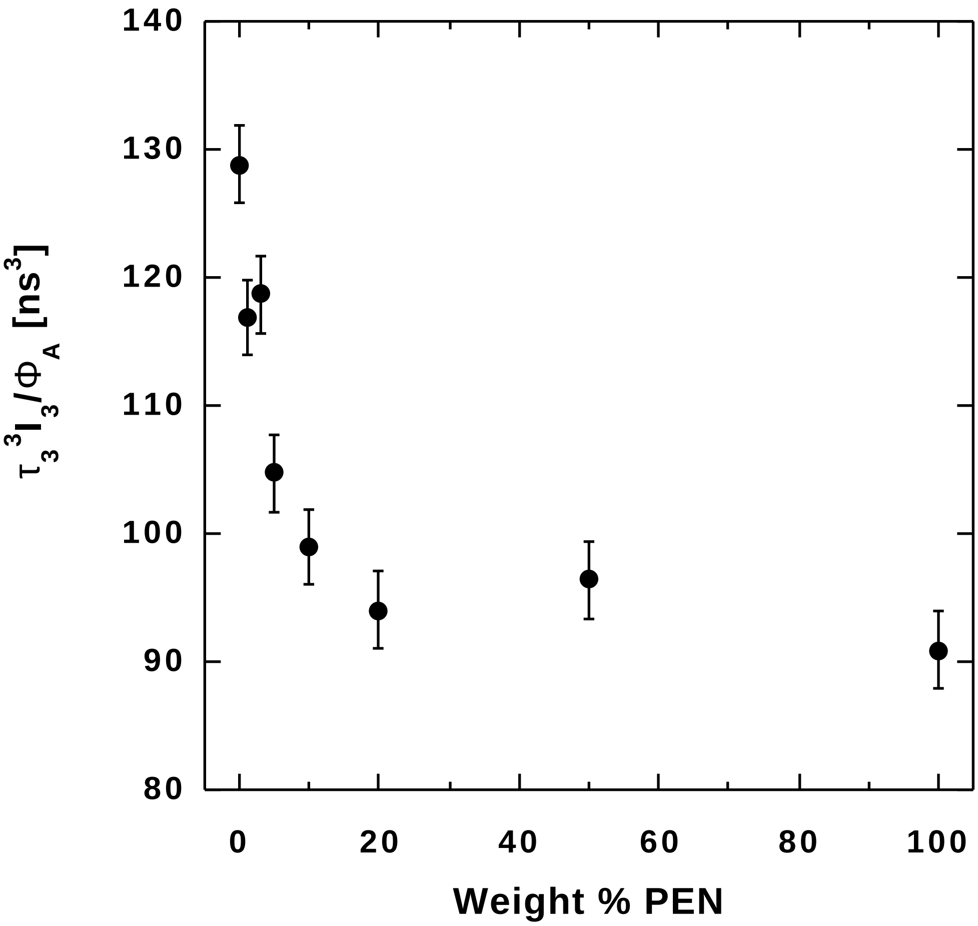

Figure 4.5. Relative Free Volume in the Amorphous Regions of PET/PEN Copolymers as Probed by PALS

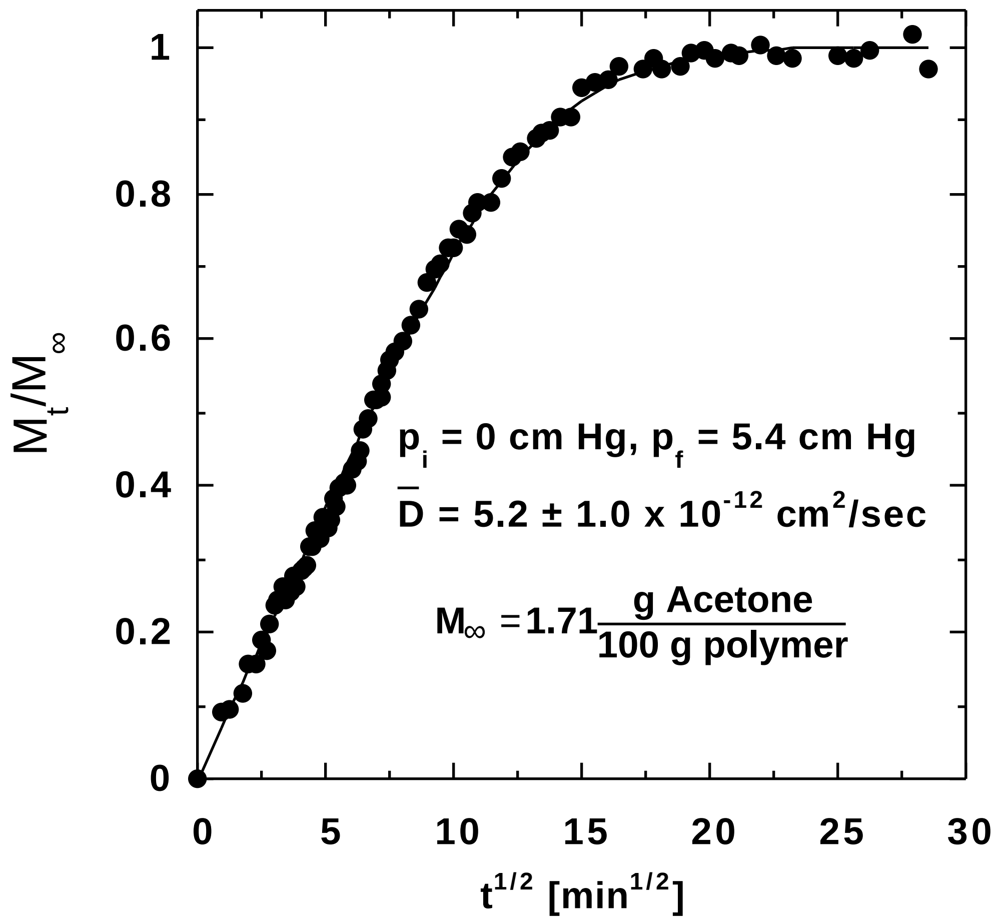

Figure 4.6. Acetone Sorption Kinetics in As-cast PET Film at 35˚C. p_i is the initial acetone pressure. At t=0, the acetone pressure is in increased to p_f. At 35˚C, the saturation vapor pressure of acetone is 36.0 cm Hg.[43]

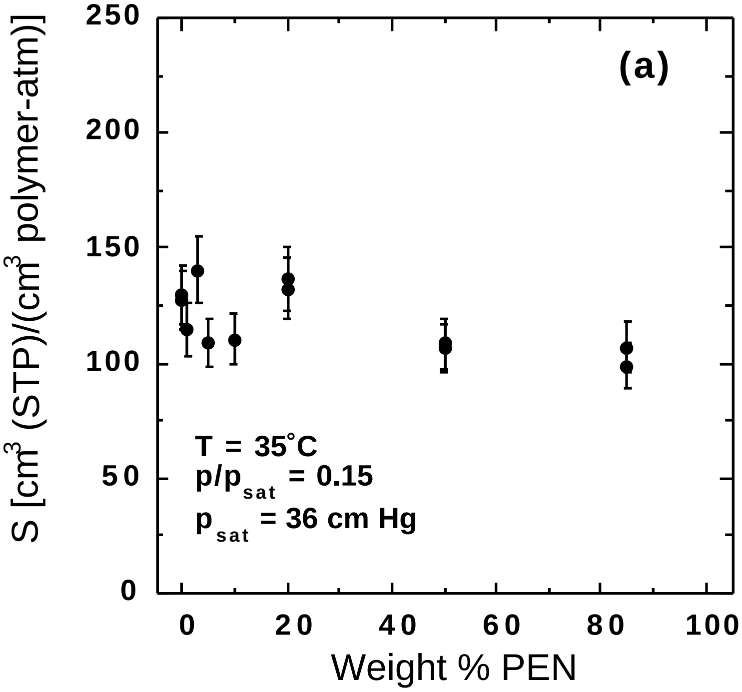

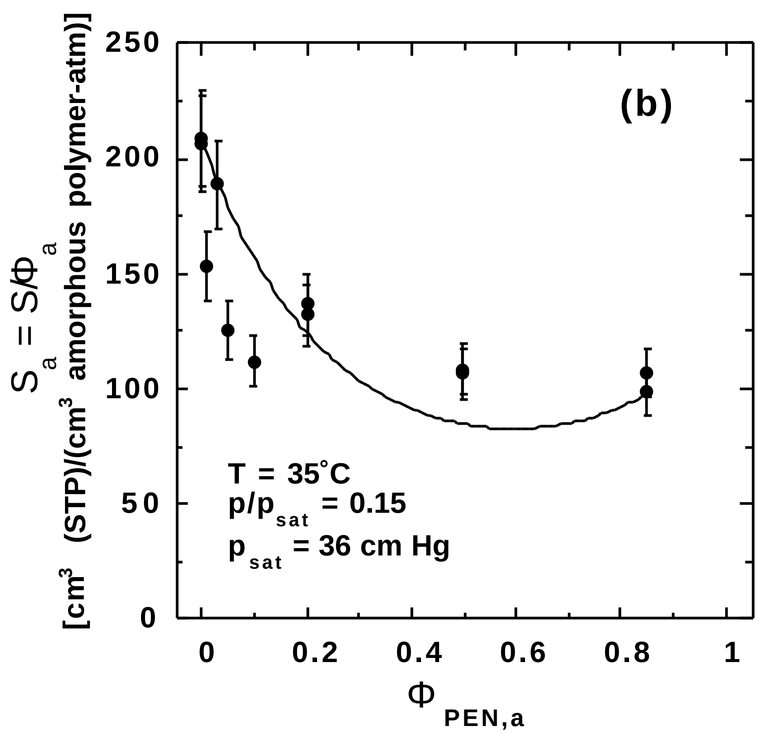

Figure 4.7. Solubility of Acetone in PET/PEN Copolymer Films at 35˚C. The PET/85PEN data point was determined using the micromelt extruded sample. (a) Solubility in semicrystalline polymer versus weight percent PEN (b) Calculated amorphous solubility versus volume fraction PEN in the amorphous phase. The curve is the best fit to Equation 4.13, treating γ as an adjustable parameter.

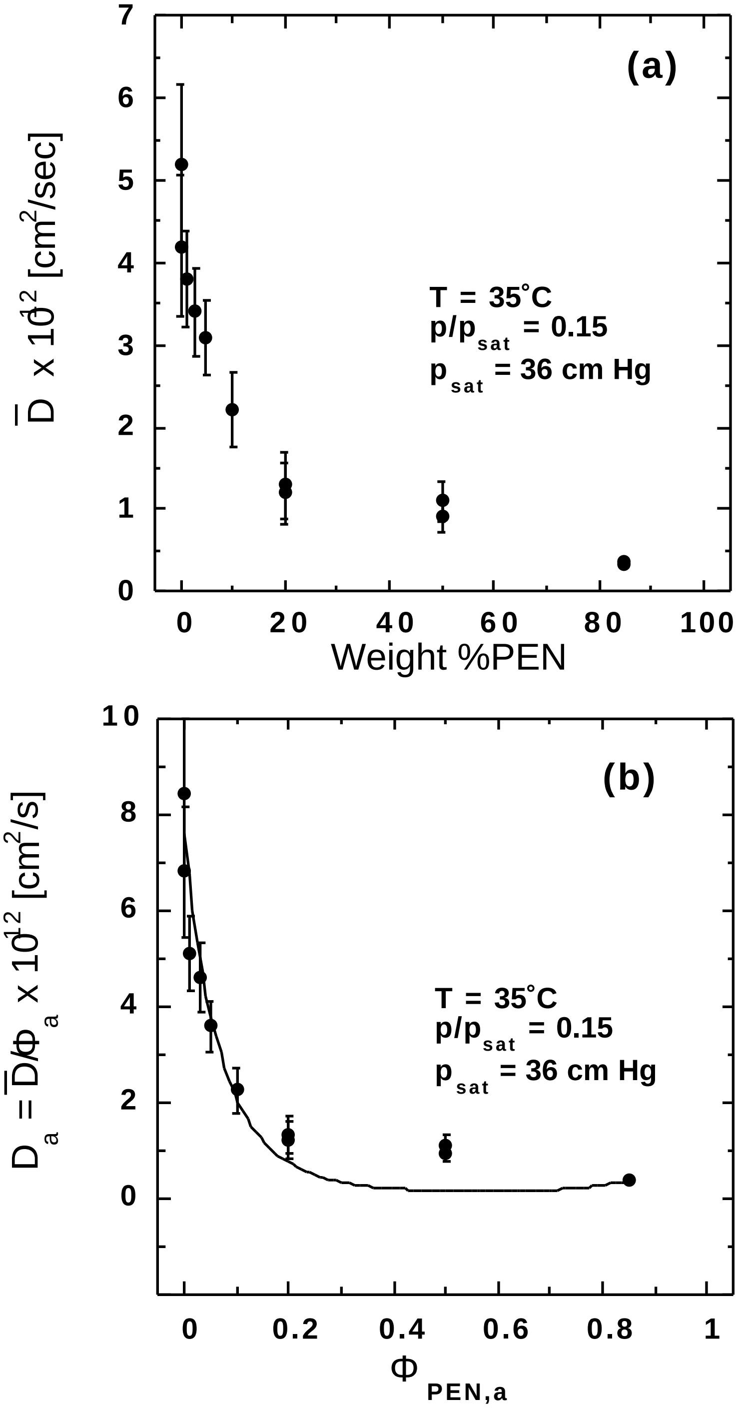

Figure 4.8. Diffusivity of Acetone in PET/PEN Copolymer Films at 35˚C. All data except for the PET/85PEN film are for as-cast films. The PET/85PEN data point was determined using the micromelt extruded sample. (a) Diffusivity in semicrystalline polymer versus weight percent PEN (b) Calculated amorphous diffusivity versus volume fraction PEN in the amorphous phase. The curve a least-squares fit to Equation 4.19, treating ω as an adjustable parameter

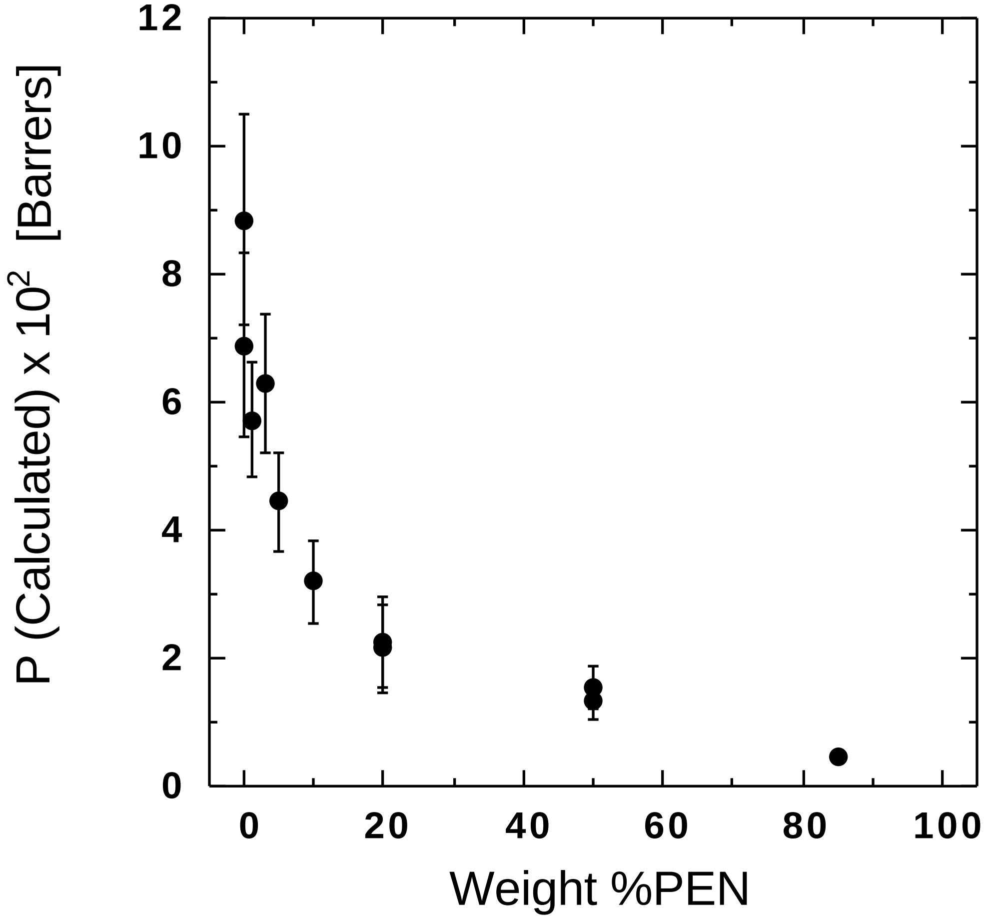

Figure 4.9. Effect of Copolymer Composition on Calculated Permeability of Acetone in PET/PEN Films.

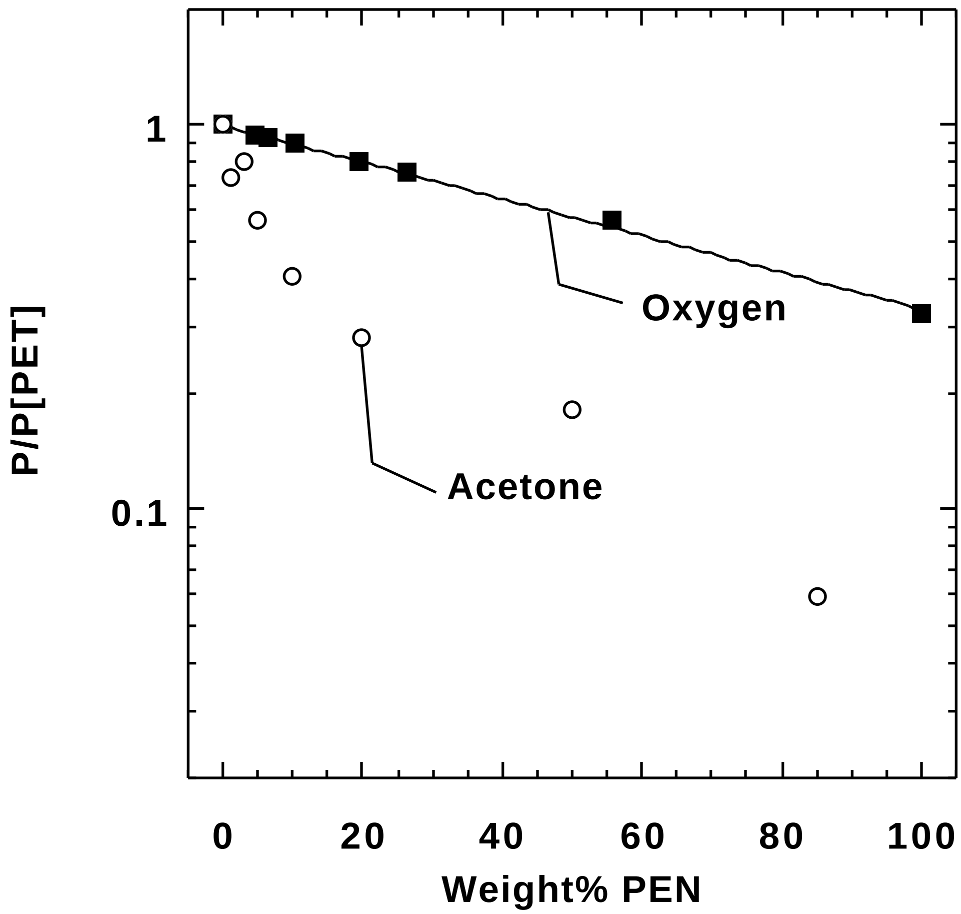

Figure 4.10. Effect of Copolymer Composition on Oxygen and Calculated Acetone Permeability in PET/PEN Copolymers. Oxygen results[25] from direct permeation experiments at 23˚C at 75% Relative Humidity. Acetone results estimated from kinetic gravimetric sorption experiments at 35˚C and p = 5.4 cm Hg.

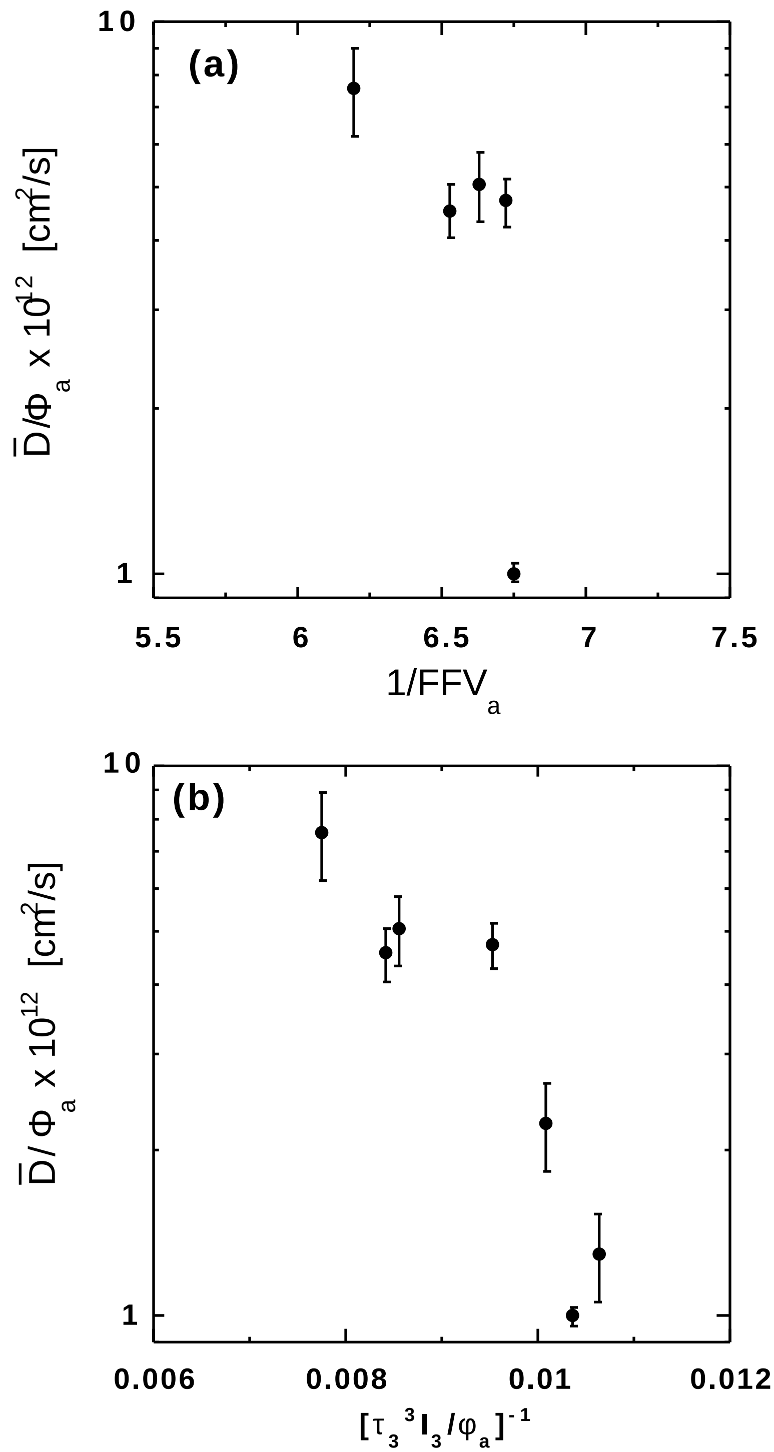

Figure 4.11. Effect of Free Volume on Acetone Diffusion Coefficient in PET/PEN Copolymers: (a) Calculated amorphous fractional free volume estimated from density and crystallinity values (b) Free Volume as Probed by PALS

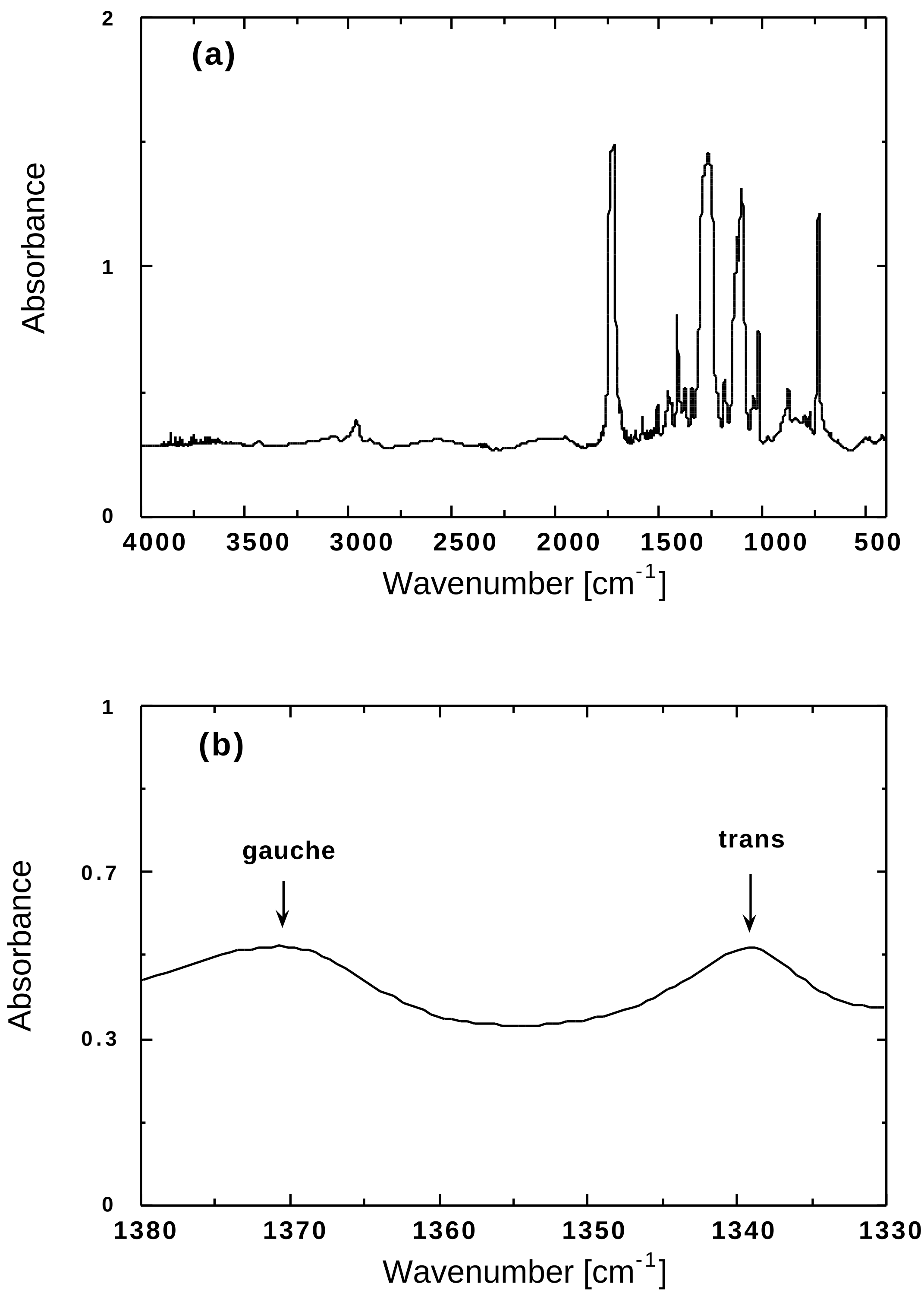

Figure 4.12 IR Spectra of As-cast PET/10PEN film (a) 500 to 4000 cm^{-1} (b) 1330 to 1380 cm^{-1}

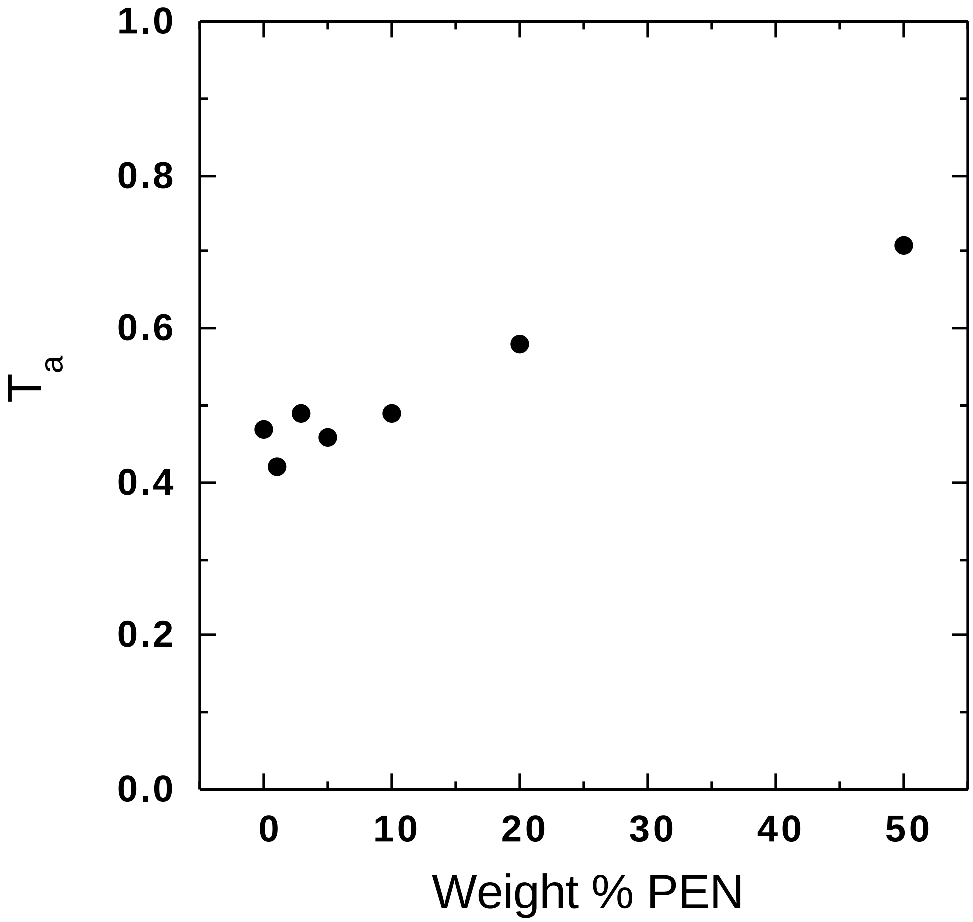

Figure 4.13. Estimated Weight Fraction of Amorphous EG units in the Trans Conformation as a Function of PEN Composition

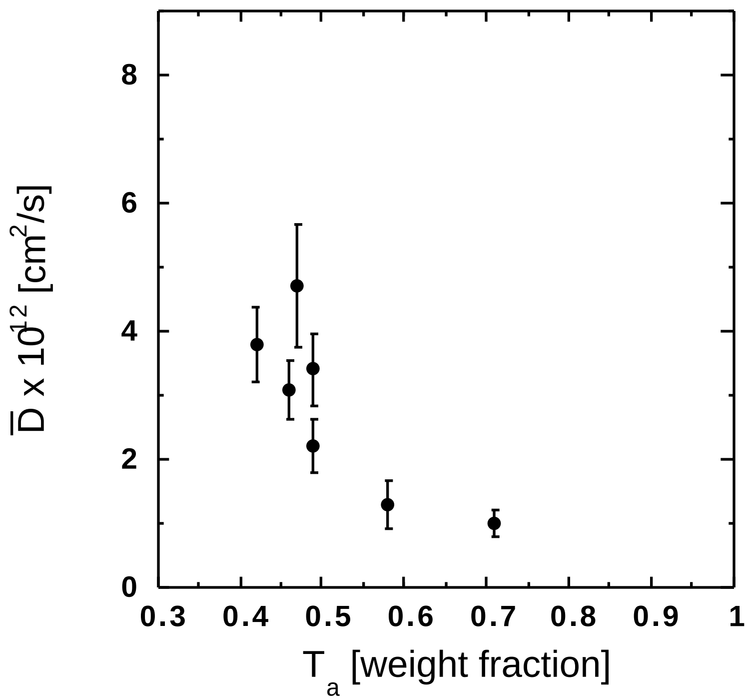

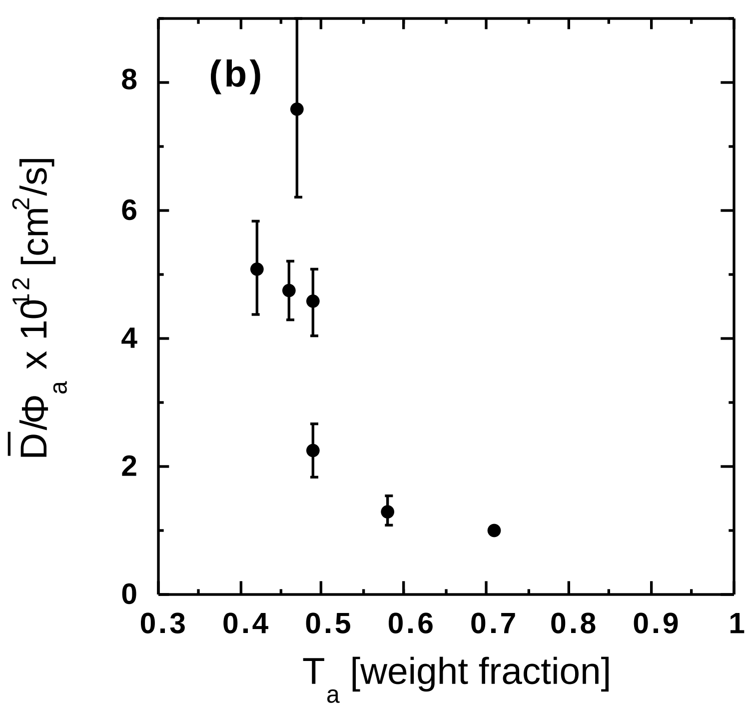

Figure 4.14. Dependence of Acetone Diffusion Coefficient on Estimated Amorphous Trans Content (a) Diffusion coefficient in semicrystalline polymer (b) Calculated Diffusion coefficient in amorphous regions of polymer

Chapter 5. Interval Kinetic Gravimetric Sorption of Acetone in Random Copolymers of Poly(ethylene terephthalate) and Poly(ethylene 2,6-naphthalate)

I. Introduction

Copolymers of poly(ethylene terephthalate) (PET) and poly(ethylene 2,6-naphthalate) (PEN) are of interest in barrier packaging because the addition of PEN to PET improves gas barrier properties and increases glass transition temperatures.[25] Increased barrier properties can lead to longer shelf life for packaged products and increased glass transition temperature makes hot-filling and steam sterilization of packages more accessible.

An important consideration in barrier packaging of food products is the loss of flavor molecules due to scalping (*i.e.* the sorption of flavor molecules into package walls).[1] A related problem, flavor molecule carry-over, is also emerging as a concern for refillable polymeric beverage bottles. In carry-over, flavor or contaminant molecules sorbed into a bottle from an initially-packaged product desorb after refill and influence the taste of the new product. To understand the sorption of flavor molecules into barrier polymers, model organic molecules are often used as markers for flavor molecules.[2]

In a previous study, the sorption of acetone in PET was reported for acetone pressures ranging from 0 to 7.3 cm Hg (*cf*. Chapter 3). The dual mode sorption model[7] provides an excellent representation of the equilibrium acetone sorption isotherm. An empirical two-stage model, which incorporates both Fickian diffusion and polymer relaxation, was used to describe the kinetics of acetone uptake in PET. The concentration dependence of the acetone diffusion coefficient was well-described by the dual mobility model[33] once the assumption of constant Henry's law and Langmuir domain diffusion coefficients was relaxed.

The diffusivity and solubility of acetone at 35˚C in solution cast films of PET/PEN random copolymers at a constant acetone partial pressure (5.4 cm Hg, or p/p_{sat} = 0.15, where p_{sat} is the saturation vapor pressure of acetone at 35˚C) were also reported (*cf*. Chapter 4). The glass transition temperature increases monotonically with increasing PEN content from 81˚C in PET to 123˚C for PEN. Films cast from PET-rich copolymers were semicrystalline while copolymers of intermediate composition were amorphous. Estimated densities of the amorphous regions of the copolymers were higher than densities of the amorphous regions of either homopolymer, suggesting that copolymerization improves amorphous chain packing. Based on positron annihilation lifetime spectroscopy [PALS] results, the free volume accessible to ortho-positronium decreases with increasing PEN content in the copolymer films. Based on infrared [IR] spectroscopy, the fraction of ethylene glycol units in the trans conformation in the amorphous phase of the copolymer matrix increases with increasing PEN content. Previous studies indicate higher amorphous phase density[75] and lower permeability[87] in PET with higher amorphous phase concentrations of glycol units in the trans conformations. Based on these composite studies, as the concentration of PEN in PET/PEN copolymers increases, crystallinity is reduced, polymer segmental mobility important to the glass/rubber transition decreases, and chain packing in the amorphous phase increases. These factors combine to decrease acetone diffusion coefficients with increasing PEN content.

In this study, the kinetics of interval acetone sorption in solution-cast films of PET/PEN random copolymers at 35˚C are reported for acetone pressures ranging from 0 to 7.3 cm Hg. The dual-mode model is used to analyze equilibrium sorption results. An empirical two-stage model incorporating Fickian diffusion and relaxation-controlled kinetics describes the acetone uptake kinetics in PET/PEN copolymers.

II. Experimental

The methods of synthesis, film casting, and gravimetric sorption experiments have been presented in the previous chapters.

III. Results and Discussion

Equilibrium Acetone Uptake

The sorption isotherm of acetone in PET at 35˚C is presented in Figure 5.1. The isotherm shape is typical for sorption of gases and condensable vapors at low activity in glassy polymers.[7] This isotherm is well-described by the dual mode sorption model for glassy polymers:[7]

$$C = k_D p + \frac{C'_H b p}{1 + bp}, \tag{5.1}$$

where k_D is the Henry's Law sorption coefficient, which characterizes penetrant sorption into the equilibrium densified polymer matrix. The Langmuir affinity parameter, b, characterizes penetrant affinity for Langmuir sites in the matrix. The Langmuir capacity parameter, C'_H, characterizes penetrant sorption in the non-equilibrium excess volume associated with the glassy polymer matrix. From the dual mode sorption model, the Langmuir capacity parameter is related to the amount of non-equilibrium excess volume by:[9]

$$C'_{H,a} = \left[\frac{V_g - V_l}{V_g}\right]\rho^* \tag{5.2}$$

where V_g is the specific volume of the glassy polymer at the temperature of the sorption measurement, V_l is the specific volume of the equilibrium densified glass, and ρ^* is the condensed penetrant density. For semicrystalline samples, V_g and V_l correspond to the glassy and equilibrium specific volumes of the amorphous (*i.e.* penetrant-accessible) regions of the polymer matrix, and $C'_{H,a}$ is the amount of penetrant sorbed into the Langmuir sites per unit volume of amorphous polymer.

The solid curves in Figure 5.1 represent a least-squares fit of the sorption data to the dual mode model. The model provides an excellent representation of the experimental data. The open circles represent as-measured values of equilibrium acetone concentration. Since this sample is semicrystalline and crystalline regions of PET are understood to preclude penetrant sorption,[18,20] the isotherm has been corrected for crystallinity to provide an estimate of the equilibrium sorption isotherm in amorphous PET. The amorphous-basis values of concentration are calculated using the relation:[18]

$$C_a = C/\Phi_a, \tag{5.3}$$

where C_a is the equilibrium concentration of acetone in the amorphous regions of the polymer, C is the measured equilibrium concentration of acetone in the semicrystalline polymer, and Φ_a is the amorphous volume fraction of material (calculated from the weight fraction crystallinity and literature values for amorphous and crystalline density of PET).[45] For the PET film, which has 40 weight percent crystallinity, Φ_a is 0.58. The filled circles in Figure 5.1 represent the calculated equilibrium concentration of acetone in amorphous polymer.

Acetone sorption isotherms for PET/PEN copolymers at 35˚C are presented in Figure 5.2. For copolymers with measurable crystallinity, the isotherms are also reported on an amorphous basis. In these cases, the open circles in Figure 5.2 represent the as-measured (semicrystalline) data and the filled circles represent the calculated amorphous basis. The PET/20PEN and PET/50PEN films are amorphous. Therefore, the filled circles for these isotherms in Figure 5.2 represent the as-measured equilibrium concentration of acetone in these amorphous copolymer films.

Table 5.1 presents the best fit dual mode model parameters for all the copolymers determined by a nonlinear least squares regression. For the semicrystalline polymers (PET, PET/5PEN, PET/10PEN) dual mode parameters are presented for both the as-measured semicrystalline and amorphous basis data. Errors in the parameters are estimated as described by Bevington.[58] For each copolymer, the b values calculated for the semicrystalline and amorphous data. The values of k_D and C'_H for the amorphous data are equal to the parameter values divided by the amorphous volume fraction, Φ_a.

As k_D and b values for all of the polymers were similar (on an amorphous basis), the amorphous basis data in Figures 5.1 and 5.2 were also fit to the dual mode model with all changes in the model parameters with polymer composition confined to C'_H, the Langmuir capacity parameter associated with the non-equilibrium glassy state. In this analysis, the best-fit model parameters are: $k_{D,a}$ = 94 cm^3(STP)/(cm^3 amorphous polymer·atm) and b=96 atm^{-1}, in good agreement with the values in Table 1. $k_{D,a}$ is the Henry's law coefficient in the amorphous phase of the polymer. These parameter values compare well with dual mode parameter values for other penetrants in PET when correlated with penetrant critical temperature (*cf*. Chapter 3).[20,33,90] The values of $C'_{H,a}$ calculated by this approach are presented as a function of weight percent PEN in Figure 5.3. Within the uncertainty, the values calculated this way are the same as those in Table 5.1.

Based on Equation 5.2 and the $C'_{H,a}$ values in Figure 5.3, the strong reduction in $C'_{H,a}$ between PET and PET/10PEN suggests a 72% reduction in the amount of excess free volume accessible to acetone as PEN content in the sample is increased from 0 to 10% PEN by weight. This reduction may be due to the ability of the naphthalate-laced polymer chains to pack more efficiently in the amorphous regions of the copolymer matrix even as the presence of PEN moieties randomly copolymerized in the chain backbone disrupts crystallinity. This result is consistent with our previous work (*cf*. Chapter 4) where increasing PEN content was accompanied by an increase in estimated amorphous phase density, a decrease in amorphous phase fractional free volume, and a decrease in free volume as measured by positron annihilation lifetime spectroscopy (*cf*. Chapter 4).

Figure 5.3 also presents the difference between the glassy and liquidous specific volume, V_g-V_l, as a function of weight percent PEN. V_g-V_l was estimated using the following relation, which is obtained from Equation 5.2:

$$V_g - V_l = V_g \frac{C'_{H,a}}{\rho^*}. \tag{5.4}$$

The estimated amorphous densities reported earlier (*cf*. Chapter 4) were used to calculate V_g, and an estimate of ρ^*, 0.774 g/cm^3 was obtained using the Hankinson-Brobst-Thomson correlation for the liquid density of pure acetone at 35°C.[43] As expected, like $C'_{H,a}$, there is a strong decrease in V_g-V_l with increasing weight percent PEN. Within the error of the measurement, there is no change in the calculated amorphous phase equilibrium specific volume, V_l, with polymer composition. Within the scope of this approximate analysis, PEN decreases non-equilibrium excess volume without markedly changing V_l. This result suggests that the most significant impact of an increase in PEN content on specific volume is the systematic reduction in non-equilibrium free volume associated with the glassy state.

Equation 5.2 is often rewritten in terms of thermal expansion coefficients and the glass transition temperature as follows:[91]

$$C'_{H,a} = \frac{\left(\frac{dV}{dT}\right)_l - \left(\frac{dV}{dT}\right)_g}{V_g}(T_g - T)\rho^* = \Delta\alpha(T_g - T)\rho^* \tag{5.5}$$

where T is the temperature of the sorption experiment, $\left(\frac{dV}{dT}\right)_l$ is the change in amorphous phase specific volume with respect to temperature above the glass transition, and $\left(\frac{dV}{dT}\right)_g$ is the change in amorphous phase specific volume with respect to temperature below the glass transition. Therefore, for a series of polymers, if $\Delta\alpha$ and ρ^* are approximately constant, $C'_{H,a}$ should vary linearly with T_g-T. This result presumes that Equation 5.2 is valid, and that V_g and V_l vary linearly with temperature between T and T_g.

A linear dependence of $C'_{H,a}$ on (T_g-T) has been reported for CO_2 sorption in a wide range of glassy polymers.[91] These data are presented in Figure 5.4. Within the context of the dual mode model, these data suggest that the dominant reason for variations in $C'_{H,a}$ among these polymers is the temperature difference T_g-T. As this difference increase, the non-equilibrium excess free volume in the polymer sample increases and, in turn, the number of Langmuir sorption sites increases. However, as shown in Figure 5.5a for our PET/PEN copolymers, $C'_{H,a}$ values generally decrease with increasing T_g, suggesting that factors other than simply the temperature difference, T_g-T, play a significant role in determining $C'_{H,a}$. Deviations from the linear relationship between $C'_{H,a}$ and T_g-T have been reported for substituted polycarbonates where sub-T_g transitions are evident above the temperature of the experiment.[92] For the substituted polycarbonates, it was found that Equation 5.2 overpredicts $C'_{H,a}$, possibly due to the existence of a maximum amount of non-equilibrium excess free-volume at temperatures below the sub-T_g transition.[92]

Another model for the variation of $C'_{H,a}$ with glass transition temperature is provided by the Boyer model.[93] The Boyer relation suggests that the product $\Delta\alpha T_g$ should be a constant.[93] Using this notion, Equation 5.5 can be rewritten as:

$$C'_{H,a} = \Delta\alpha T_g \rho \left(1 - \frac{T}{T_g}\right), \tag{5.6}$$

where $\Delta\alpha T_g$ and ρ^* are constants. Based on this model, a material with a higher T_g should have a higher value of $C'_{H,a}$. If the Boyer relation were obeyed, then a plot of $C'_{H,a}$ would increase linearly with 1-T/T_g. However, as presented in Figure 5.5b, the Langmuir capacity parameters associated with acetone sorption in PET/PEN copolymers do not change with T_g as suggested by the Boyer model.

Essentially, both of these models predict that $C'_{H,a}$ should increase with increasing T_g (*i.e.* increasing PEN content), and we observe exactly the opposite effect (*cf*. Figure 5.3). This result suggests that the amount of non-equilibrium excess volume in these glassy copolymers decreases with increasing PEN content. That is, the increase in the concentration of PEN in the polymer matrix increases chain packing efficiency sufficiently to more than offset any decreases in chain packing resulting from the phenomena described by Equations 5.5 and 5.6.

<u>Interval Acetone Sorption Kinetics</u>

Figure 5.6 presents results from representative acetone kinetic sorption experiments in PET (Figure 5.6a), PET/10PEN (Figure 5.6b), PET/20PEN (Figure 5.6c), and PET/50PEN (Figure 5.6d). The time since the penetrant pressure surrounding the polymer sample was increased from its initial value, p_i, to its final value, p_f, is t, M_t is the mass of acetone sorbed by the polymer from the beginning of the experiment until t, and M_∞ is the equilibrium mass uptake during the interval sorption experiment. At short times, the fractional mass uptake, M_t/M_∞, increases linearly with the square root of time, which is characteristic of sorption kinetics controlled by Fickian diffusion.[6] At longer times, the mass uptake exhibits a protracted, non-Fickian asymptotic approach towards equilibrium. Such two stage kinetics are often observed for organic vapor sorption in glassy polymers such as vinyl chloride monomer in PVC[55] and benzene in PET.[33] Two stage sorption

kinetics are often reported for interval organic vapor sorption in glassy polymers. Such kinetics have been reported for as methyl acetate uptake in poly(methyl methacrylate) and cellulose acetate,[56] benzene in polystyrene,[56] acetone in cellulose nitrate,[56] and ethyl benzene in polystyrene.[57]

For the data presented in Figure 5.6, at each pressure interval the diffusion process controls mass uptake at short times and polymer relaxation controls mass uptake at long times. The presence of an intermediate plateau region in each plot in Figure 5.6 (marked by arrows) separates the diffusion-controlled and relaxation-controlled regimes of mass transfer. As described below, this observation allows a separation of the kinetic parameters for mass uptake by diffusion from those associated with structural relaxation.

The fraction of weight uptake controlled by Fickian diffusion, ($1-\alpha_R$), is estimated as the fraction of weight uptake at the end of the intermediate plateau of the sorption data (indicated by the arrows in Figure 5.6). The average Fickian diffusion coefficient over the concentration range probed by the experiment, $\overline{D}$, can then be estimated from a best fit of these data to an analytical model for sorption into a uniform plane sheet:[5]

$$\frac{\frac{M_t}{M_\infty}}{(1-\alpha_R)} = 1 - \frac{8}{\pi^2}\sum_{n=0}^{\infty}\frac{1}{(2n+1)^2}\exp\left(\frac{-\overline{D}(2n+1)^2\pi^2 t}{\ell^2}\right), \qquad (5.6)$$

where ℓ is the film thickness and α_R is the fraction of mass uptake controlled by polymer relaxation. This expression is used to describe data at times up to the intermediate plateau. Polymer relaxation-controlled mass uptake kinetics at times greater than those associated with Fickian kinetics are modeled empirically by a single exponential:

$$\ln\left(1 - \frac{M_t}{M_\infty}\right) = \ln\alpha_R - \frac{t}{\tau_R}. \tag{5.7}$$

where τ_R is the first order time constant characterizing the long time, non-Fickian drift in mass uptake towards equilibrium. The curves in Figure 5.6 represent the separate diffusion and relaxation contributions to the acetone sorption kinetics as determined by these methods. The value of determined from the intercept of Equation 5.7 is often different than the corresponding value determined as the plateau value of $1-M_t/M_\infty$. However, as in PET(*cf*. Chapter 3) the value of α_R determined from the intercept of Equation 5.7 is systematically higher than those determined graphically. In each case, the value of α_R determined graphically from intermediate plateau values of M_t/M_∞ indicated by the arrows in Figure 5.6.

Figure 5.7a presents the dependence of average acetone diffusion coefficient on average acetone concentration during each interval sorption experiment for PET, PET/10PEN, PET/20PEN and PET/50PEN. C_i is the acetone concentration at the beginning of the interval sorption experiment, and C_f is the acetone concentration at the end of the interval sorption experiment. In Figure 5.7b, the average acetone concentration is reported on an amorphous basis using Equation 5.3, and the effect of crystallinity on diffusivity has been estimated using the following equation:[19]

$$\overline{D} = \overline{D}_a \Phi_a \tag{5.8}$$

where $\overline{D}_a$ is the calculated average diffusion coefficient in the amorphous regions of the polymer matrix in the concentration interval probed during the sorption experiment. In previous studies of gas diffusion in PET,[19] the effect of crystallinity on diffusion coefficients was well-described by Equation

5.8. The calculated amorphous phase diffusion coefficients increase with increasing acetone concentration for all of the PET/PEN compositions. The calculated amorphous phase diffusion coefficients for PET, PET/10PEN, and PET/20PEN are similar at the same amorphous phase concentration. The amorphous phase diffusion coefficients for PET/50PEN are generally lower than the others at the same acetone concentration.

As reported earlier, the standard dual mobility model does not adequately describe the concentration dependence of acetone diffusion coefficients in PET (*cf*. Chapter 3). However, when the assumption of constant values of diffusion coefficients in the Langmuir and Henry's law modes is relaxed, the model provides a good description of the experimental data (*cf*. Chapter 3). Presumably, acetone plasticizes the polymer matrix somewhat, and, as a result, effective acetone diffusion coefficients increase more with acetone concentration than would be expected based on the standard dual mobility model. In a similar fashion, the standard dual mobility model cannot describe the concentration dependence of acetone diffusion coefficients in PET/10PEN and PET/20PEN, suggesting plasticization of the polymer matrices by acetone. However, the standard dual mobility model, with constant Henry's law and Langmuir diffusion coefficients, can be used describe the concentration dependence of acetone diffusion coefficients in PET/50PEN. The values for the Henry's law and Langmuir diffusion coefficients are 2.3 x 10^{-12} cm^2/s and 4.6 x 10^{-13} cm^2/s, respectively. This result suggests that at higher PEN contents, the copolymers are more resistant to plasticization by acetone.

Figure 5.8 presents the structural relaxation time constant, τ_R, as a function of the final acetone concentration, C_f, for each kinetic gravimetric sorption experiment. The relaxation time does not vary systematically with acetone concentration or with copolymer composition over the ranges probed in this study.

Figure 5.9 presents the fraction of mass uptake controlled by relaxation as a function of final acetone concentration in the copolymers. α_R generally increases with increasing acetone concentration. However, there is no strong systematic impact of copolymer composition on this empirical parameter.

IV. Conclusions

The dual mode sorption model describes the equilibrium sorption of acetone in PEN/PET copolymers at acetone pressures up to 7.3 cm Hg at 35°C. Interval kinetic gravimetric sorption results over this pressure range can be described using an empirical two-stage model, with Fickian diffusion and polymer structural relaxation controlling mass uptake at short and long times, respectively.

The value of the Langmuir sorption capacity parameter decreases strongly with increasing PEN content up to PET/10PEN, implying an important reduction in the accessible non-equilibrium excess free volume associated with the glassy state of the polymer upon addition of modest amounts of PEN. For interval sorption of acetone from 0 to 7.3 cm Hg and at 35°C, the amorphous basis acetone diffusion coefficient in the PET/50PEN film is generally lower than the amorphous basis acetone diffusion coefficients in the PET, PET/10PEN and PET/20PEN films at the same acetone concentrations in the amorphous phase. The value of the first-order time constant used to describe the kinetics of acetone sorption controlled by penetrant-induced relaxation is not markedly influenced by polymer composition or penetrant concentration over the range of penetrant concentration explored in this study. For interval sorption of acetone from 0 to 7.3 cm Hg and at 35˚C, the fraction of mass uptake controlled by penetrant-induced relaxation of the polymer matrix increases with increasing acetone concentration in the polymer and does not depend systematically on copolymer composition.

Table 5.1. Dual Mode Parameters for Acetone Sorption in PEN / PET (35˚C)

Polymer	k_D [cm^3(STP)/ cm^3/atm]	C'_H [cm^3(STP)/cm^3]	b [1/atm]
PET	61 ±7.4	7.2 ± 1.1	50 ± 12
PET (amorphous basis)	101 ± 12.3	12 ± 1.8	50 ± 12
PET / 5PEN	60 ± 8.5	7.5 ± 1.1	76 ± 22
PET / 5PEN (amorphous basis)	72 ± 10	9.0 ± 1.3	76 ± 22
PET / 10PEN	82 ± 6.2	3.2 ± 1.7	83 ± 16
PET / 10PEN (amorphous basis)	84 ±6.5	3.4 ± 1.8	83 ± 16
PET / 20PEN	102 ± 6.3	4.5 ± 2.7	96 ± 37
PET / 50PEN	89 ± 7.3	4.0 ±2.9	160 ± 48

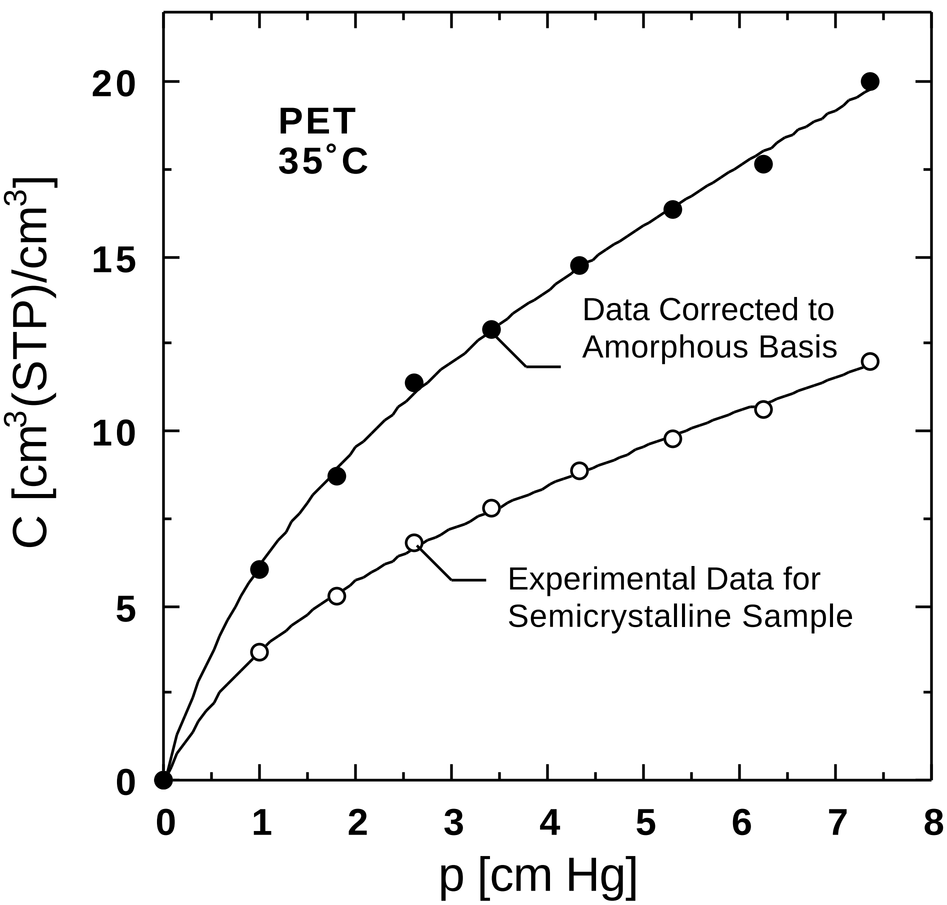

Figure 5.1. Equilibrium Sorption Isotherm of Acetone in PET at 35˚C (○ = experimental data for semicrystalline material, ● = calculated sorption data on an amorphous basis). The saturation vapor pressure of acetone in 36.0 cm Hg.[43]

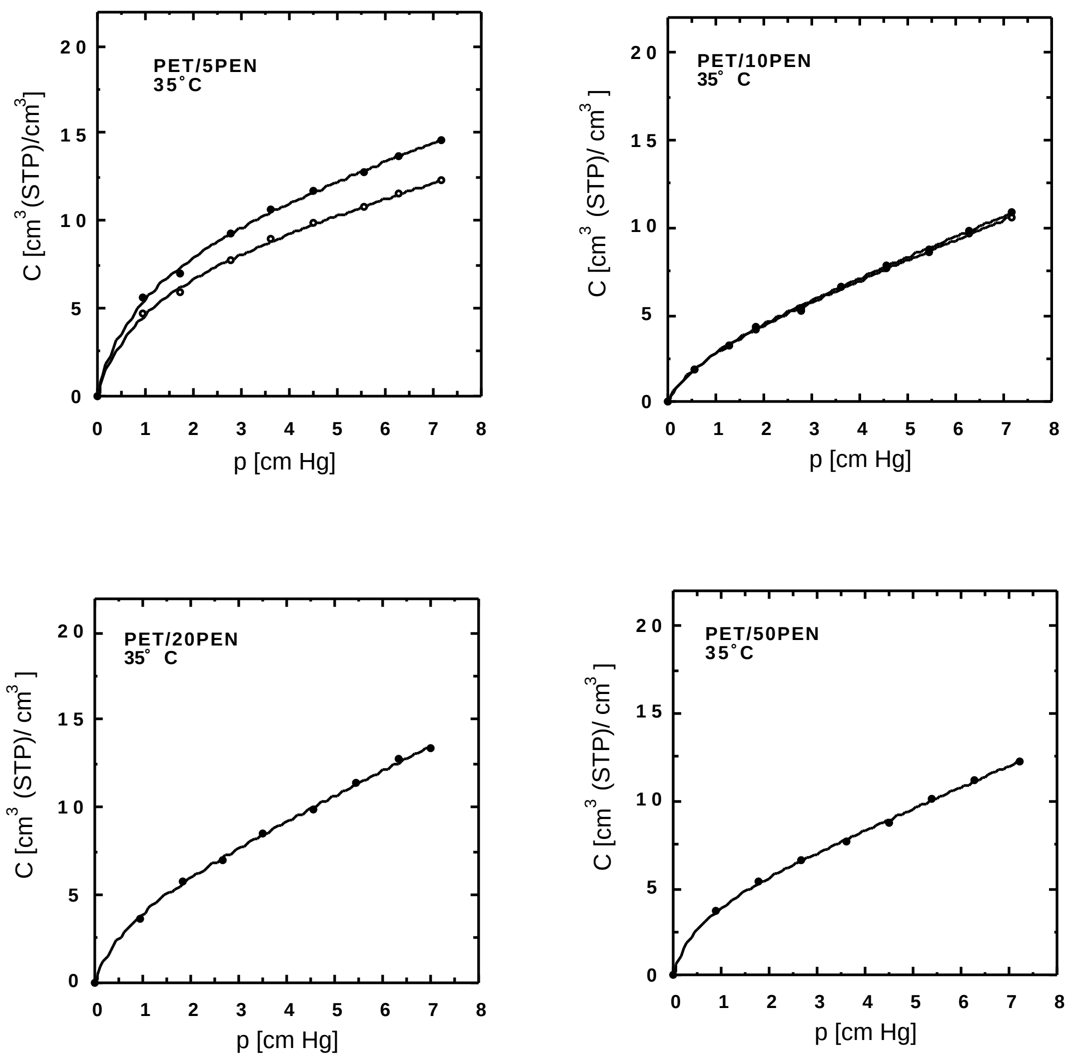

Figure 5.2. Equilibrium Sorption Isotherms of Acetone in PET / PEN Copolymers at 35˚C (○ = experimental data for semicrystalline material, ● = calculated sorption data on an amorphous basis).

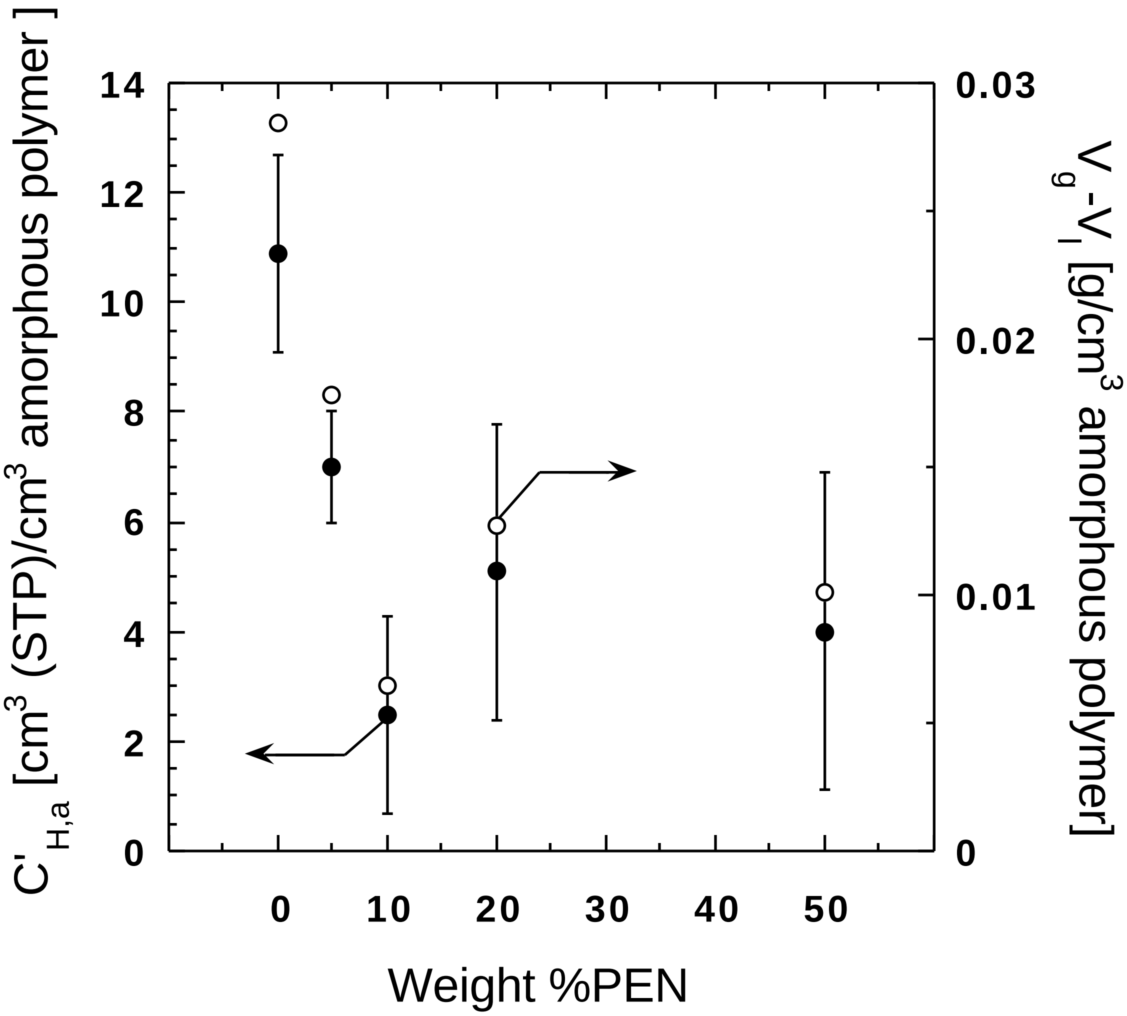

Figure 5.3. Langmuir Capacity Parameter as a Function of Weight Percent PEN in PEN / PET Copolymers

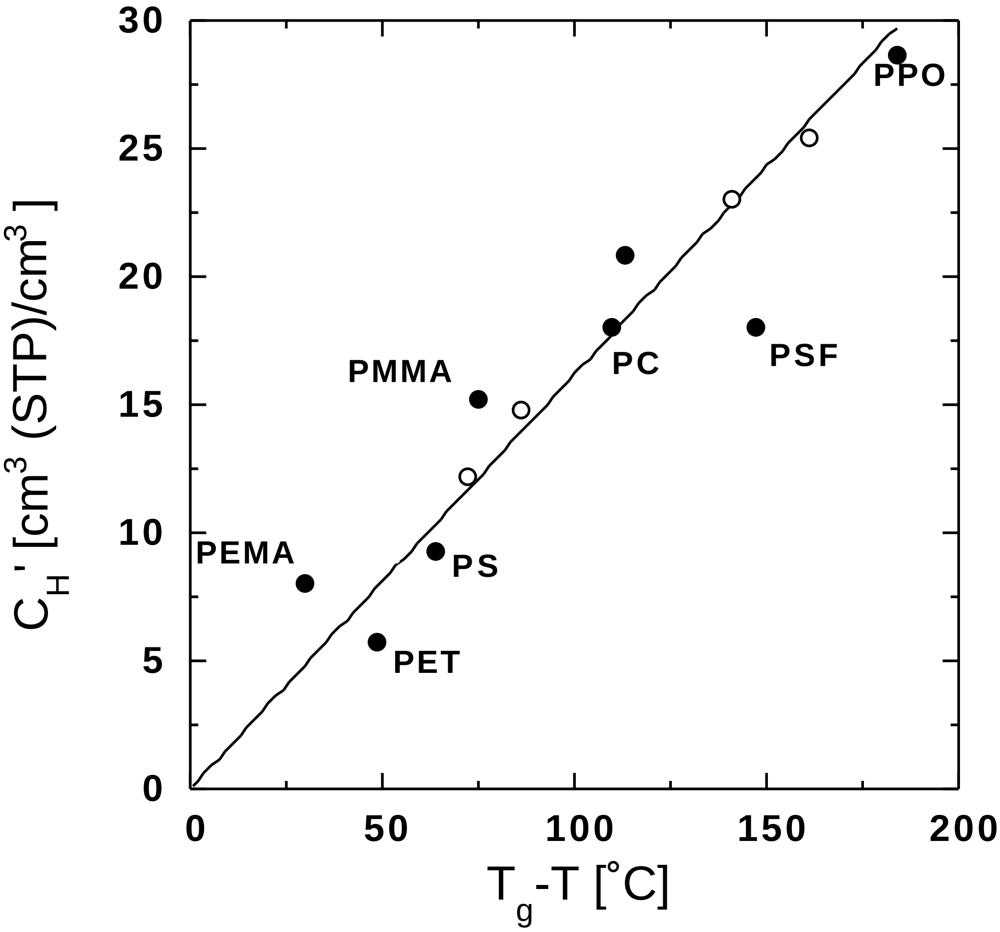

Figure 5.4. Correlation of Measured Values of Carbon Dioxide Langmuir Capacity Parameter as a Function of the Difference Between Polymer Glass Transition Temperature and Temperature of the sorption measurement, T = 35˚C. PPO = poly(phenylene oxide), PSF = polysulfone, PC = polycarbonate, PMMA = poly(methyl methacrylate), PS = polystyrene, PEMA = poly(ethyl methacrylate). Miscible blends of polymer pairs designated by open circles (PPO / PS). Data from Toi, *et al.* [91]

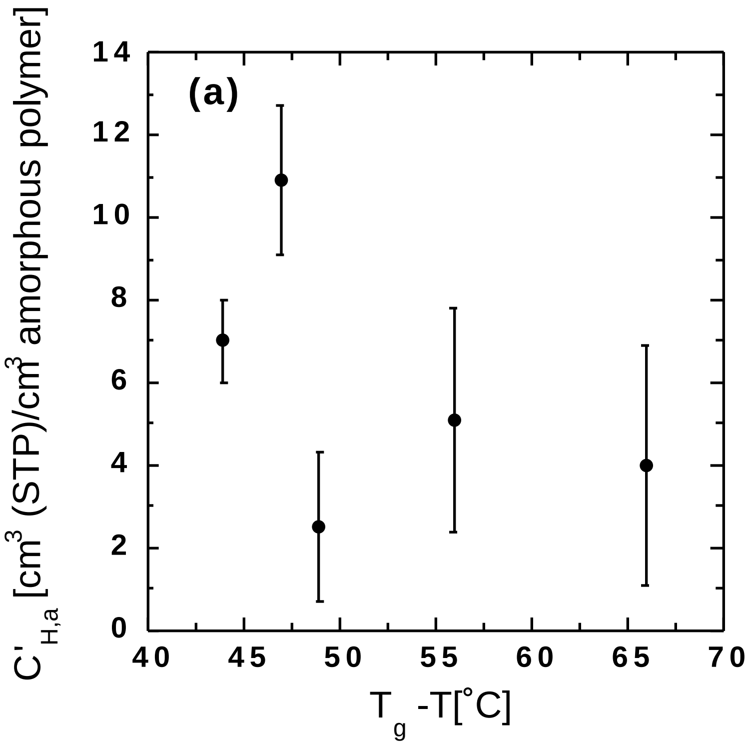

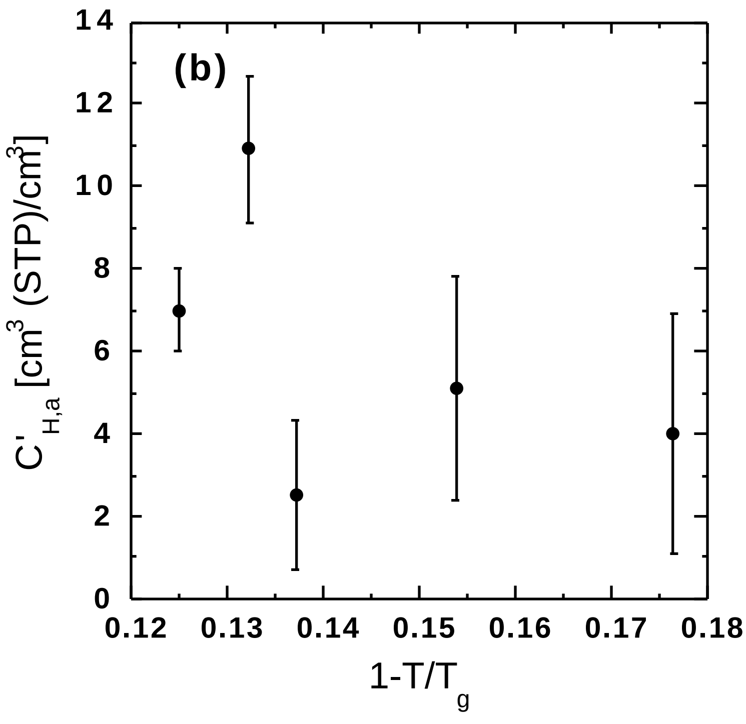

Figure 5.5. Acetone Langmuir Capacity Parameter as a Function of the Difference Between Polymer Glass Transition Temperature and Sorption Experiment Temperature for PEN / PET Copolymer Films

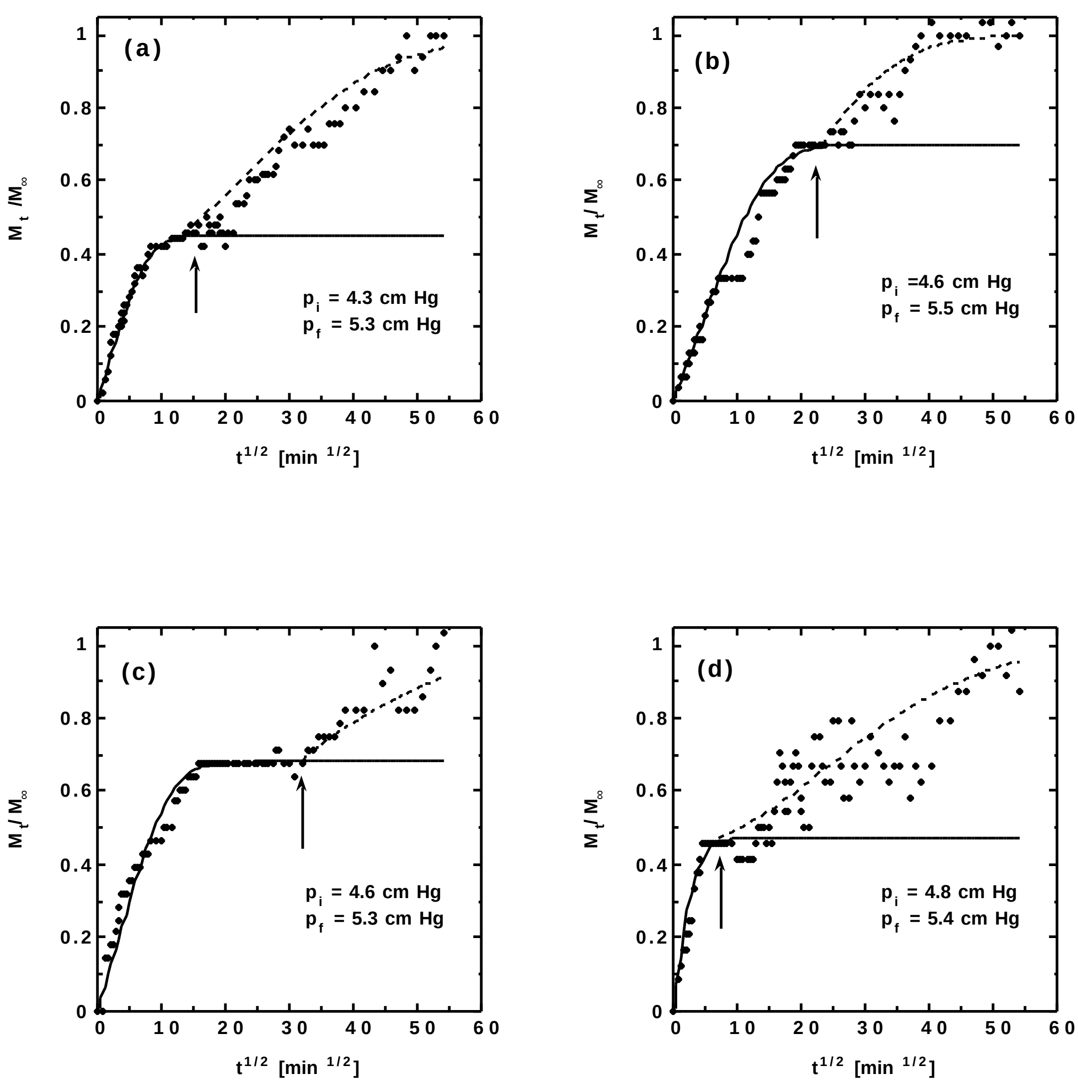

Figure 5.6. Interval Acetone Sorption in PET/PEN at 35˚C. The solid lines indicate contribution of Fickian diffusion to overall mass uptake, and the dashed lines represent the contribution of relaxation to overall uptake kinetics. (a) PET (b) PET/10PEN (c) PET/20PEN (d) PET/50PEN.

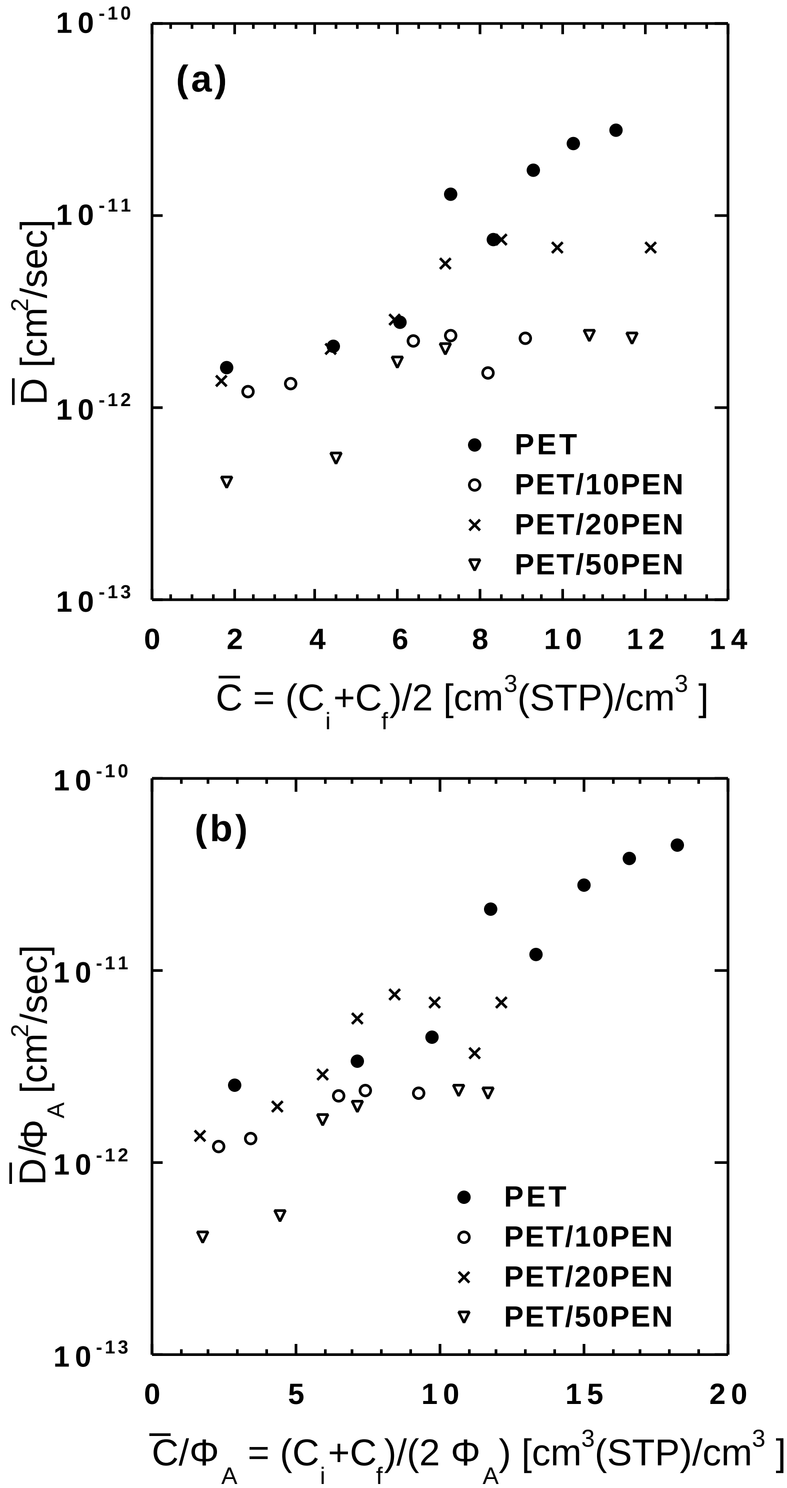

Figure 5.7. Acetone Diffusion Coefficient in PEN / PET Copolymers as a Function of Average Acetone Concentration in Amorphous Regions of the Polymer Matrix (a) As-measured Data (b) Amorphous Basis

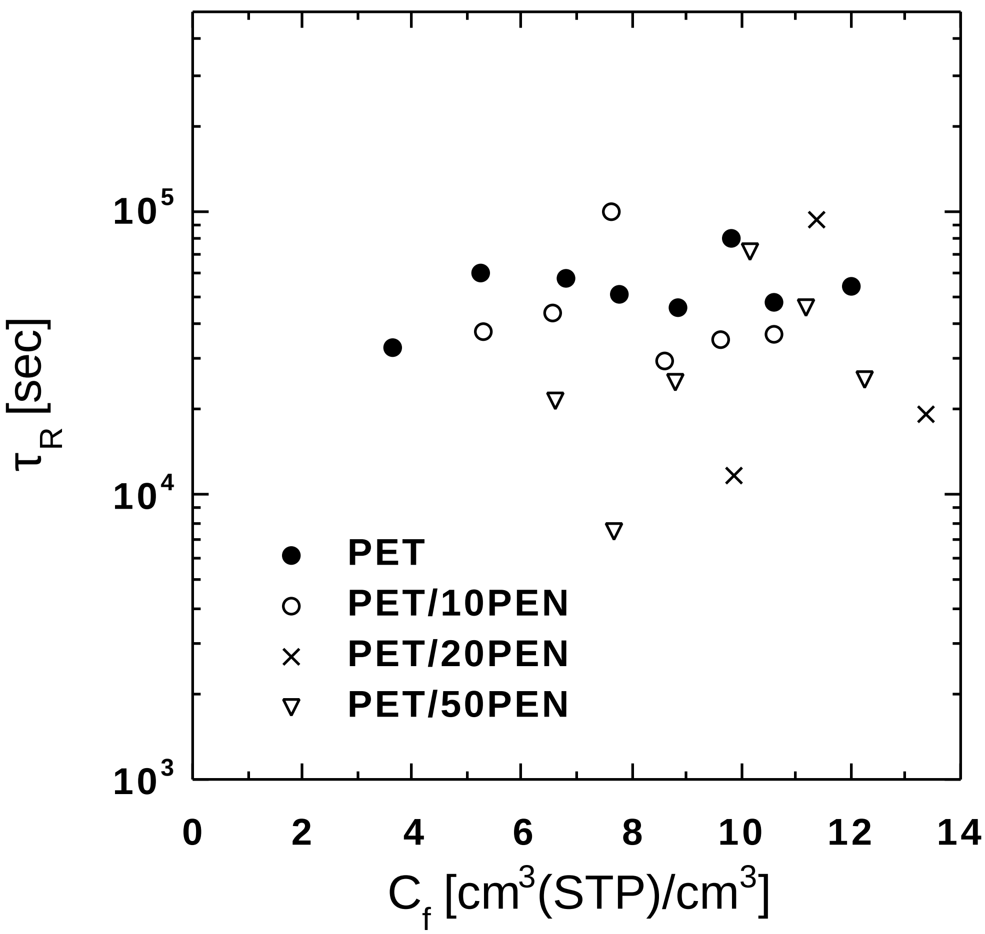

Figure 5.8. Characteristic Relaxation Time During Interval Acetone Sorption as a Function of Final Acetone Concentration

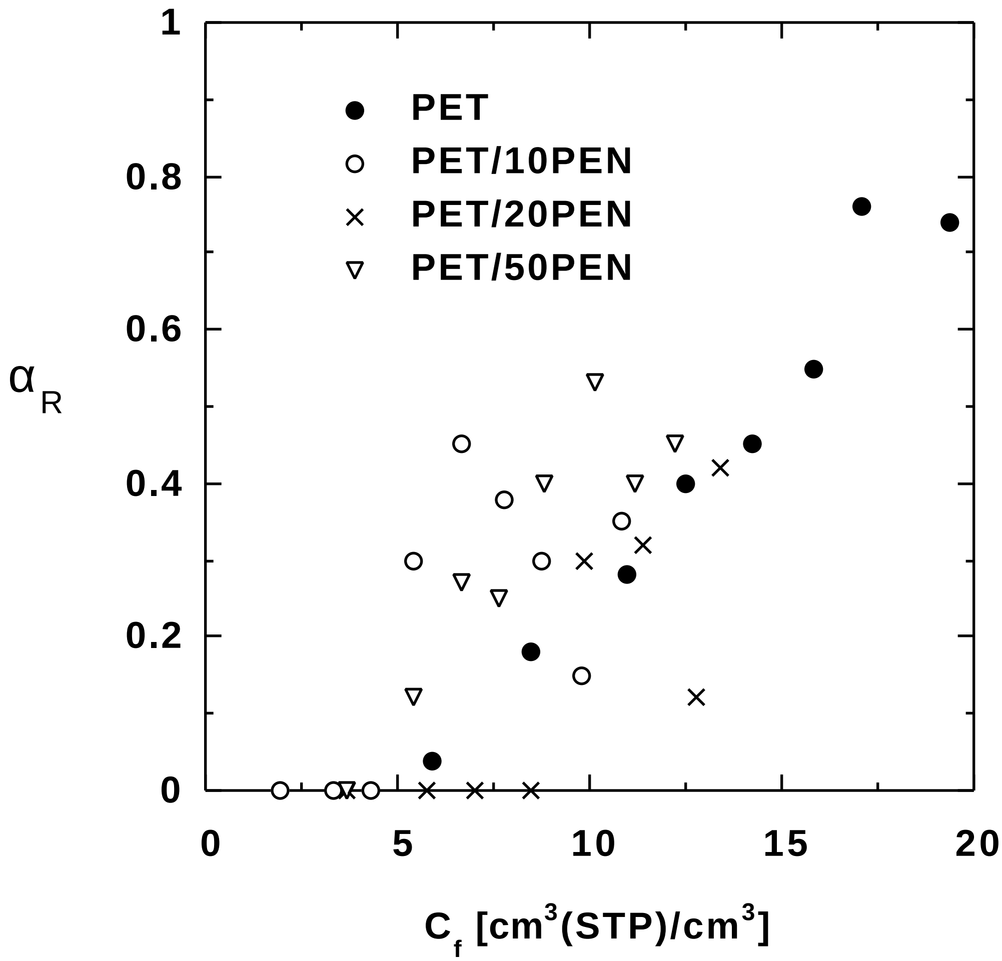

Figure 5.9. Effect Acetone Concentration on Fraction of Sorption Controlled by Kinetics of Penetrant-Induced Polymer Relaxation in PET/PEN Copolymers

Chapter 6. Acetone Solubility, Diffusivity, and Physical Characterization of Poly(ethylene terephthalate) Modified with Low Levels of 2,6-Naphthalene Dicarboxylic Acid, Isophthalic Acid, and 2,5-Bis-(4-carboxyphenyl)-1,3,4-Oxadiazole

I. Introduction

Recently, acetone sorption and transport properties of a systematic series of random copolymers of PET and poly(ethylene 2,6-naphthalate) [PEN] were reported (*cf*. Chapters 4 and 5). Based on results from this study, copolymerization of PET with PEN improves organic vapor barrier properties of PET(*cf*. Chapters 4 and 5). Previously, Light and Seymour reported a systematic investigation of the effect of polyester chemical structure on oxygen and carbon dioxide permeation properties.[69] Based on their results, copolymerizing PET with either 50% PEN or 50% poly(ethylene isophthalate) [PEI] improved barrier properties to oxygen and carbon dioxide.[69] Copolymerizing PET with 13 and 31% poly(1,4-cyclohexylene dimethylene terephthalate) [PCDT] results in a polymer with higher oxygen and carbon dioxide permeability coefficients than those of PET.[69]

In this study, the effect of copolymer composition on the sorption and transport of acetone in random copolyesters rich in PET are reported. In the preparation of the copolymers, as much as 10% weight percent of the dimethyl terephthalate [DMT] in the reaction mixture was replaced by either dimethyl 2,6-naphthalate [NDC], isophthalic acid [IPA], or 2,5-bis-(4-

carboxyphenyl)-1,3,4-oxadiazole [ODCA]. In this report, copolymers will be identified with the acronyms PET/PEN for PET modified with NDC, PET/PEI for PET modified with IPA and PET/PEOD for PET modified with ODCA. A number in front of the second copolymer component will represent the weight percent of DMT replaced by the alternate diacid. For example PET/5PEOD would be a copolymer where 5% of the DMT was replaced by ODCA. The sorption and transport of acetone at 35˚C in solvent cast films of these materials were characterized by kinetic gravimetric sorption. A Fickian model of mass uptake describes acetone sorption kinetics. These acetone sorption studies are complemented by differential scanning calorimetry [DSC], wide-angle X-ray diffraction [WAXD], and infrared spectroscopy [IR] characterization of the copolymers.

II. Experimental

Polymer Synthesis

Copolymers were synthesized similarly to PET (*cf*. Chapter 3), substituting a portion of the dimethyl terephthalate with dimethyl 2,6-naphthalene dicarboxylate [NDC], isophthalic acid [IPA] or 2,5-bis-(4-carboxyphenol)-1,3,4-oxadiazole [ODCA]. The structures of the resulting copolymers are presented in Figure 6.1.

III. Results and Discussion

Polymer Characterization

Second scan DSC thermograms of the as-cast films are presented in Figures 6.2a, 6.2b, and 6.2c. Each film exhibits a single glass transition, a crystallization exotherm, and a melting endotherm. The copolymers contain measurable levels of crystallinity, as indicated by the cold crystallization exotherms centered at T_c and the melting endotherms centered at T_m in the DSC thermogram. The cold crystallization exotherm is observed, as expected, above T_g.[46] The weight percent crystallinity was calculated as follows:

$$X_c = \frac{\Delta H_m - \Delta H_c}{\Delta H_f} \times 100, \tag{6.1}$$

where ΔH_m is the enthalpy of melting determined by DSC, ΔH_c is the enthalpy of crystallization determined by DSC, and ΔH_f is the enthalpy of fusion for PET. The enthalpy of fusion for PET is 140 J/g.[47] This calculation presumes no cocrystallization of PET with the other polyesters. While we did not find systematic studies of the crystal structure of PET/PEI or PET/PEOD copolymers, Lu and Windle report that co-crystallization occurs in PET/PEN copolymers only when samples are subject to high temperature annealing and high draw ratio.[68]

Table 6.1 summarizes the DSC results for these polyester films. There is a single glass transition at each composition, consistent with the notion that these samples are random copolymers. Figure 6.3a presents the glass/rubber transition temperature in the copolyesters as a function of weight percent modifier. The glass transition temperature increases with increasing weight percent PEOD. The weight percent crystallinity decreases with increasing PEOD content, which is expected for random copolymers.[68] The same trends in crystallinity with composition are observed for PET/PEN. However, in the narrow composition range presented in Table 6.1, PEN content has little effect on the glass transition temperature (*cf*. Figure 6.2b). The glass transition temperatures of PET/PEN copolymers are well-described using the Gordon-Taylor equation[73] for phase-continuous copolymers (*cf*.

Chapter 4). Modification of PET with 2.4 weight % IPA decreases the glass transition temperature and decreases the level of crystallinity (Figure 6.2c). The glass transition of the PEI/PET copolymer, 72˚C, is between the T_g's of PET (81˚C) and PEI (68˚C),[69] and is higher than the glass transition of PET/50PEI, 69˚C.[69] In this regard, the T_g of this polymer is in reasonable agreement with the literature values just presented. However, based in the Gordon-Taylor equation, a T_g of 80˚C would be predicted for a 2.4% copolymer, and a T_g of 74 ˚C would be predicted for a 50% copolymer. The reason for the discrepancy between the theoretical prediction and experimentally measured T_g for the PET/PEI copolymer is not known. Figure 6.3b presents the melting temperature of the copolyesters as a function of weight percent modifier. The weight percent modifier in the copolyester appears to have a stronger effect on the melting temperature than the chemical structure of the modifying agent.

In addition to the DSC data, Table 6.1 presents density values for the films. The density of PET, 1.373 g/cm^3, compares well with literature values for a sample with 40 weight percent crystallinity (*cf*. Chapter 3). The densities of the copolymers decrease with increasing weight percent modifier, largely due to a decrease in crystallinity. The amorphous density was estimated as follows:

$$\rho_a = \frac{\rho - \frac{X_c}{100}\rho_c}{(1 - \frac{X_c}{100})} \tag{6.2}$$

where ρ_a is the estimated density of the amorphous phase material in the sample, ρ is the measured density, X_c is the weight percent crystallinity determined by DSC and ρ_c is the crystalline density of PET, (1.440 g/cm^3)[45].

Fractional free volume in the amorphous phase of the sample [FFV_a] was estimated as follows:[4]

$$FFV_a = \frac{\frac{MW}{\rho_a} - V_o}{\frac{MW}{\rho_a}} \qquad (6.3)$$

where MW is the average molecular weight of a monomer unit, and V_o is an estimate of the so-called occupied volume. V_o is estimated using the equation:[4]

$$V_o = 1.3V_W, \qquad (6.4)$$

where V_W is the van der Waals volume calculated using the group contribution method suggested by Bondi.[12]

Figure 6.4 presents the WAXD spectra for a PET film and the PET/10PEOD film. The spectrum of the PET film is typical of other PET WAXD spectra reported in the literature[48] and has been described in detail previously (*cf*. Chapter 3). The spectrum of the PET/10PEOD film exhibits peaks in the same locations as the PET spectrum (2θ = 16.4, 22.0, and 25.1°) suggesting the same crystalline unit cell as PET and, therefore, no co-crystallization of PEOD with PET. The peaks are much less intense in the PET/10PEOD spectrum than in the PET spectrum because of the lower levels of crystallinity in the PET/10PEOD film. PET/10PEOD spectrum is typical of the WAXD spectra for the other copolyesters.

The weight percent crystallinity, as determined by WAXD, for each sample are included in Table 6.1. These values were obtained by computing the area under the amorphous halo and crystalline peaks after establishing a baseline for the spectrum. The weight percent crystallinity was then estimated as $A_C/(A_A+A_C)x100$ where A_C is the area associated with the crystalline peaks and A_A is the area associated with the amorphous peak. In general, the weight percent crystallinity determined by this method and by DSC are in excellent agreement. There is a discrepancy in the weight percent crystallinity as determined by the two experimental methods in the PET/5 PEOD film. As the experimental procedures and calculations were consistent, the reason for the discrepancy in this film is not well understood. The spectrum from the PET/10PEN film shows hints of crystalline peaks, but the diffraction pattern is too weak for quantitative analysis.

Acetone Sorption

Figure 6.5 presents the fractional acetone mass uptake in a film of PET/10PEOD as a function of time for a integral sorption experiment at 5.4 cm Hg and 35˚C. The sorption data for this film are representative of the sorption data for the other films. The integral sorption kinetics are well described by the following solution to Fick's Law for diffusion in a plane sheet of uniform thickness:[5]

$$\frac{M_t}{M_\infty} = 1 - \frac{8}{\pi^2} \sum_{n=0}^{\infty} \frac{1}{(2n+1)^2} \exp\left(\frac{-\bar{D}(2n+1)^2 \pi^2 t}{\ell^2} \right) \tag{6.5}$$

where M_t is the mass uptake at time t, M_∞ is the ultimate amount of mass uptake, and ℓ is the film thickness. $\bar{D}$ is approximately equal to the diffusion coefficient averaged over the concentration interval of the experiment:[5]

$$\bar{D} = \frac{1}{C_f - C_i} \int_{C_i}^{C_f} D\,dC, \tag{6.6}$$

where C_f and C_i are the penetrant concentrations at $t=\infty$ and $t=0$, respectively. The fit of the data to Equation 6.5 is shown in Figure 6.5 as a solid curve.

From a least-squares fit of the sorption data to Equation 6.5, values of $\bar{D}$ and M_∞ are determined. A value for the solubility coefficient, S, in $cm^3(STP)/(cm^3 \cdot atm)$, can be calculated from M_∞ as:

$$S = \frac{M_\infty}{M_o} \times \frac{\rho}{MW_{penetrant}} \times \frac{22{,}414}{p} \tag{6.7}$$

where M_o is the mass of the penetrant-free polymer, p is the final pressure in the experiment in atm, $MW_{penetrant}$ is the penetrant molecular weight in g/mole, and 22,414 is the conversion from moles to cm^3(STP). Table 6.2 presents acetone solubility, diffusivity, and calculated permeability values for the copolymers. The permeability of the polymer sample to acetone may be estimated as the product of solubility and diffusivity.[27]

Figure 6.6a presents the solubility of acetone in the copolymers as a function of weight percent modifier for integral sorption experiments at 35°C and an acetone relative pressure of 0.15 (5.4 cm Hg pressure). The solubility values decrease modestly with increasing PEN content, despite a decreasing level of crystallinity. The acetone solubility does not change appreciably with incorporation of 2.4% IPA, despite decreasing crystallinity. PET/PEI and PET have the same chemical structure except that some *p*-phenylene rings are replaced by *m*-phenylene rings. Therefore, changes in acetone solubility between PET and PET/PEI are expected to be more strongly dependent on morphology and non-equilibrium packing in the glassy polymer matrix than on changes in the chemical affinity between acetone and the polymer matrix. Acetone solubility increases with increasing ODCA content in the PET/PEOD copolymers. Based on the solubility parameter of acetone and estimated solubility parameters of the polymers, (*cf*. Table 6.3), acetone should be more soluble in PET/PEOD copolymers than in PET, but less soluble in PET/PEN copolymers than in PET.

Crystallites imbedded in a polymer matrix generally preclude penetrant sorption.[15,18] Therefore, a two phase model is used to describe penetrant sorption in semicrystalline polymers:[20]

$$S = \Phi_a S_a, \tag{6.8}$$

where Φ_a is the amorphous volume fraction in the semicrystalline polymer, and S_a is the solubility of penetrant in the amorphous regions of the polymer matrix. This model has been applied with excellent success to describe the effect of crystallinity on gas solubility in rubbery polymers[18] and provides a reasonable description of the effect of crystallinity on gas solubility in PET.[20] Therefore, Figure 6.6b presents the calculated amorphous-phase solubility, estimated from Equation 6.8, as a function of weight percent modifier. Since there are no data available for amorphous densities available for PEI or PEOD, the amorphous volume fractions for PET/PEI and PET/PEOD samples are estimated as $1-X_c/100$. As the density of crystalline PET and amorphous PET and PEN are all within 10% of each other, this estimate of amorphous volume fraction for PET/PEI and PET/PEOD is reasonable. Figure 6b shows that while crystallinity has an effect on acetone solubility in the copolyesters, the changes in acetone solubility cannot all be attributed to changes in crystallinity. Other effects, such as chemical affinity of the penetrant for the polymer matrix and non-equilibrium packing in the amorphous matrices of these glassy copolymers may also play a significant role in determining penetrant solubility.

The values of $\overline{D}$ from the Fickian model fit to the kinetic sorption data are presented in Figure 6.7a as a function of weight percent modifier in the copolymers. Acetone diffusivity decreases with increasing PEN in PET/PEN copolymers content even though crystallinity decreases with increasing PEN content. Since crystalline regions in a polymer matrix usually act as impenetrable barriers in a polymer matrix and, therefore, act to decrease diffusion coefficients,[17,19] the observed decrease in diffusivity is in the opposite direction expected based simply on the crystalline content of the samples. Based on the higher T_g values in copolymers with higher concentrations of PEN, the decrease in diffusivity is linked to more restricted segmental motion in the copolymers than in PET. Acetone diffusivity is higher in the PET/2.4PEI film than in PET, due in part to decreased crystallinity and to an increase in FFV_a in PET/2.4PEI relative to PET. Acetone diffusivity in the PET/PEOD films appears to go through a maximum at PET/5PEOD. There is also a maximum in FFVa (*cf*. Table 6.1) at PET/5PEOD, which may contribute to the maximum in diffusion coefficient.

Michaels *et al*. found that the effect of crystallinity on gas (O_2, N_2, CO_2, CH_4, He) diffusion in PET could be expressed as:

$$\overline{D} = \overline{D}_a \Phi_a \tag{6.9}$$

where D_a is the diffusion coefficient in the amorphous regions of the polymer matrix. Therefore, acetone diffusion coefficients in the amorphous phase of the copolymers can be estimated by dividing the measured diffusion coefficient by the amorphous volume fraction. Figure 6.7b presents calculated amorphous phase acetone diffusivity, estimated from Equation 6.9, as a function of weight percent modifier in the copolymers. If the simple model in Equation 6.9 is valid for acetone as it is for other penetrants, then the observed variations in acetone diffusivity in the polyesters cannot be ascribed solely to changes in crystallinity.

Besides crystallinity, several other factors may contribute to the observed changes in acetone diffusion coefficients with polymer composition in these copolyesters. If the modifiers restrict chain dynamics (manifested by an increase in T_g) or if they decrease amorphous fractional free volume, diffusion coefficients can decrease and vice versa. The diffusion coefficients reflect the composite results of each comonomer's ability to disrupt crystallinity, influence segmental dynamics, and effect chain packing in amorphous regions of the polymer matrix. Estimated amorphous acetone diffusivity decreases with increasing PEN content in PET/PEN copolymers due to more restricted segmental chain dynamics. The estimated amorphous phase acetone diffusivity is higher in PET/2.4 PEI than PEN due to a slightly higher FFV and less restrictive segmental dynamics. There is a maximum in amorphous acetone diffusivity in PET/PEOD copolymers at PET/5PEOD, accompanied by a maximum in FFV.

As shown in Figure 6.8, there is an interesting correlation between acetone diffusion coefficients and acetone solubility in the amorphous regions of the copolymers. The diffusion coefficients are measured at a fixed acetone pressure of 5.4 cm Hg, and, based on results in Figure 6.6b, amorphous phase acetone concentration can vary by a factor of approximately two, depending on the comonomer and it's concentration. If diffusivity changes with penetrant concentration in the polymer, then this effect can also contribute to the differences in the values of diffusion coefficients in Figure 6.7b.

Acetone permeability (calculated as explained in Table 6.2) for the copolymers are presented in Figure 6.9 as a function of weight percent modifier. Calculated acetone permeability generally decreases as PEN concentration in the copolymer increases. This decrease has been linked to an increase in amorphous phase packing with increasing PEN content as probed by positron annihilation lifetime spectroscopy [PALS], densitometry, and infrared spectroscopy [IR] (*cf*. Chapter 4). Error bars for Figures 6.6, 6.7, and 6.9 were estimated using a propagation of error technique.[58] The largest source of error in diffusivity and calculated permeability values is the uncertainty associated with the thickness of the polymer films.

The PET/2.4PEI film has a calculated acetone permeability coefficient similar to that of to the PET. This result is interesting since the oxygen and carbon dioxide permeabilities for PEI and 50/50 PET/PEI are reported to be lower than those of PET.[69] PEI has a higher amorphous density than PET,[69] suggesting that PEI packs more efficiently in the amorphous phase than PET. Typically, the free volume of meta-connected amorphous polymers is lower than that of the analogous para-connected, amorphous polymers.[94] Meta-connected aromatic rings, in contrast with para-connected rings, cannot undergo extensive ring flipping (so-called π flips) without cooperative motions of neighboring units in the polymer backbone.[94] Since a meta-linked polymer cannot sequester free volume through highly activated ring flipping motions at ambient conditions, it typically has less free volume and lower permeability coefficients than it's para-linked analog.[94,95]

The PET/5PEOD film has a higher calculated acetone permeability than either the PET film or PET/10PEOD film. This higher permeability coefficient is due to a higher acetone diffusion coefficient (*cf*. Figure 6.7), which may be attributed to a higher fractional free volume in PET/5PEOD than in PET or PET/10PEOD (*cf*. Table 6.1).

Conformational Analysis by Infrared Spectroscopy

IR studies of PET have been used to determine the conformation of ethylene glycol (EG) linkages in the chain backbone.[75] The glycol linkage conformation has been related to the density in the amorphous phase and, in turn, to transport properties of small molecules in PET. The ethylene glycol residue in PET can exist in either the trans or gauche conformations.[75] This notion is expressed mathematically as follows:

$$T + G = 1 \tag{6.10}$$

where T is the weight fraction of polymer containing EG units in the trans conformation and G is the weight fraction of polymer containing EG units in the gauche conformation. T and G are calculated from peak absorbances as previously described by Lin and Koenig,[75] using the following equations:

$$T = \frac{A_{1337\ cm^{-1}}}{A_{1337\ cm^{-1}} + A_{1365\text{-}70\ cm^{-1}}} \tag{6.11}$$

$$G = \frac{A_{1365\text{-}70\ cm^{-1}}}{A_{1337\ cm^{-1}} + A_{1365\text{-}70\ cm^{-1}}} \tag{6.12}$$

where $A_{1337\ cm^{-1}}$ is area under the peak at 1337 cm^{-1} and $A_{1365\text{-}70\ cm^{-1}}$ (associated with EG units in the trans conformation) is area under the peak located between 1365-70 cm^{-1} (associated with EG units in the gauche conformation). The 1337 cm^{-1} peak in both PET and PEN is attributed to wagging of CH_2 groups in the trans conformation.[89] The medium weak 1365 cm^{-1} peak in PET and the medium strong 1370 cm^{-1} peak in PEN are attributed to the wagging of CH_2 groups in the gauche conformation.[89] All of the ethylene glycol linkages in crystalline PET are commonly understood to be in the trans conformation, but amorphous material contains a mixture of EG linkages in the trans and gauche conformations.[75] Therefore, Equation 6.10 can be rewritten as follows:

$$T_a + T_c + G = 1 \tag{6.13}$$

where T_a is the weight fraction of polymer that is amorphous and contains EG linkages in the trans conformation. T_c is the weight fraction of polymer that is crystalline and contains EG linkage in the trans conformation. Since all EG units in crystalline PET are in the trans conformation, T_c is taken to be to $X_c/100$. Therefore, Equations 6.11-13 can be used to estimate the weight fraction of polymer in the amorphous phase and having ethylene glycol units in the trans conformation as shown in the following equation:

$$T_a = 1 - \frac{X_c}{100} - \frac{A_{1365-70\ \mathrm{cm}^{-1}}}{A_{1337\ \mathrm{cm}^{-1}} + A_{1365-70\ \mathrm{cm}^{-1}}}\,. \tag{6.14}$$

Table 6.4 presents the results of this analysis for the copolymers. Previously, trans amorphous content in PEN/PET copolymer films was found to increase with increasing PEN content (*cf*. Chapter 4). However, at low concentration of PEN, PEI, or PEOD, there is no strong systematic effect of copolymerization on ethylene glycol unit conformation.

The incorporation of naphthalene units, even at low concentration, into a PET backbone increases amorphous phase chain packing and leads to a decrease in acetone diffusion coefficients. This effect, however, is not common to all of the modifiers considered. In fact, incorporation of isophthalate and 2,5-bis-(4-carboxyphenyl)-1,3,4-oxadiazole residues at low concentration can increase acetone diffusion coefficients. While crystallinity is an important factor in sorption, diffusion, and permeation properties, these results suggest that other factors (such as amorphous phase chain packing, polymer/penetrant affinity, and macromolecular chain dynamics) also influence the sorption and diffusion of organic penetrants in polyesters.

IV. Conclusions

Random copolymers were prepared based on poly(ethylene terephthalate) and modified by replacing the terephthalate linkage in the backbone with either 2,6-naphthalate, isophthalate, or 2,5-bis-(4-carboxyphenyl)-1,3,4-oxadiazole linkages at low (up to 10 weight percent) levels of substitution. Copolymers containing 1-10 weight percent PEN exhibited higher glass transition temperatures and lower levels of crystallinity than those of PET. Copolymers containing 5-10 weight percent PEOD also exhibited higher glass transition temperatures and lower levels of crystallinity than those of PET. The copolymer containing 2.4 weight percent PEI has a lower glass transition temperature and a lower level of crystallinity than PET. The acetone diffusion coefficients were lower in copolymers containing PEN than those in PET. In PET/PEOD copolymers, there was an apparent maximum in acetone diffusivity at 5% PEOD content. The PET/PEOD copolymers had higher acetone solubilities that PET. A copolymer with 2.4 weight percent PEI had a higher acetone diffusivity a lower acetone solubility than PET. These composite studies indicate that even low levels of comonomers in PET-rich polymers can have a significant impact on the morphology, chain packing, macromolecular mobility, and, in turn, sorption and transport properties.

Table 6.1. Density, Thermal Transitions, and Crystalline Content in PET and Modified PET Films

Polymer, Modifier, Wt %, [Mol%]	**Density [g/cm^3]**	**Amorphous Fractional Free Volume**	**T_g [˚C]**	**T_c [˚C]**	**T_m [˚C]**	**X_c [wt %], DSC**	**X_c [wt %], WAXD**
PET	1.373	0.154 ± 0.06	81	141	255	40%	38%
PET / 5PEOD	1.347	0.175 ± 0.17	84	164	243	36%	26%
PET / 10PEOD	1.346	0.157 ± 0.06	89	172	234	20%	19%
PET / 1PEN	1.362	0.151± 0.06	82	-	251	27%	32%
PET / 3PEN	1.360	0.153 ± 0.06	85	149	246	28%	26%
PET / 5PEN	1.351	0.149± 0.07	79	136	244	15%	15%
PET / 10PEN	-	-	84	152	238	2%	-
PET / 2.4PEI	1.355	0.159 ± 0.11	72	124	242	29%	25%

Table 6.2. Solubility, Diffusivity, and Estimated Permeability of Acetone in Polyester Films at 35˚C

Polymer	**S [cm^3(STP)/cm^3/atm][a]**	**$\overline{D}$ x 10 [12] [cm^2/s][b]**	**Px 10^2 [Barrers][c]**
PET	129 ± 12	5.2 ± 1.0	8.9 ± 1.6
PET/5PEOD	158 ± 16	7.4 ± 1.3	15.2 ± 2.6
PET/10PEOD	167 ± 17	4.0 ± 1.1	8.8 ± 2.5
PET/1PEN	115 ± 11	3.8 ± 0.6	5.7 ± 0.9
PET/3PEN	140 ± 13	3.4 ± 0.6	6.3 ± 1.1
PET/5PEN	109 ± 11	3.1 ± 0.5	4.4 ± 0.8
PET/10PEN	110 ± 10	2.2 ± 0.5	3.2 ± 0.7
PET/2.4PEI	126 ± 14	6.8 ± 1.2	11.4 ± 2.0

[a] p = 5.4 cm Hg, p_{sat} = 36 cm Hg
[b] determined from interval sorption experiments with p_i = 0 and p_f = 5.4 cm Hg
[c] $P = S \times \overline{D}$

Table 6.3. Solubility Parameters of Polyesters and Acetone

	Solubility Parameter [$(cal/cm^3)^{1/2}$]
Acetone[81]	9.9
PEOD[a]	10.2
PET[a]	10.8
PEI[a]	10.8
PEN	11.2

[a] estimated using group contribution method of Hoy[82]

Table 6.4. Conformational Analysis of Copolymers by Infrared Spectroscopy

Polymer	**T**	**$T_c = X_c/100$**	**G**	**T_a**
PET	0.87	0.40	0.13	0.47
PET/5PEOD	0.85	0.36	0..49	0.49
PET/10PEOD	0.53	0.20	0.30	0.23
PET/1PEN	0.71	0.27	0.29	0.40
PET/3PEN	0.75	0.28	0.25	0.47
PET/5PEN	0.61	0.15	0.39	0.46
PET/10PEN	0.51	0.02	0.49	0.49
PET/2.4PEI	0.76	0.29	0.24	0.47

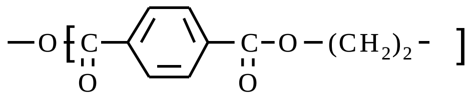

Poly(ethylene terephthalate) [PET]

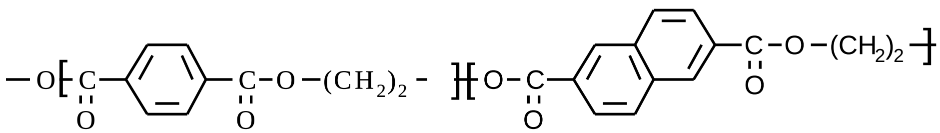

Poly[(ethylene terephthalate)-co-(ethylene 2,6-naphthalate) [PET / PEN]

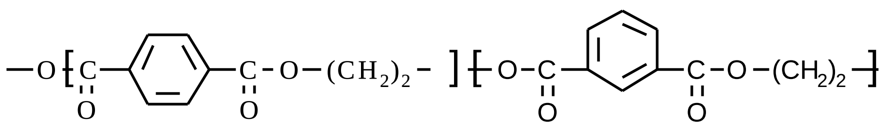

Poly[(ethylene terephthalate)-co-(ethylene isophthalate)] [PET / PEI]

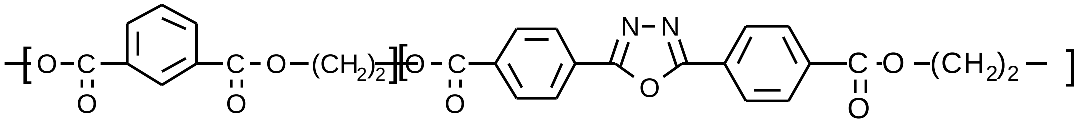

Poly[(ethylene terephthalate)-co-(ethylene 2,5-bis(4-carboxyphenyl)1,3,4-oxadiazole)-[PET / PEOD]

Figure 6.1. Primary Chemical Structures of PET and PET-based Copolymers

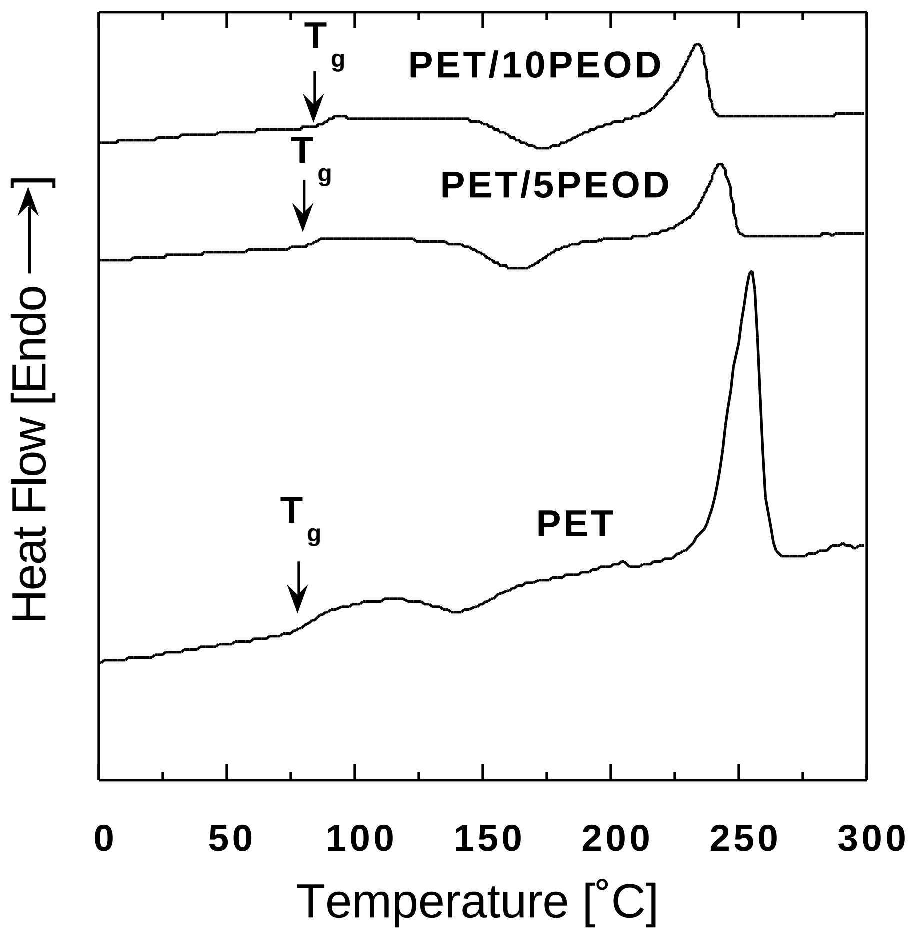

Figure 6.2a. DSC Thermograms of PET and PET Modified with PEOD

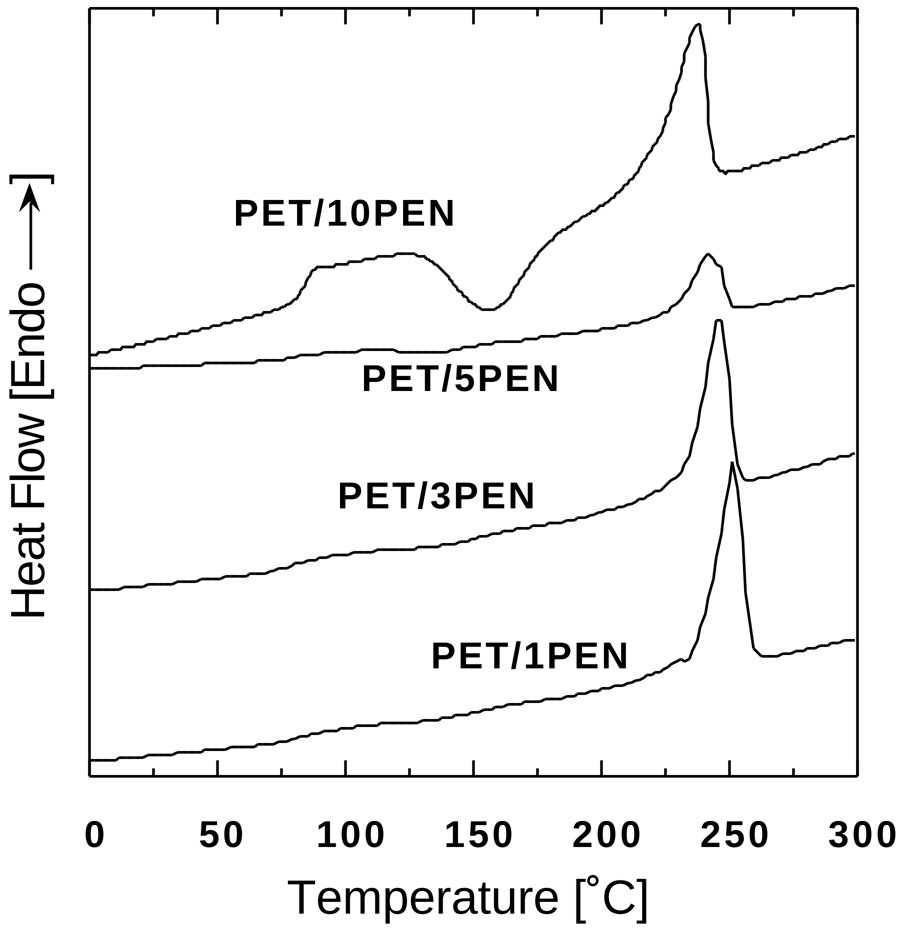

Figure 6.2b. DSC Thermograms of PET Modified with PEN

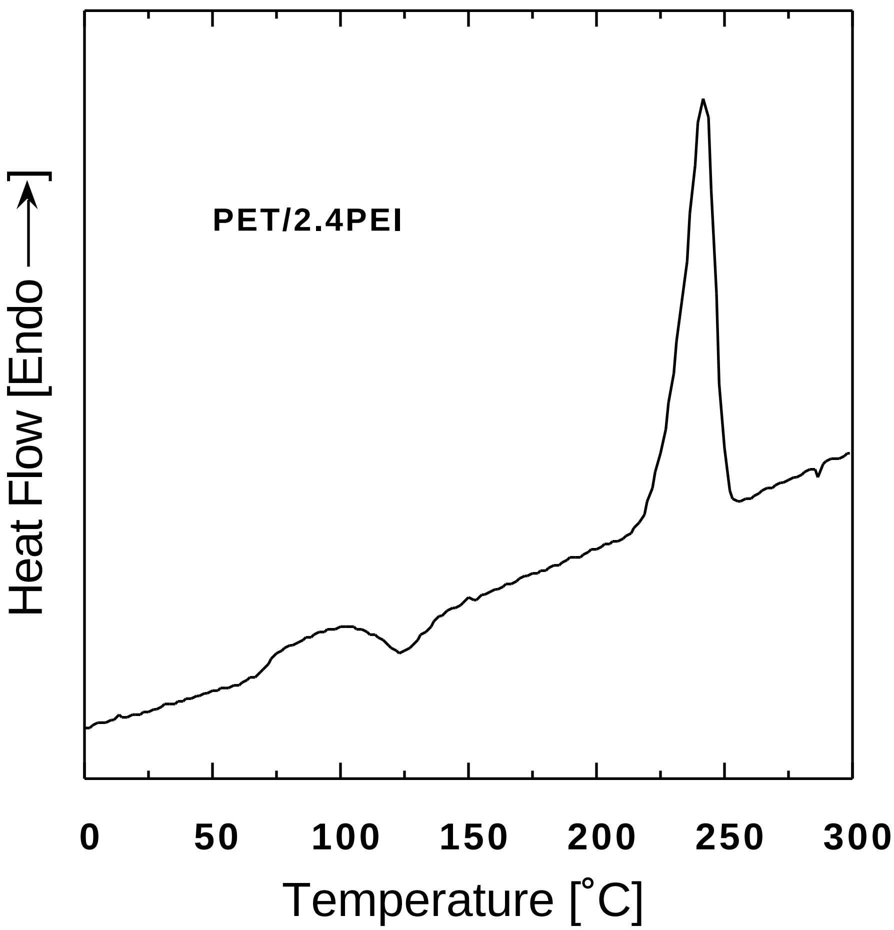

Figure 6.2c. DSC Thermograms PET Modified with PEI

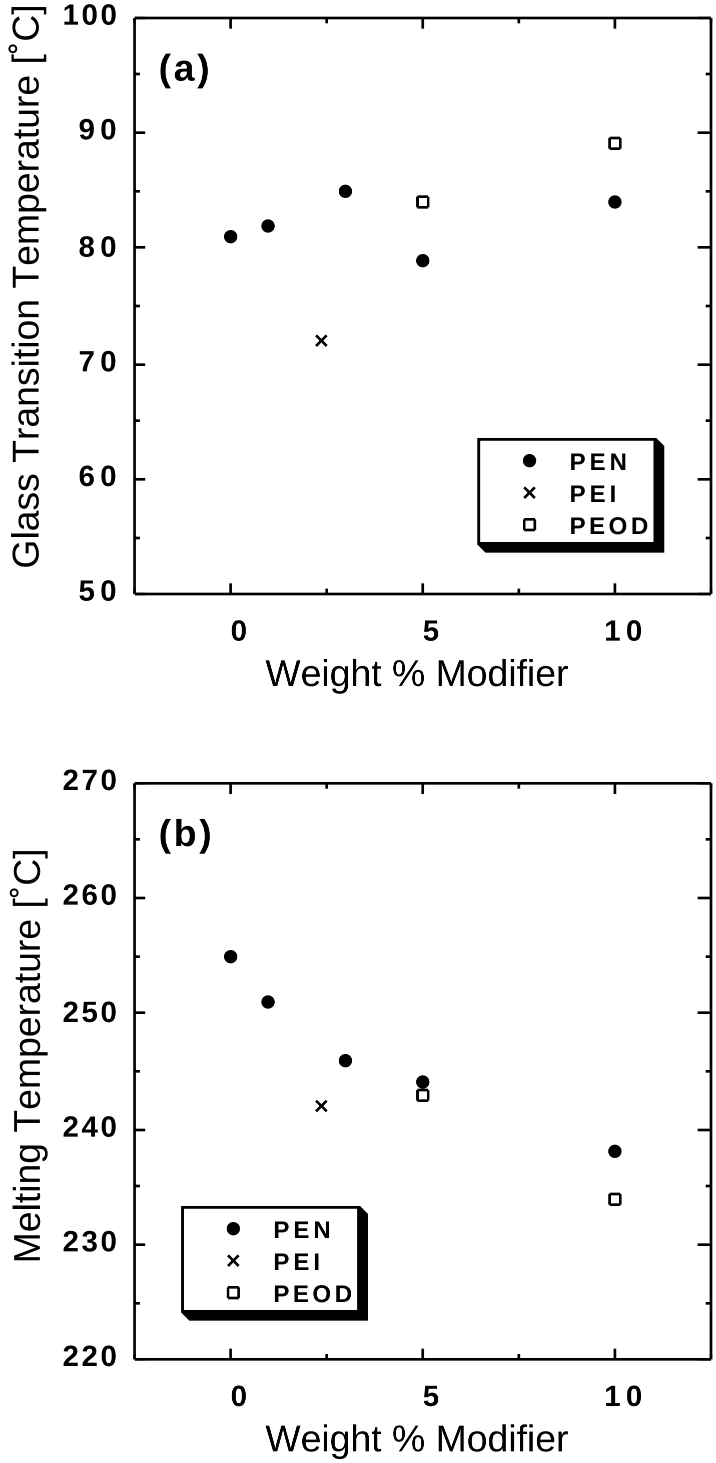

Figure 6.3. Thermal Transitions in PET-based Copolymers (a) Glass/Rubber Transition Temperature (b) Melting Temperature

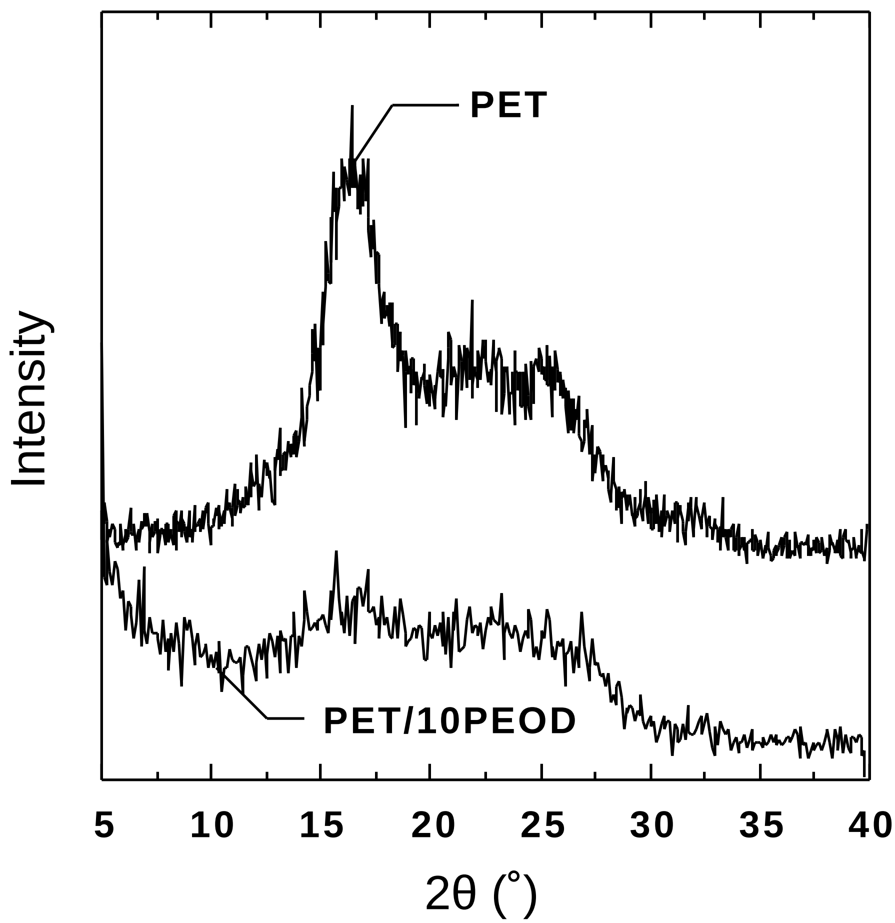

Figure 6.4. WAXD Spectrum of Solvent Cast Films of PET and PET/10PEOD

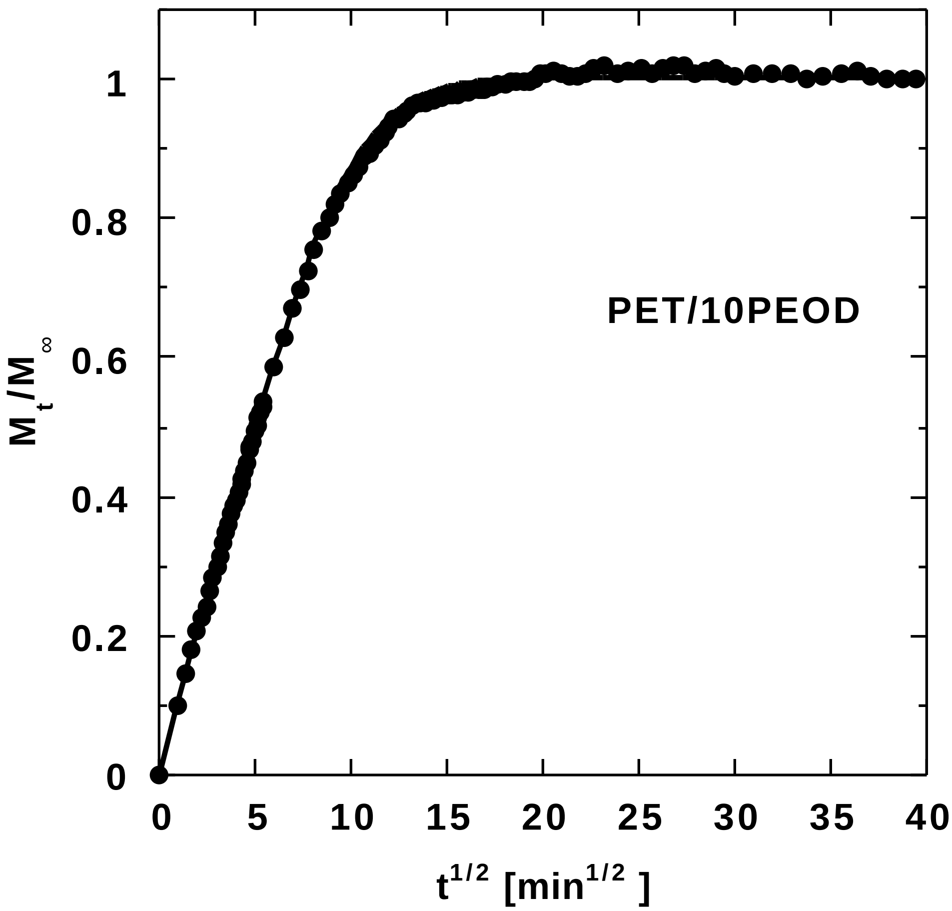

Figure 6.5. Acetone Sorption Kinetics of PET/10PEOD Film (T = 35˚C, p_i = 0 cm Hg, p_f = 5.4 cm Hg)

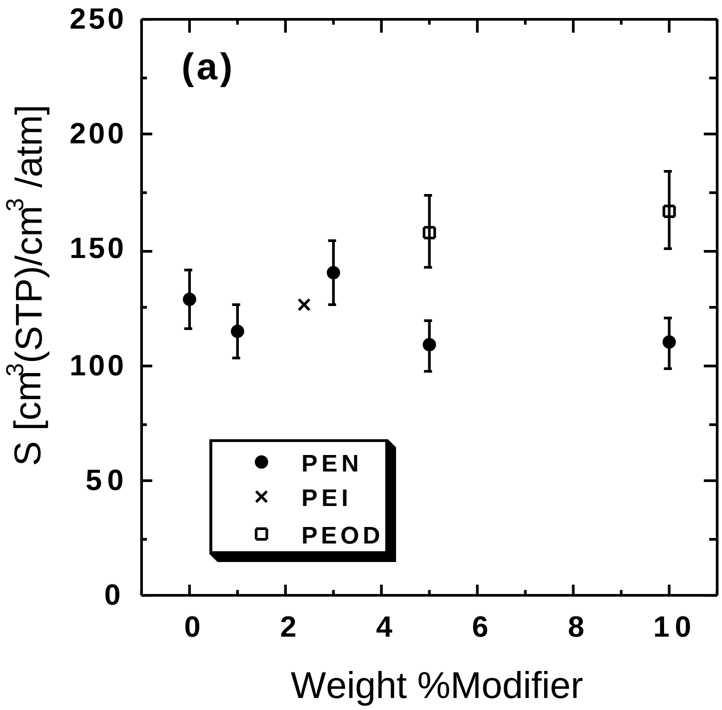

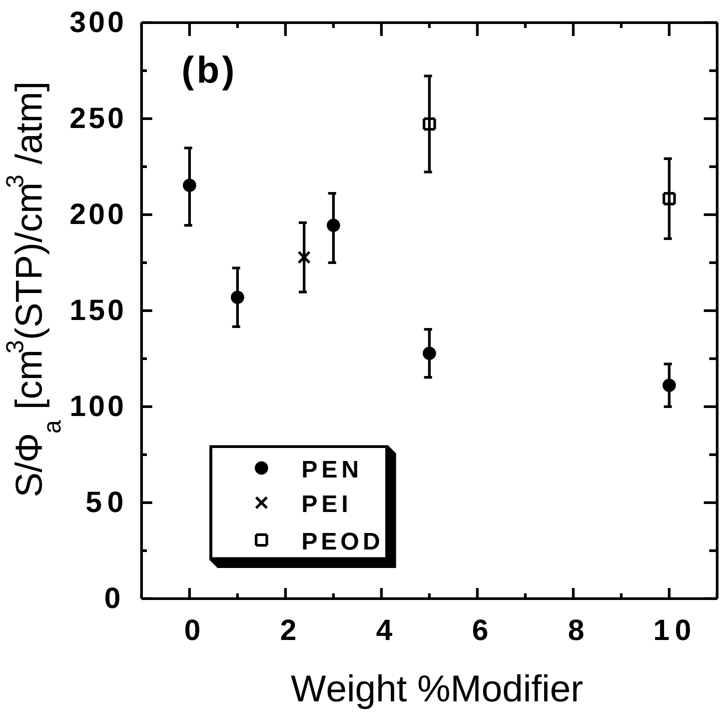

Figure 6.6. (a) Solubility of Acetone in PET Copolymers (b) Estimated Solubility of Acetone in Amorphous Regions of PET Copolymers (T = 35˚C, p = 5.4 cm Hg)

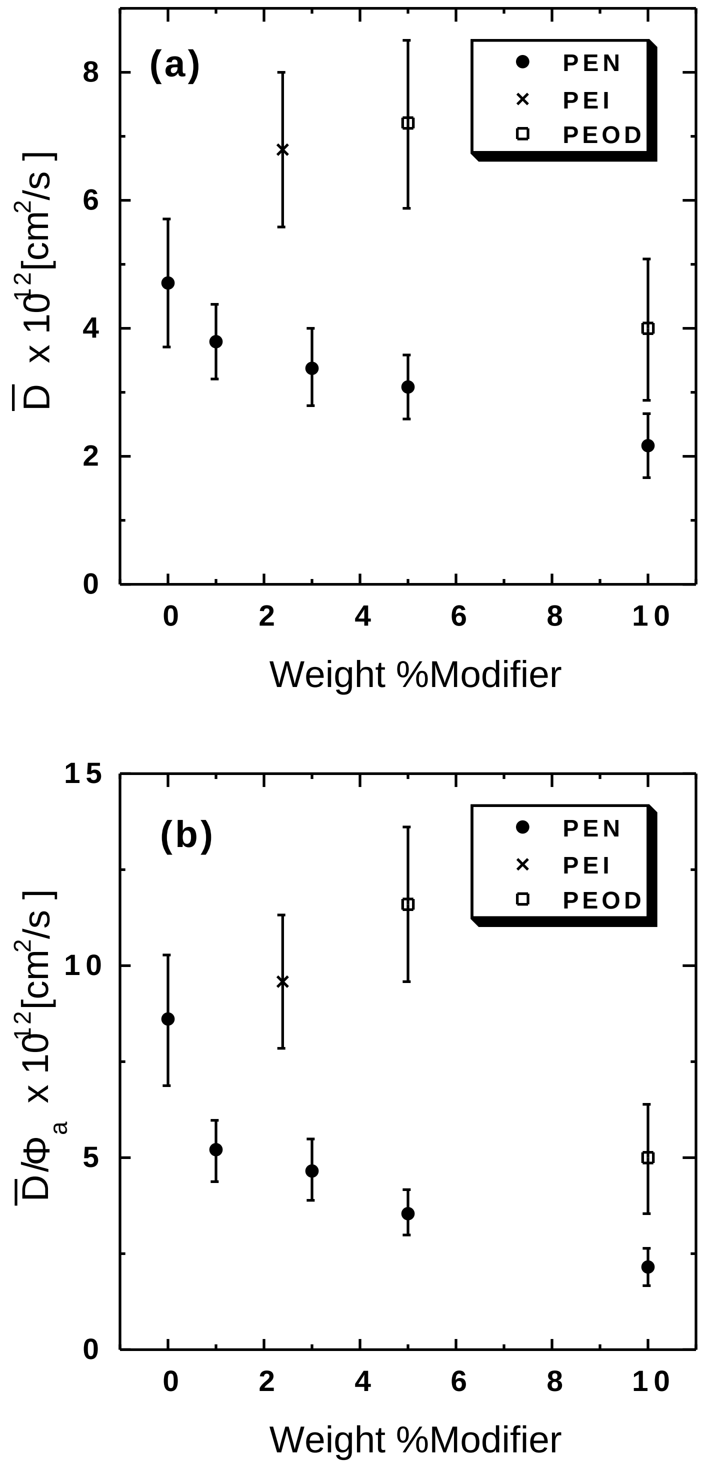

Figure 6.7. (a) Diffusivity of Acetone in PET Copolymers (b) Estimated Diffusivity of Acetone in Amorphous Regions of PET Copolymers (T = 35˚C, p_i = 0 cm Hg, p_f = 5.4 cm Hg)

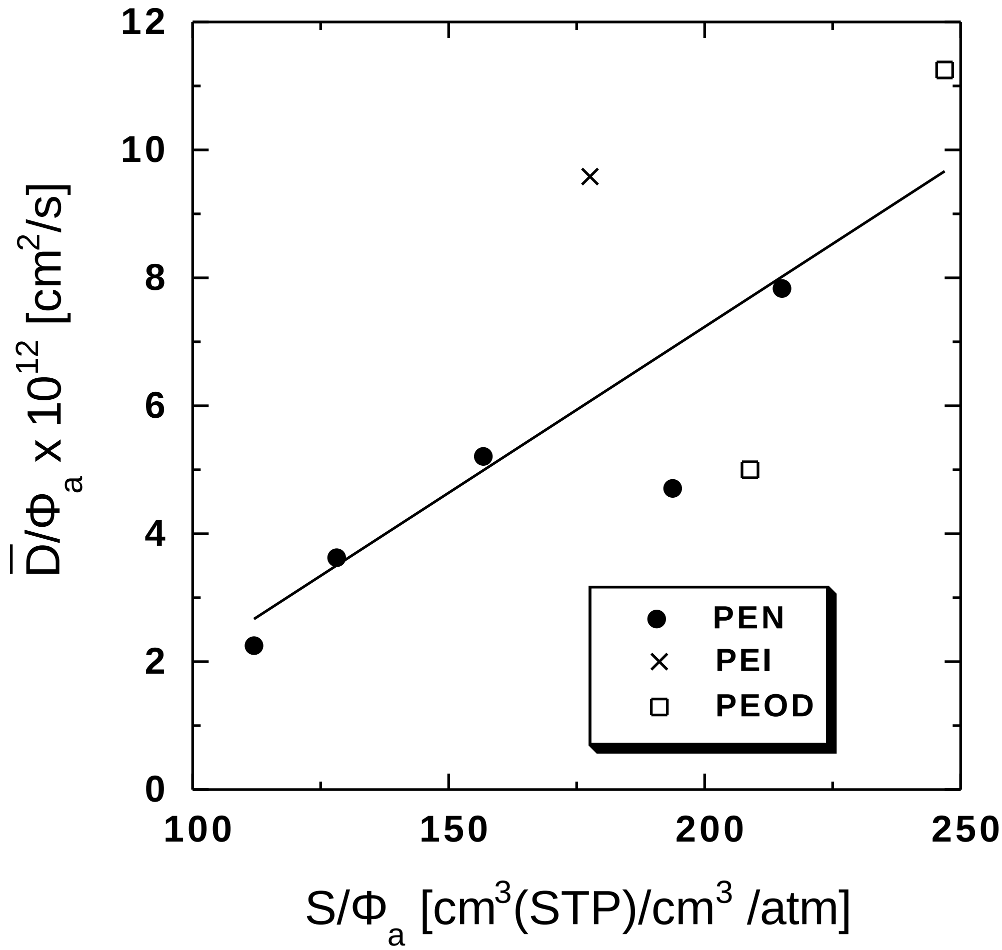

Figure 6.8. Estimated Diffusivity of Acetone in the Amorphous Regions of PET Copolymers as a Function of Estimated Acetone Concentration in the Amorphous Regions (T = 35˚C, p_i = 0 cm Hg, p_f = 5.4 cm Hg)

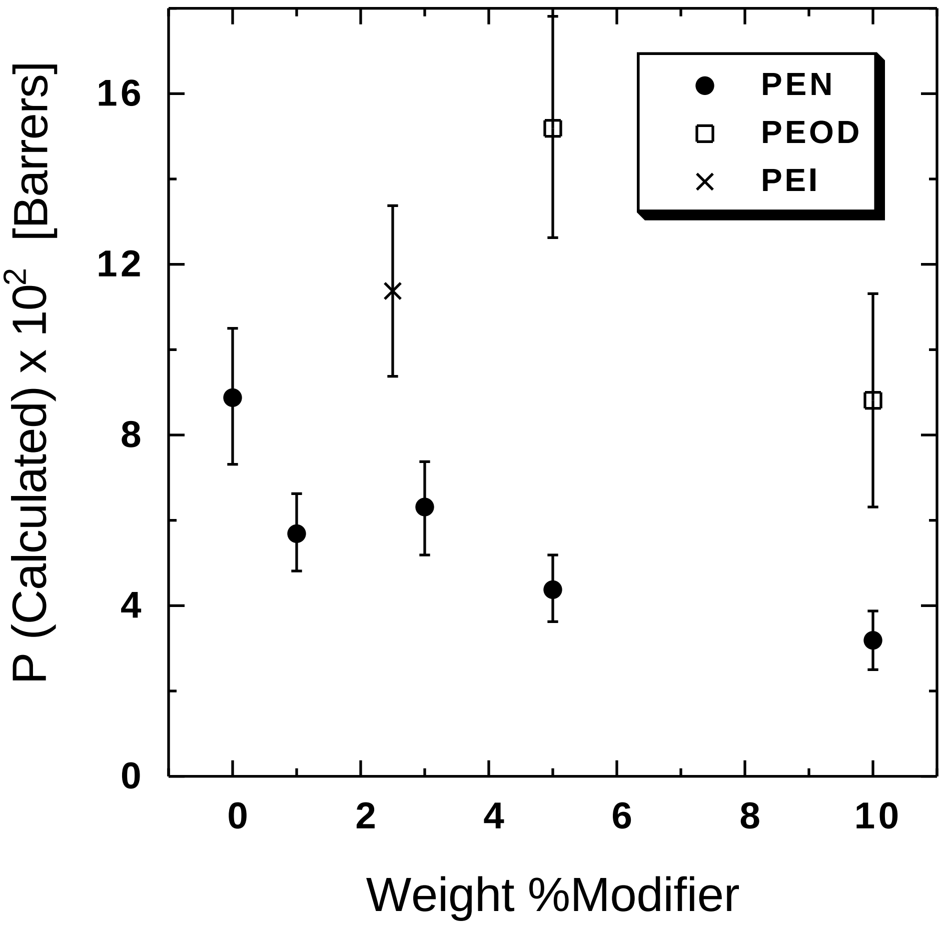

Figure 6.9. Calculated Permeability of PET Copolymers to Acetone (T = 35˚C, p_i = 0 cm Hg, p_f = 5.4 cm Hg)

Chapter 7. Conclusions and Future Work

A. Summary of the Conclusions

1. A spring balance equipped with a CCD camera, frame-grabber card, MacIntosh computer, and NIH Image software provides a straightforward, inexpensive mechanism for automation of spring balance systems to collect equilibrium uptake and kinetic sorption data.

2. The dual mode model adequately describes the equilibrium sorption of acetone in PET.

3. Interval kinetic gravimetric sorption of acetone in PET is described by an empirical two-stage model, with Fickian diffusion and polymer structural relaxation contributing to the control of mass uptake kinetics. The time constant of the relaxation process does not vary systematically with acetone concentration and has an average value of 53,000 ± 4,000 seconds (approximately 15 hours). The fraction of mass uptake associated with the relaxation process increases linearly with increasing concentration of acetone dissolved in the equilibrium densified region of the polymer matrix.

4. Acetone diffusivity increases with increasing concentration of acetone dissolved in the PET film. The standard dual mobility model cannot adequately account for this increase, implying that the acetone-induced polymer plasticization plays an important role in acetone diffusion. However, the experimental data were well described by an extended version of the dual mobility model where the diffusion coefficient of acetone in the Henry's law mode depends exponentially on concentration.

5. A series of random copolymers of PET and PEN were synthesized and characterized by DSC, WAXD, PALS, IR spectroscopy, and acetone sorption. The glass transition temperatures of the copolymers rise monotonically from 81˚C in PET to 123˚C in PEN. Copolymers with compositions rich in either homopolymer are semi-crystalline while copolymer of intermediate composition are amorphous. The estimated amorphous density is higher and amorphous fractional free volume is lower in the copolymers than in either homopolymer, suggesting that copolymerization leads to better chain packing in the amorphous regions of the polymer matrix even as copolymerization frustrates crystallinity. The amorphous phase free volume as probed by PALS decreases strongly with increasing PEN content, particularly at low concentration of PEN in PET.

6. Acetone uptake kinetics in solvent cast PET/PEN copolymer films at 35˚C and 5.4 cm Hg are well-described by Fick's law. The acetone diffusion coefficient decreases 93% from PET to PET/85PEN. The amorphous phase acetone solubility coefficient decreases by approximately a factor of two over the same composition range. The diffusion coefficient decreases 53% from PET to PET/10PEN; over the same composition range the weight percent crystallinity decreases from 40% to 0.

7. The acetone diffusion coefficients decrease as amorphous fractional free volume decreases. The acetone diffusion coefficients correlate well with the amorphous phase free volume as probed by PALS, suggesting that both static and dynamic free volume are important in the transport of acetone in these copolymers. Based on the results of an IR spectroscopy study, the fraction of amorphous phase EG units in the trans conformation increases with increasing PEN content. This increase in trans conformation may be

associated with the observed increase in chain packing and decrease in amorphous phase free volume.

8. Integral acetone sorption kinetics in PEN/PET copolymers from 0 to 5.4 cm Hg can be adequately described using a model incorporating only Fickian kinetics. The dual mode model adequately describes the equilibrium sorption of acetone in PEN/PET copolymers over a range of 0-7.3 cm Hg at 35˚C. Interval kinetic gravimetric sorption results over this pressure range can be described as a two-stage process, with both Fickian diffusion and polymer structural relaxation controlling mass uptake at short and long times, respectively.

9. The value of the Langmuir sorption capacity parameter decreases strongly with increasing PEN content up to PET/10PEN, implying an important reduction in the accessible non-equilibrium excess free volume associated with the glassy state of the polymer upon addition of modest amounts of PEN.

10. The dual mode sorption model describes the equilibrium sorption of acetone in PEN/PET copolymers at acetone pressures up to 7.3 cm Hg at 35˚C. Interval kinetic gravimetric sorption results over this pressure range can be described using an empirical two-stage model, with Fickian diffusion and polymer structural relaxation controlling mass uptake at short and long times, respectively.

11. For interval sorption of acetone from 0 to 7.3 cm Hg and at 35˚C, the amorphous basis acetone diffusion coefficient in the PET/50PEN film is generally lower than the amorphous basis acetone diffusion coefficients in the PET, PET/10PEN and PET/20PEN films at the same acetone

concentrations in the amorphous phase. The value of the first-order time constant used to describe the kinetics of acetone sorption controlled by penetrant-induced relaxation is not markedly influenced by polymer composition or penetrant concentration over the range of penetrant concentration explored in this study. For interval sorption of acetone from 0 to 7.3 cm Hg and at 35˚C, the fraction of mass uptake controlled by penetrant-induced relaxation of the polymer matrix increases with increasing acetone concentration in the polymer and does not depend systematically on copolymer composition.

12. Random copolymers were prepared based on poly(ethylene terephthalate) and modified by replacing the terephthalate linkage in the backbone with either 2,6-naphthalate, isophthalate, or 2,5-bis-(4-carboxyphenyl)-1,3,4-oxadiazole linkages at low (up to 10 weight percent) levels of substitution. Copolymers containing 1-10 weight percent PEN exhibited higher glass transition temperatures and lower levels of crystallinity than those of PET. Copolymers containing 5-10 weight percent PEOD also exhibited higher glass transition temperatures and lower levels of crystallinity than those of PET. The copolymer containing 2.4 weight percent PEI has a lower glass transition temperature and a lower level of crystallinity than PET.

13. The acetone diffusion coefficients were lower in copolymers containing PEN than those in PET. In PET/PEOD copolymers, there was an apparent maximum in acetone diffusivity at 5% PEOD content. The PET/PEOD copolymers had higher acetone solubilities that PET. A copolymer with 2.4 weight percent PEI had a higher acetone diffusivity a lower acetone solubility than PET.

B. Suggestions for Future Work

1. Effect of Penetrant Properties on Sorption and Transport Properties in PET/PEN

As shown in Chapter 3 (*cf*. Figure 3.7), the permeation properties of oxygen and acetone in PET/PEN copolymers are markedly different. There needs to be a better understanding of the effect of penetrant properties (such as size, shape, and chemical nature) on sorption, diffusion, and permeation properties of polymers. Therefore, a number of different organic and gaseous penetrants should be studied in the manner prescribed in this dissertation. Some particular penetrant groups which would be interesting to study include alkanes of different chain length (methane, ethane, propane, n-butane, *etc.*), organic molecules of similar size with different chemical properties (acetone, acetaldehyde, propane, acetic acid, *etc.*), and various gaseous penetrants (CH_4, CO_2, O_2, N_2, He).

2. Effect of Processing Conditions on Sorption and Transport Properties of PET/PEN Copolymers

There is also an effect of film processing conditions on the sorption, transport, and permeation properties of PEN/PET copolymers. This may account for some of the differences in oxygen and acetone permeation properties evident in Figure 3.7. In order to understand these differences, it would be important to study as-cast films of the random copolymers studied in this dissertation using gas permeation experiments as described by Hoffman for compatibilized, melt-processed blends.[25] A thicker film, which would be necessary for gas permeation measurements, has been successfully cast from a 50/50 PET/PEN random copolymer solution in triflouroacetic acid.

3. Effect of Diluent Concentration on the Glass/Rubber Transition Temperatures of PET/PEN

As shown in Chapters 3 and 5 of this dissertation, acetone concentration has an marked effect on properties of PET and PET/PEN copolymers. An interesting experiment to study the effect of acetone concentration on macromolecular chain dynamics would be to examine the glass transition temperature by DSC.

4. Effect of Sequence Distribution on Acetone Sorption and Transport Properties in PEN/PET Copolymers

Previously, there has been interest in examining the effect of ester monomer sequence distribution on the sorption and transport properties of polyesters.[96] Acetone sorption in PEN/PET copolymers could serve as an excellent system to study these effects. In this thesis, small changes in polymer composition (as small as substituting 1% PEN into PET) have led to measurable differences in acetone solubility and diffusion coefficients, as well as measurable differences in other polymer properties (*cf*. Chapter 4). Therefore, other subtle changes in structure, such as sequence distribution, may lead to measurable changes in acetone sorption and transport properties. Random copolymers were used in this thesis and are available for future study. More "blocky" copolymers could be prepared by melt processing blends of PEN and PET homopolymers. Blends of the homopolymers can also be used in the study. NMR could be used to confirm the "randomness" of the copolymers.

5. Effect of Copolymer Composition on Sorption and Transport Properties of PET/PEI

As shown in Chapter 6 and by Light and Seymour,[69] copolymers of PET and poly(ethylene isophthalate) [PEI] have some interesting properties. Despite the presence of the kinked isophthalate group, PEI has a higher amorphous density than PET.[69] The glass transition temperatures do not appear to very with copolymer composition according to the Gordon-Taylor equation,[73] which typically describes glass transition temperatures in copolymers and blends with homogeneous phase morphologies. PEI and 50/50 PET/PEI have lower oxygen and CO_2 permeabilities than PET. PET/PEI copolymer should be studied in a manner similar to the PET/PEN copolymers described in this dissertation. This study would enable a comparison of the properties of the two systems and evaluation of PET/PEI as a potential barrier packaging material.

6. Effect of Copolymer Composition on Sorption and Transport Properties of a Liquid Crystalline Polyesteramide

Although not a direct consequence of this research, one of the most interesting questions in the area of barrier polymers deals with the difference between thermotropic and lyotropic liquid crystalline polymers [LCP's]. Previously, it has been shown that thermotropic liquid crystalline polyesters, such as poly(hydroxybenzoate-co-hydroxynaphthanoate), have low gas permeation properties due to extremely low solubilities despite normal diffusion coefficients.[97-99] Lyotropic liquid crystalline polyamides, such as poly(*p*-phenylene terephthalamide), have low gas permeation properties due to extremely low diffusion coefficients despite normal solubilities.[100] If possible, soluble liquid crystalline polyamides should be prepared spanning a composition from pure polyester to pure polyamide. These may be possible from analogs of the liquid crystalline polyesters prepared at the University of North Carolina at Chapel Hill (*cf*. Appendix A). Acetone sorption experiments should be performed with copolymers of varying copolymer composition (as demonstrated in this dissertation) and thermal annealing protocol (as demonstrated in the dissertation of Dr. G.R. Cantrell)[96] in order to elucidate the source of the difference in sorption and transport properties between liquid crystalline polyesteramides and liquid crystalline polyesters. This research may also lead to copolymer compositions which take advantage of both the low solubilities in liquid crystalline polyesters and the low diffusion coefficients of liquid crystalline polyesteramides.

References

1. W. J. Koros, "Barrier Polymers and Structures: Overview", in Barrier Polymers and Structures, W. J. Koros, Ed., American Chemical Society, Washington, D.C., 1990, 60.

2. G. Strandburg, P. T. DeLassus and B. A. Howell, "Diffusion and Sorption of Linear Esters in Selected Polymer Films", in Barrier Polymers and Structures, W. J. Koros, Ed., American Chemical Society, Washington, DC, 1990, 333.

3. W. J. Koros and M. W. Hellums, "Transport Properties", in Encyclopedia of Polymer Science and Engineering, H. F. Mark, Ed., John Wiley and Sons, New York, 1989, 724.

4. K. Ghosal and B. D. Freeman, "Gas Separation Using Polymer Membranes: An Overview" *Poly. for Adv. Tech.*, **5**, 673, (1994).

5. J. Crank, Mathematics of Diffusion, Oxford Science Publications, Oxford, 1975, 414.

6. J. Crank and G. S. Park, "Methods of Measurement", in Diffusion in Polymers, J. Crank and G. S. Park, Ed., Academic Press Inc., New York, 1968, 1.

7. D. R. Paul, "Gas Sorption and Transport in Glassy Polymers" *Ber. Bunsenges. Phys. Chem.*, 294, (1979).

8. T. Naylor, "Permeation Properties", in Comprehensive Polymer Science, G. Allen, Ed., Pergamon Press, New York, 1989, 643.

9. R. T. Chern, W. J. Koros, E. S. Sanders, S. H. Chen and H. B. Hopfenberg, "Implications of the Dual-Mode Sorption and Transport Models for Mixed Gas Permeation", Proceedings of American Chemical Society, Washington, D.C., **Symposium Series No. 223**, 1983, 47.

10. A. R. Berens, "Transport of Plasticizing Penetrants in Glassy Polymers", in Barrier Polymers and Structures, W. J. Koros, Ed., American Chemical Society, Washington, DC, 1990, 92.

11. J. C. Schmidhausen and K. L. Longley, "Gas Transport Through Bisphenol-Containing Polymers", in Barrier Polymers and Structures, W. J. Koros, Ed., American Chemical Society, Washington, D.C., 1990, 159.

12. A. Bondi, Physical Properties of Molecular Crystals, Liquids and Glasses, Wiley, New York, 1968, 358.

13. W. M. Lee, "Selection of Barrier Materials from Molecular Structure" *Polym. Eng. & Sci.*, **20**, 65, (1980).

14. D. H. Weinkauf and D. R. Paul, "Effects of Structural Order on Barrier Properties", in Barrier Polymers and Structures, W. J. Koros, Ed., American Chemical Society, Washington, D.C., 1990, 60.

15. A. W. Myers, C. E. Rogers, V. Stannett and M. Swarc, "Permeability of polyethylene to gases and vapors" *Modern Plastics*, **34**, 157, (1957).

16. A. S. Michaels and R. B. Parker, Jr., "Sorption and Flow of Gases in Polyethylene" *J. Polym. Sci.*, **16**, 53, (1959).

17. A. S. Michaels and H. J. Bixler, "Flow of Gases Through Polyethylene" *J. Polym. Sci.*, **50**, 413, (1961).

18. A. S. Michaels and H. J. Bixler, "Solubility of Gases In Polyethylene" *J. Polym. Sci.*, **50**, 393, (1961).

19. A. S. Michaels, W. R. Vieth and J. A. Barrie, "Diffusion of Gasses in Polyethylene Terephthalate" *J. Appl. Phys.*, **34**, 13, (1963).

20. A. S. Michaels, W. R. Vieth and J. A. Barrie, "Solution of Gases in Polyethylene Terephthalate" *J. Appl. Phys.*, **34**, 1, (1963).

21. J. Brandup and E. H. Immergut, Polymer Handbook, John Wiley and Sons, New York, 1989,

22. A. C. Puleo, D. R. Paul and P. K. Wong, "Gas sorption and transport in semicrystalline poly(4-methyl-1-pentene)" *Polymer*, **30**, 1357, (1989).

23. D. R. Paul, "Gas Transport in Homogeneous Multicomponent Polymers" *J. Membrane Sci.*, **18**, 75, (1984).

24. H. B. Hopfenberg and D. R. Paul, "Transport Phenomena in Polymer Blends", in Polymer Blends, D. R. Paul and S. Newman, Ed., Academic Press, New York, 1978, 445.

25. D. C. Hoffman and J. K. Caldwell, "Predicting Barrier and Glass Transition Temperature Enhancements in PET/PEN Blends", Proceedings of Specialty Polyesters, 1995, 223.

26. J. W. McBain and A. M. Bakr, "A New Sorption Balance" *JACS*, **48**, 690, (1926).

27. G. R. Cantrell, B. D. Freeman, H. B. Hopfenburg, S. Makhija, I. Haider and M. Jaffe, "The Influence of Thermal Annealing on Vapor Sorption and Transport in a Nematogenic Copolyester", in Liquid Crystalline Polymers, C. Carfagna, Ed., Pergammon, Tarrytown, NY, 1994, 233.

28. B. M. Baumert and S. J. Muller, "Flow Visualization of the Elastic Taylor-Couette Instability in Boger Fluids" *Rheol Acta*, **34**, 147, (1995).

29. L. I. Winkler and B. A. Stevenson, "Imaging System to Monitor the Pendulum Mpde of a Vibrationally Driven Torsion Balance" *Rev. Sci. Inst.*, **68**, 4275, (1997).

30. D. C. Giancoli, Physics for Scientists and Engineers, Prentice Hall, Englewood Cliffs, New Jersey, 1988, 927.

31. J. Myers, "PET Bottle Growth is Outpacing Supply" *Modern Plastics*, 40, (1994).

32. J. Izydorczyk and J. Salwiniski, "Sorption and Permeation of Methanol and Ethyl Acetate Vapors in Polyethylene Terephthalate" *Polish J. Chem.*, **66**, 321, (1993).

33. C. J. Patton, R. M. Felder and W. J. Koros, "Sorption and Transport of Benzene in Poly(ethylene Terephthalate)" *J. Appl. Poly. Sci.*, **29**, 1095, (1984).

34. C.-P. A. Liu and P. Neogi, "Sorption of Methylene Chloride in Semicrystalline Polyethylene Terephthalate" *J. Macromol. Sci.-Phys.*, **31**, 265, (1992).

35. H. Jameel, J. Waldman and L. Rebenfeld, "The Effects of Orientation and Crystallinity on the Solvent-Induced Crystallization of Poly(ethylene Terephthalate). I. Sorption- and Diffusion-Related Phenomena" *J. Appl. Poly. Sci.*, **26**, 1795, (1981).

36. C. J. Durning and W. B. Russel, "A Mathematical Model for Diffusion with Induced Crystallization: 2." *Polymer*, **26**, 131, (1985).

37. C. J. Durning, L. Rebenfeld and W. B. Russel, "Integral Sorption with Induced Crystallization" *Poly. Eng. and Sci.*, **26**, 1066, (1986).

38. G. F. Billovits and C. J. Durning, "Penetrant Transport in Semicrystalline Poly(ethylene Terephthalate)" *Polymer*, **29**, 1468, (1988).

39. D. A. Blackadder and P.I.Vincent, "Solvent uptake as a tool for investigating polymer morphology" *Polymer*, **15**, 2, (1974).

40. N. R. Miranda, J. T. Willits, B. D. Freeman and H. B. Hopfenberg, "Organic Vapor Sorption and Transport in a Thermotropic Liquid Crystalline Polymer" *J. Membrane Sci.*, **94**, 67, (1994).

41. J. Y. Park, D. R. Paul, I. Haider and M. Jaffe, "Effect of Thermal Annealing on the Gas Permeability of HIQ-40 Films" *J. Poly. Sci.: Poly. Phys. Ed.*, **34**, 1741, (1996).

42. M. H. Cohen and D. Turnbull, "Molecular Transport in Gases and Liquids" *J. Chem. Phys.*, **31**, 1164, (1959).

43. R. C. Reid, J. M. Prausnitz and B. E. Polling, The Properties of Gases and Liquids, McGraw-Hill, Inc., New York, 1987, 741.

44. R. M. Felder and G. S. Huvard, "Permeation, Diffusion, and Sorption of Gases and Vapors", in Methods of Experimental Physics, Vol. 16C, R. Fava, Ed., Academic Press, New York, 1978, 315.

45. E. L. Lawton and E. L. Ringwald, "Physical Constants of Pol(oxyethylene-oxytereohthaloyl) (Poly(ethylene terephthalate))", in Polymer Handbook, J. Brandup and E. H. Immergut, Ed., John Wiley and Sons, New York, 1989, V/101.

46. F. W. Billmeyer, Textbook of Polymer Science, John Wiley and Sons, New York, 1984, 578.

47. S. Z. D. Cheng and B. Wunderlich, "Thermal Analysis of Thermoplastic Polymers" *Thermochimica Acta*, **134**, 161, (1988).

48. N. S. Murthy, S. T. Correale and H. Minor, "Structure of the Amorphous Phase in Crystallizable Polymers: Poly(ethylene terephthalate)" *Macromolecules*, **24**, 1185, (1991).

49. H.-C. Shen, The Characterizations of a New Soluble Main Chain Nematic Liquid Crystalline Polymer and Poly(etherketone)/Liquid Crystalline Block Copolymers, Master's Thesis, North Carolina State University, 1993.

50. G. J. VanAmerongen, "Diffusion in Elastomers" *Rubber Chem. and Tech.*, **37**, 1065, (1964).

51. V. I. Bondar, B. D. Freeman and I. Pinnau, "Characterization and Analysis of the Sorption and Pure-Gas Permeation Properties of Polyether-Polyamide Block Copolymers" *Poly. Mat. Sci. and Eng.*, **77**, 311, (1997).

52. A. Singh, Gas and Vapor Sorption and Permeation Properties in Ultra High Free Volume Glassy Polymers, Ph.D. Dissertation, North Carolina State University, 1997.

53. W. J. Koros and D. R. Paul, "Transient and steady-state permeation in poly(ethylene terephthlate) above and below the glass transition" *J. Poly. Sci.: Poly. Phys. Ed.*, **16**, 2171, (1978).

54. E. S. Sanders, High-Pressure Sorption of Pure and Mixed Gases in Glassy Polymers, Ph.D. Dissertation, North Carolina State University, 1983.

55. A. R. Berens and H. B. Hopfenberg, "Diffusion and Relaxation in Glassy Polymer Powders: 2. Separation of Diffusion and Relaxation Parameters" *Polymer*, **19**, 489, (1978).

56. A. Kishimoto, H. Fujita, H. Odani, M. Kurata and M. Tamura, "Succesive Differential Absorption of Vapors of Glassy Polymers" *J. Phys. Chem.*, **64**, 594, (1960).

57. G. F. Billovits and C. J. Durning, "Two Stage Weight Gain in the Polystyrene-Ethylbenzene System" *Polymer Commun.*, **31**, 358, (1990).

58. P. Bevington, Data Reduction and Error Analysis for the Physical Sciences, McGraw-Hill, New York, 1969, 150.

59. G. K. Fleming and W. J. Koros, "Dilation of Polymers by Sorption of Carbon Dioxide at Elevated Pressures" *Macromolecules*, **19**, 2285, (1986).

60. N. Miranda, The Effect of Primary and Higher Order Molecular Structure on Sorption and Transport Phenomena in Stiff-Chain Membranes and Barrier Polymer, Ph.D. Dissertation, North Carolina State University, 1992.

61. H. Fujita, "Organic Vapors above the Glass Transition Temperature", in Diffusion in Polymers, J. Crank and G. S. Park, Ed., Academic Press Inc., New York, 1968, 75.

62. D. R. Paul and W. J. Koros, "Effect of Partially Immobilizing Sorption on Permeability and the Diffusion Time Lag" *J. Poly. Sci.: Poly. Phys. Ed.*, **14**, 675, (1976).

63. S. A. Stern and V. Saxena, "Concentration-Dependent Transport of Gasses and Vapors in Glassy Polymers" *J. of Membrane Sci.*, **7**, 47, (1980).

64. J. S. Vrentas and J. L. Duda, "Diffusion in Polymer-Solvent Systems. I. Reexamination of the Free-Volume Theory" *J. Poly. Sci.: Poly. Phys. Ed.*, **15**, 403, (1977).

65. C. SantaCruz, F. J. Balta-Calleja, H. G. Zachmann and D. Chem, "Mechanical Properties and Structure of Glassy and Semicrystalline Random Copolymers of Poly(ethylene terephtahalate) and Poly(ethylenenapthalene-2,6-dicarboxylate)" *J. Mat. Sci.*, **27**, 2161, (1992).

66. M. E. Stewart, A. J. Cox and D. M. Naylor, "Reactive Processing of Poly(ethylene 2,6-napthalene dicarboxylate) / Poly(ethylene terephthalate) blends" *Polymer*, **34**, 4060, (1993).

67. T. A. Ezquerra, F. J. Balta-Calleja and H. G. Zachmann, "Dielectric Relaxation of Amorphous Random Copolymers of Poly(ethylene terephthalate) and Poly(ethylene-2,6-napthalene dicarboxylate)" *Acta Polymerica*, **44**, 18, (1993).

68. X. Lu and A. H. Windle, "Crystallization of Random Copolymers of Poly(ethylene terephthalate) and Poly(ethylene napthalene-2,6-dicarboxylate)" *Polymer*, **36**, 451, (1995).

69. R. R. Light and R. W. Seymour, "Effect of sub Tg Relaxations on the Gas Transport Properties of Polyesters" *Poly. Eng. & Sci.*, **22**, 857, (1987).

70. D. R. Rueda and A. Varkalis, "Water Sorption / Desorption Kinetics in Poly(ethylene napthalene-2,6-dicarboxylate) and Poly(ethylene terephthalate)" *J. Poly. Sci.: Poly. Phys. Ed.*, **33**, 2263, (1995).

71. W. Puff, "PFPOSFIT: A New Version of a Program for Analyzing Positron Lifetime Spectra with Non-Gaussian Prompt Curve" *Comput. Phys. Commun.*, **30**, 359, (1983).

72. A. J. Hill, "Positron Annihilation Lifetime Spectroscopy To Probe Free-Volume Effects in High-Temperature Polymers and Composites", in <u>High Temperature Properties and Applications of Polymers</u>, M. R. Tant, J. W. Connell and H. L. N. McManus, Ed., ACS, Washington D.C., 1995, 63.

73. M. Gordon and J. S. Taylor, "Ideal Copolymers and the Second-Order Transitions of Synthetic Rubbers. I.Non-Crystalline Copolymers" *J. Appl. Chem.*, **2**, 493, (1952).

74. H. C. Shen, C.C.McDowell, S. S. Sankar, B. D. Freeman, R. J. Kumpf, D. A. Wcks, C. W. Lantman and C. Noel, "Synthesis and Thermal Transitions of a Soluble, Main Chain, Nematic Liquid Crystalline Polymer Exhibiting a Kinetically Trapped, Disordered Structure" *J. Poly. Sci., Poly. Phys. Ed.*, **34**, 1347, (1996).

75. S.-B. Lin and J. L. Koenig, "Spectroscopic Characterization of the Rotational Conformations in the Disordered Phase of Poly(ethyelene Terephthalate)" *J. Poly. Sci.: Poly. Phys. Ed*, **20**, 2277, (1982).

76. S. Buchner, D. Wiswe and H. G. Zachmann, "Kinetics of Crystallization and Melting Behavior of Poly(ethylene napthalene-2,6-dicarboxylate)" *Polymer*, **30**, 480, (1989).

77. A. Bondi, "Van der Waals Volumes and Radii" *J. Phys. Chem.*, **68**, (1964).

78. M. D. Zipper, G. P. Simon, P. Cherry and A. J. Hill, "The Effect of Crystallinity on Chain Mobility and Free Volume in the Amorphous Regions of a Miscible Polycarbonate/Polyester Blend" *J. Poly. Sci.: Poly. Phys. Ed.*, **32**, 1237, (1994).

79. L. Xie, D. W. Gidley, H. A. Hristov and A. F. Yee, "Positronium Formation in Semicrystalline Poly(ethylene terephthalate)" *Polymer*, **35**, 14, (1994).

80. K. Okamoto, K. Tanaka, M. Katsube, H. Kita, O. Sueoka and Y.Ito, "Correlation between Positron Annihilation and Gas Diffusion Properties of Various Rubbery Polymers" *Polymer J.*, **25**, 275, (1993).

81. L. H. Sperling, Introduction to Physical Polymer Science, John Wiley and Sons, New York, 1992, 594.

82. S. Krause, "Polymer-Polymer Compatability", in Polymer Blends, D. R. Paul and S. Newman, Ed., Academic Press, New York, 1978, 15.

83. J. A. Barrie and K. Munday, "Gas Transport in Heterogeneous Polymer Blends" *J. Membrane Sci.*, **13**, 175, (1983).

84. J. Csernica, R. F. Baddour and R. E. Cohen, "Gas Permeability of a Polystyrene/Polybutadiene Block Copolymer Possessing a Misoriented Lamellar Morphology" *Macromolecules*, **22**, 1493, (1989).

85. M. L. Greenfield and D. N. Theodorou, "Structure, Rate, and Mechanism of Methane Diffusion in Glassy Atactic Polypropylene as Determined by Coarse-Grained Molecular Modelling" *Poly. Mat. Sci. and Eng.*, **76**, 429, (1997).

86. A. A. Gray-Weale, R. H. Henchman, R. G. Gilbert, M. L. Greenfield and D. N. Theodorou, "Transition-State Theory Model for the Diffusion Coefficients of Small Molecule Penetrants in Glassy Polymers" *Macromolecules*, **30**, 7296, (1997).

87. J. A. Slee, G. A. J. Orchard, D. I. Bower and I. M. Ward, "The Transport of Oxygen Through Oriented Poly(ethylene terephthalate)" *J. Poly. Sci.: Poly. Phys. Ed*, **27**, 71, (1989).

88. W. R. Vieth, L. H. Dao and H. Pedersen, "Non-equilibrium microstructural abd transport characteristics of glassy poly(ethylene terephthalate)" *J. Membrane Sci.*, **60**, 41, (1991).

89. I. Ouchi, M. Hosoi and S. Shimotsuma, "Infrared Spectra of Poly(ethyelene 2,6-naphthalate) and Some Related Polyesters" *J. Appl. Poly. Sci.*, **21**, 3445, (1977).

90. W. J. Koros and D. R. Paul, "CO2 Sorption in Poly(ethylene Terephthalate) above and below the Glass Transition" *J. Poly. Sci.: Poly. Phys. Ed.*, **16**, 1947, (1978).

91. K. Toi, G. Morel and D. R. Paul, "Gas Sorption adn Transport in Poly(phenylene Oxide) and Comparisons with Other Glassy Polymers" *J. Appl. Polym. Sci.*, **27**, 2997, (1982).

92. N. Murugandam, W. J. Koros and D. R. Paul, "Gas Sorption and Transport in Substituted Polycarbonates" *J. Poly. Sci.: Polym. Phys. Ed.*, **25**, 1999, (1987).

93. R. Simha and R. F. Boyer, "Ona General Relation Involving the Glass Temperature and Coefficients of Expansion of Polymers" *J. Chem. Phys.*, **37**, 1003, (1962).

94. C. L. Aitken, W. J. Koros and D. R. Paul, "Effect of Structural Symmetry on Gas Transport Properties of Polysulfones" *Macromolecules*, **25**, 3424, (1992).

95. K. Ghosal, R. T. Chern, B. D. Freeman, W. H. Daly and I. I. Negulescu, "Effect of Basic Substituents on Gas Sorption and Permeation in Pulysulfone" *Macromolecules*, **29**, 4360, (1996).

96. G. R. Cantrell, The Effect of Annealing on the Sorption and Transport Properties in a Liquid Crystalline Polymer, Ph.D. Dissertation, North Carolina State University, 1995.

97. D. H. Weinkauf, H. D. Kim and D. R. Paul, "Gas Transport Properties of Liquid-Crystalline Co-Poly(ethylene-co-p-Oxybenzoate)" *J. Poly. Sci.: Poly. Phys. Ed.*, 329, (1991).

98. D. H. Weinkauf and D. R. Paul, "Gas Transport Properties of Thermotropic Liquid-Crystalline Copolyesters. I. The Effects of Orientation and Annealing" *J. Poly. Sci.: Poly. Phys. Ed.*, **30**, 817, (1992).

99. D. H. Weinkauf and D. R. Paul, "Gas Transport Properties of Thermotropic Liquid -Crystalline Copolyesters. II. The Effects of Copolymer Composition" *J. Poly. Sci.: Poly. Phys. Ed.*, **30**, 837, (1992).

100. D. H. Weinkauf, H. D. Kim and D. R. Paul, "The gas transport properties of poly(p-phenylene terephthalamide)" *Macromolecules*, **25**, 788, (1992).

Appendix A. Additional Experimental Data

• Small Molecule Sorption in Liquid Crystalline Polymers, Liquid Crystalline/ Amorphous Block Copolymers, and PENBB

Figures A-1 to A-6

Figures A-1 through A-6 present data from acetone sorption studies of a series of liquid crystalline polyesters from Hoechst-Celanese Corporation. All of the experiments were performed in a Cahn RG-2000 electrobalance system at 35˚C and an acetone partial pressure of 5.4 cm Hg. The films used in the study were melt processed by Hoechst Celanese in Greer, SC and were 5-15 µm thick. The composite results of these copolymers are presented in Table A-1.

Table A-1. Acetone Sorption, Transport, and Permeation in HCC LCP's

Polymer	M_∞ [g/100g Polymer]	D [cm^2/s]	S [cm^3(STP)/ cm^3/atm]	Calculated P [Barrers]
A950	0.019	1×10^{-11}	1.5	3×10^{-3}
B950	0.021	2×10^{-12}	1.6	3×10^{-4}
A950 + 0.2% SSI	0.023	2×10^{-12}	1.8	2×10^{-4}
L950	0.060	1×10^{-12}	4.6	3×10^{-4}
NDA-D	0.041	1×10^{-11}	3.1	6×10^{-3}
RD1009	0.34	7×10^{-12}	26	1×10^{-2}

Figures A-7 to A-10

Figures A-7 through A-10 present data from acetone sorption experiments on a series of liquid crystalline polymers synthesized at The

University of North Carolina at Chapel Hill by Mr. Theo Dingemanns. All of the experiments were performed at 35˚C and an acetone partial pressure of 5.4 cm Hg. The films were cast from a 5% (w/v) solution in triflouroacetic acid. The fiber samples were supplied by Mr. Dingemanns.

Figure A-7 presents an acetone sorption run for a copolymer melt polymerized by reacting oxadiazole dicarboxylic acid [ODCA] with a model monomer. The model monomer was made by capping ethylene glycol with two hydroxybenzoic acid molecules. The chemical structure of this copolymer is:

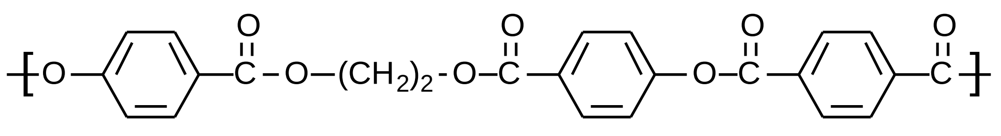

The diffusion coefficient reported in Figure A-7 was calculated using the long time estimation since the initial weight uptake is not a linear function of $t^{1/2}$.

Figures A-8 and A-9 present acetone sorption runs for a copolymer melt polymerized by reacting terephthalic acid [TA] with the model monomer. The chemical structure of this copolymer is:

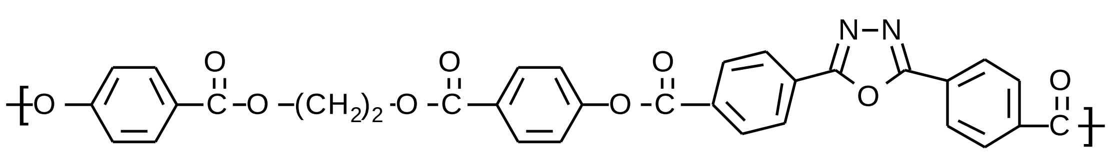

The initial mass uptake is followed by a decrease in mass, as shown in Figure A-8. Since this result was not expected, the experiment was repeated. The resulting data are shown in Figure A-9. The subsequent desorption of the film showed an initial decrease in mass followed by an increase. There is not an explanation of the anomalous results at this time.

Figure A-10 presents acetone sorption in fibers drawn from the same TA-based LCP. The kinetics of the experiment were very slow due to the low diffusion coefficient and the thickness of the fibers. Therefore, the system did not reach equilibrium over the time scale of the experiment. The diffusion coefficient was estimated assuming the kinetics were Fickian and all the data were linear (short-time solution to Fick's law).

<u>Figure A-11 and A-12:</u>

Figures A-11 and A-12 present the results of propane sorption experiments in block copolymers of PICT and bisphenol-A polyether ether ketone [PEEK]. PICT is an aromatic polyester composed of 25 mole% phenyl hydroquinone, 10 mole% isophthalic acid, 40 mole% chloroterephthalic acid, and 25 mole% *t*-butyl hydroquinone. The chemical structures of PICT and PEEK are:

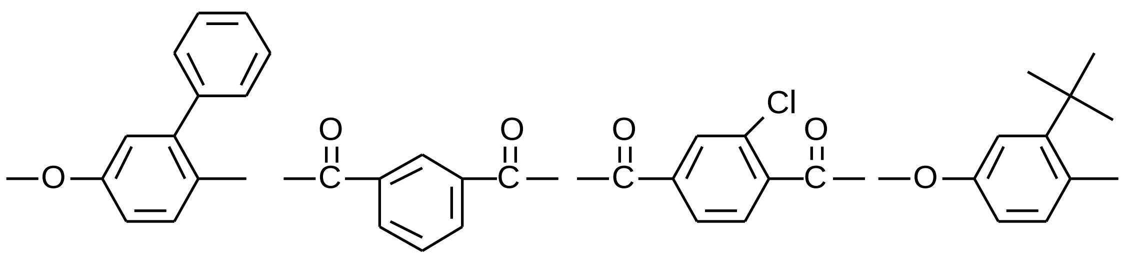

25 mol% phenyl hydroquinone | 10 mol% isophthalic acid | 40 mol% chloroterephthalic acid | 25 mol% *t* -butyl hydroquinone

PICT

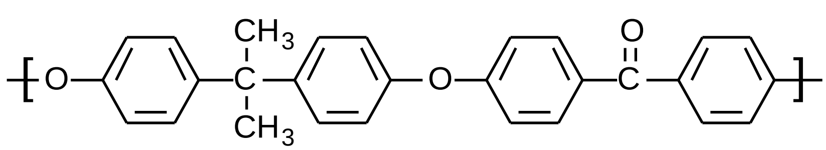

PEEK.

PICT, PEEK, and PICT/PEEK copolymers have been thoroughly characterized previously in the M.S. thesis of Dr. Hsin-Chen Shen (Dept. of Chem. Eng., N.C. State, 1993). The data for acetone sorption in PICT in Figures A-11 and A-12 were taken from the Ph.D. dissertation of Dr. Nathaniel Miranda (Dept. of Chem. Eng., N.C. State, 1992). All of the experiments were performed at 35˚C. The films were cast from a 5%(w/v) solution in methylene chloride. The films were not annealed after casting. The details of the casting process is available elsewhere (Hsin-Chen Shen, M.S. Thesis, Dept. of Chem. Eng., N.C.

State, 1993). The experiments were run in interval mode (starting at zero pressure).

Figure A-11 presents the equilibrium concentration of propane in the copolymers as a function of propane partial pressure in the experiment. The data are well described by the dual-mode sorption model for each copolymer. Figure A-12 presents the propane diffusion coefficient as a function of propane partial pressure. The diffusion coefficient was estimated by fitting the solution of Fick's law for a plane sheet to the propane sorption data.

Figure A-13:

Figure A-13 presents the sorption kinetics in poly(ethylene 2,6-naphthalate bibenzoate) [PENBB] film at 35˚C and an acetone partial pressure of 5.4 cm Hg. The chemical structure of PENBB is:

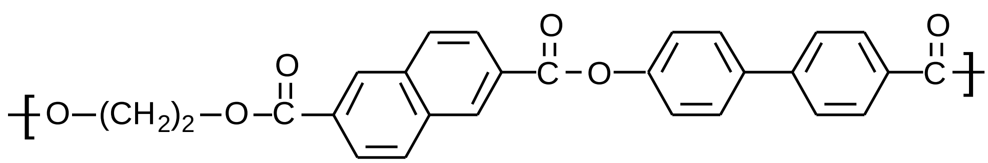

The 1 µm PENBB film was provided by the Hoechst-Celanese Corporation in Charlotte, NC. The data are well described by a Fickian model (Solid curve in Figure A-13).

• Acetone Sorption in PET and PET Copolymers

Figure A-14:

Figure A-14 present acetone sorption kinetics in a PET film cast from TFAA. The experimental conditions were 35˚C and an acetone partial pressure of 5.4 cm Hg. While the initial (up to ~30 $min^{1/2}$) data can be described using a Fickian model, there is a decrease in mass with time following the initially Fickian portion of the data. This is attributed to penetrant-induced crystallization of the film. Acetone is a known crystallizing agent for PET. The polymer film loses 7% of the weight that it initially sorbed as a result of the crystallization, suggesting an increase in crystallinity of 4%. Subsequent to this experiment, the PET/PEN copolymers were exposed to acetone at a pressure of 7.2 cm Hg prior to other sorption experiments in order to avoid solvent-induced crystallization during sorption.

Figures A-15 to A-21:

Figures A-15 to A-21 present acetone sorption kinetics in PET copolymer films cast from TFAA. The experimental conditions were 35˚C and an acetone partial pressure of 5.4 cm Hg.

Figures A-22 to A-46

Figures A-22 to A-48 present acetone sorption kinetics in PET/PEN copolymer films cast from TFAA. The experimental conditions were 35˚C and an acetone partial pressure range of 0 - 7.2 cm Hg.

•WAXD in PET Copolymer Films

Figure A-47 to A-52

These figures present WAXD spectra of PET copolymer films cast from TFAA. The PET/85PEN film was made using a micromelt extruder as described in Chapter 4.

•DMA in PET/PEN Copolymer Films

Figures A-53 to A-57

These figures present dynamic mechanic mechanical analysis of PET, PEN, and PET/50PEN films. The PEN film was made with a micromelt extruder as described in Chapter 4. The PET and PET/50PEN films were cast from TFAA solution. The Seiko DMA used in the experiments are located in the Department of Chemistry at UNC-Chapel Hill.

•IR in PET Copolymer Films

Figures A-58 to A-65

Figures A-58 to A-67 present the IR spectra of PET copolymer films cast from TFAA. More details on these spectra are available in Chapters 4 and 6.

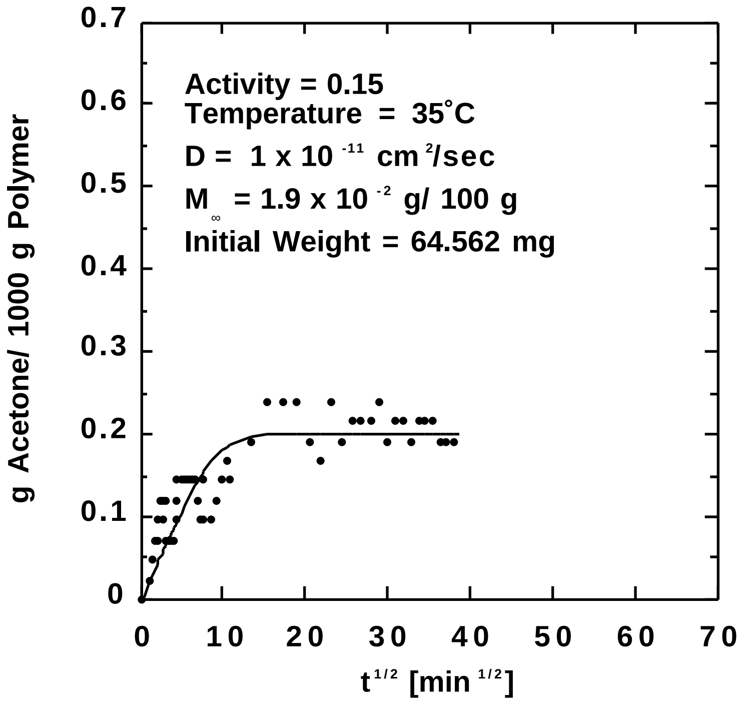

Figure A-1. Acetone Sorption Kinetics in Vectra A950

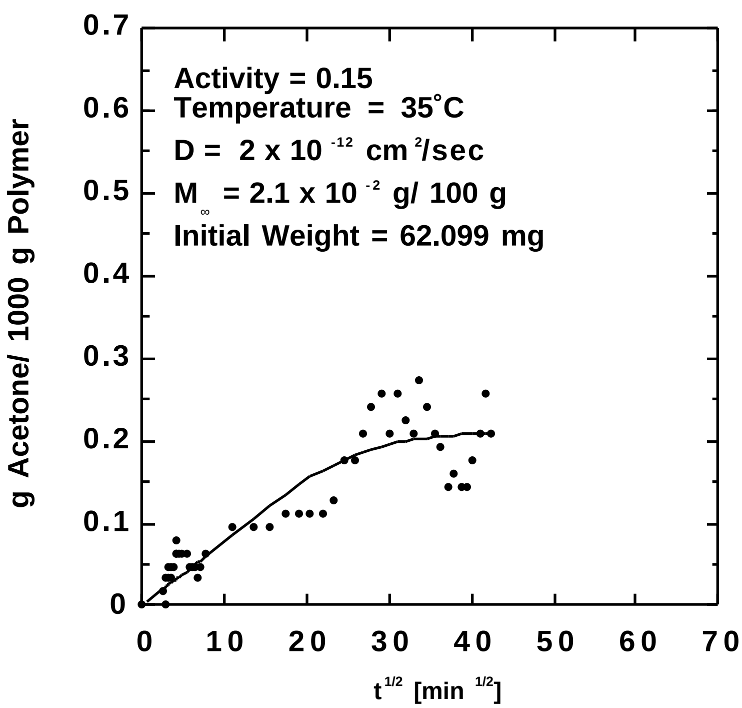

Figure A-2. Acetone Sorption Kinetics in Vectra B950

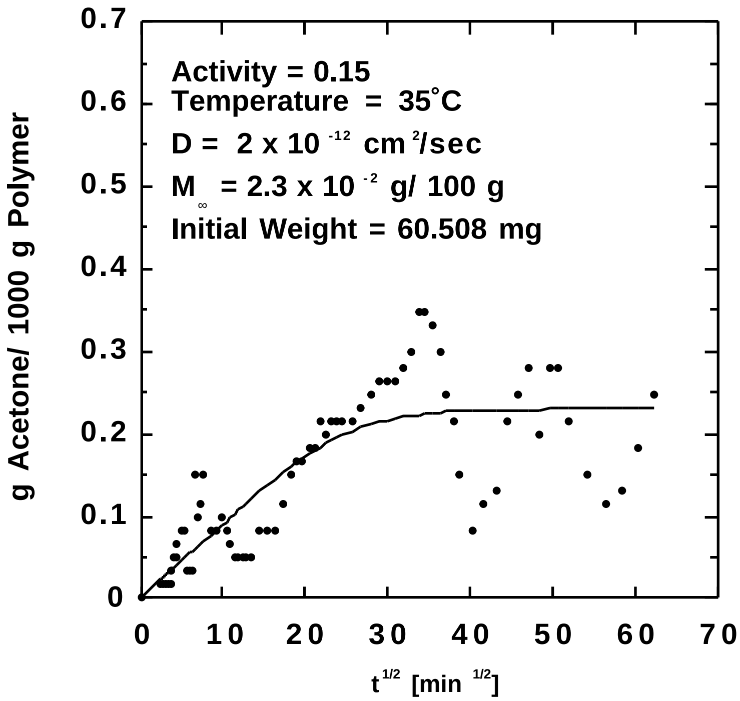

Figure A-3. Acetone Sorption Kinetics in Vectra A + 0.2% Ionic Comonomer

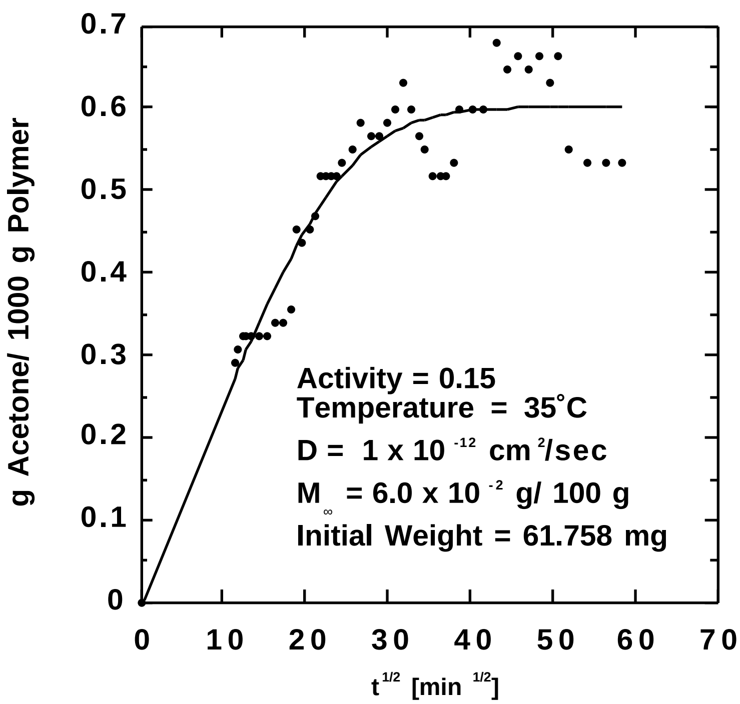

Figure A-4. Acetone Sorption Kinetics in Vectra L950

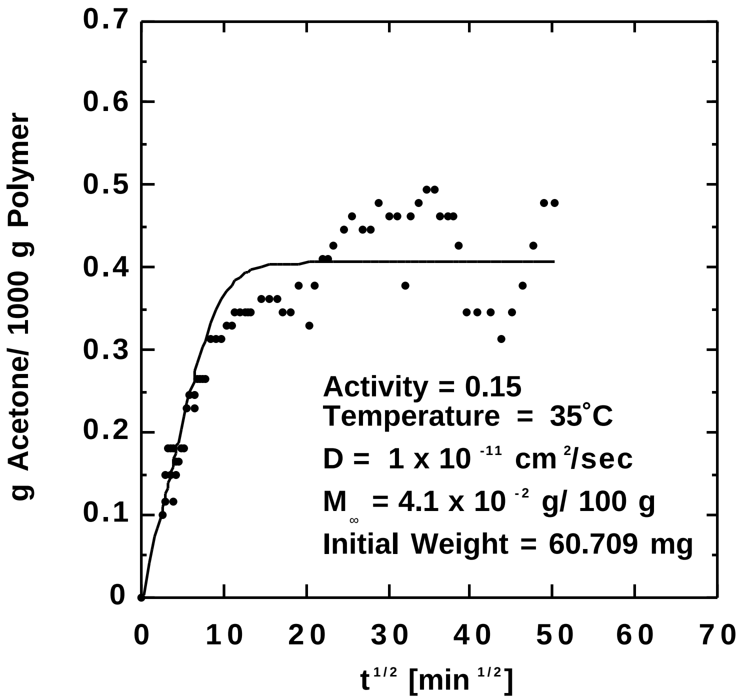

Figure A-5. Acetone Sorption Kinetics in Vectra NDA-D

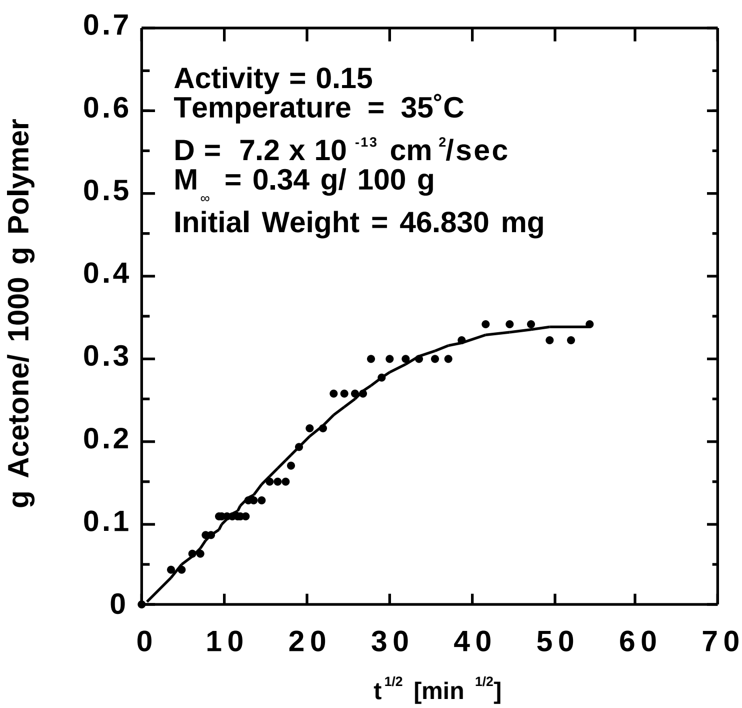

Figure A-6. Acetone Sorption Kinetics in Vectra RD1009

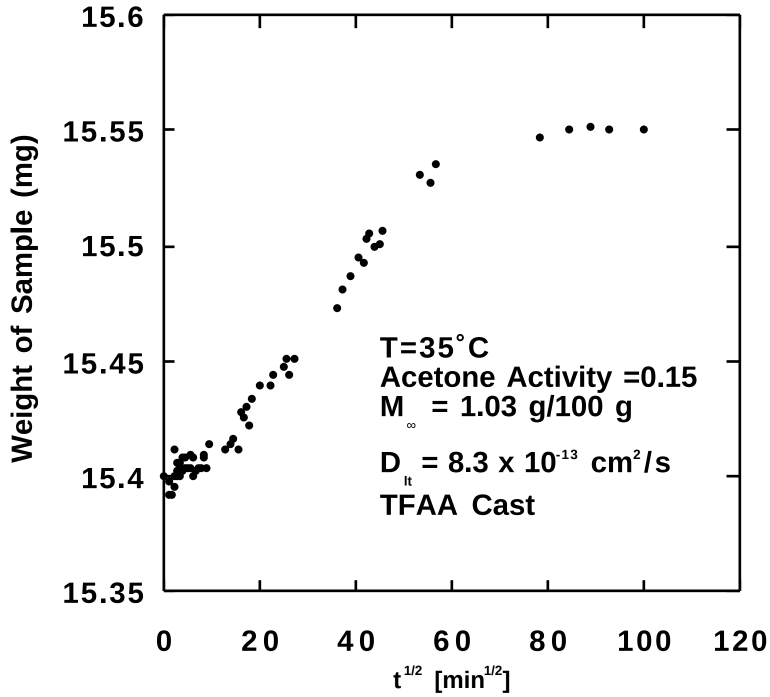

Figure A-7. Acetone Sorption Kinetics in ODCA-based LCP Film

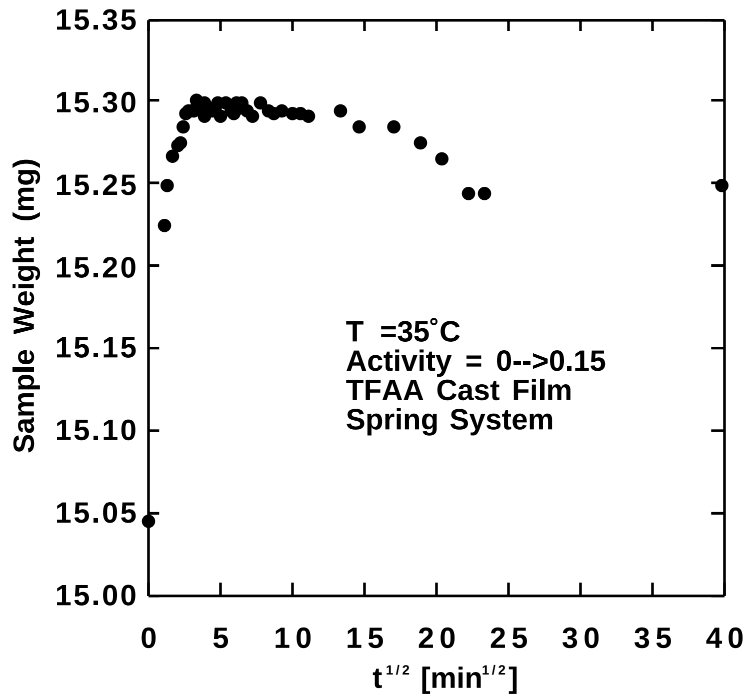

Figure A-8. Acetone Sorption Kinetics in TA-based LCP Film(Initial Run)

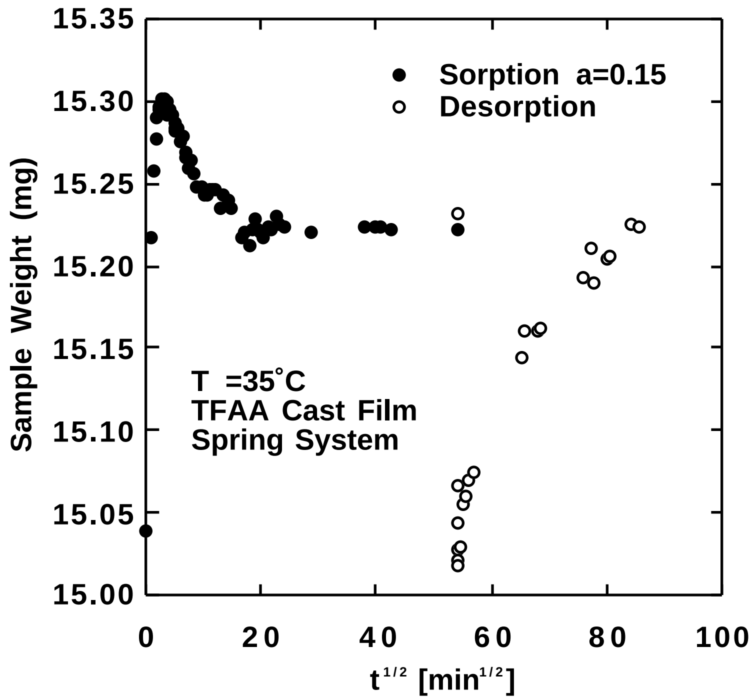

Figure A-9. Acetone Sorption Kinetics in TA-based LCP Film (Subsequent Run and Desorption)

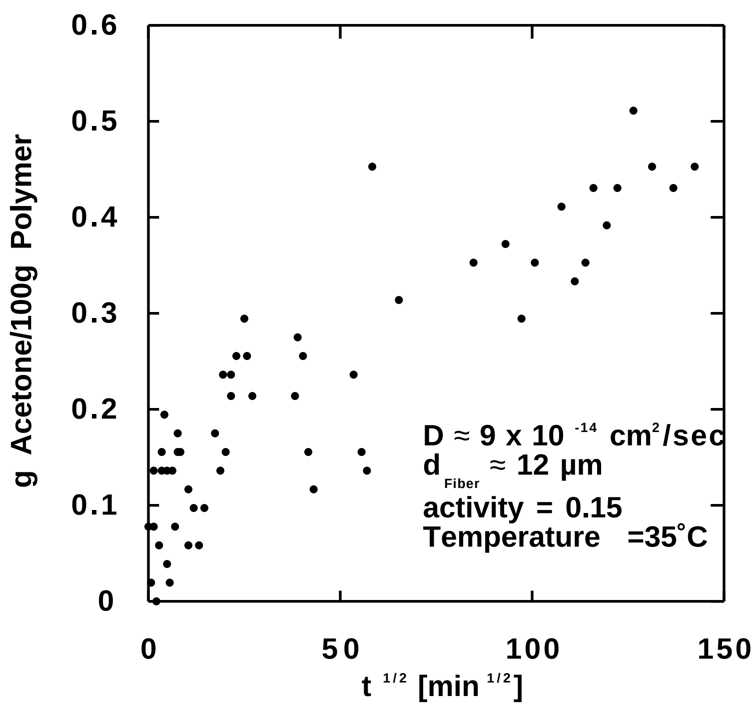

Figure A-10. Acetone Sorption Kinetics in TA-based LCP Fiber

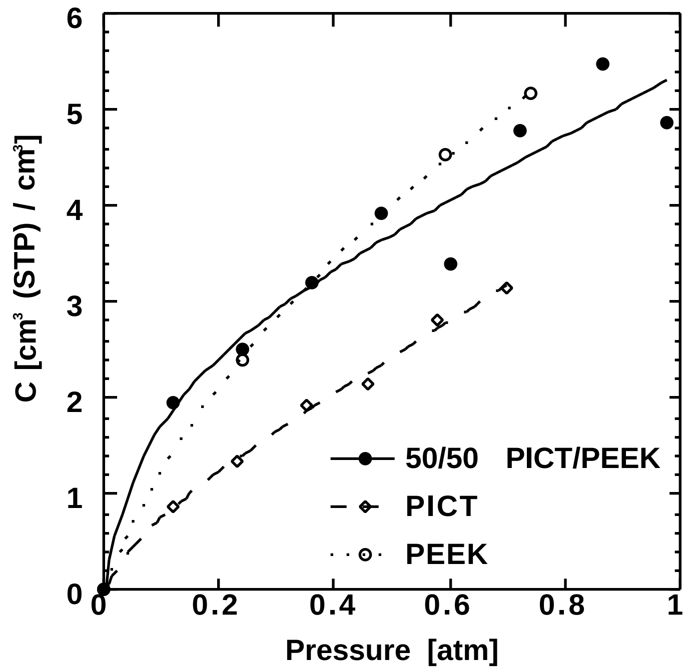

Figure A-11. Equilibrium Concentration of Propane in As-Cast PICT/PEEK Copolymer Films as a Function of Pressure

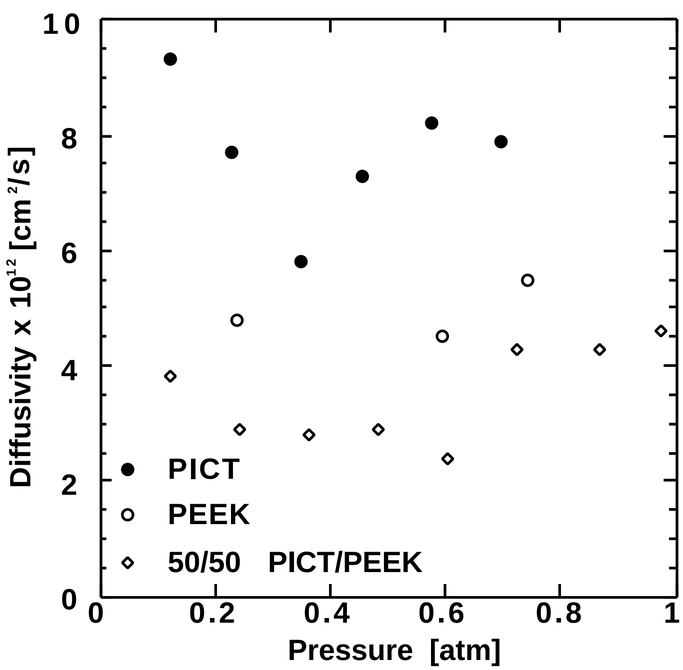

Figure A-12. Propane Diffusion Coefficient as a Function of Pressure in As-Cast PICT/PEEK Copolymer Films

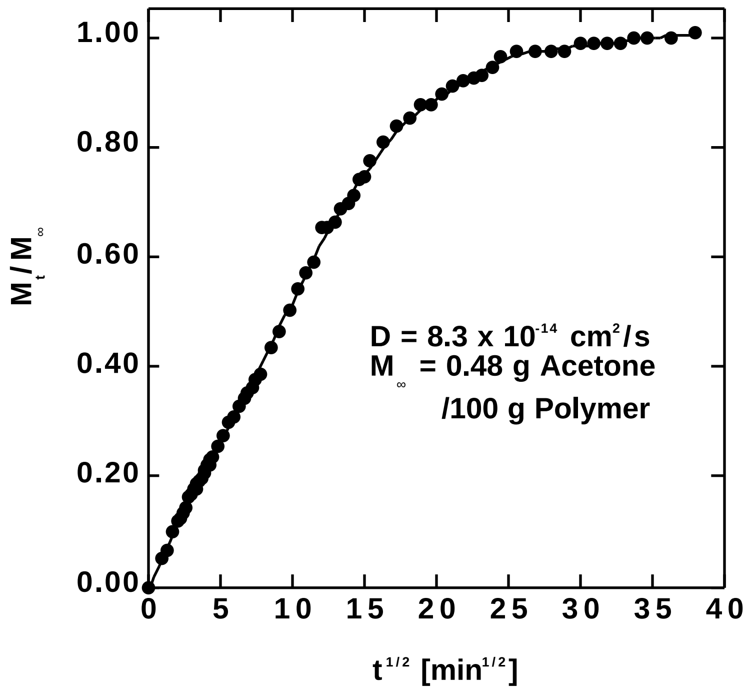

Figure A-13. Acetone Sorption Kinetics in PENBB Film

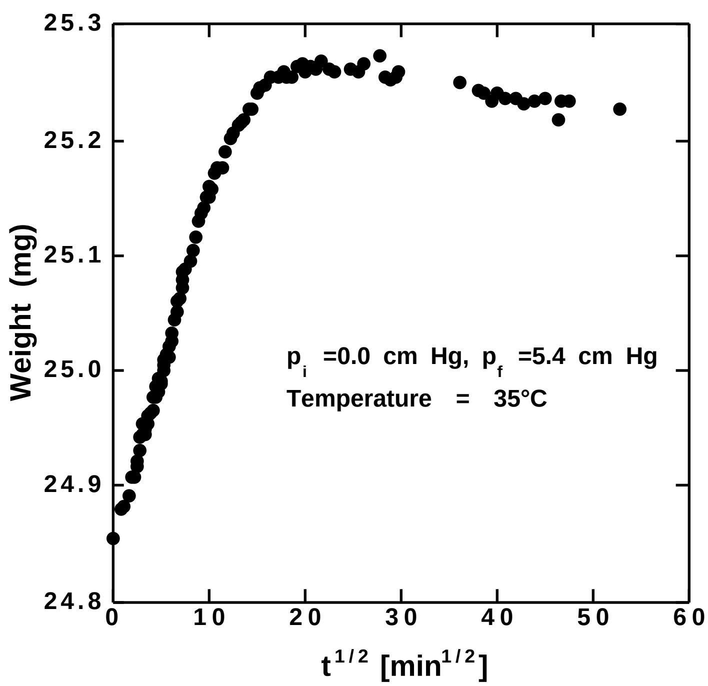

Figure A-14. Acetone Sorption Kinetics with Penetrant-Induced Crystallization in an As-Cast PET film

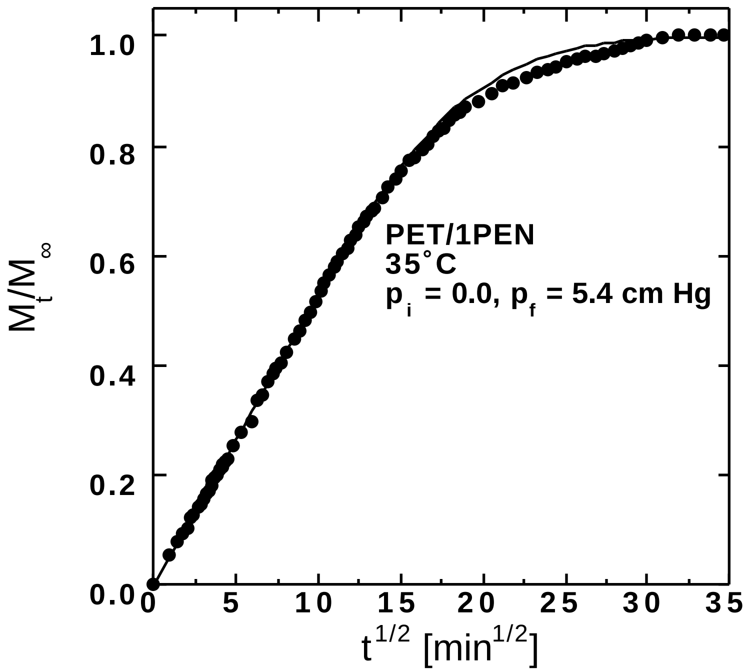

Figure A-15. Acetone Sorption Kinetics in PET / 1PEN

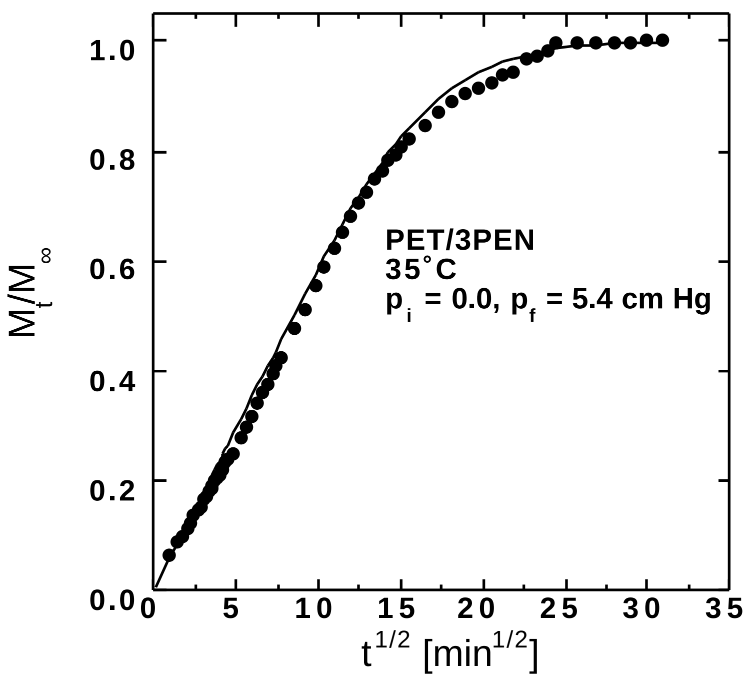

Figure A-16. Acetone Sorption Kinetics in PET / 3PEN

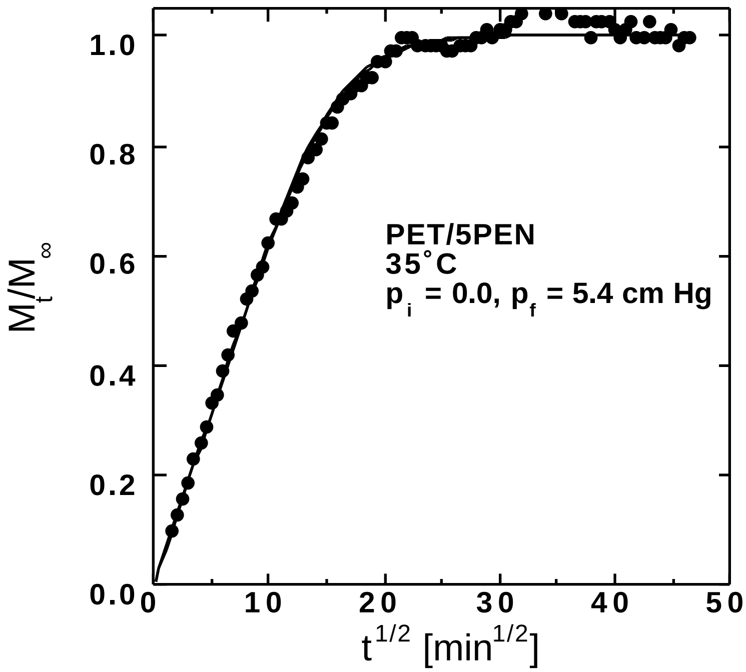

Figure A-16. Acetone Sorption Kinetics in PET / 5PEN

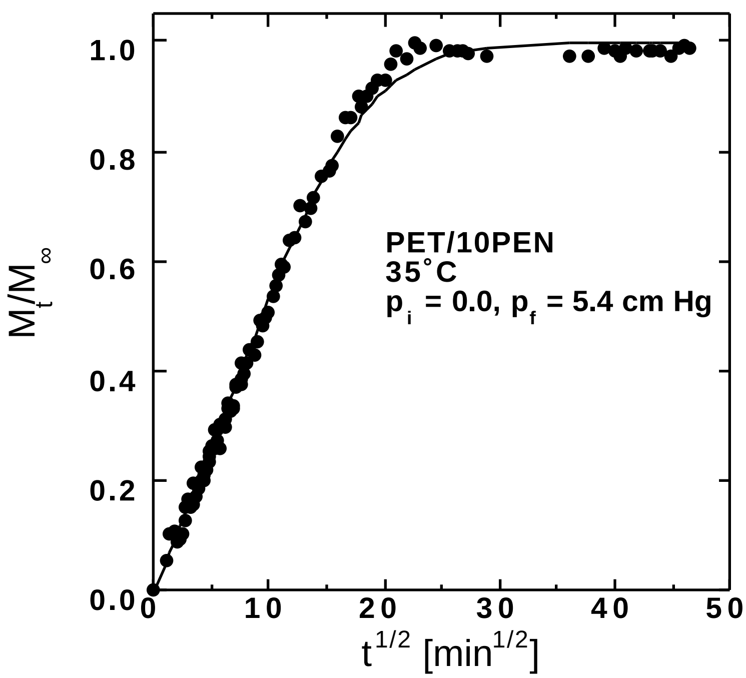

Figure A-17. Acetone Sorption Kinetics in PET / 10PEN

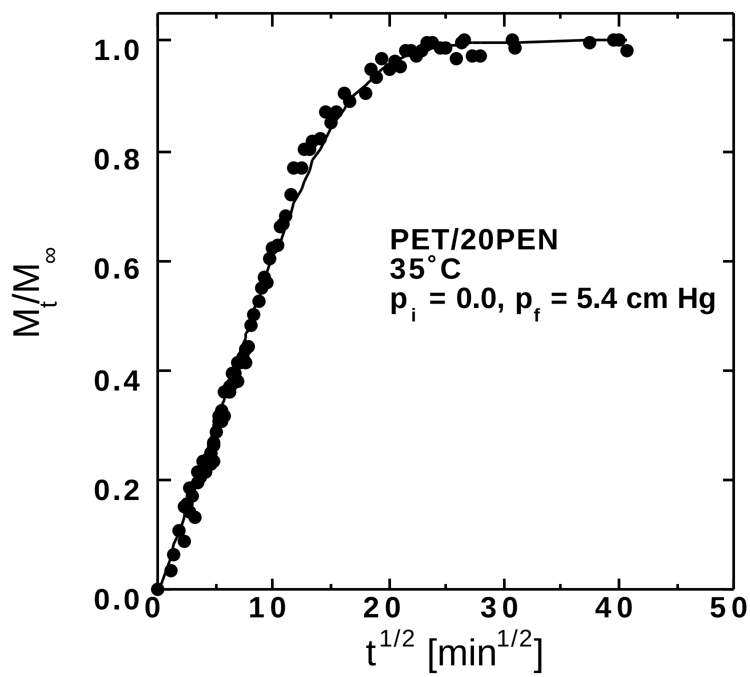

Figure A-18. Acetone Sorption Kinetics in PET / 20PEN

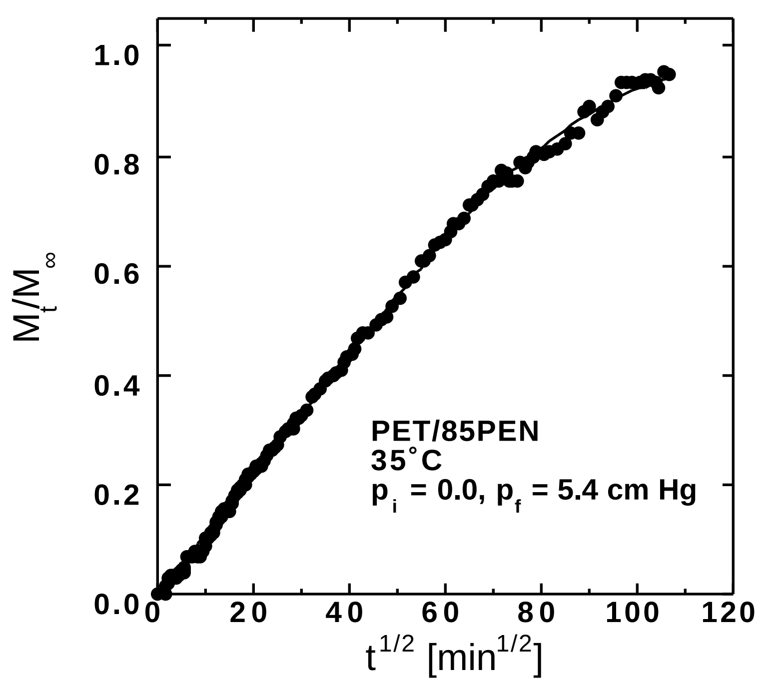

Figure A-19. Acetone Sorption Kinetics in PET / 85PEN

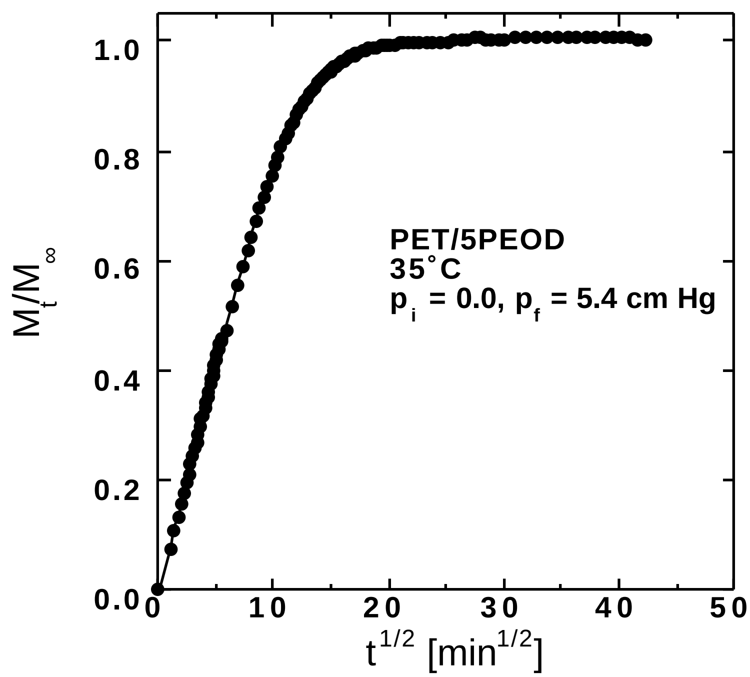

Figure A-20. Acetone Sorption Kinetics in PET/5PEOD

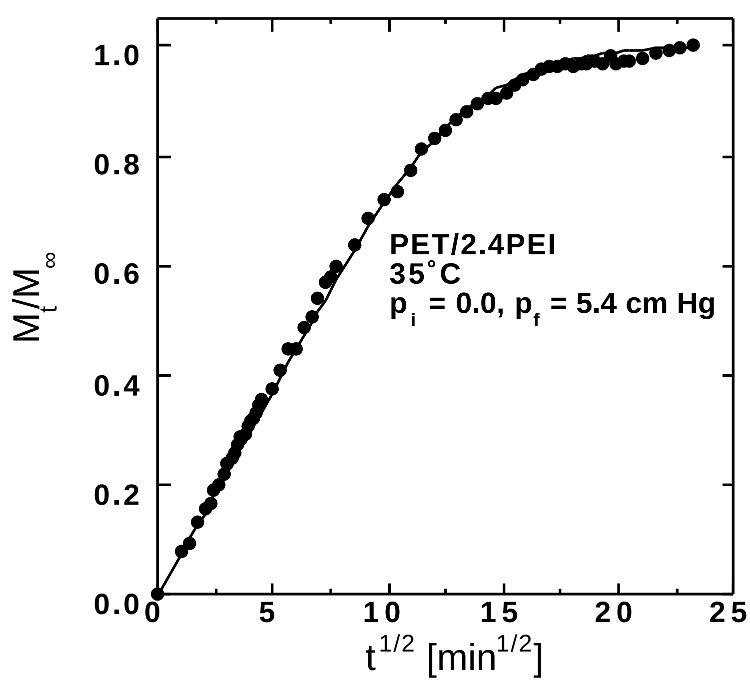

Figure A-21. Acetone Sorption Kinetics in PET/2.4IPA

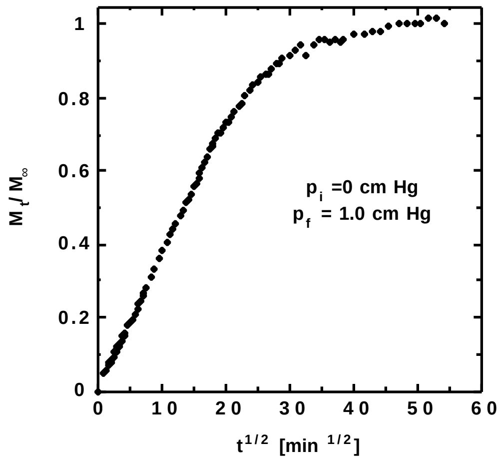

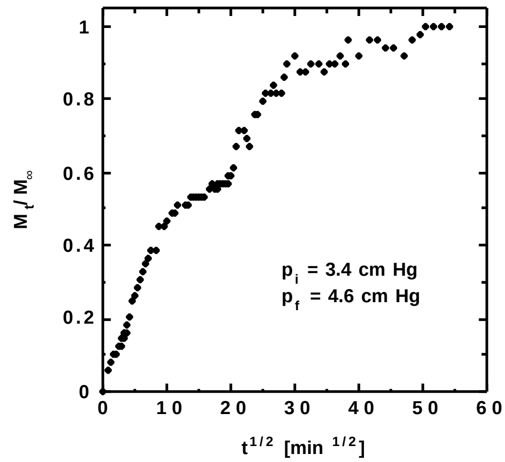

Figure A-22. Acetone Sorption in PET p_i =0.0 cm Hg, p_f = 1.0 cm Hg
Figure A-23. Acetone Sorption in PET p_i =3.4 cm Hg, p_f = 4.6 cm Hg

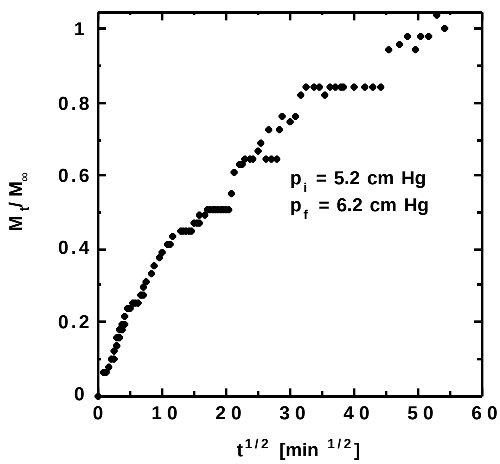

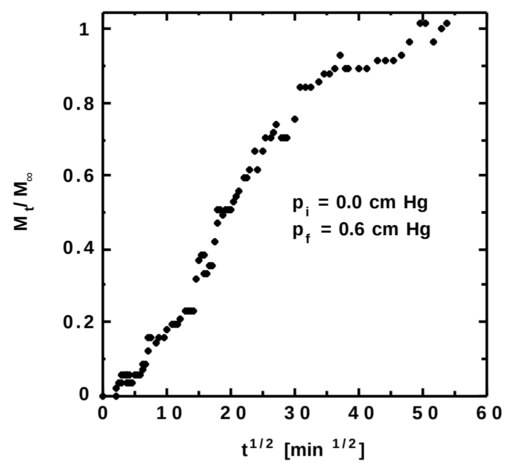

Figure A-24. Acetone Sorption in PET p_i =5.2 cm Hg, p_f = 6.2 cm Hg
Figure A-25. Acetone Sorption in PET/10PEN p_i = 0.0 cm Hg, p_f = 0.6 cm Hg

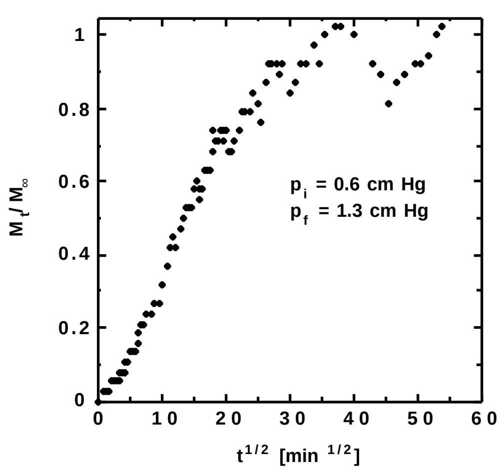

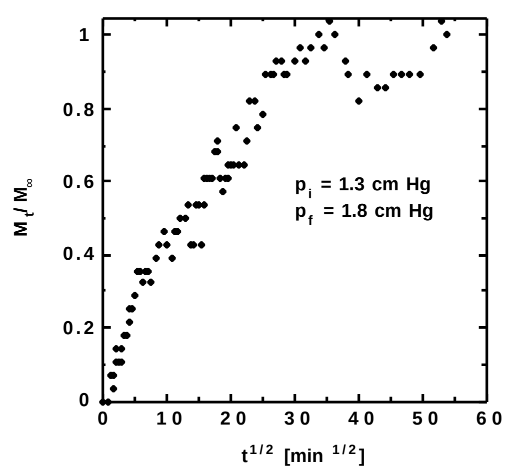

Figure A-26. Acetone Sorption in PET/10PEN p_i =0.6 cm Hg, p_f = 1.3 cm Hg
Figure A-27. Acetone Sorption in PET/10PEN p_i = 1.3 cm Hg, p_f = 1.9 cm Hg

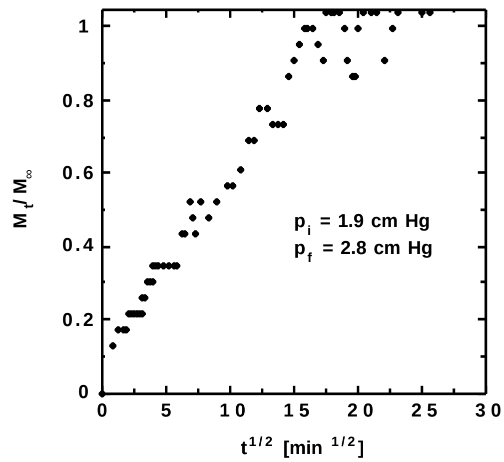

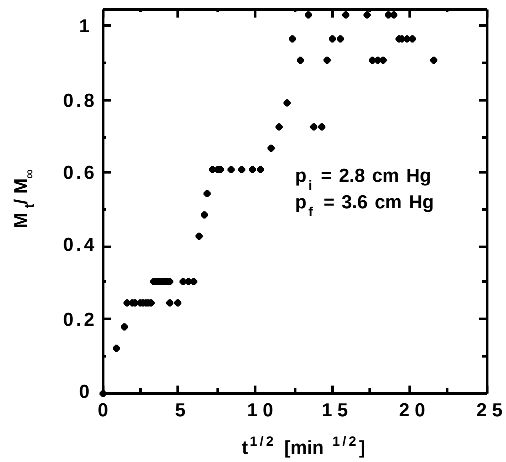

Figure A-28. Acetone Sorption in PET/10PEN p_i =1.9 cm Hg, p_f = 2.8 cm Hg
Figure A-29. Acetone Sorption in PET/10PEN p_i = 2.8 cm Hg, p_f = 3.6 cm Hg

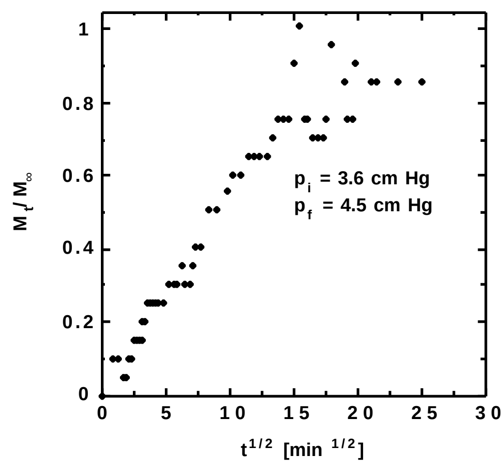

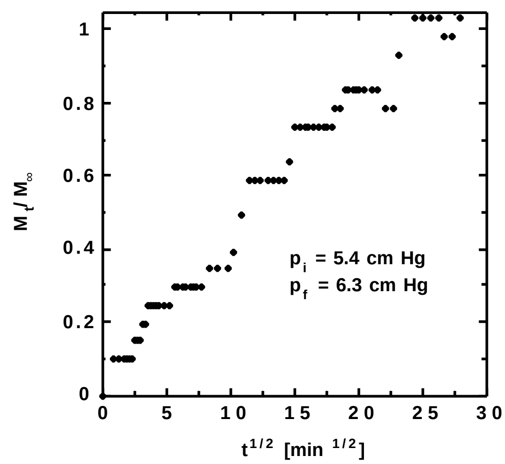

Figure A-30. Acetone Sorption in PET/10PEN p_i =3.6 cm Hg, p_f = 4.5 cm Hg
Figure A-31. Acetone Sorption in PET/10PEN p_i = 5.4 cm Hg, p_f = 6.3 cm Hg

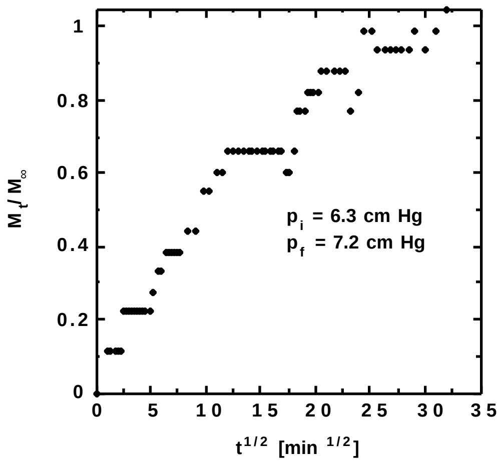

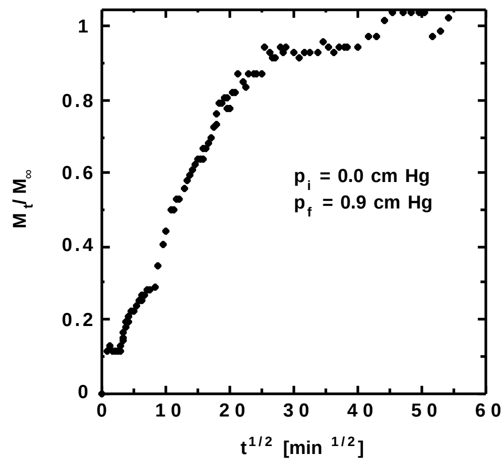

Figure A-32. Acetone Sorption in PET/10PEN p_i =6.3 cm Hg, p_f = 7.2 cm Hg

Figure A-33. Acetone Sorption in PET/20PEN p_i = 0.0 cm Hg, p_f = 1.0 cm Hg

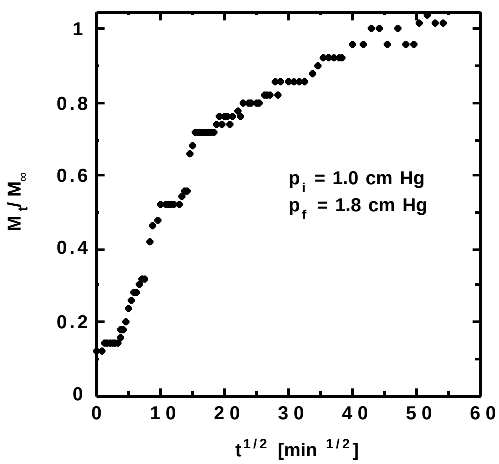

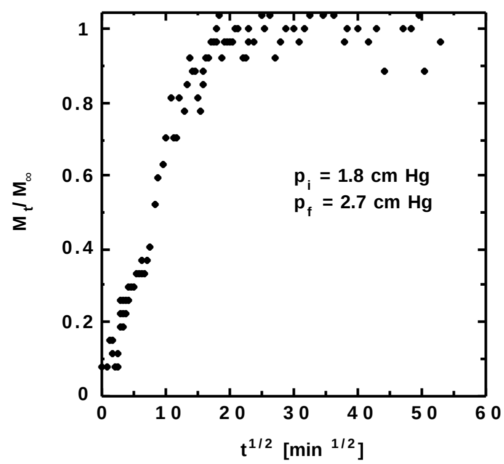

Figure A-34. Acetone Sorption in PET/20PEN p_i = 1.0 cm Hg, p_f = 1.8 cm Hg

Figure A-35. Acetone Sorption in PET/20PEN p_i = 1.8 cm Hg, p_f = 2.7 cm Hg

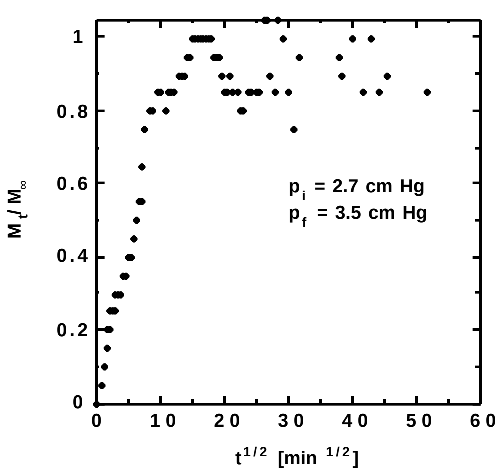

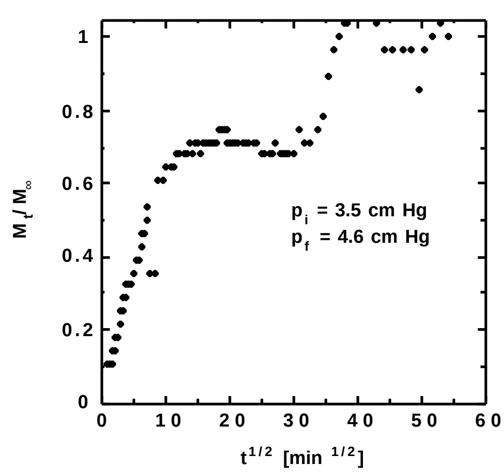

Figure A-36. Acetone Sorption in PET/20PEN p_i = 2.7 cm Hg, p_f = 3.5 cm Hg

Figure A-37. Acetone Sorption in PET/20PEN p_i = 3.5 cm Hg, p_f = 4.6 cm Hg

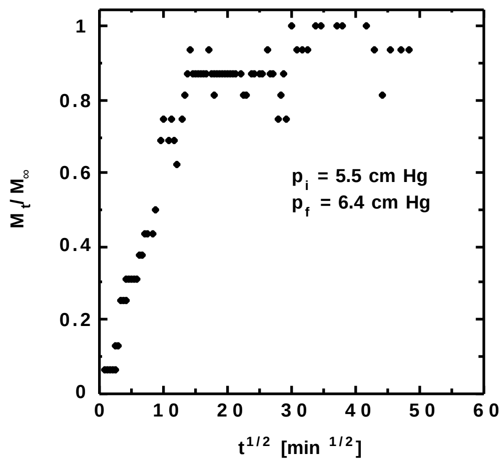

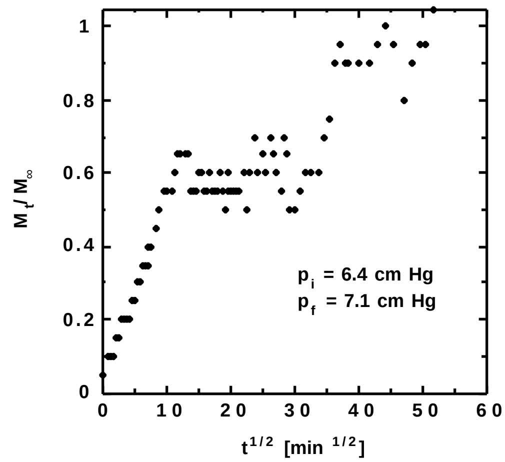

Figure A-38. Acetone Sorption in PET/20PEN p_i = 5.5 cm Hg, p_f = 6.4 cm Hg
Figure A-29. Acetone Sorption in PET/20PEN p_i = 6.4 cm Hg, p_f = 7.1 cm Hg

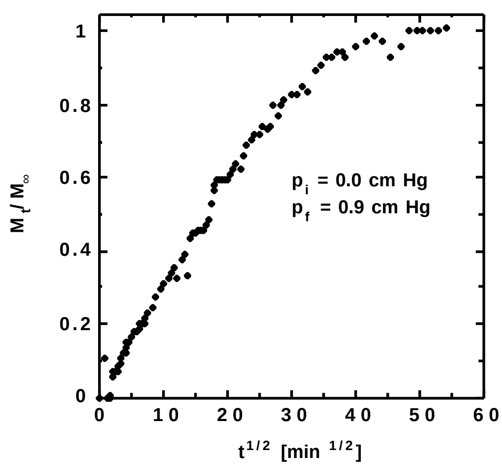

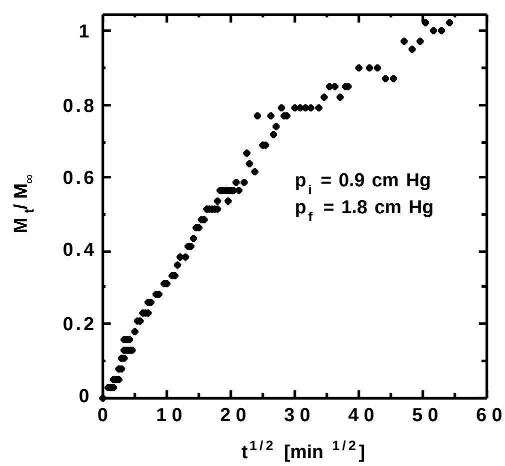

Figure A-40. Acetone Sorption in PET/50PEN p_i = 0.0 cm Hg, p_f = 0.9 cm Hg
Figure A-41. Acetone Sorption in PET/50PEN p_i = 0.9 cm Hg, p_f = 1.8 cm Hg

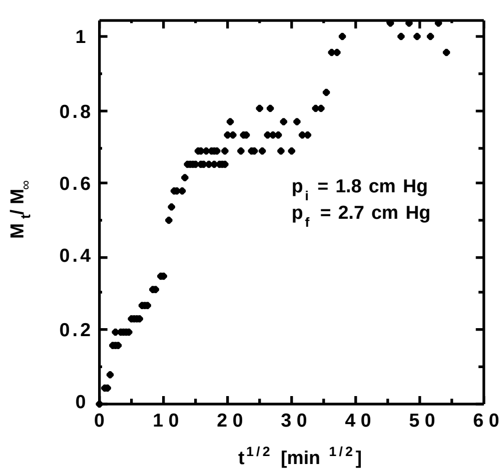

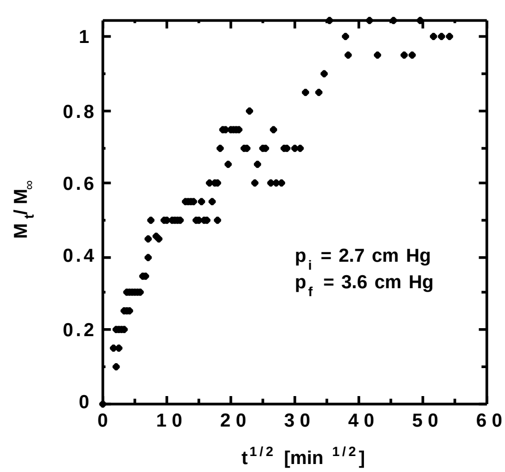

Figure A-42. Acetone Sorption in PET/50PEN p_i = 1.8 cm Hg, p_f = 2.7 cm Hg
Figure A-43. Acetone Sorption in PET/50PEN p_i = 2.7 cm Hg, p_f = 3.6 cm Hg

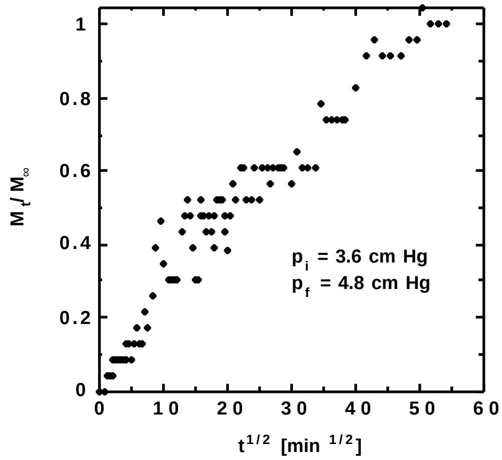

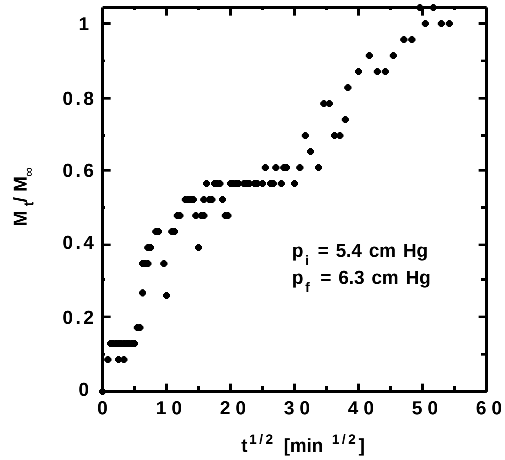

Figure A-44. Acetone Sorption in PET/50PEN p_i = 3.6 cm Hg, p_f = 4.8 cm Hg
Figure A-45. Acetone Sorption in PET/50PEN p_i = 5.4 cm Hg, p_f = 6.3 cm Hg

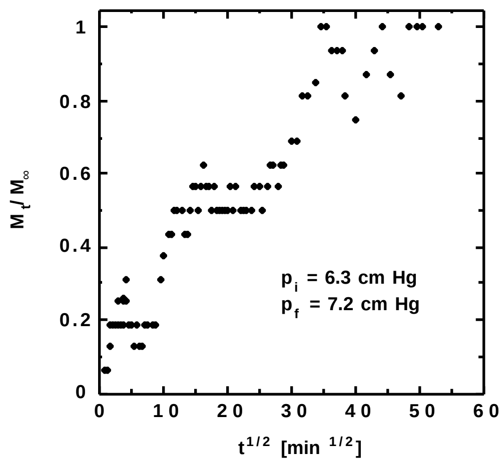

Figure A-46. Acetone Sorption in PET/50PEN p_i = 3.6 cm Hg, p_f = 4.5 cm Hg

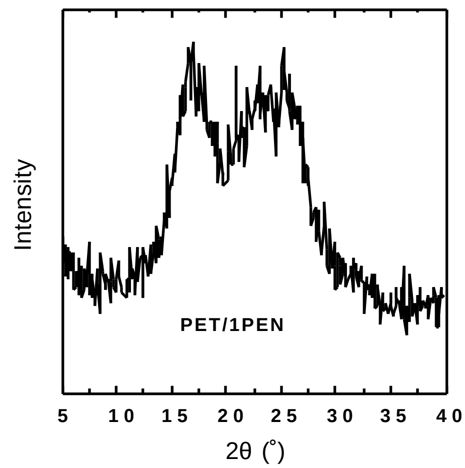

Figure A-47. WAXD Spectrum of PET/1PEN

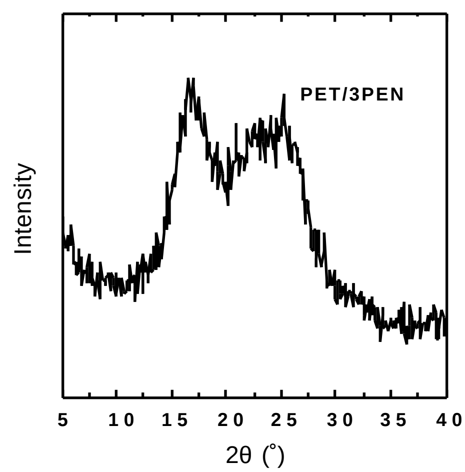

Figure A-48. WAXD Spectrum of PET/3PEN

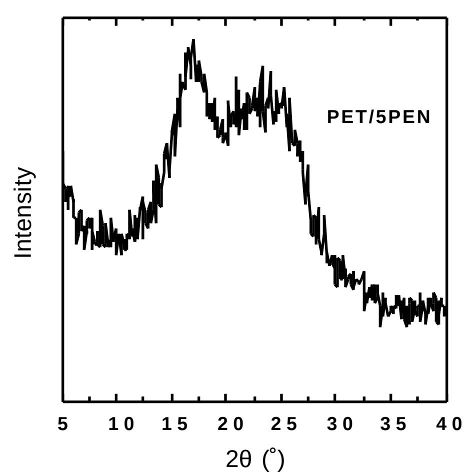

Figure A-49. WAXD Spectrum of PET/5PEN

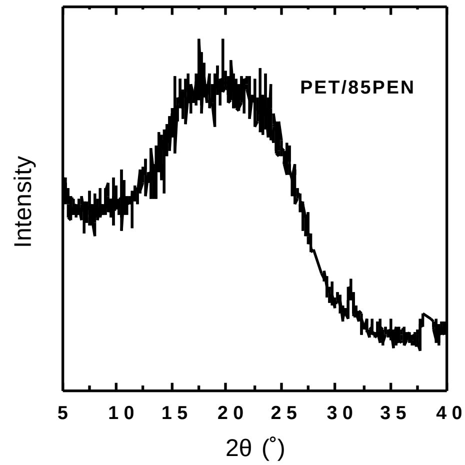

Figure A-50. WAXD Spectrum of PET/85PEN

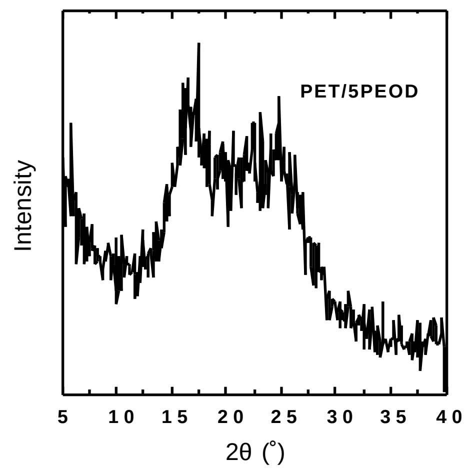

Figure A-51. WAXD Spectrum of PET/5PEOD

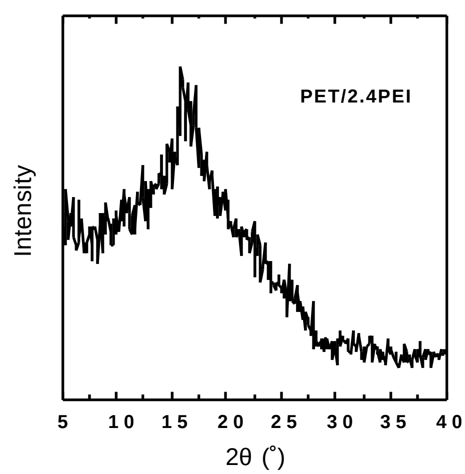

Figure A-52. WAXD Spectrum of PET/2.4PEI

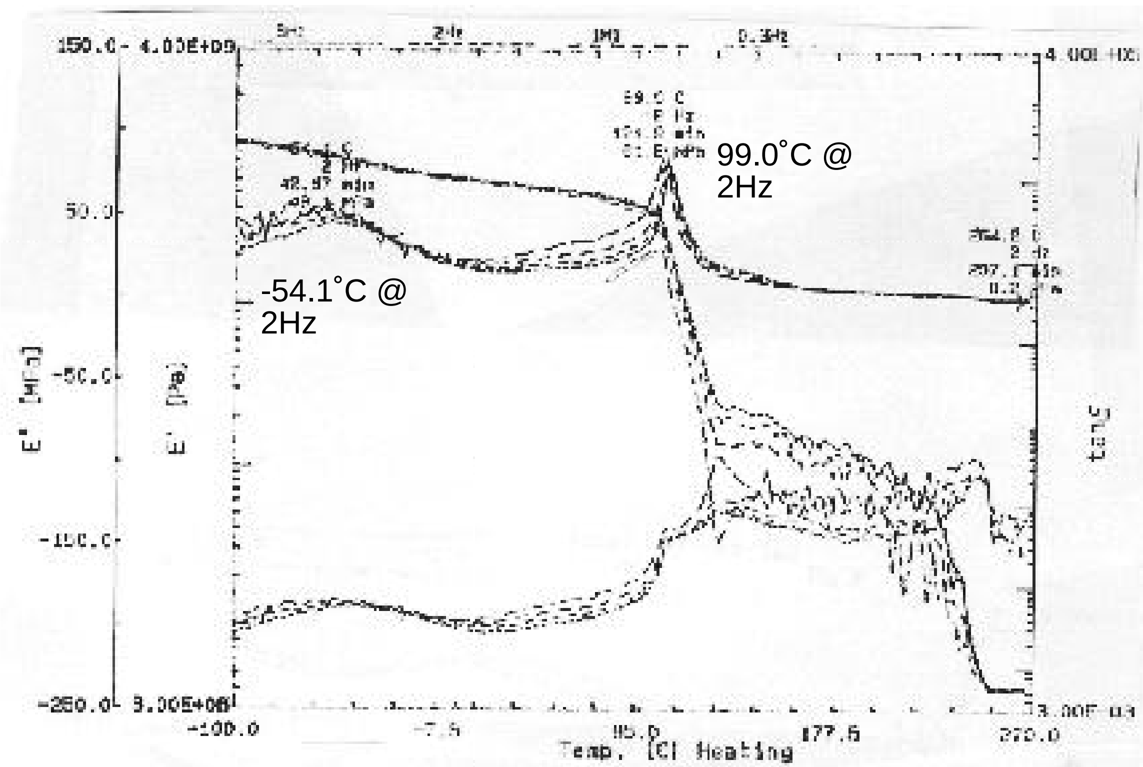

Figure A-53. DMA Spectrum of PET

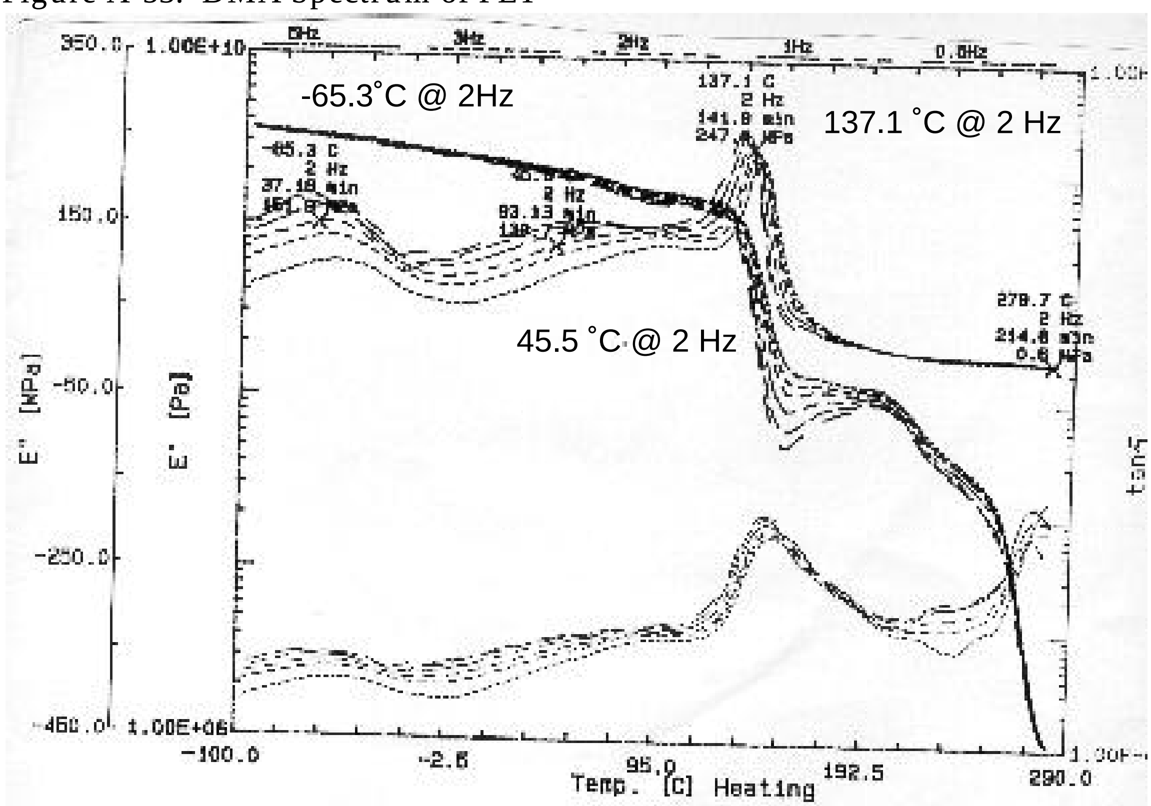

Figure A-54. DMA Spectrum of PEN

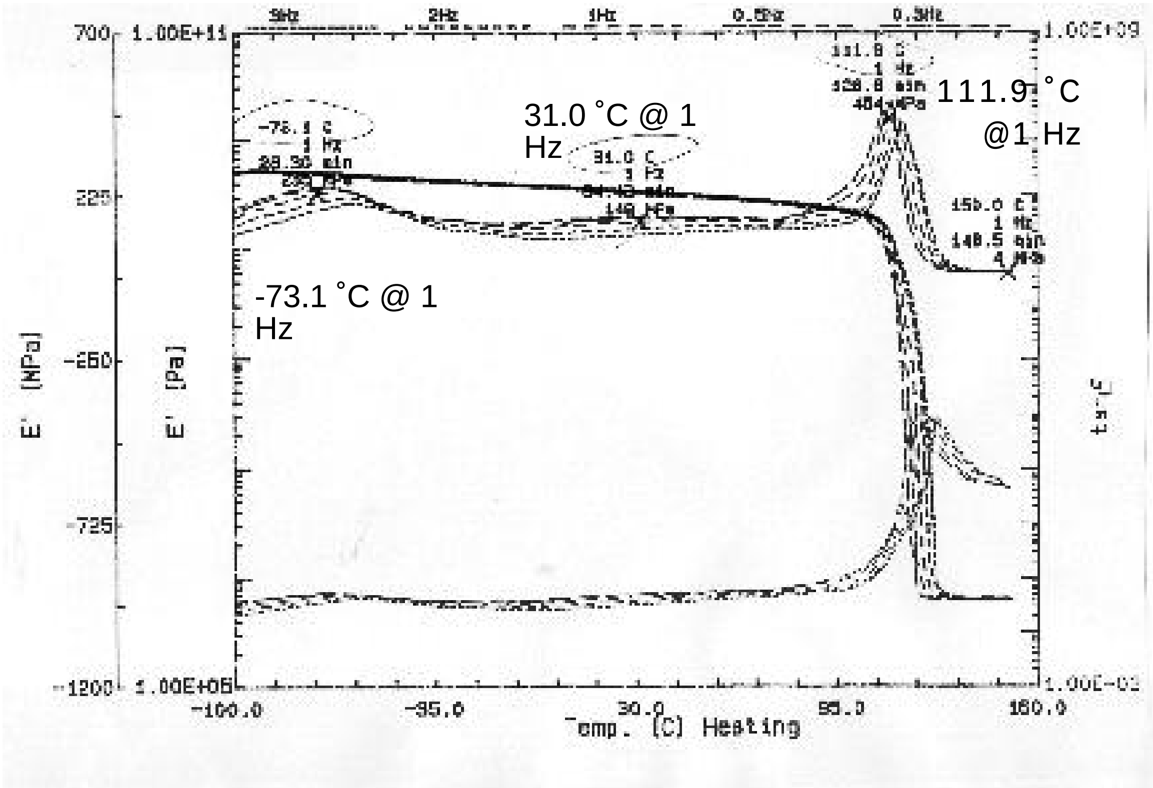

Figure A-55. DMA Spectrum of PET/50PEN

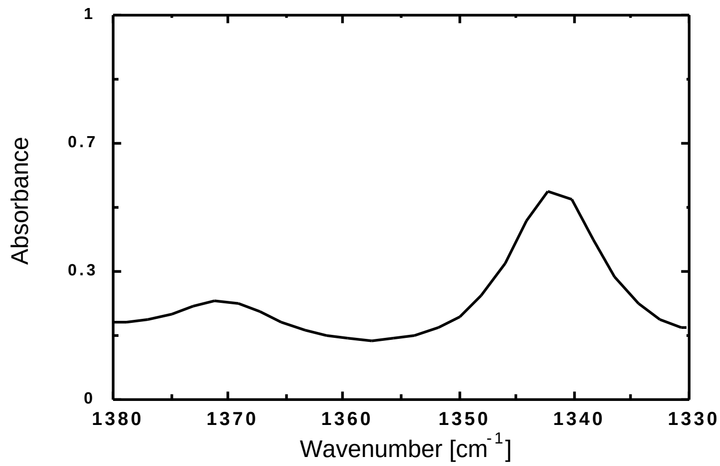

Figure A-56. IR Spectrum of PET/1PEN

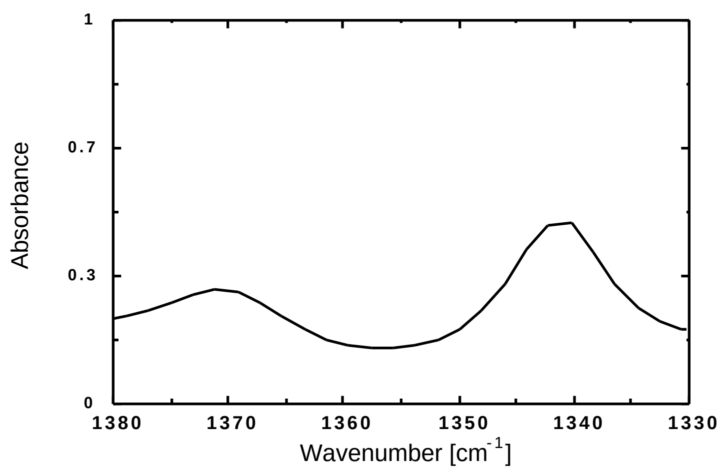

Figure A-57. IR Spectrum of PET/3PEN

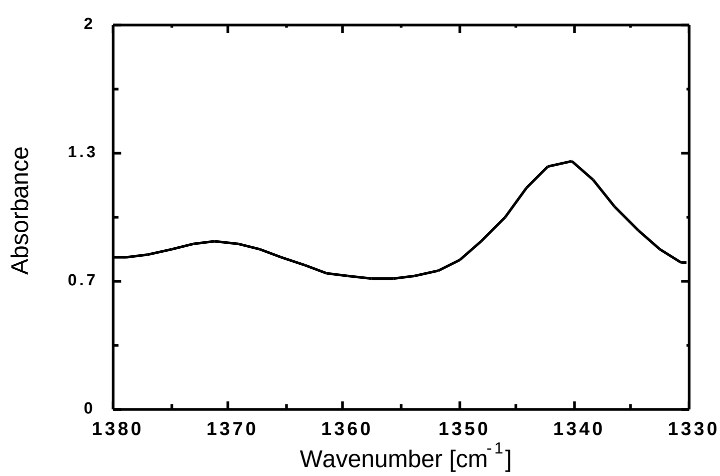

Figure A-58. IR Spectrum of PET/5PEN

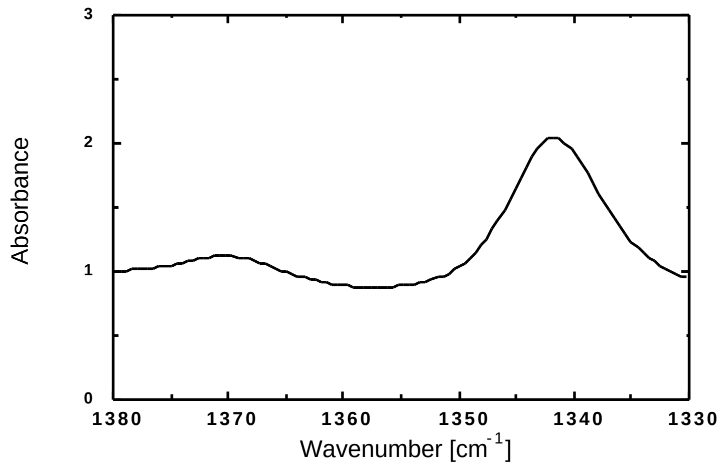

Figure A-59. IR Spectrum of PET

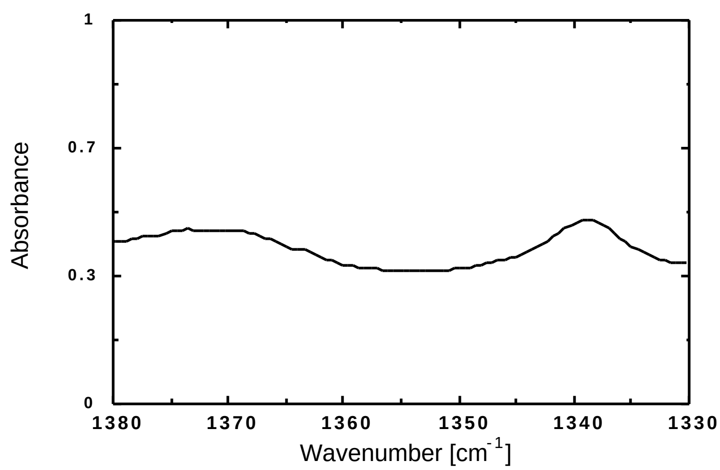

Figure A-60. IR Spectrum of PET/20PEN

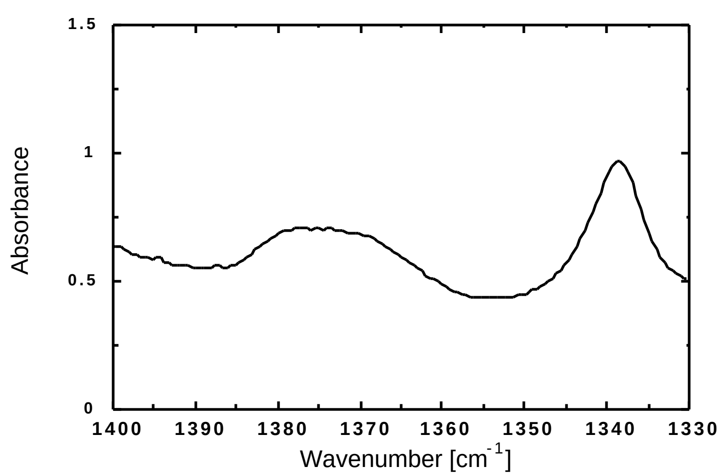

Figure A-61. IR Spectrum of PET/50PEN

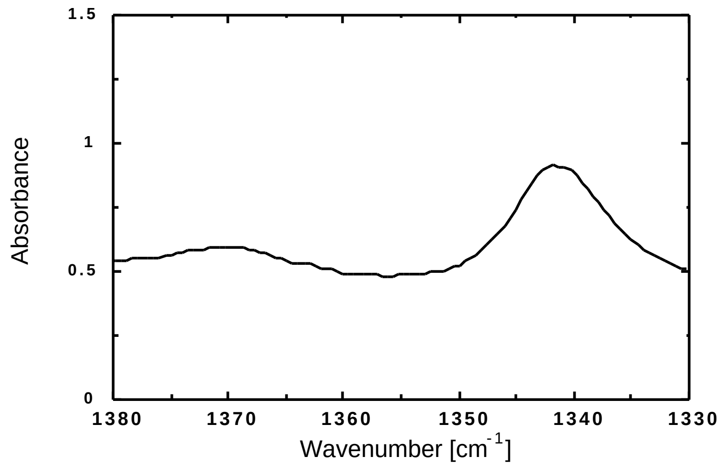

Figure A-62. IR Spectrum of PET/5PEOD

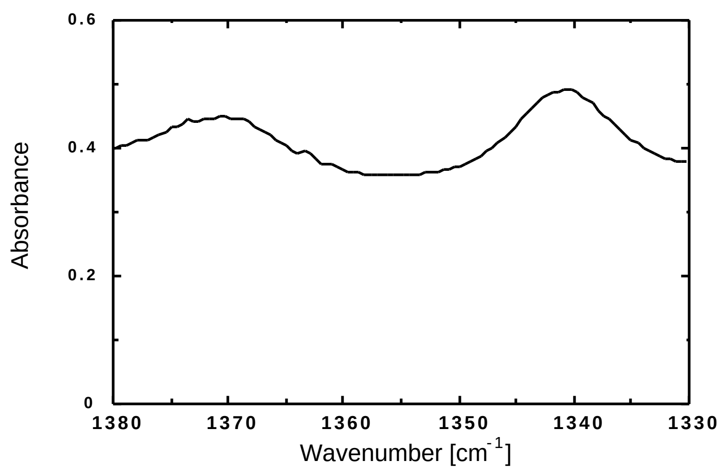

Figure A-63. IR Spectrum of PET/10PEOD

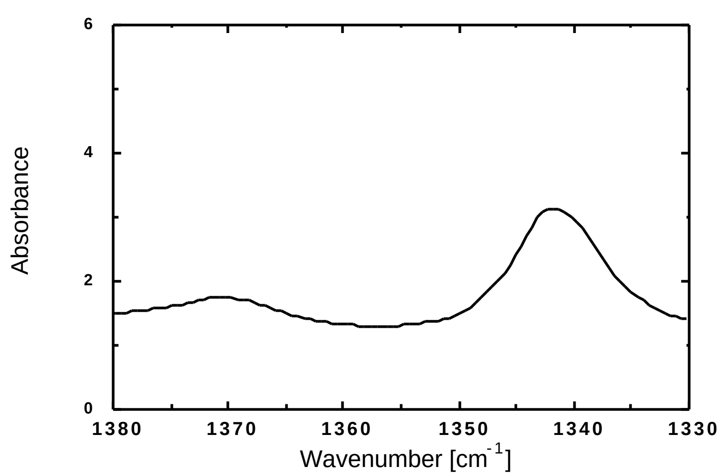

Figure A-64. IR Spectrum of PET/2.4PEI

Appendix B. Data for Figures in Dissertation Text

This appendix contains the data for all the figures in the dissertation in tabular form text except for raw data such as data from sorption runs, IR spectra, WAXD spectra, and DSC thermograms. These data are available in electronic form from the author.

Figures 1.3-1.5

1/FFV	D_{CO_2} [cm^2/s]	D_{CH_4} [cm^2/s]	S_{CO_2} [cm^3(STP)/ cm^3/atm]	S_{CH_4} [cm^3(STP)/ cm^3/atm]	P_{CO_2} [Barrers]	P_{CH_4} Barrers]
4.65	$2.4x10^{-7}$	$3.5x10^{-8}$	4.24	1.20	129	6.53
5.48	$1.4x10^{-7}$	$2.0x10^{-8}$	2.25	1.09	71.1	6.00
5.86	$6.5x10^{-8}$	$7.3x10^{-9}$	2.47	0.914	27.8	1.67
6.11	$3.3x10^{-8}$	$6.8x10^{-9}$	1.44	0.388	10.0	0.60
6.42	$2.0x10^{-8}$	$3.2x10^{-9}$	2.06	0.582	7.74	0.43

Figure 1.6

Volume % Crystal [Ar]	S_{Ar} [cm^3(STP)/ cm^3/atm]	Volume % Crystal [O_2]	S_{O_2} [cm^3(STP)/ cm^3/atm]	Volume % Crystal [N_2]	S_{N_2} [cm^3(STP)/ cm^3/atm]
0.0	0.00	0.0	0.00	0.0	0.00
16.0	0.015	19.1	0.013	19.1	0.0060
19.6	0.017	20.0	0.015	20.4	0.0081
19.6	0.019	29.3	0.019	22.2	0.0069
21.3	0.020	29.8	0.022	30.7	0.013
22.2	0.021	31.1	0.020	30.7	0.011
29.3	0.027	32.4	0.025	47.1	0.016
30.2	0.029	36.9	0.028	50.7	0.018
60.4	0.059	45.8	0.029	57.3	0.023
61.8	0.061	50.7	0.036	58.2	0.025
59.6	0.064	56.4	0.042	68.0	0.027
100.0	0.098	59.1	0.042	99.6	0.041
		58.7	0.045		
		59.6	0.046		
		57.3	0.047		
		66.2	0.051		
		100.0	0.075		

Figure 1.7

Volume % Crystal [CH_4]	S_{CH_4} [cm^3(STP) /cm^3/atm]	Volume % Crystal [CO_2]	S_{CO_2} [cm^3(STP) /cm^3/atm]
24.2	0.169	24.2	0.468
31.7	0.175	31.7	0.507
39.2	0.175	39.2	0.513
38.9	0.182	38.9	0.500
48.7	0.221	48.7	0.610
49.4	0.208	49.4	0.580
61.9	0.240	61.9	0.669
80.0	0.312	80.0	0.818

Figure 3.3

p [cm Hg]	C [cm^3(STP)/cm^3]
0.00	0.00
1.00	3.64
1.80	5.24
2.62	6.82
3.43	7.76
4.34	8.83
5.32	9.81
6.24	10.61
7.37	12.03

Figure 3.4

Critical Temperature [K]	k_D [cm^3(STP)/ cm^3/atm]	k_D* [cm^3(STP)/ cm^3/atm]	b [1/atm]
5.2	0.0078	0.0078	
126.2	0.058	0.0580	
151.8	0.082	0.0820	
154.4	0.10	0.10	
190.7	0.24	0.24	
304.2	0.83	5.46	0.322
508.0	98	679	35.1
562.6	185	427	150

Figure 3.9

C_f [cm^3(STP)/cm^3]	τ_R [s]
3.64	33,200
5.24	59,900
6.82	58,100
7.76	50,800
8.83	45,700
9.81	79,400
10.6	47,200
12.0	53,800

Figure 3.10

C_f [cm^3(STP)/cm^3]	C_D [cm^3(STP)/cm^3]	α_R
3.64	0.56	0.04
5.24	1.01	0.18
6.82	1.47	0.28
7.76	1.93	0.40
8.83	2.44	0.45
9.81	2.99	0.55
10.6	3.51	0.76
12.0	4.14	0.74

Figures 3.11 and 3.14

C_{avg} [cm^3(STP)/cm^3]	D x 10^{12} [cm^2/s]
1.82	1.60
4.44	2.07
6.03	2.76
7.29	12.8
8.30	7.58
9.32	17.1
10.3	23.6
11.3	27.6

Figure 3.12

K/ (1+bp_i)/(1+bp_f)	D[1+K/ (1+bp_i)/(1+bp_f)] x 10^{11} [cm^2/s]
3.16	5.79
1.67	5.53
1.07	5.70
0.751	22.4
0.561	11.8
0.415	24.2
0.319	31.1
0.250	34.5

Figure 3.13

C_D [$cm^3(STP)/cm^3$]	$D_D \times 10^{12}$ [cm^2/s]	C_H [$cm^3(STP)/cm^3$]	$D_H \times 10^{12}$ [cm^2/s]
0.40	6.77	1.43	-
1.12	8.16	3.38	3.33
1.80	8.043	4.25	5.57
2.52	29.7	4.84	32.9
3.16	15.1	5.19	24.0
3.84	30.2	5.46	66.4
4.64	37.4	5.70	115
5.40	40.5	5.88	164

Figure 4.4

Weight % PEN	ρ_A [g/cm^3] pellets	FFV_a pellets	ρ_A [g/cm^3] film	FFV_a film
0	1.283 ± 0.018	0.183 ± 0.0025	1.317 ± 0.010	0.161 ± 0.007
1	1.342 ± 0.018	0.145 ± 0.0020	1.340 ± 0.012	0.151 ± 0.005
3	1.340 ± 0.018	0.146 ± 0.0019	1.330 ± 0.010	0.153 ± 0.004
5	1.313 ± 0.038	0.163 ± 0.0047	1.335 ± 0.015	0.149 ± 0.004
10	1.303 ± 0.027	0.169 ± 0.0035		
20	1.340 ± 0.013	0.144 ± 0.0014		
50	1.319 ± 0.013	0.153 ± 0.0015	1.326 ± 0.013	0.148 ± 0.004
80	1.317 ± 0.013	0.149 ± 0.0015		
90	1.306 ± 0.026	0.155 ± 0.0031		
100	1.283 ± 0.017	0.169 ± 0.0023		

Figure 4.5

Weight % PEN	$\tau_3{}^3$ [ns^3]	I_3 [%]	$\tau_3{}^3 I_3/\varphi_A$ [ns^3]
0	4.83	16.53	128.8
1	4.64	18.85	116.9
3	4.42	19.99	118.7
5	4.78	19.03	104.8
10	4.79	20.31	99.0
20	4.78	19.73	94.0
50	4.54	21.23	96.4
100	3.76	21.76	90.9

Figure 4.7-4.9

Weight % PEN	S [cm^3(STP) /cm^3/atm]	D x 10^{12} [cm^2/s]	P x 10^2 [Barrers]
0	129 ± 0.3	5.2 ± 0.9	8.9 ± 1.6
0	128 ± 0.3	4.2 ± 0.9	6.9 ± 1.4
1	115 ± 0.2	3.8 ± 0.6	5.7 ± 0.9
3	141 ± 0.3	3.4 ± 0.5	6.3 ± 1.1
5	109 ± 0.2	3.1 ± 0.5	4.4 ± 0.8
10	110 ± 0.2	2.2 ± 0.5	3.2 ± 0.7
20	132 ± 0.3	1.3 ± 0.4	2.3 ± 0.7
20	137 ± 0.3	1.2 ± 0.4	2.2 ± 0.7
50	107 ± 0.2	1.1 ± 0.2	1.5 ± 0.3
50	108 ± 0.2	0.93 ± 0.2	1.3 ± 0.3
85	107 ± 0.2	0.34 ± 0.04	0.48 ± 0.05
85	98.6 ± 0.2	0.35 ± 0.04	0.45 ± 0.05

Figure 4.10

Weight % PEN	$P_{O_2}/P_{O_2,PET}$	Weight % PEN	$P_{Acetone}/P_{Acetone}$
0	1.00	0	1.00
4.4	0.94	1	0.73
6.4	0.92	3	0.80
10	0.89	5	0.56
20	0.80	10	0.41
26	0.75	20	0.28
56	0.56	50	0.18
100	0.32	85	0.06

Figures 4.11, 4.13, 4.14

Weight % PEN	$1/FFV_a$	$\tau_3{}^3 I^3/\varphi_A$ [ns^3]	T_a	D/Φ_A x 10^{12} [cm^2/s]
0	5.47	128.8	0.47	7.6
1	6.90	116.9	0.42	5.1
3	6.84	118.7	0.49	4.6
5	6.14	104.8	0.46	4.7
10	5.93	99.0	0.49	2.2
20	6.97	94.0	0.58	1.3
50	6.56	96.4	0.71	1.0

Figure 5.1

p [cm Hg]	C [cm^3(STP)/cm^3]	C/φ_A [cm^3(STP)/cm^3]
0.0	0.00	0.00
1.0	3.64	6.07
1.8	5.24	8.73
2.6	6.82	11.4
3.4	7.76	12.9
4.3	8.83	14.7
5.3	9.81	16.3
6.2	10.6	17.7
7.4	12.0	20.0

Figure 5.2

5% PEN			10 % PEN			20% PEN		50% PEN	
p [cm Hg]	C [cm^3 (STP) /cm^3]	C/φ_A [cm^3 (STP) /cm^3]	p [cm Hg]	C [cm^3 (STP) /cm^3]	C/φ_A [cm^3 (STP) /cm^3]	p [cm Hg]	C [cm^3 (STP) /cm^3]	p [cm Hg]	C [cm^3 (STP) /cm^3]
0.0	0.00	0.00	0.0	0.00	0.00	0.0	0.00	0.0	0.00
1.0	4.70	5.60	0.6	1.92	1.96	1.0	3.68	0.9	3.65
1.8	5.88	7.01	1.3	3.25	3.31	1.8	5.75	1.8	5.39
2.8	7.77	9.25	1.9	4.24	4.33	2.7	7.00	2.7	6.63
3.7	8.97	10.7	2.8	5.30	5.41	3.5	8.44	3.6	7.67
4.5	9.88	11.8	3.6	6.56	6.69	4.6	9.88	4.5	8.79
5.6	10.8	12.8	4.6	7.62	7.77	5.5	11.4	5.4	10.2
6.3	11.5	13.7	5.5	8.61	8.79	6.4	12.8	6.3	11.2
7.2	12.3	14.6	6.3	9.60	9.80	7.1	13.4	7.2	12.2
			7.2	10.6	10.8				

Figure 5.3

Weight % PEN	C_H' [cm^3(STP)/cm^3]	V_g-V_l [g/cm^3]
0	10.9	0.028
5	7.0	0.019
10	2.5	0.0064
20	5.1	0.013
50	4.0	0.010

Figure 5.4

Polymer	T_g - 35 [˚C]	C_H' [cm^3(STP) /cm^3] (various polymers)	C_H' [cm^3(STP) /cm^3] (PPO/PS)
PEMA	30.2	8.1	
PET	48.9	5.7	
COP	51.6	9.4	
PS	64.1	9.3	
	72.1		12.2
PMMA	74.8	15.2	
	86.4		14.7
PC	109.6	18.0	
	113.2	20.8	
	140.9		23.1
PSF	147.1	18.0	
	161.4		25.4
PPO	183.8	28.7	

Figure 5.6

T_g - 35 [˚C]	C_H' [cm^3(STP)/cm^3]	1-T/T_g
47	10.9	0.132
44	7.0	0.125
49	2.5	0.137
56	5.1	0.154
66	4.0	0.176

Figure 5.7

PET		10% PEN		20% PEN		50% PEN	
C/φ_A [cm^3 (STP) /cm^3]	D/φ_A x 10^{12} [cm^2/s]	C/φ_A [cm^3 (STP) /cm^3]	D/φ_A x 10^{12} [cm^2/s]	C/φ_A [cm^3 (STP) /cm^3]	D/φ_A x 10^{12} [cm^2/s]	C/φ_A [cm^3 (STP) /cm^3]	D/φ_A x 10^{12} [cm^2/s]
2.94	2.6	0.59		1.71	1.4	1.82	0.41
7.17	3.0	2.36	1.2	4.37	2.0	4.51	0.54
9.74	4.5	3.42	1.4	5.91	2.9	6.00	1.7
11.8	21	4.36		7.16	5.6	7.14	2.0
13.4	12	5.42		8.49	7.5		
15.0	27.6	6.48	2.3	9.84	6.8	9.45	
16.6	38.1	7.42	2.4	11.2	3.7	10.7	2.4
18.3	44.6	8.34	1.5	12.1	6.8	11.7	2.3
		9.24	2.3				

Figure 5.8

PET		**10% PEN**		**20% PEN**		**50% PEN**	
C_f [cm^3 (STP) /cm^3]	**τ_R [s]**	**C_f [cm^3 (STP) /cm^3]**	**τ_R [s]**	**C_f [cm^3 (STP) /cm^3]**	**τ_R [s]**	**C_f [cm^3 (STP) /cm^3]**	**τ_R [s]**
3.64	33,200	1.92		3.68		3.65	
5.24	59,900	3.25		5.75		5.39	
6.82	58,100	4.24		7.00		6.63	21,400
7.76	50,800	5.30	37,900	8.44		7.67	7,450
8.83	45,700	6.56	43,200	9.88	11,600	8.79	24,700
9.81	79,400	7.62	248,000	11.4	92,300	10.2	
10.6	47,200	8.61	29,900	12.8		11.2	45,900
12.0	53,800	9.60	35,600	13.4	19,400	12.2	25,700
		10.6	36,900				

Figure 5.9

PET		**10% PEN**		**20% PEN**		**50% PEN**	
C_f/ [cm^3 (STP) /cm^3]	**α_R**	**C_f [cm^3 (STP) /cm^3]**	**α_R**	**C_f [cm^3 (STP) /cm^3]**	**α_R**	**C_f [cm^3 (STP) /cm^3]**	**α_R**
3.64	0.04	1.92	0.00	3.68	0.00	3.65	0.00
5.24	0.18	3.25	0.00	5.75	0.00	5.39	0.12
6.82	0.28	4.24	0.00	7.00	0.00	6.63	0.27
7.76	0.40	5.30	0.30	8.44	0.00	7.67	0.25
8.83	0.45	6.56	0.45	9.88	0.30	8.79	0.40
9.81	0.55	7.62	0.38	11.4	0.32	10.2	0.35
10.6	0.76	8.61	0.30	12.8	0.12	11.2	0.40
12.0	0.74	9.60	0.15	13.4	0.42	12.2	0.45
		10.6	0.35				

Figure A-11

PICT		PEEK		50/50 PICT/PEEK	
p [atm]	**C [cm^3(STP)/ cm^3]**	**p [atm]**	**C [cm^3(STP)/ cm^3]**	**p [atm]**	**C [cm^3(STP)/ cm^3]**
0.00	0.00	0.00	0.00	0.00	0.00
0.120	0.87	0.238	2.40	0.12	1.96
0.23	1.34	0.594	4.54	0.24	2.51
0.35	1.94	0.743	5.16	0.36	3.20
0.46	2.14			0.48	3.92
0.58	2.81			0.60	3.40
0.70	3.14			0.72	4.80
				0.87	5.48
				0.98	4.88

Figure A-12

PICT		PEEK		50/50 PICT/PEEK	
p [atm]	**D x 10^{12} [cm^2/s]**	**p [atm]**	**D x 10^{12} [cm^2/s]**	**p [atm]**	**D x 10^{12} [cm^2/s]**
0.120	9.3	0.238	4.8	0.12	3.8
0.23	7.7	0.594	4.5	0.24	2.9
0.35	5.8	0.743	5.5	0.36	2.8
0.46	7.3			0.48	2.9
0.58	8.2			0.60	2.4
0.70	7.9			0.72	4.3
				0.87	4.3
				0.98	4.6